I.O.S.

FIELD OBSERVATIONS OF WAVE-INDUCED MOTION ABOVE THE SEABED AND OF THE RESULTING SEDIMENT MOVEMENT

BY

A. G. DAVIES

REPORT NO. 179

1984

NATURAL ENVIRONMENT RESEARCH COUNCIL

INSTITUTE OF OCEANOGRAPHIC SCIENCES

INSTITUTE OF OCEANOGRAPHIC SCIENCES

Wormley, Godalming,
Surrey, GU8 5UB.
(0428 - 79 - 4141)

(Director: Dr. A.S. Laughton FRS)

Bidston Observatory,
Birkenhead,
Merseyside, L43 7RA.
(051 - 653 - 8633)

(Assistant Director: Dr. D.E. Cartwright)

Crossway,
Taunton,
Somerset, TA1 2DW.
(0823 - 86211)

(Assistant Director: M.J. Tucker)

When citing this document in a bibliography the reference should be given as

DAVIES, A.G. 1984 Field observations of wave-induced motion above the seabed and of the resulting sediment movement.
Institute of Oceanographic Sciences, Report, No. 179, 171pp.

ERRATA IOS REPORT NO. 179

"Field observations of wave-induced motion above the seabed and of the resulting sediment movement" by A G Davies

p.13, para.1, 1.4 p.16, para.1, 1.9 p.16, para.2, 1.10	Davies (1980a) not (1980)
p.64, para.2, 1.21	Run 12 not Fig. 12
p.71, para.2, 1.9	$0.01\hat{u}_*/\sigma$ not $0.02\hat{u}_*/\sigma$
p.74, para.2, 1.8	Treloar and Abernethy (1978)
p.84, para.1, 1.1	remove ; that is, $f'(\zeta) = 1$ for $\zeta = \infty$. replace by for $\chi > 0$.
p.89, Eq. (22)	$U_0 a$ not Ua
p.103, para.2, 1.2	transport by waves not of waves
p.161	Grain size for Run 8: $D_{50} = 0.0225$ not 0.0025

INSTITUTE OF OCEANOGRAPHIC SCIENCES

TAUNTON

Field observations of wave-induced motion above the seabed and of the resulting sediment movement

by

A.G. Davies

I.O.S. Report No. 179

1984

CONTENTS

LIST OF FIGURES

TABLES

LIST OF SYMBOLS

a	vortex separation in the irrotational model
a_r	radius of rotational vortex core
A	area of rotational vortex core
$\hat{A}_\infty = d_o/2$	near-bed excursion amplitude
$b = \eta/2$	ripple amplitude
C_1	constant in relationship of bed roughness to ripple height
$C_2(x)$	near-bed potential velocity amplitude function
$d_o = 2\hat{U}_\infty/\sigma$	near-bed orbital excursion
D	grain diameter
D_{50}	median grain diameter
E	grouped estimate of spectral energy
$\tilde{f}$	instantaneous wave drag coefficient
$f( )$	conformal mapping function in the irrotational model
f_w	Jonsson's (1967) friction factor
g	acceleration of gravity
h	water depth
J	Jacobian of the transformation in the irrotational model
$k = 2\pi/\lambda_w$	surface wavenumber
k_s	equivalent roughness of bed surface
$\ell = 2\pi/\lambda$	ripple wavenumber
m	counter in summations
$M = \hat{U}_\infty^2/g\gamma D$	"mobility number"
M_c	critical "mobility number " at the onset of sediment motion
n	vortex number in the row
$\tilde{n}$	number of wave cycles after the first appearance of ripples on a flat bed
N	inward directed normal to surface S
N_r	number of ripples on the bed in the calculation of vortex energy
P	typical point in the ζ-plane
$q = \sqrt{(u^2+v^2)}$	speed of the fluid
Q	typical point in the z-plane
r	modulus of ζ in the ζ-plane (also r_o, r_1....)
$R = \hat{U}_\infty/(\sigma\nu)^{\frac{1}{2}}$	nondimensional parameter in the analysis of Sleath (1975a)
$RE = \hat{U}_\infty\hat{A}_\infty/\nu$	wave Reynolds number

S	surface enclosing the fluid
S_*	dimensionless sediment parameter of Grant and Madsen (1982)
t	time
T	wave period
T_k	kinetic energy of the fluid
ΔT	average measured wave half-period
$u = -\phi_x$	velocity component in x-direction in z-plane
$\tilde{u}$	velocity component in ξ-direction in ζ-plane
$u_* = \sqrt{\tau_o/\rho_f}$	shear velocity
$\hat{u}_*$	peak shear velocity in a wave cycle
U	measured horizontal velocity component in shoreward direction (also U_1, U_2, U_3)
$U_T = \mathrm{sgn}(U)\sqrt{(U^2+V^2)}$	total measured horizontal velocity
U_{ROT}	rotated component of measured horizontal velocity
U_∞	free-stream velocity
$\hat{U}_\infty$	free-stream velocity amplitude
$\hat{U}_{\infty c}$	critical value of $\hat{U}_\infty$ at the onset of sediment motion on a flat bed
U_o	free-stream velocity in the irrotational flow model
$v = -\phi_y$	velocity component in y-direction in z-plane
$\tilde{v}$	velocity component in χ-direction in ζ-plane
V	measured horizontal velocity component in longshore direction (also V_3)
V_f	volume of fluid
w	width of the flow
W	measured vertical velocity component (also W_1, W_2)
x	co-ordinate in physical z-plane
y	" " " z-plane
y_b	height of the bed surface
$z = x + iy$	position in the z-plane
$\beta = \sqrt{\sigma/2\nu}$	shear wavenumber
$\gamma = (\rho_s-\rho_f)/\rho_f$	relative density of sediment
δ_1	wave boundary layer thickness of Jonsson (1967)
$\zeta = \xi + i\chi = re^{i\theta}$	position in the ζ-plane
η	ripple height
$\eta' = \lambda/7$	assumed ripple height for equilibrium ripples
θ	argument of ζ (also θ_o, θ_1 ....)

$\theta' = \frac{1}{2} f_w M$	Shields' parameter
θ_c	critical value of Shields' parameter at the onset of sediment motion
κ	vortex strength or circulation
$\lambda = 2\pi/\ell$	ripple wavelength
$\lambda_w = 2\pi/k$	surface wavelength
ν	kinematic viscosity
ξ	co-ordinate in transform ζ-plane
ρ_f	density of fluid
ρ_s	density of sediment
$\sigma = 2\pi/T$	wave frequency
τ_o	bed shear stress
$\hat{\tau}_o$	peak bed shear stress in the wave cycle
φ	angle of repose of sand
ϕ	velocity potential in irrotational model ($\bar{\phi}$ when normalised)
χ	co-ordinate in transform ζ-plane (also χ_o, χ_1 ....)
ψ	streamfunction in irrotational model ($\bar{\psi}$ when normalised)
ψ_r	angle of rotation in forming reduced velocity time series
ψ_1'	Manohar's (1955) dimensionless parameter representing the lift on sediment particles
ω	angular velocity of rotational vortex core
$\Omega = \phi + i\psi$	complex potential in irrotational model ($\bar{\Omega}$ when normalised)

subscripts (§7)

I	irrotational flow region
R	rotational flow region
r	rotational velocity component
s	free-stream velocity component
v	velocity components associated with the infinite row of vortices

SUMMARY

Although there have been many laboratory studies of sediment movement by waves and of the properties of oscillatory flow above erodible sand beds, there have been comparatively few field studies of these topics. The present report is based upon two field studies carried out to determine both the critical conditions at the threshold of sand motion beneath irregular sea waves, and the nature of the associated near-bed oscillatory flow. The experiments were conducted in waters of depth 4-10 m outside the breaker zone at Blackpool Sands, Start Bay, S Devon, England, in a region where the bed was reasonably level and comprised a mixture of sand grain sizes. A bottom rig was placed on the bed, which enabled water velocity and bottom pressure measurements to be obtained. The associated sediment motion was monitored with an underwater television system, and the physical properties of the bed were measured by divers.

From the synchronous video and near-bed velocity records, critical conditions at the threshold of sediment motion have been established in terms of the free-stream velocity amplitude and wave period. Despite the irregular nature of the (swell) waves and the mixture of grain sizes on the bed, agreement between the present field, and previous laboratory, results has been found to be reasonable, provided that proper allowance is made for the presence of sand ripples on the bed. For the rippled beds which were present during the experiments, critical conditions for the onset of vortex formation and shedding above the bed have also been established. Again, reasonable agreement with laboratory results has been found. In particular, it has been shown that vortex formation occurs above the lee slopes of ripples only if the near-bed orbital excursion exceeds the ripple wavelength. Prior to certain experimental runs, the area of the seabed in the vicinity of the rig was flattened by divers, and an (equilibrium) ripple pattern was allowed to develop. The wavelengths of the ripples which formed are in close agreement with the field results of previous workers.

In order to define sediment threshold motion conditions on a more rational basis than simply in terms of the measured free-stream velocity amplitude, calculations of the bottom stress have been made on the basis of laboratory-derived wave drag coefficients. The threshold motion conditions thus established from the field data are in good agreement with sediment threshold values from Shields' curve derived from laboratory work. For rippled beds above which there was vortex formation and shedding, it was not possible to calculated the skin friction acting directly on the surface layer of sand grains. In such cases only the total stress was calculated, that is the sum of skin friction and form drag. From the

results obtained, and from a knowledge of the Shields' threshold stress for the sand size in question, it has been shown that there is an order of magnitude difference between the (larger) form drag and (smaller) skin friction contributions to the total stress.

In order to examine in detail some of the properties of separating flow above a rippled bed, an irrotational standing vortex model has been considered. This has been used to relate the near-bed velocity field to the outer free-stream velocity, and to calculate the kinetic energy associated with near-bed vortices for a range of parameter settings. While the proposed quasi-steady model is deficient in respect of certain properties of the oscillatory (unsteady) flow over ripples, it provides a useful framework for analysis of the present field data.

Finally, the present report includes an extensive literature survey concerned with previous observations of sand ripple formation, with the mechanisms of ripple formation and with aspects of the near-bed oscillatory flow above sand ripples.

§1 INTRODUCTION

1.1 General considerations

This report is based on two field experiments carried out to study aspects of the problem of sediment movement by waves. These experiments were a continuation of the earlier field studies reported by Davies et al (1977), Davies and Wilkinson (1979) and Davies (1980), which were carried out to determine the critical conditions at the threshold of sediment motion by waves.

Most previous studies of sediment movement by waves have involved either theoretical or laboratory work; comparatively little work has been carried out in the field. The theory has been concerned mainly with properties associated with surface waves, such as the wave-induced motions in the body of the fluid and the nature of the oscillatory boundary layer above the bed; while the laboratory work has concentrated on the transition from laminar to turbulent flow in the wave boundary layer, with the threshold of sediment motion in oscillatory flow, and with aspects of ripple formation on the bed (see the review of Davies (1983)). The present study is concerned, to a greater or lesser extent, with all of these matters.

The principal differences between the idealised cases usually treated both in theory and in the laboratory, and the situation in the field, are, firstly, that sea waves are rather irregular and not simply sinusoidal and, secondly, that the seabed comprises a mixture of grain sizes and not a single size. Furthermore, mobile seabeds are generally rippled, not flat, and this further complicates matters, since the processes at work near the seabed depend rather critically upon whether or not ripples are present. If the bed is flat, sediment entrainment by an oscillatory flow must result from processes such as turbulent diffusion. However, if the bed is rippled, the near-bed oscillatory motion may induce a pattern of vortex formation and shedding in each wave half-cycle, which both stabilises the rippled bed structure, and also picks sediment up into the flow as a suspended load. Although there have been laboratory studies of the detailed nature of separating flow above ripples, no equivalent field studies have been undertaken. Vortex formation and shedding is associated with high wave drag coefficients and, hence, high wave energy dissipation rates. It is therefore a phenomenon of considerable practical importance.

Very little previous work has been carried out on the sediment transport rates which occur when waves are present, largely as a result of the inadequacy of existing instrumentation. Although for a symmetrical to- and fro- wave-induced

motion the net sediment transport must be zero, the importance of wave action in the problem as a whole is its ability to mobilise sediment by generating large shear stresses within the thin wave boundary layer. If, for any reason, a steady current is superimposed on the wave action, the resulting net sediment transport rate may be unexpectedly large. Even small steady currents, not capable of causing sediment motion on their own, may be found to transport quite a substantial sediment load. However, before such effects can be treated adequately, it is necessary to achieve a basic understanding of the properties of sediment movement in comparatively simple situations in which the flow is oscillatory. This is the aim of the present study; no consideration is given to the problem of sediment movement resulting from the combined influence of waves and currents.

1.2 Previous field studies of the wave boundary layer and of sediment transport by waves

There have been rather few previous field studies related to the present investigation. Those pertaining to topics which are directly relevant to the present report, for example to sand ripple formation by wave action, are discussed in §2. Some other less directly related field observations are discussed briefly here.

Measurements of the boundary layer flow beneath surface waves have been made in the field by Lukasik and Grosch (1963) and, more recently, by Lambrakos (1982). Lukasik and Grosch attempted to check the basic relationships of linear wave theory concerning wave phase angle and velocity amplitude. In particular, they measured the pressure at the seabed with an absolute pressure gauge, and the velocity at various heights above the bed with a thermistor, and used spectral analysis methods to test for the existence of regions of potential flow, and of boundary layer flow, above the bed. For waves having periods of 8 and 13 seconds, they demonstrated the in-phase behaviour of the velocity and pressure at a height of 38 cm above the bed, and verified the predictions of linear theory for the relative magnitudes of these quantities. In the layer between 38 cm height and the bed itself, they demonstrated the existence of a laminar boundary layer by the departure of their observations from the predictions of the theory. Lambrakos (1982) also made velocity measurements at two levels above the bed, in order to demonstrate the existence of a wave boundary layer. For swell waves of (representative) period 13.5 s, he found that wave velocities measured at 69 cm above the bottom were generally larger in magnitude, and also shifted in phase, relative to velocities measured at a height of 185 cm.

Previous field studies of sediment movement caused by wave action have tended to relate the general wave climate at a field site to the sediment motion induced by the waves; in no previous studies have detailed comparisons been made between properties of the oscillatory flow and the resulting sediment movement on the bed. For example, Cook and Gorsline (1972) studied wave-generated currents, and the associated sand transport, in the offshore zone off southern California in waters of depth 3-30 m. They measured the oscillatory currents with a mechanical current meter, and detected grain motion by the use of sediment traps. They also used close-up cinematography to examine the water circulation over sand ripples, and the resulting motion of sand grains. However, they did not make any direct measurements of, for example, critical sediment threshold velocity amplitudes of the kind described in the present report. The same is true of the field study of Sternberg and Larsen (1975). These workers obtained bottom photographs, from which turbidity levels could be assessed, in water of depth 167 m on the Washington continental shelf. Simultaneously, surface wave conditions were recorded in 35 m depth, on the summit of Cobb Seamount, 465 km to the west of this shelf experiment. These wave observations were used to estimate threshold conditions for sediment motion on the continental shelf. Again, not least on account of the large distance between the sites where the turbidity and the waves were measured, no instantaneous correlations of wave motion and the resulting sediment movement were made. More recently, Lavelle et al (1978) performed field experiments to investigate the relationship between the near-bottom fluid velocity and the suspended sediment concentration, in water of depth 10.5 m on the inner continental shelf south of Long Island, N.Y. Burst sampling of the (instantaneous) velocity and sediment concentration fields was undertaken, and statistical analyses were performed on the data. Again, however, no instantaneous wave-by-wave correlations of the kind described in the present report were attempted.

1.3 The present study

In the earlier field studies cited in §1.1, attempts were made to determine critical conditions for the threshold of sediment motion by waves in the sea. Threshold motion results were obtained both in terms of the measured free-stream velocity well above the bed, and also in terms of the bed shear stress, which was deduced by theoretical and semi-empirical methods. The underlying aim of this earlier work was to assess the general validity, for use in the field, of the many previous laboratory results which had been obtained in idealized situations, usually involving monochromatic waves above a flat bed comprising

grains of a single size. In the field, rather greater variability in sediment threshold results is expected than in the laboratory, but mean values of quantities defining the threshold of sediment motion should be closely similar. This was the essential finding of the earlier field investigations. The greatest complication in the analysis of this earlier data was that the seabed was generally rippled. However, since the flow was always nonseparating above the ripples, it was possible to partition the problem into a study of the irrotational flow over the ripple profiles, and then to make a boundary layer correction in the thin layer adjacent to the bed (Davies, 1980). The thickness of the boundary layer was typically two orders of magnitude less than the ripple wavelength. For this type of flow, the form drag on the bed was zero, and the bottom friction was entirely skin friction.

As noted in §1.1, a more generally occurring, and more important situation is that in which the flow over the ripples separates, with vortices forming above, and being shed from, the ripples in each wave half-cycle. In such situations, the waves and the seabed are generally "in equilibrium", as opposed to the case of nonseparating, non-equilibrium, flow mentioned above, in which the ripples are usually the result of some previous, more vigorous, wave activity. In the equilibrium case, in which both the skin friction and form drag components of the total stress are non-zero, the analysis of the problem is more difficult. The aim of the present report is to extend the earlier work of Davies et al (1977), Davies and Wilkinson (1979) and Davies (1980), to encompass these physically more interesting and important conditions. Results are presented for quite active wave-induced flows, involving separation above the bottom ripples. Also, certain experimental runs are described in which the formation of equilibrium ripples from an initially flattened bed has been observed.

The detailed aims of the present field study were

i) to determine the conditions at the threshold of sand motion in terms of the measured free-stream velocity and to make comparisons with laboratory results;

ii) to determine on a wave-by-wave basis whether the boundary layer was laminar or turbulent and also, for rippled beds, whether vortex formation and shedding was occurring;

iii) to determine a criterion for the onset of vortex formation above a rippled bed, in terms of the ratio of the observed ripple wavelength and the (deduced) orbital excursion of the near-bed motion;

iv) to calculate bottom stresses at the threshold of motion on a wave-by-wave basis, and to compare the skin friction component of the total

stress with Shields' threshold stress from the laboratory; and

v) to determine the relationship between the equilibrium wavelengths of evolving sand ripples and the orbital excursions of those measured waves which were capable of moving sediment.

Under each of the above headings, a comparison has been made between the field observations made in irregular waves, and laboratory results made in idealised conditions. A final aim of the study has been to obtain a quantitative understanding of some of the features of separating flow over a rippled bed on the basis of an irrotational flow model.

In §2, a literature review is presented which is concerned with sand ripple formation and the properties of oscillatory flow over ripples. In §3, the field experiments are described, and some examples of the measured data are shown. Results of spectral analysis are presented in order to classify the waves; and the properties of the bed, namely the grain size and the ripple dimensions, are also described. In §4, results for the threshold of sediment motion are presented in terms of the directly measured (free-stream) velocity data. Here it is shown that there is reasonable agreement with some widely used sediment threshold motion criteria from the laboratory. In §5, an initial flow classification is made, aimed at establishing an experimental criterion for the onset of vortex shedding above the bed. This involves the calculation of a representative value for the orbital excursion of the water particles in each wave half-cycle, and the comparison of such values with the ripple wavelength. Also, in this section, results of some ripple formation trials are discussed, and comparisons are made with laboratory results. In §6, a secondary flow classification is made, this time aimed at determining whether the flow in the boundary layer was laminar, transitional or turbulent. Two contrasting cases are described; one in which the flow was almost always nonseparating and in which the (thin) wave boundary layer was almost always transitional, and another in which the flow was separating and in which the wave boundary layer was generally rough turbulent. In the former case, the total bed shear stress is equal to the skin friction and, in the latter case, it is equal to the sum of skin friction and form drag. The bottom stress is calculated, in the first case, by a combination of theoretical and semi-empirical arguments and, in the second, by semi-empirical arguments alone. A comparison of the results obtained is made with the usual Shields' threshold stress for the sand size in question. Finally, in §7, some theoretical considerations of the structure of a vortex above a rippled bed are presented. Although the analytical model described

is strictly for steady flow, the results obtained have a direct bearing on the interpretation of the earlier field results.

Throughout this report, we are concerned with the principal, first-order, features of the flow, and with the response of the bed to this flow. We are not concerned with any small, second-order, effects such as the residual mass-transport flows which are induced near the bed by bottom friction.

§2 PREVIOUS STUDIES OF SAND RIPPLE FORMATION AND OF THE OSCILLATORY FLOW OVER RIPPLES

It was stated in §1 that the processes at work near the seabed depend rather critically upon whether sand ripples are present. In this section, we review the previous literature on sand ripple formation in oscillatory flow, with particular reference to field observations, and also assess the present state of knowledge on the flow over ripples. Some of the results are discussed further in §5 in connection with the present field observations.

2.1 The properties of wave-generated sand ripples

2.1.1 Laboratory studies

An extensive and illuminating review of the early literature on this subject has been provided by Kennedy and Falcon (1965). For a more recent literature survey, the reader is referred to the valuable contribution of Lofquist (1978). The studies of ripple formation in oscillatory flow described by these, and other, workers have been carried out mainly in the laboratory, though there have also been several field studies. The laboratory work has been conducted in wave flumes, in pulsating water tunnels and with oscillating beds. We consider below studies of all these kinds, though we give special emphasis to field results, and to particular aspects of laboratory studies which have a bearing on field work.

In general, sand ripples in simple (sinusoidal) oscillatory flows may be characterised as long-crested, symmetrical, regularly spaced features on the bed, having crest lines which are transverse to the plane of the orbital motion of the fluid. Most experimental studies have attempted to relate the principal geometrical, features of such ripples (in particular, ripple wavelength (λ), height (η) and steepness (η/λ)) to properties of the flow and of the sediment in question. The most widely accepted conclusion from these studies has been that, in the first stage of ripple formation after the threshold of sediment motion is exceeded, the ripple wavelength (λ) scales on the near-bed orbital excursion (d_o). This quantity is calculated, for a notional flat bed, from $d_o = 2\hat{U}_\infty/\sigma$, where $\sigma = 2\pi/T$ is the wave

frequency, T is the wave period and $\hat{U}_\infty$ is the (irrotational) near-bed velocity amplitude. In the initial stages of ripple formation, at small values of the ripple steepness ($\eta/\lambda \lesssim 0.10$), it is generally accepted that evolving sand ripples are of "rolling grain" type (described below), above which the flow is always nonseparating. Whether such ripples are "stable" features on the bed, or are transitory features in the overall process of ripple formation, is rather unclear. In most situations, sand ripples develop with roughly constant wavelength but increasing steepness (up to values of $\eta/\lambda \simeq 0.15$) becoming, at some stage, ripples of "vortex" type. For ripples in this category, the flow separates in each wave half-cycle, and a vortex is formed above the lee slope of each ripple. These vortices are shed upon flow reversal, to be replaced in the following half-cycle by new vortices above the lee slopes. If the flow becomes more active then, at some point in the process of ripple development, a "cut-off" or "break-off" point occurs at which the scaling of λ upon d_o breaks down. For increasing d_o above this point, the ripple wavelength remains essentially constant, or even diminishes somewhat. At the same time, the ripple steepness (η/λ) decreases, mainly as a result of a decrease in ripple height (η). As the flow becomes still more active and ripple steepnesses diminish to low values, it has been suggested (Sleath, 1976) that the vortex ripples give way to a second stage of ripples of rolling grain type. Ultimately, the ripples vanish and the bed becomes flat; at the very high flow stages in question, so-called "sheet flow" conditions prevail, in which there is a substantial suspended sediment load.

The essential features of sand ripple formation were observed in the laboratory by Bagnold (1946), who conducted experiments with an oscillating bed in still water. Bagnold found that the ripple wavelength (λ) increased with the orbital excursion (d_o), at least for a small values of d_o. However, above a "cut-off" point, in particular for $d_o > 2\lambda$, he concluded that λ varied as the square root of the grain diameter D (independently of the grain density). He found also that, for non-uniform sand, the ripple wavelength λ followed exactly the same curve as for a uniform sand having the dominant diameter in the grain size distribution. Bagnold described in detail the nature of the flow over sand ripples, and distinguished between the stages of rolling grain and vortex ripple formation. He considered that the essential distinguishing feature of rolling grain ripples was the absence of grain movement within the ripple troughs; the ripples in question were of such small steepness that the flow was always non-separating. He observed that rolling grain ripples were stable, for a given value of d_o, between the critical velocity amplitude $\hat{U}_{\infty c}$ for the first movement of sedi-

ment on a smoothed surface, and about $2\hat{U}_\infty c$. However, for $\hat{U}_\infty > 2\hat{U}_\infty c$, he observed that the ripples attained such a height that an abrupt change took place in the character of the oscillatory water motion, and that ripples of vortex type developed. Ripple steepness (η/λ) reached a maximum value of between 0.20 and 0.22 near to the "cut-off" point, and then decreased with further increases in d_o. Bagnold also observed the similarity between the profiles of steep ripples and steep surface water waves. In particular, he noted that the crest angle of steep sand ripples was 120°, which is the limiting crest angle for surface water waves. This conclusion has been reached also by Brebner (1981), and has been exploited by Longuet-Higgins (1981a) in a model of the flow over steep ripples. However, Longuet-Higgins (1981b) has pointed out, on the basis of experimental data summarised by Nielsen (1979), that ripple steepnesses are often greater than suggested by Bagnold, the angle at the crest being closer to 108° than 120°.

A subsequent laboratory study of sand ripple formation was described by Scott (1954). Since the ripples in Scott's experiments were asymmetrical, and migrating up a steeply sloping sand beach, only tentative comparisons are possible with results obtained on initially flat beds. Scott found that, despite considerable scatter, the ripple wavelength was proportional to the horizontal component of the near-bed orbital excursion, in accordance with the results of Bagnold (1946). He found also that the shape of ripples was related to their velocity of movement, ripples with higher velocities of propagation being more skewed. More recently, Sunamura (1981) conducted an experimental study of the nature of asymmetrical ripple profiles caused by steep surface waves beneath which the oscillatory velocity field is asymmetrical.

Further experiments on sand ripple formation were carried out by Manohar (1955). For every near-bed velocity amplitude $\hat{U}_\infty$, Manohar proposed that there was a stable ripple profile. For increasing $\hat{U}_\infty$, he found that both the ripple wavelength and height increased. However, above a critical value of $\hat{U}_\infty$, he noted that increases in $\hat{U}_\infty$ resulted in decreases in ripple height, and increases in wavelength, until, ultimately, the ripples completely disappeared. For the conditions tested, Manohar concluded that the ripple steepness for each sediment size was dependent on $\hat{U}_\infty$, and not upon d_o. Manohar presented his results in terms of a dimensionless parameter ψ_1', representing the intensity of lift on the sediment particles, namely $\psi_1' = \hat{U}_\infty/[(\gamma g)^{0.4}\ \nu^{0.2}\ D^{0.2}]$, where g is the acceleration of gravity, ν is the kinematic viscosity, and $\gamma = (\rho_s - \rho_f)/\rho_f$ is the relative density of the sediment (ρ_s and ρ_f are the densities of the sand and fluid, respectively). He found that, for $\psi_1' = 7.45$, initial sediment movement occurred

on a flat bed; for $\psi_1' = 8.2$, general sediment movement occurred; for $\psi_1' = 9.23$, ripples were initiated and, for $9.23 < \psi_1' < 12.5$, ripple heights, wavelengths, and also steepnesses, increased; for $12.5 < \psi_1' < 20.9$, ripple wavelengths continued to increase, but heights, and therefore steepnesses, decreased; finally, for $\psi_1' = 20.9$, the ripples disappeared completely. The above values were proposed by Manohar for grain sizes up to D = 3.17 mm. Manohar's data was re-analysed by Sleath (1976) who suggested that the ripples in question (having steepnesses $\eta/\lambda < 0.08$) were of rolling grain type.

A rather different approach to the problem of ripple formation was provided by Yalin and Russell (1963), who interpreted laboratory results on the basis of similarity arguments. They also confirmed that ripples disappear at high flow stages because their heights, not wavelengths, tend to zero. At around this time, contributions to the study of ripple formation were made by various Japanese workers. Homma and Horikawa (1962) obtained laboratory data on sand ripples, as part of a study of suspended sediment in oscillatory flow. On the basis of their own data, and also that of Scott (1954) and Inman (1957), they found that the maximum value of ripple steepness was about 0.23, equal approximately to $\frac{1}{2} \tan \varphi$, where φ is the angle of repose of the sand. They noted further that d_o must be greater than λ, in accordance with the results of previous studies. Homma and Horikawa (1963), and Homma et al (1965), made further observations of sediment in suspension above ripples. In the latter paper, relationships for both the ripple wavelength and ripple steepness were proposed on the basis of laboratory data. The study of Homma et al (1965) was extended by Horikawa and Watanabe (1967), who confirmed the principal results of the earlier work.

Results of theoretical and experimental studies were reported by Kennedy and Falcon (1965). From their experimental observations they postulated a zone of ripple existence, from initial formation through to sheet flow, but they did not delineate this zone because of the insufficient data set available. They noted that the heights of steeper ripples were limited by the angle of repose of the sand; slope angles of up to 32° were measured in intermediate sand, corresponding to a (minimum) crest angle of 116°. As far as ripple wavelengths (λ) were concerned, they found that, for fixed $\hat{U}_\infty$, λ increased with increasing orbital excursion d_o and that, for a fixed value of d_o, the ripple wavelength increased with increasing $\hat{U}_\infty$. Ripple wavelengths (λ) were smaller than d_o by a factor of anything up to 10. The data of Kennedy and Falcon was replotted by Lofquist (1978), and shown to be consistent, up to a point, with the predictions of Mogridge and Kamphuis (1973) which are discussed shortly.

An extensive, and often cited, laboratory study of ripple formation was conducted by Carstens and Neilson (1967) and Carstens et al (1969). The paper of Carstens and Neilson was descriptive, and concerned primarily with rolling grain ripples. These were found to be temporary bed forms, unlike vortex ripples which were found to be more permanent features on the bed. Ripples were classified as having been formed spontaneously on a flat bed, or as having been induced by some disturbance on the bed. Rolling grain ripples were found to occur spontaneously at near-bed velocity amplitudes at which the boundary layer had started to become turbulent, and at which some surface grains were in motion all over the bed. Carstens and Neilson also presented a result for the mean velocity at which a pattern of induced ripples spreads over an initially flat bed. They concluded that, since ripples can be induced to form in less active flow conditions than those associated with incipient motion on a flat bed, the usual incipient sediment motion condition should not be regarded as a comprehensive lower limit for the development of a rippled bed. They suggested further that, since any natural bed is almost certain to be littered with flow obstructions, a disturbed-flow, deformed-bed, incipient motion criterion is the logical lower limit for a rippled bed; in particular, they proposed the criterion $\hat{U}_\infty/[\gamma g D]^{\frac{1}{2}} = 1.3$. The initial study of Carstens and Neilson was extended by Carstens et al (1969). They found that, for conditions somewhat in excess of incipient sediment threshold motion, ripple amplitudes increased until $d_o/2D \approx 775$. In this range of conditions, the ripples were two-dimensional, with steepnesses between 0.15 and 0.20 and wavelengths which increased with d_o. However, in the range $775 < d_o/2D < 1700$, the ripples were three-dimensional with wavelengths which were nearly independent of d_o. At the upper limit of this range, the ripples disappeared and the bed became flat.

Results very similar to those of Bagnold (1946) and Carstens et al (1969) were obtained in the laboratory by Mogridge and Kamphuis (1973). They found that, as $d_o/2D$ increased, the ripple wavelength λ was initially dependent only on d_o, whereas, for large values of $d_o/2D$, λ was directly proportional to the grain diameter D. Both the ripple height and steepness were found to increase at first with increasing $d_o/2D$, to reach maximum values and then to decrease until the bedforms disappeared. A useful contribution of this paper was the inclusion of design curves, by means of which it is possible to predict the length and height of bedforms that will develop on any specified bed as a result of prescribed wave-induced flow conditions.

On the basis of both the laboratory data of Kennedy and Falcon (1965) and others, and also the field data of Inman (1957), Komar (1974) proposed a basic

linear relationship between λ and d_o which gave way, beyond the "cut-off" point, to a relationship between λ and D. In particular, for sands with median diameters in the range 88-177 μm, Komar suggested that the ripple wavelength λ increases, as d_o increases, up to a maximum value of about λ = 21 cm; beyond this, above the "cut-off" point, λ decreases with further increases in d_o until, finally, a value of d_o is reached at which the ripples cease to exist. For coarser sand sizes ($\sim$ 500 μm), Komar found the same dependence of λ on d_o below the "cut-off" point, but did not have sufficient data to define the "cut-off" point itself. For the data analysed, Komar proposed the relationship $\lambda = 0.8d_o$ below the "cut-off" point. By comparison, he found that the laboratory data of Scott (1954) suggested $\lambda = 0.87d_o$; that the field measurements of Tanner (1971) yielded $\lambda = 0.7d_o$, though with a pronounced scatter; and that the field study of Newton (1968) suggested the rather lower value $\lambda = 0.3d_o$, again with considerable scatter.

Dingler and Inman (1977) presented a study concerned with the entire range of ripple occurrence, from initial ripple formation through to sheet flow. They re-affirmed the existence of a relationship between λ and d_o (for low values of d_o), the existence of the "cut-off" point, and the fact that λ decreases with increasing d_o for large values of d_o. A further study concerned with the entire range of ripple occurrence was conducted by Komar and Miller (1975). They presented a delineation of the regimes of ripple occurrence, and proposed a disturbed-bed threshold conditon for ripple formation (of the kind proposed by Carstens and Neilson (1967)). They suggested that this condition was particularly suitable for field applications since, firstly, the seabed contains many irregularities and protuberances, so that sediment threshold motion will be achieved "at lower boundary stress values" than for a flat bed; secondly, the ripples observed on a natural bed may be "fossil ripples" caused by previous, higher, waves; and, thirdly, irregular surface waves may only occasionally cause ripple formation (see the reference to Dingler and Inman in §2.1.2). The general implication of these three considerations is that, in the field, wave-generated ripples may be formed under conditions which are normally considered to lie below the threshold of sediment motion. For the disappearance of ripples, and for sheet flow, Komar and Miller found good agreement among the data sets which they examined, and confirmed the criterion proposed by Bagnold (1946).

More recently, Miller and Komar (1980a) studied ripples generated by various types of laboratory device, in a further attempt to determine a consistent relationship between λ and d_o. On the basis of flume and water tunnel data, they proposed the relationship $\lambda = 0.65d_o$, rather than $\lambda = 0.8d_o$ as suggested earlier

by Komar (1974) on the basis of both laboratory and field data. Departures from this relationship occur for large d_o, maximum values of λ depending upon the grain size D. A tentative empirical relationship identifying the "cut-off" point (at which λ usually takes its maximum value) was suggested, namely $\lambda = 0.0028D^{1.68}$, where D is in microns and λ is in centimeters. Miller and Komar concluded that ripples formed in oscillating bed devices do not correspond well with those developed under progressive waves in flumes or in oscillating water tunnels. In fact, they suggested that not all types of ripples generated in the laboratory exist in the field; in particular, that rolling grain ripples are only stable on oscillating beds and are not found, or are unstable, in wave flumes and water tunnels. This conculsion differs from that of Sleath (1976).

A rather different approach, and a particularly valuable one from the point of view of field workers, was adopted in the laboratory by Lofquist (1978). Initially, on the basis of previous studies, Lofquist presented a composite curve for the threshold of sand motion. From a re-analysis of the results of Mogridge and Kamphuis (1973), he also proposed the relation $\lambda/d_o = 2/3$, for $10^2 < d_o/2D < 5 \times 10^3$ and $0 < M < 30$ (where the "mobility number" M is defined by $M = \hat{U}^2_\infty/[g\gamma D]$). In his own experiments conducted in an oscillatory water tunnel, he studied ripples formed both on an initially flat bed, and from a pattern of previously established (fossil) ripples. The latter situation raises the important issue for field workers of the change in wave conditions which is needed to enable a rippled bed to be transformed from one equilibrium state to another. Initial ripple wavelengths were found to be independent of d_o, but to depend slightly upon D. However, equilibrium wavelengths were found to conform to $\lambda/D = 2/3(d_o/D)$, at least up to the "cut-off" point, above which signs of a decrease in λ/d_o with d_o/D were noted. In general, the character of the bedforms was found to confirm the design curves of Mogridge and Kamphuis (1973). The notion of "compressed" and "extended" ripples was introduced, in relation to a range of "stable" ripples having $0.55 < \lambda/d_o < 0.80$ (and $0.22 < \eta/\lambda < 0.125$). Compressed or extended ripples, caused by changing wave conditions, were defined as having values of λ/d_o less than, or greater than, 2/3 (ie the value at about the middle of the "stable" range). A hysteresis effect was demonstrated in respect of changes in ripple wavelength. Moreover, the temporal growth rate of η/d_o and λ/d_o was found to be a function of $(2D/d_o)\tilde{n}$, where $\tilde{n}$ denotes the number of wave cycles since ripples first appear on a flat bed, or since the start of an experiment with a previously rippled bed. It was concluded that ripples attain maturity if $\tilde{n} > d_o/2D$. More generally, it was concluded that an equilibrium ripple profile on an unconfined region of bed is independent of its time history;

initial bedforms were found to converge to final forms dependent only on d_o and the wave period T.

Valuable contributions to the study of sand ripple formation were made by Nielsen (1979, 1981). Nielsen's conclusions were expressed in terms of the "mobility number" M (defined above), which is essentially the quotient of the near-bed velocity amplitude and the sediment settling velocity, and also of the Shields' parameter θ', defined by $\theta' = \frac{1}{2} f_w M$ where f_w is the wave friction factor of Jonsson (1967). Here f_w is evaluated in respect of the grains on the bed, such that θ' represents the non-dimensionalised skin friction on the surface layer of sand grains (which, in some sense, is spatially averaged over the ripples). Nielsen's conclusions were as follows. Firstly, ripples exist from the onset of grain motion at $\theta' \approx 0.045$ up to about $\theta' \approx 1$. Secondly, the ripple steepness η/λ depends upon both θ' and φ, the angle of repose of the bed material. When $\theta' < 0.20$, η/λ is independent of θ' and equal to about $0.32 \tan\varphi$ (which may be compared with the limiting value of $0.5\tan\varphi$ suggested by Homma and Horikawa (1962)); and, when $0.20 < \theta' < 1$, η/λ tends to zero with increasing θ' according to the rule

$$\eta/\lambda = 0.182 - 0.24\,\theta'^{1.5} .$$

The ripples finally disappear when $\theta' \approx 1.0$; Nielsen argues that this criterion in terms of θ' is to be preferred over Dingler and Inman's (1977) equivalent criterion (quoted later) on the grounds that it eliminates much of the scatter in their presentation of results. Thirdly, the ripple wavelength λ is of the same order of magnitude as $d_o/2$, the most important single parameter determining λ/d_o being M. The quotient (λ/d_o) is nearly constant (≈ 0.65) when $M \lesssim 20$; as M increases in the range $M > 20$, λ/d_o decreases in such a way that λ either decreases slowly, or remains constant. The empirical formula suggested by Nielsen for laboratory conditions is

$$2\lambda/d_o = 2.2 - 0.345\,M^{0.34} . \qquad (1)$$

He has also provided a rule for the direct determination of the ripple height.

A further laboratory study has been described by Brebner (1981). Brebner found that bedforms are not initiated until the "mobility number" M is greater than 3. For fine sands, he found that ripple wavelengths decrease as the mobility number increases, that the maximum ripple steepness is 0.14, and that the crest angle at this steepness is 120°. Brebner also found that a high mobility number

results in the flattening of bedforms, and in massive amounts of sand in suspension.

More recently, a valuable study of ripple formation has been provided by Grant and Madsen (1982). They have suggested that the "cut-off" point can be predicted from the empirical expression $\theta'/\theta_c = 1.8S_*^{0.6}$, where θ'/θ_c is the quotient of the maximum value in the wave cycle of the Shields' parameter θ' (skin friction) and the critical value of the Shields' parameter θ_c for initiation of motion on a flat bed, and where $S_* = (D/4\nu)(\gamma g D)^{\frac{1}{2}}$ is a dimensionless sediment parameter. Grant and Madsen have found the parameter (θ'/θ_c) to be useful also in characterising both the behaviour of the ripples, and the sediment transport; below the "cut-off" point, the ripple steepness (η/λ) is nearly independent of θ'/θ_c but, as the ripples decay, their steepness becomes dependent upon θ'/θ_c. The rate of sediment transport also increases with increasing θ'/θ_c. On the basis of the data of Carstens et al (1969) and others, Grant and Madsen have proposed the following relationships for the ripple height and steepness: below the "cut-off" point, $\eta/d_o = 0.11(\theta'/\theta_c)^{-0.16}$ and $\eta/\lambda = 0.16(\theta'/\theta_c)^{-0.04}$; above the "cut-off" point, $\eta/d_o = 0.24\ S_*^{0.8}(\theta'/\theta_c)^{-1.5}$ and $\eta/\lambda = 0.28\ S_*^{0.6}(\theta'/\theta_c)^{-1.0}$.

2.1.2 Field studies

Certain comments relating to field studies have been made already; for example, aspects of the work of Lofquist (1978) are highly relevant to the question of ripple evolution on natural sand beds. Here we review the principal results of previous field studies, by way of introduction to the study described in this report. As noted earlier, one of the most important considerations in field studies is that sand ripples observed on the seabed may not be in active formation as a result of the prevailing wave conditions. Such ripples, which may be the product of storm waves that have long since subsided, are termed fossil or relict ripples. Inman (1957) remarked that, for ripples in coarse sand, the existence of an equilibrium profile is made less certain by the slow response of the ripples to changes in wave conditions, than is the case for ripples in fine sand which are more rapidly modified.

The most comprehensive set of field observations of wave-generated sand ripples has been made by Inman (1957), who provided data for water depths of up to 50 m. Ripple heights and wavelengths were measured, and ripple asymmetry was estimated. Some of the observations were made by divers with a greased comb, others with a transparent plastic stick on which ripple dimensions were marked. Inman classified symmetrical wave-generated ripples as (a) "solitary ripples" having flat troughs and isolated crests, and (b) "trochoidal ripples" having

rounded troughs and somewhat peaked crests (either sharp or slightly rounded). He further classified the ripples as to their pattern, the basis for this being the quotient of the average ripple crest length and the ripple wavelength λ. For values of this quotient greater than 8, Inman adopted the term "long-crested ripples"; for values in the range 3-8, "intermediate crested ripples"; and, for values less than 3, "short-crested ripples". In certain cases, Inman recorded wave data during the period of ripple observation. Estimates of wave period and significant wave height were then used to calculate the near-bed orbital excursion d_o. These estimates were based on the significant wave, rather than the rms wave, in order to emphasise the importance of larger surface waves on the ripple geometry. Inman concluded that grain size is the most important factor in determining the size of ripples (larger ripples forming in coarse sand and smaller ripples in fine sand). He also found that the ripple wavelength λ did not exceed d_o, and that λ decreased as d_o increased, at least for sufficiently large values of d_o. In general, he concluded that ripples in the ocean tend to be large because the surface waves are long and, consequently, have large orbital excursions; that ripples occurring near the surf zone are usually somewhat smaller (and are absent altogether in the breaker zone); and that ripples occurring in bays, lakes and other areas of limited fetch, tend to be smaller still, as a result of the small values of d_o for the (short) waves which occur there. Inman found that ripple steepnesses were, on average, between about 0.10 and 0.125 for fine and very fine sands, and about 0.13 for coarser sands. The variation in steepness for fine sands was substantial (0.05 to 0.20) whereas, for coarse sands, it was rather less (0.125 to 0.22). The steepest ripples were commonly "trochoidal" in profile, and were of vortex type. "Solitary ripples" were found typically in fine sand in very shallow water, and tended to be less steep. In general, ripples tended to be less steep for relatively large values of d_o.

Inman compared his field observations with the laboratory results of Bagnold (1946) and Manohar (1955). He concluded that maximum ripple wavelengths obtained in the laboratory were less than those obtained in nature for the same sand size, and that his observed ripple steepnesses were in accord at least with Bagnold's observations. Inman also found that the patterns and profiles of natural ripples varied systematically with depth. In shallow water, fine sand ripples were characteristically long-crested and were solitary in profile. At progressively deeper stations, there was a change in profile from solitary to trochoidal, accompanied by the tendancy for the ripples to be "intermediate" or "short-crested". In general, the ripple profiles tended to imitate in miniature the surface waves

which generated them. Finally, Inman found that sand grain sizes on the ripple crests tended to be coarser than those in the troughs. He also observed that ripple systems in active formation had the capacity to sort out and remove fine sand, particularly as the ripple size increased; fine material, placed in suspension by vortices shed from the ripple crests (see §2.3), was either carried away from the area or was deposited in the ripple troughs.

On the basis of the observations and definitions of Inman (1957), an attempt was made by Lofquist (1978) to establish conditions for the occurrence of two-dimensional and three-dimensional ripples on the seabed. Lofquist noted the tendency for longer-crested ripples to be associated with larger values of both the mobility number M and also d_o/D. (Inman found a tendency for long-crested ripples to occur nearshore in shallow water, which also implies an association with larger values of M.) However, the effect of depth appeared so strong as to suggest to Lofquist the importance of some factor other than M, such as the increasingly two-dimensional character of surface waves as they advance over a shoaling bottom.

More recent field studies have been undertaken by Newton (1968), Tanner (1971), Komar et al (1972), Tunstall and Inman (1975), Dingler and Inman (1977) and Miller and Komar (1980b). Newton (1968) made an extensive set of observations of sand ripples in shallow water (in depths less than 3 m) in the Baltic and North Seas. He examined the internal structure of the ripples, and used a ripple profiler to measure their dimensions. For grain sizes in the range 125-320 μm, he found a good correlation between the orbital excursion d_o and both the ripple height (η) and wavelength (λ). However, on account of the method adopted for determining the properties of the surface waves, there is possibly some uncertainty about the results obtained. Tanner (1971) contributed data both from shallow water (lakes), and also from water of depth up to about 30 m in the Gulf of Mexico. The results of both Newton and Tanner were re-analysed by Komar (1974), as mentioned earlier.

Komar et al (1972) made observations of wave-generated sand ripples on the Oregon Continental Shelf in water depths of up to 200 m. The ripples in question were considered to be consistent with winter storm conditions. (Average summer waves in the same area were considered to be capable of producing ripples only in depths of up to about 50-100 m.) The significance of this study was that it extended to deeper waters the earlier field observations of Inman (1957), by use of a camera system with which stereo pairs of bottom photographs were obtained. In particular, Komar et al related their observations to Inman's ripple classification system. They found no "solitary ripples", probably because the study was confined to deep water. However, they found that "trochoidal ripples" were

extremely common. They also introduced a third type of profile into the classification scheme for symmetrical ripples, namely a "rounded-type" ripple, resembling a smooth sine curve. Such ripples were commonly observed off Oregon. According to Inman's system most ripples observed on the Oregon Shelf were "intermediate-crested" or "long-crested" and ripple steepnesses were between 0.14 to 0.33 for sand sizes in the representative range 67μ to 203μ.

Tunstall and Inman (1975) suggested the range of steepness of natural wave-generated ripples as 0.14 to 0.20, at least in the regime in which the flow is not sufficiently intense to begin destroying the ripples. In addition, for equilibrium ripples, they quoted the range of values of d_o/λ as ($\gtrsim$) 1 up to about 6. Hence, for natural conditions, they suggested that ripple heights (η) should be such that $2.75 < d_o/2\eta < 22$.

Dingler and Inman (1977) studied wave-formed sand ripples both in a wave tank, and in a high energy nearshore environment using a high resolution sonar. Their conclusions were as follows. Firstly, once ripples have formed, their steepness is controlled by the mobility number M. The steepness remains constant ($\eta/\lambda \approx 0.15$) until $M \approx 40$, and then decreases to zero (flat bed) for sheet flow conditions ($M \geqslant 240$). This decrease in steepness is caused by a decrease in ripple height, since the wavelength remains essentially constant (or decreases somewhat). For $M \geqslant 240$, ripples in fine sand disappear, and the bed becomes flat after the passage of only one or two large waves. However, a rippled bed re-appears after the passage of a few smaller waves. Secondly, grain size appears to have a negligible effect on ripple steepness, though maximum ripple wavelengths and heights are grain-size dependent. Dingler and Inman correlated ripple profiles both with individual waves, and with the wave spectrum. In addition, they proposed a criterion for the onset of grain motion, and presented results both for ripple migration rates and also for the asymmetry of ripple profiles.

A significant study in connection with field observations was conducted by Miller and Komar (1980b). They examined the relationship between d_o and λ for a range of natural wave energy environments and a range of grain sizes (81-913 microns). Of particular concern in this study was the evaluation of a truly representative value for d_o under field conditions. They obtained spectra of the bottom pressure and, hence, calculated mean square pressures for each spectral peak present. From this they estimated a value of d_o for each significant peak. Ultimately, these values were combined to yield a rms value of d_o. This was related to the significant value of d_o by multiplying by the factor 1.41, a procedure which is valid at least for a broad spectrum. It was concluded that

the field data showed best agreement with laboratory results if the calculation of d_o was based on the significant wave height, particularly in respect of the rule $\lambda = 0.65 d_o$ proposed by Miller and Komar (1980a). This confirms the approach of Inman (1957), who also used significant wave height, rather than rms wave height and period, in the calculation of d_o. Miller and Komar found that their field data fell into two categories, namely larger ripples of wavelength about 20 cm, and smaller ripples of about 9 cm, and they suggested that there may be two possible equilibrium wavelengths for a given value of d_o, and a given grain size. In particular, they noted that the larger ripples occurred, in almost all cases, under a polymodal wave spectrum, that is when more than one wave train was present. By comparison, the smaller ripples were associated with wave spectra having a single pronounced peak. However, an explanation for the difference was not proposed.

On the basis of a re-analysis of the field data of Inman, Dingler, and Miller and Komar, Nielsen (1981) reached the following conclusions. Firstly, the size and shape of ripples in the field are strongly influenced by the irregularity of the surface waves. Under irregular waves, ripples are shorter and flatter than under regular waves. Nielsen suggested that ripple steepnesses in the field are best represented by

$$\eta/\lambda = 0.342 - 0.34\sqrt[4]{\theta'},$$

and that ripple wavelengths, which are shorter than those in the laboratory, are well represented by

$$2\lambda/d_o = \exp\left(\frac{693 - 0.37\ln^2 M}{1000 + 0.75\ln^7 M}\right) \qquad (2)$$

(cf Eq (1)). He also suggested a rule for the direct determination of ripple height. Secondly, field measurements of ripples conform best with laboratory measurements when the near-bed fluid motion is calculated on the basis of the significant wave height, in accordance with the comments made above.

2.2 Mechanisms of formation of sand ripples in oscillatory flow

We consider here briefly the possible mechanisms of formation of wave-generated sand ripples which have been proposed. This topic has been reviewed previously, in a rather more general way, by Davies and Wilkinson (1977).

In §2.1, we have simply been concerned with the physical properties of "rolling grain" and "vortex" ripples. Clearly, these properties are dependent, at least in part, on the nature of the near-bed oscillatory flow. For example, it is thought that the stability and growth of "rolling grain" ripples depends upon friction-induced residual circulation cells above the bed, which tend to drag bed material from ripple trough to crest positions. As the ripples gradually become steeper, a critical ripple profile is attained for which the flow separates in the region of the ripple crest in each wave half-cycle. Thereafter, a process of vortex formation and shedding becomes established in each wave half-cycle, and this leads to further ripple growth. This growth is due, in part, to the fact that the instantaneous near-bed flow is everywhere towards the crest positions (as described in more detail in §6). It is due also to the properties of the suspended sediment load when there is vortex shedding from the bed. Ultimately, an equilibrium ripple profile is attained, as discussed earlier.

Kennedy and Falcon (1965) approached the problem of predicting the characteristics of wave-generated ripples by developing a kinematical, irrotational, model of the flow above a slightly (sinusoidally) deformed, though otherwise flat, bed. They introduced a continuity equation for sediment movement, an assumed sediment transport rate formula and a criterion to define the wavelength of the ripples most likely to develop on the bed. This dominant wavelength was taken to be that which maximised the growth rate of the disturbance of the bed. Their analysis, which was restricted to ripples of small amplitude, involved neither flow separation, nor organised vortex formation, above the bed. Thus the model was capable of predicting trends only in the early stages of ripple development. Categories of stable, unstable and neutrally stable ripples were defined, corresponding to decaying, growing or neutrally stable bedforms of a particular wavelength. Central to the argument was the phase lag between the bed shear stress (and hence sediment movement) and the (irrotational) water motion. However, since Kennedy and Falcon regarded this phase lag as a "factor of ignorance" in the problem, they did not pursue their analysis to the point of making any firm quantitative predictions about the characteristics of the ripples which were most likely to develop under given flow conditions.

A different approach was adopted by Sleath (1976) who examined the formation of rolling grain ripples. For ripples of small steepness, he developed analytical relations for the ripple wavelength, on the basis of solutions of the two-dimensional equation of vorticity. Such solutions were developed for the cases of both small and large values of the parameter $(d_o/2\lambda)$, though the former case was thought

to have little, if any, practical application. In each case, a pattern of friction-induced, residual, mass transport velocities above the bed was predicted. For small $(d_o/2\lambda)$, Sleath determined a limiting ripple wavelength by arguing that, close to the bed, the fluid particles tend to drift towards the ripple crests and, hence, that sediment particles close to the bed must have the same behaviour. By varying parameters such as to maximise the residual drift of fluid particles (though without introducing any specific device to model the sediment transport), Sleath proposed as a realistic range of rolling grain ripple wavelengths: $4.5 < \beta\lambda < 17.7$, where $\beta = \sqrt{\sigma/2\nu}$. For large $(d_o/2\lambda)$, the residual streamlines also showed a tendency for the fluid motion at a small distance above the bed to be towards the ripple crests. In this case, Sleath proposed that the ripples most likely to form on the bed were those for which the oscillating fluid particles remain predominantly over a single ripple. He concluded that the associated, critical, value of $(d_o/2\lambda)$ is independent of $\beta\lambda$, but displays a functional relationship with βD. In order to examine his theoretical predictions, Sleath investigated ripple formation in the laboratory, using three different sediment sizes on a bed oscillating in its own plane. His findings were generally consistent with the theoretical arguments for the case in which $(d_o/2\lambda)$ was large.

Sleath (1975a) also considered the problem of the formation of vortex ripples having steepnesses rather greater than those of rolling-grain ripples. In this case, he developed a numerical solution of the two-dimensional equation of vorticity. Underlying his analysis was the proposition that the flow remains reasonably laminar under conditions of practical importance. Even if the flow is turbulent, he suggested that the mean velocity distribution may still be well represented by the solutions obtained if, as is likely, the transfer of momentum between different fluid layers remains dominated by essentially laminar effects such as vortex formation and decay. As in the case of rolling grain ripples, he demonstrated that the fluid close to the bed drifts towards the ripple crests, and thus provides a mechanism for the formation of ripples. Moreover, detailed examples of the calculated velocity vectors above rippled beds were found to reveal the existence of vortices in the instantaneous streamline pattern (see Sleath 1973, Figure 3; and 1974, Figure 1). Again, Sleath suggested that the ripples which form on the bed are those associated with the maximum drift of near-bed fluid, and hence sediment, towards the ripple crests. The particular situation which he considered was that in which the fluid velocity is only just strong enough to move sediment, the mobile grains remaining at all times in close contact with the bed. The vortex above the lee slope of each ripple was assumed to be insufficiently

strong to lift sediment grains, such that any grains carried over the ripple crest simply cascade down the downstream ripple face. Under these conditions, there is very little exchange of sediment between adjacent ripples. At higher fluid velocities, a different situation (not treated by Sleath (1975a)) arises, in which any sediment carried over the crest is lifted away from the bed by the lee vortex, possibly to be deposited on the next ripple. In this situation, there is considerable exchange of sediment between adjacent ripples. For the less active conditions which he modelled, Sleath proposed the following relationship for the wavelength of those ripples most likely to grow:

$$d_0/2\lambda = 0.492\, R^{0.064} \quad \text{where} \quad R = \hat{U}_\infty/(\sigma\nu)^{1/2} .$$

He found that this result was little affected by changing ripple steepness. Moreover, he found that, over a range of (relatively low) values of R for which the exchange of sediment between adjacent ripple crests was small, there was reasonable agreement between the above theoretical result and the experimental results of several previous workers.

Although the studies cited above have provided an initial understanding of the physical mechanisms which are important in the development of sand ripples, much work remains to be done on this topic. This is particularly so for active flow conditions in which the process of vortex formation and shedding is fully developed.

2.3 The nature of oscillatory flow over sand ripples

The essential distinction between the flow patterns above equilibrium "rolling grain" ripples (also fossil ripples) and "vortex" ripples is that, in the former case, the oscillatory flow is always nonseparating while, in the latter case, the flow separates above the lee slopes of the ripples in each wave half-cycle. A study of irrotational, deep, nonseparating flow above symmetrical sand ripples with prescribed profiles was presented by Davies (1979). Further theoretical results for the case of deep flow were discussed by Davies (1983). The general aim of these studies was to relate the velocity of the outer (free-stream) flow, well above the bed, to the flow velocity near the bed, and also to determine the height of influence of bottom ripples on the flow. For natural ripple profiles, it was found that surface crest velocities exceed velocities in the outer flow by a factor of up to about 2, surface trough velocities being correspondingly diminished. Typically, there may be a ratio 3 : 1 between surface

crest and trough velocities. The height of influence of a rippled bed was shown to be less than one wavelength and, for practical purposes, less than one half a wavelength. Davies (1980, 1982a, 1982b, 1983) also studied the propagation of progressive free-surface waves above a rippled bed. It was shown that the interaction between such waves and the bed may, in certain circumstances (which are not discussed here), lead to the reflection of wave energy incident upon a region of bedforms. It was shown also that the presence of a free surface may give rise to a velocity field near the bed which differs somewhat from that for deep flow.

There have been various studies of deep nonseparating viscous flow above rippled beds (eg Sleath (1976), Matsunaga et al (1981)). A central aim of such studies has been to model the pattern of residual flow induced by oscillatory motion above a rippled surface. In the fluid layers immediately adjacent to the bed, this residual motion involves the gradual migration of fluid particles from ripple trough to crest positions. Above this, the residual flow is in the opposite direction, such that recirculating cells of water exist above each half ripple wavelength. As mentioned in §2.2, Sleath (1976) has proposed a mechanism for the formation of rolling grain ripples on the basis of analytical predictions of this kind. Matsunaga et al (1981) have produced similar results for the residual flow using numerical methods, and have also demonstrated, both theoretically and experimentally, residual cells having double structures in each half ripple wavelength. Results of flow visualisation of the residual circulation cells above ripples have been presented by Honji et al (1980).

Sleath (1975b) made velocity measurements in oscillatory flow above a rippled bed in order to investigate the way in which such a flow becomes turbulent. He discussed the important difference between situations in which $\beta\lambda$ is large and small ($\beta = \sqrt{\sigma/2\nu}$). For very large $\beta\lambda$, in laminar flow and in the absence of vortex formation, the flow near the bed consists of a thin viscous layer, beneath an inviscid outer layer. In this situation, the flow in the viscous boundary layer and the flow in the inviscid outer layer may be treated separately. For very small $\beta\lambda$, the bed roughness is totally immersed in the viscous boundary layer, and the flow over the ripples may be expected to behave at each instant in the same way as a uniform flow having the same velocity profile above each point on the bed. Sleath found that random instability in the flow, associated with the ripples rather than the grain roughness, occurred for values of (d_o/λ) greater than about 1.0. He emphasised that the nature of this instability was rather different from that of turbulence in the usual sense. He also found that transition to turbulence was a gradual process and that, for a given value of (d_o/λ), the velocity $\hat{U}_\infty$ at

which the flow was clearly turbulent was many times greater than that at which the first signs of instability appeared. He suggested further that the motion of sediment inhibits the transition to turbulence. Although Sleath was able to propose a criterion for initial instability, he concluded that no similar criterion for a fully turbulent flow was meaningful. For natural equilibrium ripples, he suggested that $1.0 < d_o/\lambda < 10$, with values of ripple steepness ranging down to zero, but commonly lying between 0.1 and 0.2. This is in broad agreement with the conclusions of Tunstall and Inman (1975), quoted in §2.1.2. For nonequilibrium conditions, Sleath noted that (d_o/λ) may be small, since the orbital motions of waves which are unable to move sediment are likely to be much smaller than those of the larger waves which originally created the ripples. More recent measurements of velocity above both self-formed vortex ripples and artificial ripples have been reported by DuToit and Sleath (1981).

The nature of separating flow above vortex ripples has been described by several workers. Bagnold (1946, §4) described the formation, and subsequent shedding, of a vortex above the lee slope of each ripple in each wave half-cycle. Another fine description of the phenomenon has been provided by Tunstall and Inman (1975). These workers carried out laboratory experiments to obtain values for the three parameters: vortex size, vortex circulation (or strength) and the radius of the vortex core. Their results are discussed in detail in §7. In their laboratory experiments, they generated a pattern of equilibrium ripples, which they solidified and then used in a study of oscillatory flow above a nonequilibrium rippled surface. Particular attention was given to determining the phase angle in the wave cycle at which vortices begin to form above the lee slopes of ripples. For equilibrium conditions, they found that the vortex forms very close to the time of maximum velocity. For nonequilibrium conditions (with the solidified bed), and for larger values of velocity amplitude ($\hat{U}_\infty$) than the equilibrium value, they found that the vortex tends to form before the time of occurrence of maximum free-stream velocity. Conversely, for a lower velocity amplitude, the vortex tends to form after the time of maximum free-stream velocity. Bijker et al (1977) also gave a description of the process of vortex formation and shedding, and provided photographs of the development of the lee eddy. Like Tunstall and Inman, they considered the relationship between the phase of the orbital velocity and the development of the vortex. They found that vortex formation starts at about the time of maximum velocity in the free stream flow, and they presented a graph showing vortex diameter plotted against time. Further descriptions of the phenomenon have been provided by Nakato et al (1977) and Nielsen et al (1979).

Sawamoto (1980) performed three experiments to obtain quantitative data on organised vortices, and turbulence, in oscillatory flow above a rippled bed. In the first experiment, he measured the phase-averaged turbulence velocity over an artificial, fixed, sand ripple. Thus he identified two layers: (i) a near-bed "vortex layer" in which organised vortices were clearly observed, and (ii) a "diffusion layer" in which the structure of the flow was best described stochastically. In the second experiment, an enlarged model of a sand ripple (steepness 0.1) was placed in a wave tank with a view to estimating the rate of growth of the lee vortex. The vortex was found to grow during the interval $0 < \sigma t < \frac{11}{16}\pi$ ($\sigma t = 0$ when $U_\infty = 0$), and then to keep its intensity up to $\sigma t = \frac{7}{8}\pi$. On the basis of this experiment, a semi-theoretical procedure for the calculation of the vortex strength at any instant in the wave cycle was proposed. In the third experiment, turbulence was measured in the diffusion layer with a laser-doppler current meter. The turbulence intensity was found to decrease with height above the bed; a standard diffusion approach was recommended for modelling this region. Wave entrainment of sand particles was also treated, again on the basis of a diffusion model.

The flow above ripples was visualised in an oscillatory water tunnel by Honji et al (1980). For $d_o << \lambda$, patterns of steady (residual) streaming were photographed; at higher flow stages, separation vortices were photographed. In addition, dye streaks were used to illustrate the pairing of separation vortices above the ripple troughs. A further flow visualisation exercise was conducted by Matsunaga and Honji (1980) with a model of a beach step running parallel to the shoreline. They observed, and photographed, the evolution of a patch of sand ripples growing in the offshore direction away from the step.

Theoretical studies of separating oscillatory flow above ripples have been undertaken by Tunstall and Inman (1975), Sawamoto and Yamaguchi (1979), Shibayama and Horikawa (1980) and Longuet-Higgins (1981a). The steady-state, "standing" vortex, model of Tunstall and Inman (1975) is discussed and developed in §7, and is therefore not described in detail here. Essentially, these workers based their arguments on a uni-directional flow model, in which they assumed that the vortices above the lee slopes of ripples each comprised a rotational core and an outer potential region. As noted earlier, they used laboratory data to determine the vortex size, the circulation and the radius of the vortex core. Hence, they deduced the energy associated with each vortex formed in each wave half-cycle. Sawamoto and Yamaguchi (1979) suggested that, in the near-bed "vortex layer" (see also Sawamoto (1980)), a potential flow model was appropriate, and they proposed

an extension of the model of Tunstall and Inman (in fact, a model of the same type as that discussed in §7). They suggested that the vortex circulation may be estimated from the vorticity flux supplied from the boundary layer, and gave a procedure for the calculation of circulation (Prandtl's rule). This idea was developed by Shibayama and Horikawa (1980) who studied, both theoretically and experimentally, not only the vortex circulation, but also the movement of the vortex centre and the velocity field associated with the presence of vortices. Like Tunstall and Inman, these workers considered a single-vortex, irrotational model. They calculated the circulation of the vortex from the integral of the vorticity flux, and they modelled the dissipation of circulation. They also calculated the velocity components and the movement of the vortex centre, and estimated the amount of sand in suspension by a method similar to that used by Madsen and Grant (1976) to estimate the bedload transport rate. From their model of vortex circulation and sand movement, they found that the formation of a sediment-laden vortex above the lee slope of a sand ripple starts at $0.05T \sim 0.15T$ after flow reversal in each wave half-cycle, and ends at $0.45T \sim 0.50T$, where T is the wave period. They found also that there was reasonable agreement, between calculated values and experimental results, for both the vortex circulation and the movement of the vortex centre. Finally, they applied their model to the problem of onshore/offshore sediment transport with a view to understanding beach profile changes.

A rather different model of vortex shedding from ripples in oscillatory flow was proposed by Longuet-Higgins (1981a). In this model, discrete vortices were assumed to be generated at the (sharp) ripple crests, again with strengths related to the rate at which vorticity was shed from the boundary layer as given by Prandtl's rule. The rotational core of each vortex was assumed to expand with time, and it was shown that, ultimately, combinations of vortices may escape from the bed as vortex pairs. The horizontal force on the bottom was expressed in terms of the vortices in the flow at any instant.

The future development of theoretical models of the type outlined above holds out the prospect of an improved understanding of the properties of the flow above vortex ripples, and of the mechanisms involved in their formation. At present, both of these topics are poorly understood in quantitative terms.

2.4 The drag coefficient of a rippled sand bed in oscillatory flow

Most comments on practical aspects of this topic are reserved until §6.4, where procedures for calculating wave drag coefficients are discussed. However,

in the light of some of the comments made earlier in this section, it is appropriate to present some preliminary discussion here. The definition of drag coefficient adopted throughout this report is that of Jonsson (1967), who expressed the peak bed shear stress ($\hat{\tau}_o$) in a sinusoidal wave cycle by

$$\hat{\tau}_o = \frac{1}{2} \rho_f f_w \hat{U}_\infty^2 , \qquad (3)$$

where f_w is the wave friction factor and ρ_f is the fluid density. It should be noted that the peak values of stress ($\hat{\tau}_o$) and free-stream velocity ($\hat{U}_\infty$) do not occur simultaneously in the wave cycle.

The value of the drag coefficient is critically dependent upon the presence or absence of sand ripples on the bed, and may vary over two orders of magnitude on this account. The results of Bagnold (1946) for a fixed bed suggested that the drag coefficient is constant if $d_o/2\lambda < 1$, and that it decreases like $(d_o/2\lambda)^{-3/4}$ for larger values of $(d_o/2\lambda)$. In the light of Sleath's criterion (discussed earlier) for the onset of "random instability" in the flow (namely $d_o/\lambda \gtrsim 1.0$), it can be seen that the range $d_o/2\lambda < 1$ encompasses both stable and slightly unstable oscillatory flows. The decreases in f_w which occur for $d_o/2\lambda > 1$ are associated with a greater degree of instability in the flow and, ultimately, with a fully developed process of vortex formation and shedding from the bed. Longuet-Higgins (1981a) explained the decrease in terms of ripple troughs becoming filled with vorticity, such that "for very long strokes (ie large $d_o/2\lambda$) an almost steady flow is achieved on each stroke". For movable beds Longuet-Higgins noted, on the basis of the data of Carstens et al (1969), that the drag coefficient is relatively large at $d_o/2\lambda \approx 0.75$, and decreases for larger values of this quotient. He suggested also that there is a consistent dependence of the drag coefficient on the ripple steepness. Further comparisons based on the laboratory data of Bagnold (1946) and Carstens et al (1969) were made by Tunstall and Inman (1975), who showed that the experimental observations are accounted for by values of f_w in the range 0.09 to 0.5, the actual value depending upon $d_o/2\lambda$, and decreasing as this quotient increases. This range of values indicates that the drag coefficient for a rippled bed is at least one order of magnitude greater than that for a flat sand bed. If the ripples vanish in active flow conditions ($\theta' \gtrsim 1$), the drag coefficient is expected to decrease somewhat. However, on account of sediment transport in the near-bed layer, f_w is not expected to fall to a value appropriate to a flat immobile bed of, say,

$f_w = 0.01 - 0.02$ (see Grant and Madsen (1982)). This emphasises the need for reliable information about the nature of the bed if wave drag coefficients, and hence energy dissipation rates, in the field are to be quantified properly.

In this connection, attempts have been made to determine how much wave energy is bound up in the vortices which are formed above, and shed from, a rippled bed, compared with the wave energy which is dissipated by bottom shear, sediment transport and other processes. Tunstall and Inman (1975) calculated that shed vortices account for only about 7% of the total energy dissipated by bottom effects, whereas Vitale (1979), on the basis of his definition of the equivalent bed roughness, concluded that the percentage contribution to bottom resistance by ripples is 25-34%. This would appear to be consistent with Lofquist (1981), who concluded that the form drag contribution to the mean drag coefficient was roughly one third. Commenting on the discrepancy between this result and that of Tunstall and Inman, Lofquist observed that the result of these workers was for a rounded ripple crest, and that the relative sharpness of a naturally skewed crest may substantially enhance flow separation and vortex formation. On the basis of an essentially inviscid theory, Longuet-Higgins (1981a) has determined drag coefficients which indicate that vortex shedding may have an even greater relative importance than has been suggested by Lofquist and Vitale.

Whereas most experimental studies of wave drag on rippled beds have concentrated on determining the mean drag coefficient, Lofquist (1981) made detailed measurements of the <u>instantaneous</u> drag on a naturally rippled bed in an oscillating water tunnel. He presented results both for cases in which the ripple profiles were natural (with $\lambda/d_o = \frac{2}{3}$) and also for cases in which they were "strained" (by the manner of their generation in the tank). He found the drag coefficient, $\tilde{f}$, to be a complicated function of phase angle in the wave cycle, such that the instantaneous stress was not simply related to the instantaneous velocity. However, he noted that certain features of the drag coefficient were common to all the results obtained. In particular, for a free stream flow given by $U_\infty = \hat{U}_\infty \sin \sigma t$, he found, firstly, that the bottom stress was positive at $\sigma t = 0$; secondly, that either one or two maxima in $\tilde{f}$ occurred in $0 < \sigma t < \pi/2$; and, thirdly, that a single maximum in $\tilde{f}$ occurred in $\pi/2 < \sigma t < \pi$. He argued that this behaviour of $\tilde{f}$ is consistent with the process of vortex formation and shedding above a rippled bed.

An adequate knowledge of wave drag coefficients is necessary for the reliable calculation of wave energy dissipation rates (see Kamphuis (1978)).

The subject of wave energy dissipation is rather broader than the single consideration of dissipation by bottom friction however, as pointed out by Shemdin et al (1978) and Hsiao and Shemdin (1979). These authors assessed various field determinations of drag coefficients based on observations of wave energy dissipation rates, and discussed in detail various additional dissipation mechanisms that may arise in the field, such as bottom percolation for permeable beds and 'bottom motion' for beds comprising soft mud (see also Rosenthal (1978) and Macpherson (1980)). The relative importance of the various dissipation mechanisms at a site is strongly dependent upon both the wave and bottom sediment properties. The above authors concluded that percolation is most effective in coarse sand ($D > 0.5$ mm), and that bottom friction is generally dominant when the bed is composed of fine sand ($D = 0.1 - 0.4$ mm). As far as bottom friction is concerned, they emphasised that the friction coefficient is critically dependent upon the existence of sand ripples on the bed, and they suggested that the effect of bottom ripples may have given rise to the wide variations in wave energy decay rates at the various field sites considered. However, Grant and Madsen (1982) have suggested more recently that such variations may be attributed also to the effects of near-bed sediment transport.

2.5 Sediment in suspension above rippled sand beds

Since the present report is not concerned primarily with the problem of sediment in suspension as a result of wave action, this topic is not reviewed here in as detailed a manner as the topics in the previous subsections. Instead, the reader is referred to the reviews of experimental and theoretical studies given by Kennedy and Locher (1972), Davies and Wilkinson (1977) and Nielsen (1979, §6). The review of Davies and Wilkinson provides an assessment of the work of Homma and Horikawa (1963), Homma et al (1965), Horikawa and Watanabe (1971), Kennedy and Locher (1972), Wang and Liang (1975), and others. Some more recent studies are discussed below.

Vortex formation and shedding above rippled sand beds is a potent mechanism for carrying sand into suspension. Nakato et al (1977) carried out a detailed experimental study, in an oscillatory water tunnel, of the mechanism of sediment suspension from a rippled bed. They found that suspended sediment was confined to a relatively thin layer near the bed. They also found that the vertical distribution of the time-mean sediment concentration was different above the ripple crest and trough positions, and that the mean sediment concentration at any height was distributed along the channel in an oscillatory manner, similar to the bed

profile. In all their experiments four distinct peaks, with amplitudes that diminished rapidly with increasing distance from the bed, were found in the temporal distributions of measured concentration. These peaks, which were of the same type as those observed by Homma and Horikawa (1963) and Homma et al (1965), originated from convection past the measuring point of sediment in suspension within the eddies produced in the lee of each ripple during each wave half-cycle. (The experiments were conducted with $d_o/\lambda = 1.6 - 1.8$). They also found that the presence of sediment significantly altered the flow characteristics near the bed.

More recently, Sleath (1982a) made detailed measurements, also in an oscillatory water tunnel, of the instantaneous concentration of sediment above a rippled sand bed. He observed that sediment is entrained from the bed in two ways. Firstly, during most of each wave half-cycle, sediment grains carried as bedload up to the ripple crest are hurled out over the lee vortex; and, secondly, at the end of each half-cycle the lee vortex is ejected from the bed upon flow reversal, throwing up a plume of sediment. While Sleath provided a detailed description of both of these modes of entrainment, he concentrated on an analysis of the former mode in which sediment leaves the ripple crest in the form of a thin jet. He attempted to link the sediment transport in this jet with that on the bed. Also, for sediment suspended by vortices ejected from the bed, he examined the variation of concentration with height.

In early theoretical studies of sediment in suspension in oscillatory flow, the basic aim was invariably to produce expressions for the average suspended sediment concentration during the wave cycle, as a function of height above the bed. This time-averaged distribution was then used, in conjunction with any secondary residual flows present, to evaluate the overall movement of suspended sediment. Nielsen (1979, §6) gave a detailed discussion of the properties of the diffusivity of sediment in steady state formulations of the problem. He discussed the effects of sediment grading on mean concentration profiles, and also the differences in the diffusivity for uniform horizontal oscillations and for the oscillatory flows beneath both non-breaking, and breaking, waves. He concluded that wave breaking increases the diffusivity greatly down to a few centimeters above the bed. He also proposed an empirical expression for the reference sediment concentration at the bed level.

Probably the first comprehensive attempt to predict the instantaneous sediment concentration, as a function of both height and phase angle during the wave cycle, was that of Bakker (1975). He used numerical modelling methods to determine instantaneous sediment concentrations, at various heights, for rough

turbulent oscillatory flow. Having calculated the associated velocity distributions, he went on to determine suspended sediment fluxes. The main problem which Bakker encountered in his study was providing a realistic boundary condition for the (suspended) sediment concentration at the bed.

Nielsen (1979, §7) and Nielsen et al (1979) presented an analytical model for the prediction of time-varying sediment concentration profiles. Despite the regular nature of the vortex shedding phenomenon, the agitating process tending to keep the sediment in suspension was assumed to be diffusive. The novel feature of this work lay in the use of a "pick-up" function to model the entrainment of sediment. In the mathematical formulation, this function acts as the source for the diffusion equation, providing a bottom boundary condition which is independent of the settling of sediment grains. An advantage of this formulation is that it is easier to suggest physically realistic descriptions for the pick-up function than, for example, the bottom concentration, which is often used as a boundary condition in suspension models. To evaluate the sediment diffusivity, sediment concentrations were measured in a wave flume. It was found that the diffusivity was nearly constant under non-breaking waves. Moreover, it was concluded, on the basis of the study of Svendsen et al (1977), that the sediment diffusivity was, to all intents and purposes, equal to the turbulent eddy viscosity. Two examples concerning onshore/offshore sediment motion in different types of wave field were analysed on the basis of the theory. Finally, the model was compared with measurements of sediment flux in a flume, and reasonable agreement was demonstrated.

In a more recent contribution, Nielsen et al (1982) described a field sediment sampler with which concentration profiles were measured under breaking and non-breaking waves. They also analysed theoretically the motion of suspended sediment particles, giving particular attention to the problem of sand grains trapped within vortices. They argued that the essential nature of the trapping mechanism is such that grains of nearly all sizes travel together inside migrating vortices. They concluded from this that the process of sediment entrainment is convective, and is fundamentally unlike gradient diffusion which leads to different vertical distributions of sediment concentration for different grain sizes.

It should be noted, finally, that this section has been concerned exclusively with the interaction of oscillatory flows with sand beds. The interaction of such flows with clay beds poses rather different problems, not least because of the absence of ripples in such cases. A recent study of clay suspensions under water waves was described by Thimakorn (1981).

§3 FIELD EXPERIMENTS

3.1 The field site

Two field experiments were carried out at Blackpool Sands, Start Bay, Devon in May 1978 and in April/May 1980. This site, which has been described by Davies et al (1977), and Davies and Wilkinson (1979) was chosen for several reasons. Firstly, it was exposed to wave attack, but not to significant steady flows or tidal currents. The absence of such flows was due in part to the fact that the beach was between two headlands. Secondly, on account of the nature of the beach profile, it was possible to make measurements well outside the breaker zone, in positions where the effects of shoaling were of minor importance. Typically, such positions were about 100 m from the still water line, where the local bottom slope was about 1 in 20 and the water depth was 4-10 m. The breaker zone was confined to a narrow strip close to the pronounced berm on the beach face. Thirdly, the bed comprised localised regions of both coarse and fine sand. This meant that different sediment grain sizes could be examined by shifting the rig relatively short distances. Finally, the existence of an accessible sea wall, about 150-200 m from the positions in which the bottom rig was placed, made it possible to run a cable from the rig to a mobile laboratory on the sea wall. While the field site was suitable for all of the above reasons, it suffered the one major disadvantage that, on occasions, the underwater visibility was poor; this hampered some of the underwater television observations of sediment motion.

3.2 The measuring equipment and the logging system

The aim of the experiments was to measure and observe the wave-induced flow near the bed, and to monitor any associated sediment movement, in order to determine the conditions at the threshold of sediment motion. The experimental set-up, which was designed for this purpose, is shown in schematic outline in Fig 1. Here the instruments are shown mounted on a bottom rig, positioned on a bed of rippled sand. The flow measurements were made with electromagnetic (EM) flowmeters with 10 cm diameter discus-shaped heads, positioned at either two or three heights (between about 10 cm and 160 cm) above the bed. The upper measurement (at 130 cm height in 1978, and at 160 cm in 1980) was of the two components of horizontal velocity in a plane above the rig, and the lower measurements were of one component of vertical, and one of horizontal, velocity. Whenever necessary, the rig was levelled and aligned by divers, such that these latter measurements were made, as far as possible, in the plane of the orbital motion associated with the waves passing over the rig in the direction of the beach. Associated measurements of

the bottom pressure were made with FM pressure transducers, positioned either in the immediate vicinity of the rig or 5 m on either side of it in the direction of wave advance. The observations of sediment motion were made with an underwater television system. Thus, the sediment motion analysis was restricted to determining threshold motion conditions; the measurements did not provide any infomation about sediment transport rates. The positions of the EM-flowmeters, and general information about the experimental runs, are given in Table 1.

In both the 1978 and 1980 experiments, the velocity and pressure data were logged on a Bell and Howell FM-tape recorder. The standard experimental run length was 30 min, during which a 1 sec period timing pulse was recorded on both the FM-tapes and also the video tapes. This pulse was used as a trigger for the subsequent digitization of the data, and also as a means of synchronizing the velocity and TV records. After the data had been low-pass filtered, digitization was carried out at a rate of 5 Hz; an appropriate correction was made later for the filtering procedure by a simple spectral analysis method. The noise of the flowmeter system was equivalent to a velocity of about 1 cm/sec, and the pressure transducer system had a resolution of about 1 cm of water. Since the details of the data logging, of the calibration of the recording system and of the digitization of the data, were essentially the same as in the earlier experiment described by Davies et al (1977), they are not repeated here.

3.3 The recorded data

In Fig 2, two representative, though contrasting, 5 minute portions of the measured data are shown, one from the 1978 experiment and one from the 1980 experiment. For the 1978 data, the parameters plotted in Fig 2(i) are as follows: firstly, two components of horizontal velocity (U_3, V_3) measured at a nominal height of 130 cm above the bed; secondly, two pairs of horizontal and vertical velocity components, (U_2, W_2) and (U_1, W_1), measured at nominal heights of 90 cm and 20 cm above the bed, respectively; and, thirdly, a record of impressions gained from the TV-system of sediment movement on the bed. The sign convention adopted was that U-components of velocity were positive in the shoreward direction, and negative in the seaward direction (see Fig 1). In practice in this run (Run 9), the base of the rig was slightly buried, such that the velocity components (U_1, W_1) were actually measured at a height of 11 cm above the bed surface; the heights at which the other velocity measurements were made were reduced by a corresponding amount. The measurements were made above the crest of a sand ripple of wavelength about 74 cm and height about 12 cm, composed of sand of median diameter

D_{50} = 0.078 cm. The first point to note about the velocity measurements is that the V_3 component of velocity was always very small, suggesting that the rig was correctly aligned to measure the dominant wave action on the three U-channels. The three U-components of velocity are similar in all their essential details, except for certain features of the U_1-record which are associated with vortex shedding from the bed; this is discussed later in §5. The vertical velocity component W_2 was generally very small, as expected for long waves in relatively shallow water. The near-bed W_1-component of vertical velocity was rather larger, though still small compared with the horizontal U_1-component. It is suggested later that the near-bed vertical velocity field gave an indication of flow instability above, and vortex shedding from, the rippled bed surface. We defer discussion of the sediment motion observations in Fig 2(i), and also the justification for the various statements made above, until later.

For the 1980 data in Fig 2(ii), the parameters plotted are, firstly, the velocity components from two EM-flowmeters, one measuring in the horizontal plane and one in the vertical plane, at nominal heights of 160 cm and 60 cm respectively; secondly, the bottom pressure in the immediate vicinity of the rig; and, thirdly, the impressions gained from the TV-system of sediment movement on the bed. It may be seen from the two upper time series that the rig was aligned such that the dominant wave action was measured on the U-channels. However, in this run (Run 10), the alignment was worse than in almost every other run in either the 1978 or 1980 experiments, the ratio of the variances of the V- and U-components being 0.21:1. This matter is discussed in greater detail in §4 (Table 3). It may be seen from the measured velocities obtained with the lower flowmeter that the vertical velocity was negligibly small compared with the horizontal, as expected for long waves in relatively shallow water. Also, the record of bottom pressure may be seen to be very nearly in phase with the horizontal velocity. It follows that the waves at the field site were progressive waves which passed over the rig, and then dissipated their energy on the beach face, with little energy being back-reflected.

3.4 Spectral analysis

In Fig 3, two sets of energy spectra are presented which cover the complete experimental periods in both 1978 and 1980. Each spectrum is for a 10 minute recording period (3000 digitized values), and has been obtained by standard spectral analysis techniques based on the use of a Fast Fourier Transform. In forming the spectra in Fig 3, groups of five adjacent harmonics have been averaged such that spectral estimates have been obtained every $\frac{1}{120}$ Hz in the frequency

domain. (Note that for the choice of 5 grouped harmonics, the 80% confidence limits on the spectral estimates are 0.62E and 2.0E, where E is any one of the grouped estimates of energy.) The spectra plotted, which are for the U_3 velocity component, give an impression of the variety of wave conditions experienced during the experiments. For example, the two spectra which relate to the time series plotted in Figure 2 indicate very different conditions. On the one hand, for Run 9, 1978, the spectrum is very strongly peaked at a frequency of 0.080 Hz, corresponding to a wave period of 12.5 s, that is to swell wave conditions. On the other hand, for Run 10, 1980, the main spectral peak is at a frequency of about 0.163 Hz, corresponding to a wave period of 6.1 s and indicating much more localised wind-wave content in the spectrum. This is consistent with the short steep waves which were observed at the field site during this run. The approximate wavelengths (λ_w) of (monochromatic) waves having these frequencies, in a representative water depth (h) of 6 m, are 90-95 m and 40-45 m, respectively. In both cases therefore, the waves were relatively long compared with the depth ($kh = 2\pi h/\lambda_w \approx 0.4$ and 0.9, respectively), and this explains the rather small W_2-components of measured vertical velocity in both Figures 2(i) and (ii). On the basis of linear theory and for the parameter settings given above (for assumed monochromatic waves), the ratio of the amplitude of W_2 to that of U_2 is expected to be about 0.05 for Run 9, 1978, and about 0.09 for Run 10, 1980. The remaining spectra in Figure 3 demonstrate a wide variety of experimental conditions, both in respect of frequency content and wave intensity, and may be associated with the various histogram presentations of results in §4-6. The most general conditions experienced during the experiments were swell waves, having spectral peaks associated with which the wave period was 10-13 s. Significant wind-wave content was experienced less frequently.

3.5 Grain size analysis

Samples of the surface layer of sand were obtained by divers in both the 1978 and 1980 experiments. The results of the sieve analyses carried out are presented in Figure 4. In Figure 4(i), cumulative size distribution curves are shown for samples obtained at the crest and trough positions on two consecutive days in the 1978 experiment. These curves have been assumed to be representative of the sediment grain size distribution throughout this experiment. It was possible to sample the crests and troughs separately, since the wavelength of the ripples was relatively large (λ = 50-80 cm, see §3.6). The curves show that the material on both the crests and troughs was rather similar and comprised mainly coarse, or very coarse, sand with median grain diameter D_{50} = 0.078 cm, and with D_{10} = 0.038 cm and

D_{90} = 0.135 cm. In Figure 4(ii), three size distribution curves are shown for the 1980 experiment. Again, these curves have been assumed to be representative of conditions on the bed. The ripple wavelengths were much shorter in this experiment, and no distinction is made between material on the crests and troughs. While the three curves are similar, they now indicate material predominantly in the medium to fine size range, with a representative median grain diameter D_{50} = 0.026 cm, and with D_{10} = 0.015 cm and D_{90} = 0.062 cm. It should be noted that the experiments in 1978 and 1980 were carried out with rather different sand sizes, as had been intended.

3.6 Sand ripple profiles

In general, the sand ripples on the bed were relatively long-crested (two-dimensional) with their crest lines parallel to the surface wave crests. Also, their profiles were reasonably symmetrical, as expected for ripples generated by wave action. In the 1978 experiment, the ripples on the bed were fossil, or relict, ripples (see §2.1.2) formed by previous, more active, wave conditions than those measured during the experiment. By comparison, in the 1980 experiment, the ripples were "equilibrium" ripples formed by the measured waves.

In the 1978 experiment, complete ripple profiles were obtained by divers, who inserted thin rigid (formica) sheets into the seabed, and then marked the ripple profiles on these sheets with underwater pencils. The profiles thus obtained have been discussed and analysed previously by Davies (1979, 1980b and 1982a); they are reproduced here in Figure 5(i). The measured ripple wavelengths were in the range 54 cm < λ < 81 cm.

In the 1980 experiment, the ripple wavelengths were rather shorted, and different measuring techniques were required. For the most part, measurements of ripple wavelength and height were made by divers with an underwater tape measure. While this simple approach was sufficiently accurate as far as the measurement of wavelength (λ) was concerned, it was not particularly good for the measurement of ripple height; this difficulty is discussed later (see §6) in connection with the determination of the bed roughness. An alternative approach was to use a "ripple profiler" of the same type as used by Newton (1968). This involved setting up a row of needles in a light-weight frame, mounting this frame horizontally a short distance above the bed, and releasing the needles such that each one fell vertically downwards to strike the bed. With the tip of each needle resting on the bed, the row of needles was clamped, thus preserving the ripple profile. The frame was then brought ashore so that the results could be recorded. Although this technique was

rather better for the determination of ripple height, it was rather too cumbersome to use frequently. A ripple profile obtained with the profiler, and associated with Run 16, 1980, is shown in Figure 5(ii). The ripple wavelength may be seen to be about 15-18 cm, and the height about 2 cm. However, since the needle spacing was about 3.5 cm, the ripples in question were rather too small for the technique to be totally effective. The wavelengths and heights of the ripples, throughout both the 1978 and 1980 experiments are listed in Table 2, together with comments about their two-dimensionality. (The presence of the bottom rig caused local complications in the ripple pattern on some occasions, but normally such rig effects did not extend into the region of interest directly below the instruments.) Prior to certain runs in the 1980 experiment, the bed in the vicinity of the rig was flattened out by the divers, and an "equilibrium" ripple pattern was allowed to develop; such runs are indicated in Table 2. The interpretation of the role of sand ripples on the bed is the subject of much of the remainder of this report.

§4 RESULTS FOR THE THRESHOLD OF SAND MOTION

4.1 General considerations

In this section, we examine the relationship between the impressions of sediment transport gained from the TV-records and the measured wave-induced flow. The observations of sediment motion from the television records (shown in Figure 2) involved the classification of each wave half-cycle during the experiments as follows: The basic classification was between those wave half-cycles in which sediment motion occurred, and those in which it did not. A secondary classification of half-cycles of the former kind was then made according to the numbering scheme 1, 2 and 3, where a wave was designated:-

1. if it caused the sporadic (incipient) to- or fro-motion of a few grains here and there on the bed;
2. if it caused general to- or fro- bedload motion; or
3. if it caused bed material to be taken into suspension.

The distinction between incipient and general bedload motion has been made previously by Manohar (1955) (see §2.1.1) and other workers. Vertical bars of length commensurate with the above classification scheme are shown in Figures 2(i) and (ii) for each of the wave half-cycles during which sediment motion occurred; the direction of sediment motion, shoreward or seaward, is indicated by + and - signs, respectively. The absence of a bar indicates no motion. When the bed was rippled, sediment motion was sometimes confined to the region of the ripple crests; and, when it was flat (as it was at the start of the experimental run shown in

Fig 2(ii)), motion occurred over the entire bed surface. It may be seen in Figs 2(i) and (ii) that there is a reasonable correlation between the largest waves and sediment motion observations of types 2 and 3, as expected.

The use of an underwater television system in the experiments has restricted the present analysis to qualitative judgements of the above kind about both the flow, and the type of sediment motion, occurring. However, although the sediment motion results are necessarily rather subjective for this reason, they have been arrived at after careful and repeated examination of the video records by several observers. It is believed, therefore, that the results obtained are self-consistent. This does not mean that it is possible to relate, directly and unambiguously, the present results to those of other workers, since different sediment threshold motion criteria have been adopted in previous studies. However, by making comparisons of several types with laboratory results in §4 - §6, we shall find that agreement exists between the present field, and previous laboratory, results, within acceptable limits of uncertainty.

The observations of sediment motion made on the rippled sand beds were of two rather different kinds. In the 1978 experiment, the ripples were nonequilibrium features in the sense that they were not generated by the measured waves, but were left over from some previous wave activity. Above these ripples the flow was nonseparating for all the measured waves except the largest in the records, and sediment motion tended to be confined to the region of the ripple crests. In the 1980 experiment, sand ripples were observed to form on a region of bed which had been flattened by divers, and they were thus in equilibrium with the measured waves. Ripple wavelengths were almost an order of magnitude smaller (O(5-15 cm)) than in the 1978 experiment. Flow separation above the bed was a generally more common occurrence than sediment movement and, when sand motion occurred, it was over the entire bed surface.

In this section, the relationship which we seek is between the observations of sediment motion from the television records and the measured parameters. The most obvious starting point is to consider the correlation between the velocity measured in a horizontal plane above the rig and the observed sediment motion. The particular approach adopted here is aimed at providing sediment threshold motion conditions, which may be compared directly with the results of previous laboratory work. Workers in the laboratory have typically defined "critical waves" of single frequency which are just capable of causing sediment motion on a flat sand bed. Such waves have been defined by their periods and velocity amplitudes in the irrotational free-stream flow above the bed, and the bed material

by its size and density. In both the 1978 and 1980 experiments, the measuring heights above the bed (130 cm and 160 cm, respectively) were well above the bottom wave boundary layer (see §6) in a region of essentially irrotational flow. However, the waves were generally rather irregular, the bottom was invariably rippled, and the sand comprised a mixture of grain sizes. Therefore, the basis for comparing the present field results with previous laboratory results has to be considered carefully.

An important initial consideration is what measure of velocity in the field experiments should be considered comparable with the well defined free-stream velocity amplitudes in laboratory work. The difficulty which exists in this respect was illustrated in Fig 2 where it was shown that, despite attempts by divers to align the rig to measure velocities predominantly in the onshore-offshore direction, there was still a small transverse horizontal velocity V-component. Whatever the reason for this V-component (eg misalignment of the rig or an actual rotary velocity vector at the measuring height resulting, possibly, from directional differences associated with the various wave frequencies in the spectrum), some allowance has to be made for it in defining sediment threshold velocity amplitudes. Here, results obtained on three separate bases are compared with one another. Firstly, the measured U-component of velocity above the rig has been taken as the required velocity. Secondly, time series of the total velocity at the measuring height have been derived from the measured data, and have been taken as the required velocity; the expression adopted for the total velocity namely $\mathrm{sgn}(U)\sqrt{U^2 + V^2}$, allows its sign to change whenever the sign of the (dominant) U-velocity changes. Although this introduces discontinuities in velocity at zero crossings, this is not important since, in what follows, we are concerned only with velocity amplitude values. Thirdly, a further time series has been derived from the measured data by a simple rotation of axes. In particular, the required velocity has been taken as the resolved component of measured velocity in a single fixed direction (for any given run), this direction being that which minimises the variance of the transverse velocity component. The criterion used here in determining the necessary angle of rotation (ψ_r) has been derived by Davies et al (1977, Eq A 27). In Table 3, the variances of the measured U- and V-components of horizontal velocity are given for each run in both the 1978 and 1980 experiments, together with the ratio of these variances and the calculated optimum angle of rotation (ψ_r). It may be seen that the variance of the measured transverse component is generally in the range 0.1 to 0.2 times the variance of the measured onshore-offshore component, and that the angles of rotation needed to minimise the

variance of the (deduced) transverse component are rather varied, but are of the order of 0.1 radians. Rotation was generally found to reduce the ratio of variances quite appreciably; for example, for Run 10, 1980, rotation by ψ_r = 0.291 rad reduced the ratio from 0.208 to 0.102. We now consider results obtained on each of the three bases described above.

4.2 Results for the 1978 experiment

A convenient method of presenting sediment threshold motion results is in the form of a histogram. In Fig 6, histograms are shown for the 1978 data, in which the peak value of velocity (shoreward+, seaward-) in a wave half-cycle is plotted on the horizontal axis, and the number of half-cycles having peak velocities falling in each unit incremental range is plotted on the vertical axis. The velocity which, in each case, was measured with the upper EM-flowmeter at a height of 130 cm above the bed, has been taken, firstly, as the measured U-component of velocity (Fig 6(i)); secondly, as the total velocity $\mathrm{sgn}(U)\sqrt{U^2 + V^2}$ (Fig 6(ii)); and, thirdly, as the rotated (rectilinear) component of velocity U_{ROT} (Fig 6(iii)). The process of rotation has been carried out on a run by run basis, with angles of rotation (ψ_r) as given in Table 3. In Fig 6, results for Runs 1 and 3 to 5 have been combined for convenience; the justification for this is that the bedforms were of essentially the same type through these runs (see Tables 1 and 2). The general bimodal shape of each histogram is associated with the prevailing pattern of irregular swell waves (see Fig 3(i)). The bimodal distribution is most pronounced in respect of the total velocity amplitude (Fig 6(ii)), which suggests that waves with the smallest U-velocity amplitudes were generally associated with appreciable (in-phase) V-velocity amplitudes. The larger the waves, however, the smaller was the relative importance of the V-component, as may be seen from the closely similar shapes of the histograms in Figs 6(i) and (ii) for velocity amplitudes greater than about 20 cm/s. As far as sediment movement is concerned, the differently shaded regions in each histogram indicate those wave half-cycles in which there was no sediment motion, and motion of types 1, 2 and 3, as defined earlier. It may be seen from Fig 6 that the recorded waves in Runs 1 and 3 to 5 comprised a majority in which there was no motion, and a minority in which there was incipient and general bedload motion. No wave velocities were sufficient to cause the coarse sand (D_{50} = 0.078 cm) to be suspended. It may be seen also from the histograms that each of the above categories of motion merges with the next so that, although ranges of velocity amplitude values may be assigned to each category of motion, these ranges generally overlap. Estimated ranges of velocity amplitude

for each category of motion, and each run in the 1978 experiment, are given in Table 4. For the three different velocity parameters plotted in Fig 6, it may be seen that the differences between the velocity ranges are small, the total velocity values (based on $\mathrm{sgn}(U)\sqrt{U^2 + V^2}$) being 0(10%) larger than the corresponding U-values, and the rotated values being essentially the same as the original U-values despite a rotation of the order of 0.1 rad. The tabulated velocity ranges have been determined subject to the exclusion of "rogue values" at the extremities of the main ranges in the histograms. Rogue values have been defined as those values in a particular category which occur singly, and which are separated from the main range by two or more incremental widths.

The remaining results for the 1978 experiment are shown in Figure 7, in which the data for Runs 8-14 has been combined. The histogram shown is based simply upon the measured U-component of velocity at a height of 130 cm above the bed (cf Figure 6(i)). As before, rather few waves had peak velocities in excess of 30 cm/s. As far as sediment movement is concerned, it may be seen from the shaded regions in the histogram (see also Table 4) that, for velocity amplitudes less than about 10 cm/s in both directions, no sediment movement occurred; between about 10 and 30 cm/s, a proportion of the measured waves caused incipient sediment motion; above about 20 cm/s, a proportion of the measured waves caused general bedload motion; and, above about 30 cm/s all the measured waves caused general motion. From the above figures, and also from the results in Figure 6(i), representative values for the threshold velocity amplitude for incipient motion, and for general bedload motion, of the coarse sand in question may be taken as 20 and 25 cm/s, respectively. The equivalent results for Runs 8-14, based upon the total horizontal velocity (cf Figure 6(ii)), are essentially the same as those in Figure 7 (see Table 4).

The present experiments (Figures 6 and 7) were carried out on a rippled bed of representative steepness η/λ = 0.15-0.16 (symbols defined in Table 2), and sediment motion was observed in the region of the ripple crests only. It follows that direct comparisons between the threshold values quoted above, and previous threshold velocity values determined in the laboratory, are not possible since, in the latter case, the experiments were carried out with flat beds. It is possible, however, to correct the threshold velocities on the rippled beds, and thus enable comparisons to be made, by following the procedure suggested by Davies (1979, 1982a). This relates the measured velocity "well away" from the bed, say one ripple wavelength above it, to the velocity "close to" the rippled surface. However, the procedure is valid only if the boundary layer thickness is small compared with a ripple wavelength (see §6), and if the flow is nonseparating. As will be seen later

in §5 (Figure 13), the flow was fully separating for only a minority of the waves in the 1978 experiment, and so the flow pattern in a frictionless sense, was generally similar to the idealised streamline pattern shown later (Figure 24, §7) for nonseparating flow. For the ripples in question, the representative near-bed (potential) velocity in the region of the ripple crests has been calculated to be about 1.80 times the measured velocity. The respective threshold velocities for incipient and general bedload motion on a notional flat bed may therefore be taken as 1.80 x 20 = 36 cm/s and 1.80 x 25 = 45 cm/s. (It should be noted that no allowance has been made here for the fact that the oscillatory flow was not quite normal to the ripple crest lines in certain runs. However, since the observed angles of attack of the waves were always less than 10°-15° from the normal direction (see Table 1), the errors involved in making no correction for this effect are very small (< 3%).)

There are many criteria which may be adopted to compare the above values with threshold velocity amplitudes for flat beds in the laboratory (see Silvester and Mogridge (1971)). Three typical formulae which define the critical conditions at the threshold of sand motion in oscillatory flow are as follows:

Bagnold (1946)
$$\frac{\sigma^{1/4}\,\hat{U}_\infty^{3/4}}{\gamma^{1/2}\,D^{0.325}} = 21.5 \qquad \text{(c g s units)}$$

Manohar (1955)
$$\frac{\hat{U}_\infty}{(\gamma g)^{0.4}(\nu D)^{0.2}} = \begin{cases} 7.45 & \text{(initial movement)} \\ 8.20 & \text{(general movement)} \end{cases}$$

Komar and Miller (1975)
$$\frac{\hat{U}_\infty^{\,2}}{\gamma g D} = \begin{cases} 0.21\left(\dfrac{d_o}{D}\right)^{1/2} & (D < 0.05 \text{ cm}) \\ 0.46\pi\left(\dfrac{d_o}{D}\right)^{1/4} & (D > 0.05 \text{ cm}) \end{cases}.$$

Here $\hat{U}_\infty$ is the free-stream velocity amplitude, σ is the wave frequency, $\gamma = ((\rho_s - \rho_f)/\rho_f)$ is the relative density in which ρ_s and ρ_f are the densities of the sand and fluid respectively, D is the grain size, g is gravity, ν is the kinematic viscosity and d_o is the orbital excursion of the water particles in the free-stream flow above the bed, defined by $d_o = 2\hat{U}_\infty/\sigma$. Bagnold's formula is for the "first motion" (ie incipient motion) of grains on a flat bed, in what was stated by Bagnold to be a laminar boundary layer flow. Manohar's formula is for either incipient or general motion depending upon the choice of constant, and is for a turbulent boundary layer flow; this formula is independent of the wave period.

Komar and Miller's formulae are based upon the results of five previous laboratory studies, including those of Bagnold and Manohar, and they therefore encompass a wide range of conditions.

In order to calculate the threshold velocity amplitude, at least on the basis of the criteria of Bagnold and of Komar and Miller, it is necessary initially to determine the wave period ($T = 2\pi/\sigma$). Here we have estimated a representative wave period for the waves which moved sediment in each run, on the basis of graphs of which a typical example for Run 9, 1978, is shown in Fig 8. In this figure, the average half-period (ΔT) of those wave half-cycles having measured horizontal velocity amplitudes in each unit incremental range is plotted against the amplitude of the U-component of velocity itself (measured in the free-stream flow at a height of 130 cm). The half-periods have been defined simply by zero-crossings of velocity. The ΔT-values may be seen to increase fairly linearly with $\hat{U}$ for $|\hat{U}| \lesssim 10$ cm/s. This sharp increase then gives way to a rather more settled value for $|\hat{U}| \gtrsim 20$ cm/s, though the scatter is considerable. In the present example, the waves which moved sediment may be seen to be associated with a representative value $\Delta T \approx 5\frac{1}{2}$s, corresponding to a wave period of 11 s. (This value is rather larger than the zero crossing period of 9.3 s for <u>all</u> the waves in Run 9. It may be contrasted also with the period of 12.5 s, associated with the main spectral peak at 0.08 Hz for this run (see Fig 3).) Representative values of ΔT, estimated for each run in the 1978 experiment, are listed in Table 4, together with threshold velocity amplitudes calculated for the appropriate D_{10}, D_{50} and D_{90} grain sizes from the formulae of Bagnold, Manohar, and Komar and Miller. The tabulated values are only weakly dependent on the wave period, which justifies the use of a representative wave period for each run; in fact, variations with period are less pronounced than the differences between the predictions of the various formulae at the <u>same</u> period. The variations with grain size are quite marked however; and herein lies a difficulty in making comparisons, since the laboratory results were determined with sand of a single size, rather than a mixture of sizes as in the present field experiments. Despite this, it may be seen that the calculated threshold values in Table 4 compare quite well with the earlier estimates of 36 and 45 cm/s for incipient and general motion, respectively. The former value is in reasonable agreement with calculations made from the formulae for the D_{50} size, while the latter value is in rather better agreement with values for the D_{90} size. This is logical since it may be only the fine grains which are moved when there is incipient motion, whereas all the surface grains must move for general motion. The agreement obtained is encouraging and it suggests that, at least in this comparatively simple

case, there is a sound basis for comparing field and laboratory results.

Finally, in connection with the 1978 velocity data, results have been obtained with two EM-flowmeters mounted in the vertical plane at nominal heights of 20 and 90 cm above the bed. It may be seen from Table 1 that, in the typical case of Run 8, the lower flowmeter was actually 11 cm above the ripple crest, from which it follows that the upper flowmeter was at a height of 81 cm. At these heights, and for the ripple dimensions in question, it is expected on the basis of potential theory (see §7) that there should be a measurable difference in velocity resulting from the convergence of streamlines over the ripple crests. The upper flowmeter, at a height approximately equal to one ripple wavelength above the bed, may be shown to have been in an "outer" region of unperturbed flow, whereas the lower flowmeter was within the region of flow perturbed by the bottom ripples. As shown later in §7 (Fig 24), potential theory suggests that, for nonseparating flow above the ripples in question, the velocity at a height of 11 cm above the crest of the ripples is about 15% (±2%) greater than the velocity in the "outer" flow. Such differences have, in fact, been found between measurements made with the lower and upper flowmeters. For example, in Run 8, the r m s value of horizontal velocity at the height of 11 cm was about 20% greater than the value at the height of 81 cm. As far as the estimated horizontal velocity amplitude ranges for sediment motion are concerned, the range for incipient motion was (13-27)cm/s with velocity measured at the height of 11 cm, and (10-23)cm/s at 81 cm; for general bedload motion, the lower limit of the range was 21 cm/s at 11 cm, and 15 cm/s at 81 cm (the upper limit being undetermined). These differences are of the order of 20% and are therefore in tolerable agreement with the predicted difference of 15% quoted above. The discrepancy of about 5% is probably due in part to the fact that the actual ripple profiles in Run 8 were different in detail from the idealised profile in §7. Also the magnitude of the near-bed velocity measured with the 10 cm diameter EM-head was probably overestimated on account of the nature of the vertical profile of horizontal velocity (see Fig 24); in particular, on account of the inability of a sensor of such a physical size to make highly localised, accurate, measurements in a velocity field containing large local spatial variations. This effect was probably small however (O(1%)).

4.3 Results for the 1980 experiment

We consider next results for the 1980 experiment. Again these are presented in histogram form, but now for individual runs rather than combinations of runs. In Figs 9(i)-(vi), histograms based upon the measured horizontal U-velocity at a

height of 160 cm above the bed are presented for Runs 5, 10, 11, 12, 14 and 15. The principal features of the histograms are the same as those in Figs 6 and 7. The peak velocity values are rather larger however. In fact, they were sufficient to carry some of the (medium to fine) sand into suspension and, thus, it has been possible to estimate critical velocity amplitude ranges not only for incipient and general bedload motion, but also for suspension. The results obtained for each run are given in Table 5. As in Table 4, the results are based not only on the measured U-component of velocity, but also on the total velocity $U_T = \text{sgn}(U)\sqrt{U^2 + V^2}$ and the (rectilinear) rotated velocity U_{ROT}. Since the results are closely similar for each of these three parameters, for brevity no histograms based upon U_T or U_{ROT} are presented here. Also included in Table 5 are the representative periods of the waves which moved sediment, which have been obtained on a run by run basis from results equivalent to those shown in Fig 8. An example of the results is shown in Fig 10, in which ΔT is plotted against the measured velocity amplitude $\hat{U}$, for a case in which the waves were of relatively short period (Run 10, 1980; see Fig 2(ii)). More generally, it may be seen that there was quite a substantial variation in wave period, from swell wave periods in Runs 4 and 5, to local sea wave periods in Runs 10-15. With these estimated periods, representative threshold velocity amplitudes have been calculated for the appropriate D_{10}, D_{50} and D_{90} grain sizes, from the formulae of Bagnold, Manohar, and Komar and Miller (Table 5). As before, these values relate to a flat sand bed. The results based upon Bagnold's and Komar and Miller's formulae are in reasonable agreement, and correspond generally at the D_{50} size to a value lying within the estimated velocity amplitude range for motion of type 1 (incipient motion). The results based upon Manohar's formulae, for both incipient and general motion, are rather larger and, at the D_{50} size, lie generally within the estimated velocity amplitude range for motion of type 2. From all the results for the 1980 data, representative values for the threshold velocity amplitude for incipient motion, general bedload motion and suspended motion, of the fine to medium sand in question, have been estimated as 23, 34 and $\geq$ 40 cm/s respectively. The first of these estimates is rather larger than the values of threshold velocity amplitude given by the formulae of Bagnold and Komar and Miller for the D_{50} size, but is smaller than the equivalent values for the D_{90} size. The second estimate is well above the predictions of these two formulae, even for the D_{90} size, but is in fair agreement with results based on Manohar's formula. The third value for suspension is a very approximate estimate; it is roughly twice the threshold velocity values for bedload motion given by the formulae of Bagnold, and Komar and Miller, and is also

rather larger that the values from Manohar's formula.

Care needs to be exercised in making direct comparisons of the above kind between the present field results and previous laboratory results, since the bed surface was always rippled during the experimental runs (see Table 2). Unfortunately, since the present situation was rather different from that which existed in the 1978 experiments, it cannot be analysed in such a simple way. In the 1978 experiments, sediment motion was always confined to the crests of the rather long wavelength sand ripples, and little interchange of bed material appeared to occur between one crest and the next; more is revealed about this in §5, where the orbital excursions of the near-bed water particles are estimated. In the 1980 experiments, the ripple wavelengths were much shorter and, when sediment motion was observed, it occurred over the entire bed surface with much interchange of material between one ripple and the next. Since local variations in velocity resulting from the presence of the ripples, and hence local variations in bottom stress, were not easily quantifiable for these runs, the sediment motion events included in the histograms in Fig 9, and the estimated velocity amplitude ranges for the three motion types given in Table 5, should be considered as spatially averaged results for the entire bed. Although, in general, bottom protuberances such as ripples are expected to cause an apparent lowering of the threshold of motion, this does not appear to have happened in a systematic way in the present runs, as may be seen from the broad agreement between the present field results and the laboratory threshold results calculated for an assumed flat bed (Table 5). If we compare the results obtained in the 1978 and 1980 experiments (Tables 4 and 5, respectively), we see, firstly, that the measured free-stream threshold velocity amplitudes were rather similar in the two experiments for motion of both types 1 and 2, the measured threshold values being, if anything, rather smaller in the 1978 experiments than in the 1980 experiments. Secondly, the equivalent flat bed threshold velocity amplitudes from the laboratory were of the order of 50% greater in 1978 than in 1980, mainly on account of differences in the sediment grain size. In particular, the rough agreement between the laboratory and field results for the 1980 experiments may be contrasted with the lack of agreement in the 1978 experiments. As noted earlier, the apparent discrepancy in the latter case can be well explained by the fact that sediment motion occurred only in the region of the ripple crests and that, for the non-separating flow in question, the local velocity at the crest may be shown on the basis of potential theory to have been about 80% greater than the measured free-stream velocity.

In the remaining sections, we extend our analysis of the experimental results to some considerations of the nature of the near-bed flow. In §5, we determine

critical conditions for the formation of vortices above the bottom ripples, since this has an important bearing on any calculations of the bed shear stress. In §6, we discuss the classification of the wave boundary layer, and go on to estimate the bed shear stress on a wave-by-wave basis. Finally, in §7, we return to the question of the structure of vortices above a rippled surface, and present some theoretical results which enable the velocity measured in the free-stream flow to be related to the velocity near the bed.

§5 OBSERVATIONSOF THE NEAR-BED FLOW AND OF SAND RIPPLE FORMATION

5.1 Flow visualisation tests

Although we shall concentrate mainly in this section on the nature of the flow above the rippled beds in the field experiments, we start with some comments about the flow observed above a flattened area of sand bed. In this relatively simple case, the conditions in the boundary layer were reasonably uniform in the horizontal direction as revealed, in certain experiments, by the presence of dye in the flow. Such a flow visualisation test was carried out at the start of Run 6 in the 1980 experiment, immediately after the flattening of the bed of fine sand (D_{50} = 0.0225 cm). Dye crystals were placed on the bed by divers in small patches in the field of view of the television camera; the crystals (of potassium permanganate) were contained in small capsules, which were broken just above suitable positions on the bed. The wave conditions were essentially the same as those during Run 8 (see Table 3), few waves achieving free-stream velocity amplitudes in excess of 20 cm/s. For the representative period quoted in Table 5 of about 10 s (for the largest waves), this meant that the peak values of wave Reynolds' number ($\hat{U}^2/\sigma\nu$) achieved during the run were of the order of 10^5. As seen in §6, this implies that the flow above the flat bed was, at most, transitional, and almost certainly not turbulent in the usual sense. (Only above a rippled bed would the flow in the boundary layer have been rough turbulent for the range of values of wave Reynolds' number in question.) The relatively low velocity amplitudes gave rise to very little sediment movement, so that the dye crystals remained where they had been placed on the bed for a period of many minutes. Conditions were, therefore, very suitable for the kind of flow visualisation test carried out.

The observations were of interest, and constituted a recognisable and repeatable sequence of events, for only the largest of the measured waves. For these waves the near-bed flow above the flat bed appeared to behave, at the instants in the wave-cycle characterised by the sequence of numbers 1 to 4 in Fig 11(i), in the following way. At instant 1, as the speed of flow in the typical half-cycle was

increasing, the dye appeared to "hug" the bed; in particular, dye streaks were confined to a thin layer of the order of a few millimeters thickness (Fig 11(ii)). At instants 2 and 3, during the period of both peak and diminishing flow speeds, dye was occasionally mixed upwards but, as often as not, remained in well defined streaks close to the bottom. When some form of instability in the flow did cause upward mixing, dye could be seen dispersing into the bottom couple of centimeters (Fig 11(iii)). In such cases, the wave Reynolds' number was probably sufficiently large for the boundary layer to be turbulent (though this could not be checked since, unfortunately, a (permanent) video record was unobtainable). Between instants 3 and 4^-, the dye was generally confined to a thin layer immediately above the bed of the order of a few millimeters thickness. However, upon flow reversal (instant 4^-), there was a noticeable upward dispersion of dye to heights of the order of 2-3 cm, or even more (Fig 11(iv)); the low velocities pertaining at the instants in question allowed this to be observed quite clearly. As the sequence of events (1,2 ...) recommenced in the next wave half-cycle, the upwardly convected cloud of dye tended to vanish from the field of view. The overall effect of this was the upward dispersion of dye to heights of the order of 10 cm, or more. This was not due to turbulent mixing within one wave half-cycle but, rather, was a general effect over many cycles; this suggestion is supported by the discussion in §6, where it is shown that the oscillatory boundary layer thickness was generally rather small during the experiments. However, since the flow in the region well above the bed was out of the field of view of the television camera, all that can be stated is that no signs of (relatively large scale) instability were noted on the EM flowmeter records at the measuring heights of 60 and 160 cm.

Observations with dye in the field of view were also made above the rippled beds in both the 1978 and 1980 experiments. These flow visualisation tests have given rise to more quantitative results than for the case of the flat bed above, as described in the following subsection. In general, it was found that a good impression of the nature of the flow could be obtained not only from dye in the water, but also from the ever-present particulate matter in the flow, and even, on occasions, from the movement of sediment grains in suspension.

5.2 Threshold conditions for the onset of vortex formation above rippled beds in oscillatory flow

Many of the same video records which were used to determine conditions at the threshold of sediment motion have been used also to study vortex formation and shedding above the rippled beds in both the 1978 and 1980 experiments. As

mentioned above, it was generally possible to see the near-bed flow quite clearly from the motion of particulate matter in the water, though in some runs dye crystals were placed on the bed to give a more clear-cut impression of the fluid motion. On this basis, each wave half-cycle in the experiments was classified according to whether or not flow separation occurred. When separation occurred, it was possible to observe a discrete vortex above the lee slope of the ripple. Although it was not possible to estimate the size of this (two-dimensional) vortex, or its internal velocities, with any accuracy, the diameter of the vortex generally appeared to be of the order of the ripple height. Often a vortex could be seen dragging sand towards the ripple crest, in the direction opposite to that of the outer free-stream flow. Upon flow reversal, vortices were generally carried over the crests, sometimes retaining their identity for sufficient time to be seen on the other side of the crests as discrete vortices. Between the two extremes of separating and nonseparating (or contouring) flow, there was an intermediate class of wave half-cycles in which the flow was unstable above the lee slopes of the ripples, but in which a discrete vortex did not form. The term 'instability' is used here to classify wave half-cycles in which such perturbations in the flow were observed; it should be emphasised that these perturbations were unlike those associated with turbulence in the usual sense.

A typical portion of record from the 1978 experiment, which illustrates some of these features, is shown in Fig 12. In each of the two (negative) wave half-cycles marked with an asterisk, the horizontal velocity record contains a perturbation associated with the passage of a vortex below the EM-head positioned at a height of 11 cm above the crest. Essentially the same behaviour has been measured in the laboratory by DuToit and Sleath (1981, Fig 15a). There workers noted small perturbations in velocity records measured above a ripple crest, at phase angles of about 40° after that at which flow reversal occurred. They concluded that this perturbation corresponded to "the surge in velocity as the vortex in the lee of the crest is carried back over the crest when the flow reverses".

In Fig 13, histogram results are presented for the same data (Runs 8-14, 1978) which gave rise to Fig 7, but in which the shaded regions now depict wave half-cycles for which there was flow instability or vortex formation. In these runs, observations were possible only above one slope of the ripple in the field of view of the television camera; in particular, relevant observations were made only for wave half-cycles in which the horizontal velocity was negative. Thus the shading in Fig 13 appears only in the left tail of the histogram, and not in the right tail (for which equivalent results must be assumed). Estimated ranges of

the measured U-component of free-stream horizontal velocity amplitude for instability and vortex formation are given in Table 6. (On the basis of the discussion in §4, it is expected that closely similar results would have been obtained in terms of the total horizontal velocity U_T, or the rotated component of horizontal velocity U_{ROT}.) Representative values of measured velocity amplitude for the onset of instability and vortex shedding are about 21 and 25 cm/s, respectively. While the former value has been confirmed by the results from Runs 1-5, 1978, there was insufficient data to confirm the latter value on account of the less active waves in these runs. Although the estimates are almost equal to those quoted earlier for the measured thresholds of incipient and general bedload motion, this has no general significance as seen shortly in the discussion of the results for the 1980 experiment.

Previous work on oscillatory flow above rippled beds (see §2.3) has suggested that the flow starts to become unstable when the orbital excursion (d_o) of the water particles near the bed is approximately equal to the ripple wavelength (λ), and that vortex formation above the lee slopes of the ripples occurs when the orbital excursion is rather greater than the ripple wavelength (Sleath, 1975b). In order to test this criterion, an approximate orbital excursion (d_o) has been calculated for each of the wave half-cycles contributing to Fig 13 from the expression $d_o = 2\hat{U}.\Delta T/\pi$, based upon the assumption that each half-cycle was sinusiodal, and characterised by its peak velocity ($\hat{U}$) and its zero-crossing (half-wave) period (ΔT) (see Figs 8 and 10). Half-cycles which obviously violated this assumption by having two or more velocity maxima between zero-crossings have been discarded. Thus, in Fig 14, a histogram based upon calculated orbital excursions associated with the measured U-component of horizontal velocity, but otherwise equivalent to the histogram in Fig 13, has been obtained. Unlike Fig 13, the new histogram is not bimodal, due to the preponderance of low orbital excursion values. More importantly, the shaded region in the left tail of the histogram (the only tail for which results were obtained) suggests representative orbital excursion values of about 70 and 100 cm for the onset of flow instability and vortex formation, respectively. These values may be compared with the ripple wavelength of 77 cm, and thus support quite well the laboratory criterion for the onset of instability. The representative value of orbital excursion of 70 cm for instability has been confirmed by the results of Runs 1-5 during which the ripple wavelengths were of approximately the same magnitude (Table 2). Estimated ranges of values of orbital excursion associated with instability and vortex formation are given in Table 6.

Equivalent results have been obtained for certain runs in the 1980 experiment, for which the ripple wavelengths were considerably smaller (7-20 cm) than in the 1978 experiment. Estimated ranges of values of free-stream velocity amplitude and orbital excursion for instability and vortex formation are quoted in Table 7 for the five runs for which results were obtained, and two representative pairs of histograms for the contrasting cases of Runs 8 and 17 are shown in Figs 15 and 16, respectively. Television observations were possible on both sides of the ripple crests in these runs; thus the shading in Figs 15 and 16, indicating instability and vortex formation, appears in both the left and right tails of the histograms. The ranges of values quoted in Table 7 suggest a representative free-stream velocity amplitude for the onset of instability of about 14 cm/s. (This is a rather lower value than the velocity amplitude needed for incipient sediment motion.) The equivalent velocity amplitude value for the onset of vortex formation has been rather more difficult to estimate on account both of the limited duration of the available data sets and of the scatter in the results (Figs 15(i) and (ii)). However, a value of approximately 20 cm/s would appear to be appropriate. Both of these representative values apply for each of the five experimental runs, despite the fact that the ripple wavelength was rather smaller in Runs 3 and 8 than in Runs 11, 16 and 17. During Run 8, the ripple wavelength was about 7 cm while, during Run 17, it was about 15-20 cm (Table 2). This apparent anomaly may be explained, in part, by the fact that the ripples in the former case were not fully developed, that is they had not achieved their final (equilibrium) steepness following the flattening of the bed. The rather longer wavelength ripples in the latter case were almost certainly in equilibrium with the measured waves, having had considerably longer to develop and more active wave conditions in which to do so. The values in Table 7 suggest a representative orbital excursion for the onset of instability of about 30 cm, which is rather larger than the ripple wavelength (7-20 cm) in any of the experimental runs. However, this result is in accordance with the statement of Sleath (1975b, para 29) that, provided a bed of natural ripples has had time to reach equilibrium, the value of the quotient (d_o/λ) usually lies between 1 and 10. This may be taken as a necessary condition to be satisfied by <u>equilibrium</u> bottom ripples. (Sleath adds that values of the quotient of the ripple height and wavelength may range down to zero, but are commonly between 0.1 and 0.2.) Again, the equivalent criterion for the onset of vortex formation has been rather more difficult to assess. On the basis of the available data, the representative orbital excursion for the onset of vortex formation is rather greater than 30 cm, but well within

the range of values attributed above to Sleath for the existence of equilibrium ripples.

In conclusion, from results for both the 1978 and 1980 experiments, it has been found consistently that instability in oscillatory flow over natural sand ripples is associated only with those waves having (calculated) orbital excursions which are greater than the ripple wavelength. This is in accordance with laboratory results.

5.3 Ripple formation experiments

In the 1980 experiment, certain runs were carried out with an initially flat sand bed, which deformed into an (equilibrium) rippled bed during the recording period. In particular, prior to Runs 2, 6, 10 and 12, the bed was flattened out in the region of the rig by divers. The subsequent evolution of ripples on the bed was then monitored, while velocity measurements were made in the free-stream flow (see Table 2). As noted in §3, the evolving ripples were symmetrical and relatively long-crested (two-dimensional), with crest lines parallel to the surface wave crests. Moreover, as found previously in the laboratory (see §2.1.1), the flattened sand beds were readily deformed into rippled beds, if the threshold of sediment motion was exceeded. The first signs of ripple formation tended to occur almost immediately after the flattening of the bed. Typically, bands of bottom debris and shell could be observed moving to and fro in the oscillatory flow. These bands shortly stabilised their positions on the bed, and the process of ripple growth commenced. An initial period during which the ripples were of "rolling grain" type was followed by a longer period of ripple consolidation and growth during which the ripples were of "vortex" type. These categories of ripple type, and their physical causes, are discussed in §2.2, and the flow over an idealised rippled bed is modelled in §7. It is interesting to note that Miller and Komar (1980a) made the statement: "There are no reports of rolling grain ripples having formed in the field, but this is not surprising in that Bagnold showed that when bottom irregularities are present, vortex ripples preferentially form .... (in the laboratory) it would appear that the oscillating bed device somehow suppresses the formation of vortices, permitting stable rolling grain ripples to exist". While rolling grain ripples were observed in the early stages of each of the present experiments, they were not stable bedforms, but merely transitory features in the development of equilibrium vortex ripples. In terms of Inman's (1957) ripple classification scheme (see §2.1.2), the profiles of these equilibrium ripples were of "trochoidal" type, not of "solitary" type. (In terms

of Komar et al's (1972) extension of this scheme, they were possibly also of "rounded" type in some cases.) The ripples did not appear to have sharp crests, whatever their development time. In fact, they tended to be smooth crested, unlike the ripples generated in sinusoidal flow in the laboratory by Bagnold (1946) and others. The inability of the ripples to develop sharp crests in any of the experimental runs was most probably associated with the irregular nature of the waves (see §2.1.2 and Nielsen (1981)). Ripple migration rates were negligible on the timescale of the experimental runs, due partly to the intermittent nature of the sediment motion; in any case, the fact that the ripple profiles were, to all intents and purposes, symmetrical suggests very small, or negligible, migration rates.

In the present experiments, the length of the entire process of ripple growth was of the order of one hour (or more) when only a few occasional waves exceeded the threshold of sediment motion, though it was rather more rapid in more active wave conditions. On account of the intermittent nature of the sediment motion, it is probably inappropriate to use Lofquist's (1978) criterion for the ripple growth time (see §2.1.1); in the present context, this criterion provides, at best, a lower bound on the growth time. Following the period of ripple development, and the attainment of (what appeared to be) an equilibrium rippled bed, there was a slow, steady increase in the ripple wavelength, on the timescale of many hours. This may be noted in Tables 2 and 8 for Ripple Trials 2 and 3 (Runs 10 to 11 and Runs 12 to 17, respectively). The reason for the increasing wavelength is not entirely clear. One might expect it to have been associated with a steadily increasing amount of wave activity and, hence, with steadily increasing orbital excursion values. However, the results in Table 3 show that this was probably not the case. An alternative explanation is suggested by the conclusion of Miller and Komar (1980b) based on their field observations (see §2.1.2) that, in almost all cases, longer ripple wavelengths were associated with polymodal wave spectra, and that smaller ripple wavelengths were associated with wave spectra having a single pronounced peak. In Table 8, a classification of the wave spectra shown in Fig 3 has been made for each run. Except in a minority of cases (eg Fig 12), the classification could be made quite unambiguously. It is evident that, whereas in Ripple Trial 1 the spectrum had a single peak, in Trials 2 and 3 it tended to develop overnight from a spectrum with a single peak into a polymodal spectrum. The tendency for ripple wavelengths to increase with time in these cases is consistent with the findings of Miller and Komar.

The basic condition to be satisfied by any surface waves forming ripples is

that they should be capable of moving sediment, and the dimensions of the (equilibrium) sand ripples formed should be consistent with their properties. For vortex ripple formation, the ripple wavelength should be rather less than the orbital excursion of those waves which both move sediment, and produce flow instability or separation. Consider the typical case of Run 12, 1980, during which a ripple pattern developed in fine sand (ripple wavelength 10 cm, height 1-2 cm; see Tables 2 and 8). The representative free-stream velocity amplitude ($\hat{U}_\infty$) quoted earlier for flow instability of about 14 cm/s lies just below the range of values quoted in Table 5 for incipient sediment motion of 15-37 cm/s. Likewise, the representative orbital excursion (d_o) for flow instability of about 30 cm lies just below the range of values of orbital excursion ($\gtrsim$ 30 cm) associated with sediment motion. This is illustrated in Fig 17; similar results have been obtained for all other runs considered in this way. This confirms that ripple wavelengths caused by irregular waves in the field are of the order of, though rather less than, the orbital excursions of those waves which move sediment, as expected from laboratory work.

In Table 8, representative values are quoted for the mobility number M and the ratio ($2\lambda/d_o$), for each experimental run. These estimates have been based upon values of velocity amplitude ($\hat{U}_\infty$) and wave period (T), representative of conditions at the centre of the bedload (general motion) range. In other words, the values quoted for M and ($2\lambda/d_o$) are representative of those waves which moved an appreciable amount of sediment. The approach adopted for the calculation of d_o differs from that of Inman (1957), Dingler and Inman (1977) and Miller and Komar (1980b) (see §2.1.2), who based their estimates of d_o on significant wave parameters. The present approach has the advantage of taking into account, quite explicitly, the question of whether or not the measured waves moved sediment. It also overcomes the difficulty inherent in Miller and Komar's approach of relating the wave period at which a peak occurs in the wave spectrum to the actual, required, wave period. In general, the peak in the spectrum is associated with rather longer period waves than the required period, as may be inferred from the values calculated earlier (§4) for the period of those waves which moved sediment. It may be noted, initially, that the calculated values of mobility number M lie in the range (12, 29). According to the classification of Dingler and Inman (1977) (see §2.1.2), vortex ripples occur for values of M up to M $\approx$ 40, at least provided that the waves are capable of moving sediment (as in the present case). It would appear from this that conditions in the present experiments were consistent with the formation of vortex ripples. As far as the quotient ($2\lambda/d_o$) is concerned,

the calculated values lie in the range $0.15 < 2\lambda/d_o < 0.62$, with values at the upper end of this range probably being consistent with the existence of equilibrium ripple profiles. These values are rather lower than those predicted by the relationship of Miller and Komar (1980a), namely $\lambda = 0.65d_o$ (valid for relatively small d_o), or by the relationship of Lofquist (1978), namely $2\lambda/d_o = {}^4/_3$ (for $10^2 < d_o/2D < 5 \times 10^3$ and $0 < M < 30$). However, when the present results are plotted on a graph of $(2\lambda/d_o)$ against M, agreement with previous field data is quite convincing. In Fig 18, the results tabulated in Table 8 are plotted on two graphs presented by Nielsen (1979), one (Fig 18(i)) showing results from a number of previous laboratory studies, and the other (Fig 18(ii)) results from previous field studies. The present data is plotted as a single point for Ripple Trial 1, and as a sequence of connected points for Ripple Trials 2 and 3. When compared with laboratory data, the present data is in poor agreement, ripple wavelengths in the laboratory being considerably larger, in fact about twice as large. However, when compared with the field data of Inman and Dingler, the present results are in good agreement. This not only emphasises the fact that ripple wavelengths in the field are considerably shorter than in the laboratory, but it also supports the use of Nielsen's suggested relationship (Eq (2) quoted in §2.1.2) for field applications. The contrasting predictions of Nielsen's relationships between $(2\lambda/d_o)$ and M, for laboratory (Eq (1)) and field (Eq (2)) work, may be seen in Fig 18(ii). The ripple steepness may also be deduced from the ripple dimensions quoted in Tables 2 and 8. However, in most cases, there is some uncertainty in the measured ripple height and, for this reason, no comparisons have been made with previous laboratory and field results for steepness.

A further comparison is shown in Fig 19 in which the present data (Table 8) is plotted on the graph of M against $(d_o/2D)$ presented by Lofquist (1978, Fig 32). This graph delineates the regimes of no ripples (or fossil ripples), equilibrium ripples and sheet flow, and it also includes the field data of Inman and Dingler. The present results are in reasonable agreement with these earlier results, and may be seen to lie in the region of ripple existence, just above the threshold curve for sediment motion on a flat bed. (The curve labelled $M = M_c$ is a composite curve proposed by Lofquist on the basis of the laboratory results of several previous workers.) As far as the relationship of the present results to the "cut-off" of "break-off" point is concerned, comparisons with the criterion of Grant and Madsen (quoted in §2.1.1) suggest that conditions in the present experiments were always significantly below the "cut-off" point. In other words, the ripples were in the regime in which both ripple wavelength and steepness were

increasing with increasing d_o.

In conclusion, the present experiments have demonstrated the formation of equilibrium vortex ripples, having characteristics consistent with ripples observed previously in the field by Inman and Dingler, and lying below the "cut-off" point.

§6 CALCULATIONS OF THE WAVE-INDUCED BOTTOM STRESS AT THE THRESHOLD OF SEDIMENT MOTION

6.1 General background

In this section we return to the question of determining critical conditions for the threshold of sediment motion. It will be recalled that, in §4, such conditions were determined in terms of the measured free-stream velocity well above the bed surface. In §5, we discussed the nature of the near-bed flow in some detail, and arrived at some quantitative conclusions about the conditions needed for vortex formation and shedding above a rippled bed. Now, we develop the discussion in §5, by making estimates of the magnitudes of the bed shear stresses associated with the irregular measured waves. This is a more rational way of establishing sediment threshold motion conditions than the simple approach described in §4.

It has been commonly assumed by coastal engineers that wave boundary layers in the field are always rough turbulent. Although this is certainly true in most situations of engineering importance, it is by no means true of the wave boundary layers which exist in shallow water during the long spells of relatively calm conditions between storm events. As we shall see in this section, sediment motion is possible even in boundary layers which are nonturbulent (see also Davies (1980a)). In general, the thickness of the oscillatory boundary layer which develops at the seabed is small compared with the water depth, even in rough turbulent cases. In interpreting the present field results, we shall show that we are justified in assuming that the boundary layer is confined to a near-bed layer well below the EM-flowmeters. In the three subsections which follow, we consider, in turn, the present state of knowledge on the subjects of wave boundary layer classification, wave boundary layer thickness and wave drag coefficients (or friction factors). We then apply the approaches described to the present field results.

6.2 The classification of wave boundary layers

An initial difficulty which arises in studying wave boundary layers in the field is that almost all the available laboratory information on the subject is

related to sinusoidal free-stream flows, whereas natural wave-induced flows tend to be rather irregular. This gives rise to some uncertainty in classifying boundary layers in the field, since the behaviour of the flow in one half-cycle may depend upon previous half-cycles. This is not a problem for laminar or transitional boundary layers, which may be classified on a half-cycle by half-cycle basis on the assumption of the independence of consecutive wave half-cycles. However, for turbulent boundary layers, this assumption is likely to be valid only if little or no turbulence energy generated in one half-cycle persists until the next half-cycle. In respect of sediment movement, it follows that, while the assumption of the independence of consecutive cycles may be reasonable for a to-and fro- bedload action in which grain motion both starts and stops within each half-cycle, it is almost certainly invalid if there is a suspended load which persists from one half-cycle to the next.

In order to make a boundary layer classification, it is necessary to determine the wave Reynolds number and the "relative roughness" of the bed. The wave Reynolds number is defined by $RE = \hat{U}_\infty \hat{A}_\infty / \nu$, where $\hat{U}_\infty$ is the free-stream orbital velocity amplitude, ν is the kinematic viscosity and $\hat{A}_\infty = \hat{U}_\infty / \sigma$ is the near-bottom excursion amplitude[1], in which σ is the wave frequency. The relative roughness is defined by $\hat{A}_\infty / k_s$, where k_s, the equivalent roughness of the bed surface, is determined by the sand grain size and any ripples present on the bed. For this reason, k_s may vary in time, as ripples are formed or eroded by changing wave conditions. In the classification of wave boundary layers, the most basic distinction is between laminar boundary layers, the properties of which depend only on RE, and turbulent boundary layers, the properties of which depend upon both RE and $\hat{A}_\infty / k_s$. Turbulent boundary layers are further classified as follows. If the bed roughness is small compared with the thickness of the viscous sublayer, such that the roughness does not extend into the turbulent part of the flow, then the boundary is said to be hydrodynamically smooth. In this limiting case, the properties of the boundary layer depend only on RE and are independent of $\hat{A}_\infty / k_s$. However, if the bed roughness is large compared with the thickness of the viscous sublayer, the boundary is said to be hydrodynamically rough, and the properties of the boundary layer depend only on $\hat{A}_\infty / k_s$ and are independent of RE. Between the laminar and turbulent regimes lies the so-called transitional regime.

---

[1] It has been the convention in previous studies of this topic to present results in terms of the near-bed excursion amplitude $\hat{A}_\infty$, rather than the orbital excursion $d_o = 2\hat{A}_\infty$ itself (as used in the previous sections). This practice has therefore been adopted here.

Jonsson (1967) first presented a delineation of flow regimes in terms of RE and $\hat{A}_\infty/k_s$, based upon the knowledge available at the time. His conclusions have been modified in certain respects by subsequent experimental results, and a more recent delineation of regimes has been given by Kamphuis (1975). The best presently available knowledge has been summarised by Jonsson (1978, §3)(see Fig 21), and has been discussed by Davies (1983, Part III, §1). For <u>smooth</u> beds, Jonsson suggests that the flow is laminar if RE $\lesssim 10^4$, transitional if $10^4 \lesssim$ RE $\lesssim 3 \times 10^5$, and (smooth) turbulent if RE $\gtrsim 3 \times 10^5$, "give or take a factor of two" at the interval ends. For design purposes, Jonsson suggests the value RE = 10^5 for transition to turbulence. However, there are wide variations in suggested transitional regimes for smooth beds. For <u>rough</u> beds, the situation is complicated by the need for a knowledge of the 'relative roughness' of the bed ($\hat{A}_\infty/k_s$). For a flat smoothed sand bed, the equivalent roughness k_s may be taken as the sediment grain diameter ($k_s = D$)(Madsen and Grant (1976), Hsiao and Shemdin (1979)). For a "not so well smoothed bed", Nielsen (1979) has suggested the use of $k_s = 2.5D$, which is similar to Kamphuis' (1975) recommendation of $k_s = 2D_{90}$ (in which the definition adopted is that 90% of the grains are finer than D_{90}). However, in the general case of a rippled sand bed, it is rather more difficult to estimate the roughness. Jonsson (1967) suggested use of the equivalent roughness $k_s = 4\eta$, where η is the ripple height, which has been adopted by Tunstall and Inman (1975) and has been recommended also by Hsiao and Shemdin (1979). Nielsen (1979) has also suggested that k_s should be of the order of magnitude of the ripple height, and quotes the empirical formula

$$\frac{k_s}{\hat{A}_\infty} = 25 \frac{\eta}{\lambda} \cdot \frac{\eta}{\hat{A}_\infty} \quad , \tag{4}$$

from which the relative roughness can be obtained, in which λ is the ripple wavelength. In suggesting empirical relationships for the ratios η/λ and $\eta/\hat{A}_\infty$, Nielsen distinguishes between the cases of regular waves in the laboratory and irregular waves in nature on the grounds that, in the field, ripples tend to be less steep than under laboratory conditions (see §2.1.2 and §5.3). A rather different relationship has been proposed by Vitale (1979), namely

$$\frac{k_s}{\hat{A}_\infty} = \frac{2D_{90} + 0.01\eta}{\hat{A}_\infty} \quad .$$

This expression, which has been obtained from a re-analysis of the laboratory data of Carstens et al (1969), places rather less emphasis on the ripple height than those quoted above. More recently, the same data set has been utilised by Grant and Madsen (1982) in formulating an expression for the roughness of a mobile sand bed in oscillatory flow. The roughness has been divided into two contributions, one of which arises from form drag on the ripples on the bed and which is a function of boundary geometry, and the other which is associated with near-bed sediment transport and which is a function of the skin friction component of the bottom stress. The form drag contribution, when expressed in terms of relative roughness, is very similar to the result of Nielsen quoted above, the empirical constant 25 being replaced by 27.7. In general, sand ripples dominate the roughness when they are present (at least if $\eta/\lambda \gtrsim 0.1$). However, for high values of the boundary shear stress for which the ripples have small steepness, sediment transport dominates the roughness.

Once the relative roughness of the bed is known, transition criteria may be employed to classify the flow. Jonsson (1978) has suggested the following formulae as practical lower limits for the rough turbulent regime:

$$RE = 10^4 \qquad \text{if} \qquad 1 \leq \frac{\hat{A}_\infty}{k_s} \leq 10 \quad ,$$

and

$$RE = 10^3 \left(\frac{\hat{A}_\infty}{k_s}\right) \qquad \text{if} \qquad 10 \leq \frac{\hat{A}_\infty}{k_s} \leq 10^3 \quad .$$

The first of these approximate rules is for very rough walls and is based upon Sleath's (1974) criterion for "fully developed mixing". The second is for less rough walls, and is based upon the criteria of Kajiura (1968) and Kamphuis (1975). In Figs 21 and 23, the formulae of Sleath and Kajiura have been adopted to delineate the rough turbulent regime.

6.3 The wave boundary layer thickness

Having classified the oscillatory flow according to the above criteria, we are in a position to estimate the wave boundary layer thickness. Jonsson (1967, 1978) and Jonsson and Carlsen (1976) have defined the boundary layer thickness as the distance (δ_1) between the bed and the lowest level at which the velocity equals

the free-stream velocity, when this latter velocity is maximum. On this definition Jonsson (1967) has presented a graph of $(\delta_1/\hat{A}_\infty)$ as a function of RE and $(\hat{A}_\infty/k_s)$. Essentially, in laminar and smooth turbulent flows, $(\delta_1/\hat{A}_\infty)$ is a function of RE only and, in rough turbulent flow, it is a function of $(\hat{A}_\infty/k_s)$ only. In particular, for purely sinusoidal laminar flow above a smooth bed, δ_1 may be determined analytically and is given by

$$\frac{\delta_1}{\hat{A}_\infty} = \frac{\pi}{\sqrt{2\,RE}} \qquad \text{or} \qquad \delta_1 = \pi\sqrt{\frac{\nu}{2\sigma}} \ .$$

For smooth turbulent flow, Jonsson has suggested the empirical expression

$$\frac{\delta_1}{\hat{A}_\infty} \approx \frac{0.0465}{\sqrt[10]{RE}}$$

and, for rough turbulent flow, the general rule

$$30\,\frac{\delta_1}{k_s}\,\log_{10}\left(30\,\frac{\delta_1}{k_s}\right) = 1.2\,\frac{\hat{A}_\infty}{k_s} \ . \tag{5}$$

Jonsson and Carlsen (1976) have plotted (δ_1/k_s) against $(\hat{A}_\infty/k_s)$ over the range $10 < \hat{A}_\infty/k_s < 500$, and have shown that, in the rough turbulent regime, δ_1 is typically 2-4% of the excursion amplitude. These authors have emphasised that their definition is based upon velocity deviations and that, if the boundary layer is thought of as that part of the flow where shear stresses play a role, $2\delta_1$ is a more consistent measure of the thickness.

In turbulent oscillatory flow, part of the boundary layer near the bed has a velocity profile which is logarithmic, just as in steady flow. Johns (1975) has shown that the thickness of this logarithmic layer is least when the pressure gradients in the flow are maximum, and vice versa, and this has been confirmed by the analytical solution of Smith (1977, §3) based upon similarity theory. On general arguments, Smith has suggested a total boundary layer thickness of the order of $(\hat{u}_*/\sigma)$, where σ is the wave frequency and u_* is defined by $u_* = \sqrt{\tau_o/\rho_f}$, where τ_o is the bed shear stress and ρ_f is the fluid density. He has suggested, further, that the logarithmic layer has a thickness of the order of $0.02\hat{u}_*/\sigma$. For typical wind waves, it follows that turbulent boundary layers are only a few centimeters thick, with logarithmic regions of the order of 1 mm thick. In

general, therefore, the wave boundary layer is so thin that controlled field observations within it are difficult to make. In previous field experiments, Lukasik and Grosch (1963) have demonstrated directly the existence of a thin laminar wave boundary layer, by the departure of their observations from the predictions of potential theory. By comparison, Lambrakos (1982) has presented field observations which suggest boundary layer thicknesses (δ_1) in the range 0.21 to 0.76 m. These (surprisingly large) values were based upon velocity measurements made at two levels (0.69 and 1.83 m), with waves having a zero crossing period of 13.5 s and free-stream peak to trough velocity values, measured at the upper level, in the range 0.44 to 1.5 m/s.

As far as the present field experiments are concerned, there was no evidence in any of the measured velocity records of perturbations caused by the bottom boundary (except for the isolated cases of vortex motion recorded by the lowest EM-flowmeter in certain of the runs in the 1978 experiment, eg Fig 12). On the basis of the above arguments, there is little doubt that the boundary layers associated with the measured waves were, at most, a few centimeters thick. This is consistent with the impressions gained during the flow visualisation tests described in §5.1.

6.4 The wave friction factor

Various definitions of the wave drag coefficient, or friction factor, have been adopted (see Vitale (1979)), but perhaps the most common involves Jonsson's (1967) friction factor, f_w, which is defined by the equation (Eq (3))

$$\hat{\tau}_o = \tfrac{1}{2} \rho f_w \hat{U}_\infty^2 \quad ,$$

which relates the peak bed shear stress ($\hat{\tau}_o$) in a (sinusoidal) wave cycle to the peak free-stream velocity ($\hat{U}_\infty$). It should be noted that these two peak values do not occur simultaneously. For laminar flow above a smooth bed, the bottom stress ($\hat{\tau}_o$) leads the free-stream velocity ($\hat{U}_\infty$) by 45°. However, in the rough turbulent regime, the phase difference is rather less than this, and decreases with increasing ($\hat{A}_\infty/k_s$); for ($\hat{A}_\infty/k_s$) = 10^2 and 10^3, the phase differences are expected to be approximately 29° and 11°, respectively (Jonsson (1967)). Such values have been confirmed experimentally by Jonsson and Carlsen (1976) who have reported phase differences of 30° and 25° for $\hat{A}_\infty/k_s$ = 28.4 and 124, respectively. Jonsson (1967) and, more recently, Kamphuis (1975) have presented graphs in which f_w is plotted as a function of RE and ($\hat{A}_\infty/k_s$). These graphs show that f_w has the

same general behaviour as the boundary layer thickness; in the laminar and smooth turbulent regimes, f_w is a function of RE only and, in the rough turbulent regime, it is a function of $(\hat{A}_\infty/k_s)$ only. Rather little is known about the behaviour of f_w in the transitional regime, though Zhukovets' (1963) measurements suggest that it displays a complicated dependence on the Reynolds number. More recently, Sleath (1982b, 1982c) has calculated values of f_w in this regime, which are in reasonable agreement with the measurements of Kamphuis (1975).

In the laminar regime, f_w may be determined analytically and is given by

$$f_w = \frac{2}{\sqrt{RE}} \quad . \tag{6}$$

In the smooth turbulent regime, Jonsson has proposed the empirical equation

$$\frac{1}{4\sqrt{f_w}} + 2\log_{10}\left(\frac{1}{4\sqrt{f_w}}\right) = \log_{10}(RE) - 1.55 \tag{7}$$

and, in the rough turbulent regime, the equation

$$\frac{1}{4\sqrt{f_w}} + \log_{10}\left(\frac{1}{4\sqrt{f_w}}\right) = -0.08 + \log_{10}\left(\frac{\hat{A}_\infty}{k_s}\right). \tag{8}$$

Comparable equations have been proposed by Kajiura (1968) and Kamphuis (1975), and the latter equation, which implies decreasing f_w for increasing $(\hat{A}_\infty/k_s)$, has been confirmed experimentally by Jonsson and Carlsen (1976). Equation (6) should not be used for small values of the relative roughness, however; for $(\hat{A}_\infty/k_s) < 1.57$, Jonsson (1978, §5) has suggested (on the assumption that $k_s = 4\eta$ and that the representative ripple steepness $\eta/\lambda = 1/2\pi$) that the constant value $f_w = 0.30$ should be used, which is consistent with Bagnold's (1946) measurements. This is similar to the value $f_w = 0.25$ for $(\hat{A}_\infty/k_s) < 1.67$ proposed by Kajuira (1968), and to $f_w = 0.23$ for $(\hat{A}_\infty/k_s) < 1$ proposed by Grant and Madsen (1982). The range of low values of $(\hat{A}_\infty/k_s)$ for which f_w is constant is relevant in practice if the bed is rippled; in particular, it is associated with relatively inactive flows for which vortex shedding from the bed is probably not fully developed (see §2.4). On the basis of a method of universal velocity distributions, Jonsson (1978, §7) has derived a relationship between f_w and the ratio of boundary layer thickness to equivalent roughness, namely

$$f_w = \frac{0.0605}{\log_{10}^2 (27\delta_1/k_s)} .$$

This is similar to the equation which results from the elimination of $(\hat{A}_\infty/k_s)$ from Eqs (5) and (8). Vitale (1979) has proposed a further relationship between friction factor and relative roughness in the rough turbulent regime, and has noted discrepancies between values obtained for mobile sand beds, and for the fixed sand beds of Bagnold (1946), Jonsson and Carlsen (1976) and Kamphuis (1975). More recently, Grant and Madsen (1982) have suggested a procedure for the determination of the friction factor for a mobile sand bed, using a relative roughness based upon both the form drag on the ripples, and also the near-bed sediment transport. The wave friction factor has been discussed by Knight (1978) and Nielsen (1979), and also by Davies (1983, Part III).

As a result of the work of Putnam and Johnson (1949) and others, it has been widely assumed that wave friction factors of the order of 10^{-2} are appropriate in field applications. However, more recent determinations of the friction factor have produced much higher values. For example, Iwagaki and Kakinuma (1967) carried out field studies on a number of Japanese coasts, and obtained values of f_w from 0.02 to 2.32, with a median value of 0.18. Van Ieperen (1975) computed friction coefficients from wave data obtained at Melkbosstrand, S.A., and obtained values in the range 0.12-0.20. Treloar and Abernethy used prototype wave measurements and hydraulic model data to determine wave friction factors for Botany Bay, Australia, and obtained values in the range $0.006 < f_w < 0.28$ (mean 0.0886, s.d. 0.0838). The interest of these and other studies lies not only in the high values obtained for the friction factor, but also in the development of methods to analyse irregular measured wave data (see also Hsiao and Shemdin (1979)).

6.5 Analysis of the field data: the procedure to calculate the bed shear stress

The amplitude of the bed shear stress has been calculated for each measured wave half-cycle from Eq (3). For the reasons given earlier, it has been assumed that the boundary layer was confined to the layer below the upper EM-flowmeter (at heights of 130 cm and 160 cm in the 1978 and 1980 experiments, respectively), such that the measured horizontal velocity field represented the free-stream flow. As in §4, the free-stream velocity U_∞ in Eq (3) has been taken as the measured U-component of horizontal velocity, as the total velocity U_T or as the (rectilinear) rotated velocity U_{ROT}. It has been assumed throughout that, in respect of calculations of

the bed shear stress, each wave half-cycle was independent of all previous wave cycles and also, for simplicity, that each half-cycle was sinusoidal with velocity amplitude $\hat{U}_\infty$ equal to the peak value of measured velocity and half-period equal to the observed zero-crossing period (ΔT). As a result of the properties of the friction factor f_w, variations in ΔT for waves having equal velocity amplitudes may be expected to give rise to variations in the peak stress. It follows that histograms based on peak bed shear stress will be somewhat different in overall shape from those based on peak velocity (Figs 6, 7 and 9). Furthermore, in respect of the sediment transport information in the shaded parts of the new histograms, we anticipate rather less uncertainty in critical conditions for the threshold of sediment motion defined in terms of bottom stress rather than free-stream velocity, on the grounds that the stress is the more physically relevant of the two parameters.

The validity of the first of the above assumptions, of the independence of consecutive wave half-cycles, was discussed earlier. The second assumption, that each wave half-cycle was sinusoidal, is thought to be reasonably acceptable for most of the (irregular) wave cycles for which there was sediment motion. However, some wave half-cycles, usually associated with small velocity amplitude values, departed from sinusoidal curves in a very marked way. As noted in §5, in some extreme cases wave velocities had two maxima within a single half-cycle. Clearly, such waves are not susceptible to the simple treatment adopted here for the calculation of the bed shear stress. It will be recalled that half-cycles of this kind were removed from some of the histograms of calculated orbital excursion in §5. This procedure has not been adopted in establishing histograms of calculated bottom stress however, since the final results for the threshold of sediment motion are, to all intents and purposes, unaffected.

There are two ways in which Eq (3) can be applied for rippled beds. One option is that U_∞ may be taken as the measured velocity "well away" from the bed, in which case the corresponding value of the friction factor f_w must be based upon a bed roughness defined in terms either of the ripple size, or both the ripple size and the grain diameter. The calculated value of $\hat{\tau}_o$ is then the total stress on the bed (the sum of skin friction and form drag), and the calculated friction factor itself is the appropriate one to use in estimating total wave energy dissipation rates. As may be inferred from §6.2, this approach is hampered by the uncertainty which exists in the determination of the bed roughness from the ripple height. The second option which may be adopted, at least if the flow over the ripples is nonseparating (or if the bed is flat), is that U_∞ may be taken as the near-bed

velocity just above the thin wave boundary layer, as calculated from the potential flow argument discussed in §4 (see also §7). The corresponding friction factor must then be based upon a bed roughness defined in terms of the sediment grain size, and the resulting bottom stress will comprise the skin friction component of the total stress only. Since it is the skin friction which is "felt" by the grains, it is this part of the total stress which it is relevant to compare with threshold stresses determined in the laboratory on flat beds.

Analysis procedures for the two options are illustrated schematically in Fig 20. The former option involving the calculation of the total stress has been adopted for the analysis of much of the 1980 data for which the flow was frequently separating, and the latter option involving the calculation of the skin friction only has been adopted for the 1978 data for which the flow was generally non-separating. It might be noted that the assumptions underpinning the second option (Option 2) are the same as those adopted by Davies (1980a) in an earlier, more detailed, study of transitional wave boundary layer flow; in particular, not only is the flow assumed to be nonseparating, but also the boundary layer thickness is assumed to be small compared with the ripple wavelength. It was decided that Option 1 was unsuitable for analysis of the results from the 1978 experiment, for which the boundary layer thickness was generally small compared with the ripple wavelength. The reason for this was that sediment motion was observed in the region of the ripple crests only, and it was unclear how to relate the spatially averaged bottom stress calculated by Option 1 to the local bottom stress in the vicinity of the crests. The same difficulty did not arise in utilising Option 1 for analysis of the results from the 1980 experiment, since the ripples were generally of short wavelength, and bedload motion occurred over the entire rippled surface. As shown later, the total stress calculated on the basis of Option 1 was very different from the (much smaller) skin friction on the bed, due to the dominance of form drag in the 1980 experiments. It was not possible to use Option 2 to calculate the skin friction directly, on account of vortex formation and shedding above the bed during the 1980 runs.

For Option 1, the procedure adopted has been to relate the bed roughness (k_s) to the ripple height (η) by

$$k_s = C_1 \eta$$

where C_1 is a constant. Various choices have been made for C_1, namely $C_1 = 4$ as suggested by Jonsson (1967), $C_1 = 25(\eta/\lambda)$ as suggested by Nielsen (1979), and also

C_1 = 3 and 2. The resulting variations in the calculated bottom stress are discussed later. The representative semi-orbital excursion has been calculated for each wave half-cycle as in §5 from $\hat{A}_\infty = \hat{U}_\infty . \Delta T/\pi$. Hence, the representative wave Reynolds number for each wave half-cycle has been calculated from $RE = \hat{U}_\infty \hat{A}_\infty/\nu$, where ν(= 0.0131 cm^2/s) is the molecular viscosity. For the known values of RE and relative roughness ($\hat{A}_\infty/k_s$), the friction factor f_w has been determined from the following rules which, in all their essential details, are consistent with Jonsson's (1967) Fig 6. For rough turbulent flow, equation (8) has been used for $\hat{A}_\infty/k_s > 1.57$ and the constant value $f_w = 0.3$ has been adopted for $\hat{A}_\infty/k_s < 1.57$ (see §6.4). For smooth turbulent, transitional and laminar boundary layer flows, the same rules have been used for the calculation of f_w unless larger values are given by equation (7) for $RE > 3 \times 10^4$ (smooth turbulent flow), or by equation (6) for $RE < 3 \times 10^4$ (laminar flow). In practice, rather than using equation (7) as it stands, we have used the more convenient close approximation suggested by Jonsson (1967), namely

$$f_w = 0.09\ (RE)^{-0.2} . \qquad (7a)$$

It was noted earlier that the smooth turbulent regime commences, according to Jonsson (1978), at about $RE = 3 \times 10^5$. However, Jonsson's (1967) Fig 6 suggests that equation (7)(or (7a)) is acceptable down to a value of $RE = 3 \times 10^4$, whereupon the (linear) laminar rule (equation (6)) takes over without any discontinuity. It should be noted also that the procedure described above involves extrapolating rules for rough turbulent flow into the transitional regime. Although this is consistent with Jonsson's Fig 6, inspection of Kamphuis' (1975) Fig 7 suggests that this procedure may be an oversimplification, particularly for large values of the relative roughness if $RE > 3 \times 10^4$. However, very little experimental work has been carried out in the transitional regime, and the assumption adopted here is probably quite adequate. A more refined rule for the transitional regime could have been devised on the basis of the laboratory results of Sleath (1970)(see Davies (1980a)). However, since this would have unduly complicated matters, the present procedure was adopted for simplicity.

For Option 2, the procedure has been to relate the bed roughness to the grain diameter according to Kamphuis' (1975) criterion, namely $k_s = 2D_{90}$. The effects of separation above the ripples have been neglected, and the measured (uniform) horizontal velocity U_∞ has been related to the required local bed surface potential velocity U_b by

$$U_b = U_\infty \cdot C_2(x) \qquad (9)$$

where $C_2(x)$ is given as a function of horizontal position (x) by the method of Davies (1979, 1982a)(see also §4 and §7). Since sediment threshold stresses at the ripple crests were of principal interest in the analysis of the 1978 experiments, we have set $C_2 = \hat{C}_2$, the maximum value of C_2 over the ripple profile. The wave Reynolds number in each half-cycle is then given by

$$RE = \hat{C}_2^2 \cdot \frac{\hat{U}_\infty \hat{A}_\infty}{\nu} .$$

For given relative roughness $\hat{C}_2 \hat{A}_\infty / k_s = \hat{C}_2 \hat{U}_\infty . \Delta T/(2\pi D_{90})$, the skin friction component of the total stress has been determined at the ripple crest by calculating f_w for each half-cycle, on the same basis as for Option 1. The main difficulty with this approach is that the function $C_2(x)$ as given by Davies (1979, 1982a) is inappropriate if the flow is separating, as it was for a minority of the waves in the 1978 experiments (Figs 12 to 14). In §7, we assess the probable inaccuracy involved in assuming nonseparating flow throughout the 1978 experiments.

6.6 Results for the 1978 experiment

We consider initially results for the 1978 experiment, for which the bottom stress has been calculated on the basis of Option 2 above. Since we are concerned with the prediction of the bottom stress in the vicinity of the ripple crest, we have taken $C_2(x) = \hat{C}$; in particular, on the basis of the results of Davies (1979, 1982a), we have taken $\hat{C}_2 = 1.73$ for Runs 1 to 5, $\hat{C}_2 = 1.94$ for Runs 8 to 11, and $\hat{C}_2 = 1.75$ for Runs 12 to 14, the different values of $\hat{C}_2$ reflecting the slightly different ripple profiles on the respective days of the experiment. As mentioned above, we have also assumed that the bottom roughness is expressed by $k_s = 2D_{90}$. On this basis, we have classified each wave half-cycle in the experiments, with results which are shown for Runs 8 to 14 in Fig 21. This shows the plane of wave Reynolds number and relative roughness delineated into the laminar, transitional, smooth and rough turbulent regimes, according to the recommendations of Jonsson (1978) which were discussed earlier (§6.2). It may be seen that the shaded region, which encompasses all of the pairs of values of Reynolds number and relative roughness calculated for each half-cycle during Runs 8 to 14, lies predominantly in the transitional regime with only the largest waves entering the

smooth turbulent regime. It may be seen also that the waves which moved sediment were in both the transitional and smooth turbulent regimes. No waves in the experiments were in the rough turbulent regime, according to the classification method adopted. The same was true of Runs 1 to 5 for which the wave half-cycles were almost all transitional, except for a few which were smooth turbulent.

The calculated amplitudes of bottom stress corresponding to the waves in Fig 21 (also Figs 7, 13 and 14) are shown in Fig 22. The calculations have been made on the basis of the U-component of horizontal velocity measured at a height of 130 cm above the bed. (Again, from the discussion in §4, it is expected that closely similar results would have been obtained in terms of the total horizontal velocity, U_T, or the rotated component of horizontal velocity, U_{ROT}; this is confirmed in respect of the 1980 data in §6.7.) The measured velocity has been scaled by the appropriate value of $\hat{C}_2$ to give the potential velocity at the ripple crest (Eq (9)). The resulting histogram in Fig 22, which has peak stress plotted in incremental ranges on the abscissa, is less distinctly bimodal than its counterpart in Fig 7, due to the nonlinear nature of the bottom stress calculation. Estimated ranges of the amplitude of bed shear stress for both incipient and general bedload motion are given in Table 9. (There was no suspended load in the 1978 experiments.) The representative values of threshold stress for incipient and general bedload motion, analagous to the values obtained earlier for the threshold velocity amplitude from Fig 7, are about 3 and 6 dyne/cm^2, respectively. (Corresponding values of the Shields' parameter based upon the median grain diameter are $\theta' = 0.023$ and 0.046, respectively.) These values may be compared with laboratory determinations of the threshold stress of 4.1 and 7.6 dyne/cm^2 ($\theta_c = 0.032$ and 0.034) for the grain sizes $D = D_{50} = 0.078$ cm and $D = D_{90} = 0.135$ cm, respectively. The histogram results are in fair agreement at least with the former value for the median grain diameter (D_{50}), and this confirms the general validity of the present approach for the calculation of the bottom stress in nonseparating flow. It might be noted that, if a different choice is made for the bed roughness, k_s, different estimates are obtained for the critical threshold stress. For example, if the choice $k_s = D_{50}$ is made (Madsen and Grant (1976)), the calculated critical values of stress decrease by 30-40% compared with the values quoted above. If the choice $k_s = 2.5D_{50}$ is made (Nielsen (1979)), the decrease is of the order of 10-20%. It would appear, however, from a comparison with results from Shields' curve, that the choice $k_s = 2D_{90}$ provides quite as good, if not better, agreement than is obtained on the basis of these alternative representations.

The legitimacy of comparing threshold stresses calculated for unsteady flow with threshold stresses determined in steady flow in the laboratory has been

discussed by Davies (1980a, 1983). It has been shown by Madsen and Grant (1976), and Nielsen (1979), that inertia forces acting on the surface layer of sand grains in oscillatory flow are unimportant, and that the empirical Shields' criterion is applicable as a quite general criterion for the initiation of motion in oscillatory flow, provided that the bottom stress is properly evaluated. In practice, Madsen and Grant have used Jonsson's (1967) friction factor to calculate the bed shear stress and, on this basis, have replotted the experimental sediment threshold data of Bagnold (1946), Manohar (1955) and others, on a modified Shields' diagram. Similar comparisons have been made by Komar and Miller (1975) and, in both cases, the agreement between experimental results obtained in unsteady flow, and Shields' curve for steady flow, is good. It should be emphasised that, by adopting Option 2 in the present comparisons, we have calculated the skin friction on the bed, that is the force acting directly on the exposed layer of sand grains. Clearly, it is this component of the total stress which must always be compared with results from Shields' curve. This point is reinforced by the results in §6.7 for the 1980 experiment.

In §6.5, it was suggested that there should be rather less uncertainty in critical conditions for the threshold of sediment motion determined in terms of bottom stress, rather than free-stream velocity, on the grounds that the stress is the more physically relevant of the two parameters. However, inspection of Figs 7 and 22 suggests that, while the overall shapes of the histograms are rather different, there is quite as much uncertainty in the definition of critical threshold motion conditions in the one case as in the other. It has been found that this uncertainty persists if the bottom roughness is taken as $k_s = D_{50}$ or $k_s = 2.5D_{50}$ as suggested by Madsen and Grant (1976) and Nielsen (1979), respectively. This is a less satisfactory outcome than that achieved by Davies (1980a). In this earlier work, bottom stresses were calculated for waves in the transitional regime by a more refined argument than that used here, with the result that the definition of threshold motion conditions was significantly better in terms of bottom stress than free-stream velocity. As seen in §5, the flow was separating in certain of the wave cycles in the present experiment, and this has introduced some uncertainty into the results in Fig 22 for reasons which are discussed in detail in §7. Evidently, the use of Eq (3) for the calculation of the bottom stress, subject to the assumptions which have been made in Option 2, is adequate only up to a point. Whatever approach is adopted, however, it is unrealistic to hope to eliminate entirely the uncertainty in sediment threshold motion conditions by refining the physical arguments, since much of this uncertainty arises for sedimentological and other reasons.

6.7 Results for the 1980 experiment

We consider next results for the 1980 experiment, for which the bottom stress has been calculated on the basis of Option 1. Various choices have been made for the equivalent bed roughness, namely $k_s = 4\eta$, $25(\eta/\lambda)\eta$, 3η and 2η. In practice, since it was difficult to estimate the ripple height η adequately in the field, it has been assumed for most of the calculations that the (equilibrium) ripple steepness was such that the ripple height was one seventh of the measured ripple wavelength. The values (η') calculated in this way were generally less than the equivalent measured values (η) (see Table 10). In addition, the calculations of stress have been based not only on the U-component of horizontal velocity measured in the free-stream flow, but also on the total horizontal velocity U_T and on the rotated component of horizontal velocity U_{ROT}. Each wave half-cycle in the experiments has been classified according to its Reynolds number (RE) and relative roughness ($\hat{A}_\infty/k_s$). Flow classification results for the same representative runs as were presented in Fig 9 are shown in Fig 23, together with associated histograms of calculated bed shear stress. The results in Fig 23 are for $k_s = 25(\eta/\lambda)\eta \approx 3.57\eta'$, and have been based upon the U-component of horizontal velocity measured at a height of 160 cm above the bed. It may be seen that, on account of the very much lower values of relative roughness than those in Fig 21, the boundary layer in the 1980 experiments was either transitional or rough turbulent. Moreover, the wave half-cycles which moved sediment were almost exclusively in the rough turbulent regime. This essential distinction between conditions in the 1978 and 1980 experiments is associated with the often-separating flow above the rippled beds in the latter experiments.

The results shown in histogram form in Fig 23 indicate calculated total stresses which are an order of magnitude larger than the stresses in Fig 22. Such large values are obtained whatever the choice of k_s, as may be seen in Table 10 in which estimated ranges of the amplitude of the bed shear stress are presented for each sediment motion type (cf Table 5). Although there is a significant increase in calculated stress values as k_s is increased (from, say, $2\eta'$ to $4\eta'$), the variations involved are not as great as the order of magnitude difference which distinguishes the present results from those for the 1978 experiment. In Fig 23, results for $k_s = 3.57\eta'$ are presented as representative of the middle of the range of k_s values examined. This seems a plausible choice for k_s, both on the basis of the present results and also those of other workers. In addition, the results shown are based only on the U-component of measured horizontal velocity; it may be seen from Table 10 that results based upon the total or rotated component of horizontal

velocity are closely similar in every case. Again, as for the results of the 1978 experiment, much uncertainty remains in the definition of critical conditions at the threshold of motion. This arises for the same reasons as were discussed earlier.

The results obtained suggest that the total stress is an order of magnitude greater than the skin friction; this may be demonstrated by comparing calculated total stresses in wave half-cycles which just moved sediment, with known values of the threshold stress from Shields' curve. For the results in Fig 23, the total stress at the threshold of bedload motion may be seen to have been about 30 dyne/cm^2, which may be compared with the much lower representative (skin friction) threshold stresses from Shields' curve of 2.0 dyne/cm^2 for $D = D_{50} = 0.026$ cm, or 3.3 dyne/cm^2 for $D = D_{90} = 0.062$ cm. This discrepancy suggests that form drag makes a dominant contribution to the total shear stress on a rippled bed in oscillatory flow. In this respect, oscillatory flow differs from steady flow for which form drag and skin friction are generally considered to be about equal. The essential qualitative difference between the two cases is that, in oscillatory flow, the vortices formed above a rippled bed are shed into the flow in each wave half-cycle whereas, in steady flow, the vortices remain trapped above the bed. An adequate knowledge of the process of vortex formation and shedding above the bed is clearly necessary if the nature of the bottom stress is to be fully understood. The processes involved are important also in respect of the entrainment and suspension of sand grains. (It may be noted that very approximate values of the total threshold stress for sediment suspension are obtainable from the histograms in Fig 23, and from the results in Table 10.) With a view to attaining an improved understanding of the nature of vortices formed above a rippled bed and, in particular, to explaining some of the uncertainty in the definition of sediment threshold motion conditions (at least in the 1978 experiments), we develop in §7 a simple irrotational model of the structure of a vortex above a rippled surface.

§7 A MODEL OF THE VORTICES FORMED ABOVE A RIPPLED BED

7.1 General background

In order to gain a working understanding of the nature of the velocity field in separating flow over a rippled bed, a two-dimensional "standing vortex" model has been developed, based upon methods of classicial potential flow theory. The general aim has been to calculate near-bed velocities in relation to the outer velocity well above the bed, and to examine the implications of the results for sediment transport and the total drag on the seabed in oscillatory flow. In

practice, since a steady state model has been adopted, the results are expected to apply only for that part of each wave cycle in which the free-stream velocity is near its maximum value, and in which a vortex is fully formed above the lee slope of each ripple. Despite this shortcoming, the results obtained illuminate some of the comments made in §6 concerning the calculation of the bottom stress. The use of a two-dimensional model in connection with the present field experiments is justified by the fact that the observed ripples were generally long-crested.

A description of the phenomenon of vortex formation and shedding above a rippled sand bed has been given by Tunstall and Inman (1975) (see §2). These workers proposed a steady state "standing vortex" model for the flow above a rippled bed, and justified the use of this model in unsteady cases on the basis of experimental results. Although we adopt here a simple extension of Tunstall and Inman's model, it should be emphasised that it is a model which is more appropriate for steady, than for unsteady, flows for reasons which will be clear later. We start by treating the flow over ripples as a problem in potential theory, and determine the streamlines and the near-bed velocity field for both separating and nonseparating flow. We then calculate the energy contained in the near-bed vortices; here we introduce a rotational core into each vortex, which merges with the outer irrotational flow such as to give a physically meaningful representation for each vortex. Throughout the discussion, we compare results obtained by the approach of Tunstall and Inman (and, more recently, Shibayama and Horikawa (1980)), who assumed only one vortex in the entire flow field, with results obtained by the present more general approach in which we assume one vortex in the flow per ripple wavelength. This latter approach has been adopted also by Sawamoto and Yamaguchi (1979).

7.2 The conformal mapping procedure

We start the discussion of the potential flow aspect of the problem with some considerations of the conformal mapping method. The flow in the physical z-plane is approximated by a steady two-dimensional potential flow of an incompressible inviscid fluid, and the flow area in the physical plane is considered as the one-to-one conformal image of the upper half of the transform ζ-plane. The mapping function is denoted by

$$z = f(\zeta)$$

where $z = x + iy$ and $\zeta = \xi + i\chi$. The function $f(\zeta)$ is chosen such that $\zeta = \infty$ and

$z = \infty$ are corresponding points; that is, $f'(\zeta) = 1$ for $\zeta = \infty$. Such a function is suitable for a "deep" flow, that is a flow without a free surface. The mapping function adopted by Tunstall and Inman (1975), and which is used here (see also Davies (1979, 1983)), is as follows:

$$z = \zeta + ib\, e^{i\ell\zeta} . \tag{10}$$

If the (impermeable) bed surface ($y = y_b$) is defined as $\chi = 0$, then

$$y_b = b \cos \ell\xi , \tag{11}$$

where $b(= \eta/2)$ is the ripple amplitude and $\ell(= 2\pi/\lambda)$ is the ripple wavenumber. For small b, $x \approx \xi$ and the bed is purely sinusoidal in the original coordinates. However, for increasing values of b, the ripple crests become more and more peaked, and the troughs flatter and longer, in accordance with the profiles of natural sand ripples.

The flow above the rippled bed (11) is given by the complex potential

$$\Omega = \phi + i\psi ,$$

where ϕ is the velocity potential and ψ the streamfunction. It should be noted that the values of ϕ, ψ and, hence, Ω are unchanged by the transformation; that is, values of these quantities are equal at corresponding points in the two planes. The velocity components (u, v) $(=(-\phi_x, -\phi_y))$ in the x and y directions, respectively, are given at any point of the z-plane by

$$u - iv = -\frac{d\Omega}{dz} = -\frac{1}{f'(\zeta)}\frac{d\Omega}{d\zeta} . \tag{12}$$

From (12), it may be seen that the velocity components (u_Q, v_Q), at a typical point Q in the z-plane, are related to the velocity components (u_P, v_P) at the corresponding point P in the ζ-plane by

$$u_Q - iv_Q = (u_P - iv_P)/f'(\zeta) . \tag{13}$$

It follows from (10) and (13) that

$$u_Q = J\{u_p(1 - b\ell e^{-\ell x}\cos \ell\xi) + v_p(b\ell e^{-\ell x}\sin \ell\xi)\}$$

$$v_Q = J\{v_p(1 - b\ell e^{-\ell x}\cos \ell\xi) - u_p(b\ell e^{-\ell x}\sin \ell\xi)\} \qquad (14)$$

where J, the Jacobian of the transformation, is given by

$$J = \frac{\partial(\xi,\chi)}{\partial(x,y)} = \{1 - 2b\ell e^{-\ell x}\cos \ell\xi + (b\ell e^{-\ell x})^2\}^{-1}.$$

The case of nonseparating flow above a rippled bed is modelled in the upper ζ-half plane simply by a stream of speed U_o parallel to the ξ-axis, for which the complex potential is expressed by

$$\Omega = -U_o\zeta \,. \qquad (15)$$

The case of separating flow above a rippled bed is modelled by superimposing on this underlying motion of a row of potential vortices, also parallel to the ξ-axis and in the upper ζ-half plane. Since we require the ξ-axis to be a streamline (Eq (11)), a symmetrical vortex must be placed at the complex conjugate point in the lower ζ-half plane for each vortex in the row. By mapping the upper ζ-half plane into the physical z-plane according to (10), for either nonseparating or separating flow, the streamlines in the flow area in the z-plane are obtained as images of the streamlines in the upper ζ-half plane. It should be noted that the strengths of the vortices are not changed by the mapping.

7.3 Solutions for a single vortex pair and a row of vortex pairs

Before stating the complex potential for the case in which there is a row of vortices in the upper ζ-half plane, it is convenient to summarise the results of Tunstall and Inman (1975) with which we shall later make certain comparisons. Tunstall and Inman assumed there to be only one vortex in the upper ζ-half plane. In particular, they assumed separating flow over just one ripple as the result of a vortex of strength κ at $\zeta = \zeta_o$, and nonseparating flow over all the other ripples given by (11). For this configuration (see sketch), the complex potential is expressed by

$$\Omega = -U_0 \zeta - i\kappa \log\left\{\frac{\zeta - \zeta_0}{\zeta - \bar{\zeta}_0}\right\}. \qquad (16)$$

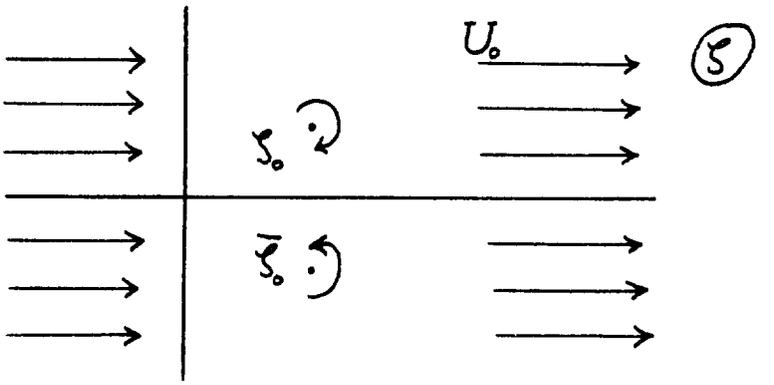

The associated velocity components $(\tilde{u}, \tilde{v})$ in the transform plane are given by

$$\tilde{u} - i\tilde{v} = -\frac{d\Omega}{d\zeta} = U_0 + \frac{i\kappa}{\zeta - \zeta_0} - \frac{i\kappa}{\zeta - \bar{\zeta}_0} .$$

The condition for the vortex at $\zeta = \zeta_0$ to be a stationary or "standing" vortex is obtained by removing from the above expression the contribution associated with the vortex at ζ_0, and setting the resulting complex velocity, evaluated at ζ_0, to zero; that is

$$-\frac{d}{d\zeta}\left\{\Omega + i\kappa \log(\zeta - \zeta_0)\right\}\Big|_{\zeta=\zeta_0} = 0 ,$$

from which it follows that

$$U_0 = i\kappa/(\zeta_0 - \bar{\zeta}_0) .$$

Since $\zeta = \xi + i\chi$, we have $\zeta_0 - \bar{\zeta}_0 = 2i\chi_0$, and so the condition for the vortex at $\zeta = \zeta_0$ to be a standing vortex is

$$U_0 = \kappa/2\chi_0 . \qquad (17)$$

In mapping the flow in the ζ-plane into the z-plane, it should be noted that, if the vortices are not standing vortices, they will not in general move so as to continue to occupy corresponding points in the two planes. However, in the event of the vortices being standing vortices, no such difficulty arises, since a stagnation point within the upper ζ-half plane is transformed into a stagnation point within the z-plane, and vice versa.

In practice, the transformation from the ζ-plane to the physical z-plane is arranged such that the vortex at $\zeta = \zeta_0$ lies above the lee slope of one of the

ripples given by (11). Tunstall and Inman (1975) have determined experimentally that the radius of a vortex is about 0.6 times the ripple height (2b), so that $\chi_o = 1.2b$. For naturally formed ripples, they have found also that the vortex lies at a point above the bed which corresponds approximately to the phase position $\ell\xi = \pi/2$ in Eq (11). This is convenient since it implies that the height of the vortex centre from the bed does not change very much as a result of the mapping; in particular, $|\frac{dz}{d\zeta}| \approx 1.006$ at $\ell\xi = \pi/2$ for typical values of ripple steepness ($b\ell = \pi/7$) and observed vortex height ($\chi_o = 1.2b$). It follows that the value of χ_o in the transform plane may be used also in the physical plane ($y_o \approx \chi_o$).

Consider next the case in which there is a row of vortices in the flow area, one vortex of strength κ above the lee slope of each ripple. For convenience, we take the vortex separation to equal a which, unless stated otherwise, will equal the ripple wavelength λ. We now require the complex potential of an indefinitely long row of vortex pairs in the ζ-plane, as shown in the sketch.

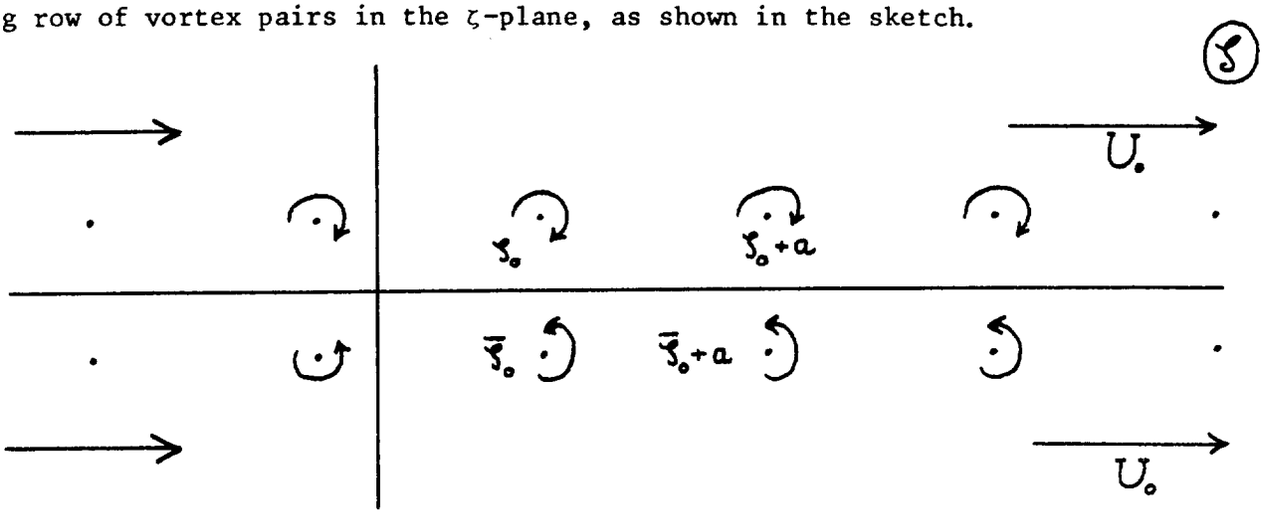

The complex potential of the (2n + 1) vortices in the upper row, centred on ζ_o, may be expressed by

$$\Omega_n = -i\kappa \log(\zeta-\zeta_o) - i\kappa \log(\zeta-(\zeta_o+a)) - \cdots - i\kappa \log(\zeta-(\zeta_o+na))$$
$$- i\kappa \log(\zeta-(\zeta_o-a)) - \cdots - i\kappa \log(\zeta-(\zeta_o-na)).$$

Omitting a constant term, we may rewrite this in the form

$$\Omega_n = -i\kappa \log\left\{\frac{\pi(\zeta-\zeta_o)}{a}\left(1-\frac{(\zeta-\zeta_o)^2}{a^2}\right)\left(1-\frac{(\zeta-\zeta_o)^2}{2^2a^2}\right)\cdots\left(1-\frac{(\zeta-\zeta_o)^2}{n^2a^2}\right)\right\}.$$

Since sin x can be expressed in the form of an infinite product (Milne-Thomson, 1968, §13.71), namely

$$\sin x = x\left(1 - \frac{x^2}{\pi^2}\right)\left(1 - \frac{x^2}{2^2\pi^2}\right)\cdots\left(1 - \frac{x^2}{n^2\pi^2}\right)\cdots\cdots ,$$

it follows that, if we let $n \to \infty$, we obtain for the upper row the complex potential

$$\Omega_u = -ik \log \sin\left\{\frac{\pi}{a}(\zeta - \zeta_0)\right\} , \qquad (18)$$

and, similarly, for the lower row

$$\Omega_L = ik \log \sin\left\{\frac{\pi}{a}(\zeta - \bar{\zeta}_0)\right\} . \qquad (19)$$

If we superimpose (18), (19) and the complex potential for a steady stream in the $+\xi$ direction, we obtain the final result

$$\Omega = -U_0\zeta - ik \log \sin\left\{\frac{\pi}{a}(\zeta - \zeta_0)\right\} + ik \log \sin\left\{\frac{\pi}{a}(\zeta - \bar{\zeta}_0)\right\} . \qquad (20)$$

The associated velocity components $(\tilde{u}, \tilde{v})$ in the transform plane are given in this case by

$$\tilde{u} - i\tilde{v} = -\frac{d\Omega}{d\zeta} = U_0 + \frac{i\pi k}{a}\cot\left\{\frac{\pi}{a}(\zeta - \zeta_0)\right\} - \frac{i\pi k}{a}\cot\left\{\frac{\pi}{a}(\zeta - \bar{\zeta}_0)\right\} .$$

To arrive at the condition for the vortices in the upper row to be standing vortices, we need only calculate velocity components based on the steady stream and the lower row, since the upper row induces no motion in itself. If we consider the typical vortex at ζ_0 in the upper row, the required condition may be expressed by

$$-\frac{d}{d\zeta}\left\{-U_0\zeta + ik \log \sin\left\{\frac{\pi}{a}(\zeta - \bar{\zeta}_0)\right\}\right\}\Bigg|_{\zeta = \zeta_0} = 0 ,$$

from which it follows that

$$U_0 = \frac{k\pi}{a}\coth\left(\frac{2\chi_0\pi}{a}\right) . \qquad (21)$$

It may be noted that (17) is recovered from (21) as the vortex spacing a tends to infinity. As far as a mapping of the ζ-plane on to the z-plane is concerned, the

same considerations apply as in the simpler case of the vortex pair. We now illustrate some results obtained on the basis of (16) and (20) in both the transform and physical planes.

7.4 Streamlines and velocity components

In the examples which follow, we adopt the typical equilibrium ripple steepness $b\ell = 0.15\pi$. The complex potential is normalised throughout by $U_o a$, where a is equal to the ripple wavelength λ, such that

$$\bar{\Omega} = \bar{\phi} + i\bar{\psi} = \frac{\Omega}{Ua} \quad . \tag{22}$$

For nonseparating flow, the complex potential is given by Eq (15), which corresponds to the streamlines shown in Fig 24 for both the transform and physical planes. In the physical plane, the streamlines near the bed converge over the ripple crests and diverge over the troughs while, away from the bed, they are unperturbed. The associated bed surface velocity components (u, v) in the physical plane are shown in normalised form in Fig 25, together with the tangential bed velocity u_T defined by

$$u_T = \sqrt{u^2 + v^2}\ \mathrm{sgn}(u) .$$

The procedure adopted to determine the velocity components was, firstly, to calculate the components in the transform plane from (12), and then in the physical plane from (14). As expected from the streamlines in Fig 24, the peak value of velocity is attained at the crest position ($\ell x = 0$) where $u/U_o = u_T/U_o = 1.891$, and the minimum value is attained in the trough where $u/U_o = u_T/U_o = 0.680$.

Equivalent results for the complex potential (16), corresponding to a single standing vortex pair in a steady stream, are shown in Figs 26 and 27. Physically, this example is somewhat artificial, since experimental observation suggests that vortices are formed simultaneously above many sand ripples. However, it is of interest because it is the case examined by Tunstall and Inman (1975). In accordance with the earlier comments, the single vortex in the transform plane has been placed at $\ell\xi_o = \pi/2$, $\ell\chi_o = 0.18\pi$ ($\chi_o = 1.2b$, $b\ell = 0.15\pi$), with strength κ satisfying (17). Again, the complex potential has been normalised according to (22). The streamlines in both the transform and physical planes comprise a single trapped circulation cell centred on the vortex, and an outer streaming flow which passes over the trapped cell. (Note that the streamlines in the lower ζ-half plane

(not shown) are the image of those shown for the upper ζ-half plane corresponding to the flow area.) The region of separating flow may be seen to lie over the lee slope of the ripple ($0 < \ell x < \pi$); the stagnation points at which the zero streamline separates from, and then rejoins, the bed are a little way downstream of the crest, and upstream of the trough, respectively. Interestingly, the perturbation in the outer flow resulting from the presence of the single standing vortex pair may be seen to be quite significant up to heights $\ell\eta$, $\ell y > \pi$, in contrast to the streamlines in Fig 24 which were effectively unperturbed at heights greater than half a ripple wavelength above the bed ($\ell y > \pi$). The surface velocity components (u, v), and the tangential velocity u_T, reveal comparatively low velocities in the region of the crest; the peak velocity in the positive direction is attained some way upstream from the crest itself. The surface velocity field in $-\pi < \ell x < \pi$ (Fig 27) is dominated by large negative velocities on the lee slope of the ripple. These large velocities are associated with relatively low surface pressures and, consequently, with form drag on the ripple in the downstream (+x) direction. It might be noted, finally, that the vertical surface velocity in $-\pi < \ell x < \pi$ is almost everywhere positive, the flow being almost everywhere directed towards the crest position. This is clearly important in cases in which the bed is erodible.

Next, results for complex potential (20), corresponding to an infinite row of standing vortex pairs in a steady stream, are shown in Figs 28 and 29. The vortices are now positioned at $\ell\xi_o = \pi/2 \pm 2m\pi$ (m = integer) and $\ell\chi_o = 0.18\pi$, with $b\ell = 0.15\pi$ and κ satisfying (21). In many respects, the results are similar to those in Figs 26 and 27. However, they are more realistic on account of the presence of a region of separating flow above the lee slope of each ripple. The streamline pattern in Fig 28 reveals a far less pronounced "doming" above each vortex than was apparent for $\ell\eta$, $\ell y > \pi$ in Fig 26. Again, the region of separating flow is confined to the lee slope of each ripple; for the lee slope in $0 < \ell x < \pi$, the stagnation points on the bed are at $\ell x = 0.326$ and 2.294. The associated surface velocity components in Fig 29 reveal rather lower peak positive and negative velocity values than those in Fig 27. The peak positive value of tangential velocity is $u_T/U_o = 1.026$ at $\ell x = -0.172$, which is some way upstream from the crest position $\ell x = 0$ at which $u/U_o = u_T/U_o = 0.900$. The peak negative value of velocity is $u_T/U_o = -2.482$ on the lee slope at $\ell x = 1.053$. In the trough ($\ell x = \pm\pi$), the velocity is relatively small and is in the +x direction, namely $u/U_o = u_T/U_o = 0.323$. In Table 11 are listed various values of peak surface velocity, equivalent to (and including) those values quoted above, obtained with an

infinite row of standing vortex pairs and with the ripple steepnesses $b\ell = 0.05\pi$, 0.1π, 0.15π and 0.2π. While the case $b\ell = 0.15\pi$ is physically the most interesting, since it corresponds to natural equilibrium ripples, the cases $b\ell = 0.1\pi$ and 0.2π are probably also physically relevant. As far as the results for separating flow are concerned, only for the case $b\ell = 0.05\pi$ in which the ripple steepness is small are the results probably physically irrelevant. Included in the table, for the case of separating flow, are the (non-peak) values of velocity in the troughs, and the positions of the stagnation points on the bed in $0 < \ell x < \pi$. Also included are peak surface velocity results at the crest and trough positions for nonseparating flow; these results are probably physically relevant only in the range $0 \lesssim b\ell \lesssim 0.1\pi$. One point of interest in the results is that the peak value of negative surface velocity in the separating case decreases, and its position migrates towards the crest, as $b\ell$ increases. Likewise, the position of the peak value of positive surface velocity migrates towards the crest as $b\ell$ increases (at least for $b\ell > 0.1\pi$). The separating region itself occupies a progressively greater proportion of the lee slope of the ripple the greater is the steepness ($b\ell$), as may be seen from the positions of the stagnation points.

Nielsen (1981) has noted that "the lee vortex is able to erode the trough as strongly as the mean flow erodes the crest". This comment is not very well supported by the results in Table 11, which indicate that the peak negative bed velocity beneath the vortex is more than double the peak positive bed velocity on the stoss face of the ripple, whatever the ripple steepness. This suggests the dominance of the erosion of the troughs in separating flow, rather than the erosion of the crests, as expected for stable (equilibrium) bedforms. Furthermore, from the tabulated results, it would appear that the ability of vortices to erode the troughs diminishes sharply as the ripple steepness increases. This is consistent with the development of an equilibrium profile with an intermediate value of steepness $0(0.15\pi)$. As far as the present field experiments are concerned, it was noted in §6.5 that inaccuracy was introduced into calculations of the bottom stress for the 1978 experiment by assuming that the flow was <u>always</u> nonseparating. A compari- of results in Table 11 for the surface crest velocities ($\ell x = 0$), in separating and nonseparating flow, indicates a very substantial difference in crest velocity, which increases with increasing ripple steepness. A more consistent definition of the critical stress at the threshold of sediment motion might have been achieved had proper allowance been made for this in the calculations for wave half-cycles during which flow separation was observed.

In Fig 30, vertical profiles of horizontal velocity are plotted for the crest and trough positions. The cases of a single vortex pair and an infinite row of vortex pairs are treated separately and, in each case, the results are compared with those for nonseparating flow over a rippled bed of the same steepness ($b\ell = 0.15\pi$). In the case of a single vortex pair, the profiles are for the crest ($\ell x = 0$) and trough ($\ell x = \pi$) positions immediately upstream and downstream of the single region of separating flow, respectively. In the case of the infinite row of vortices, the profiles apply to any crest or trough position. Near the bed, the profiles for separating and nonseparating flow are very different, at both crest and trough positions. The large surface velocities at the crest do not occur in the separating case (see Table 11), and much lower surface velocities occur at the troughs in separating flow than in nonseparating flow. Away from the bed the profiles tend to the unperturbed value $u/U_o = 1$, though they do so rather more slowly for the case of a single vortex pair than for the infinite row. In the latter case, the height of influence of the vortex row is about half a ripple wavelength (λ) above the bed, as in nonseparating flow (see Davies (1983)). Sawamoto (1980) has suggested, on the basis of laboratory measurements of separating flow over ripples, that velocity profiles over the stoss slope of a ripple agree with those given by potential theory for nonseparating flow. The results in Fig 30 suggest that this is not the case in the region of the crest. Moreover, a comparison of the surface velocities in Figs 25 and 29, for nonseparating and separating flow respectively, indicates a substantially larger bed velocity in the former case over the entire stoss slope.

Finally, in Fig 31, tangential surface velocities are presented to illustrate the effects of varying the vortex position. In Figs 24 to 30, it has been assumed that $\chi_o = 1.2b$ and that the centre of the vortex in $-\pi < \ell x < \pi$ lies above $\ell\xi_o = \pi/2$. Tunstall and Inman (1975) suggested bounds of $1.0b \leq \chi_o \leq 1.4b$ for the height of the vortex centre above the bed, and it was therefore thought useful to establish here how sensitive are the predicted bed velocities to small changes in χ_o. The cases of both a single and an infinite row of vortex pairs have been examined, the standing vortex criteria being Eqs (17) and (21), respectively. (In the former case, the results again apply only to $-\pi < \ell x < \pi$ and, in the latter case, to any ripple wavelength.) In Fig 31, results are presented for the maximum variations in vortex position permitted by the above bounds, and these new results are compared with the appropriate curves from Figs 27 and 29. The results shown are, firstly, for an upward shift in the vortex position from $\ell\chi_o = 0.18\pi$ ($\chi_o = 1.2b$) to $\ell\chi_o = 0.21\pi$ ($\chi_o = 1.4b$) with $\ell\xi_o = 0.5\pi$ and, secondly, for a sideways shift of

the same magnitude from $\ell\xi_o = 0.5\pi$ to 0.47π with $\ell\chi_o = 0.18\pi$. The variations in tangential surface velocity resulting from the change in vortex position are surprisingly small in both cases. Moreover, the results are closely similar for both a single vortex pair and an infinite row of vortex pairs. Equivalent small variations (though in the opposite sense in each case) are found if the vortex centre is shifted downwards or to the right. From these results, it may be concluded that the surface velocity field is relatively insensitive to the exact position of the vortex above the lee slope of the ripple.

7.5 Calculation of the vortex energy

In order to assess how generally valid is the model described above in the context of oscillatory flow above a rippled bed, we turn next to some considerations of the vortex energy. From their calculations of vortex energy, Tunstall and Inman (1975) produced the surprising result that only 7% of the wave energy dissipated above a rippled seabed is attributable to vortex formation and shedding. They suggested that most of the energy loss (80-85%) is associated with shear stresses within the boundary layer. This conclusion is in marked disagreement with that reached in §6 in connection with the 1980 experiment, where it was suggested that the present field results are consistent with an order of magnitude difference between the (larger) form drag and (smaller) skin friction components of the total stress acting on the bottom ripples. It is in disagreement also with the results of Longuet-Higgins' (1981a) fully time-dependent analysis in which vortices are formed and shed above the rippled bed in each wave half-cycle (see §2.4). This suggests that the formulation of the problem adopted by Tunstall and Inman may be deficient in certain important respects. In order to establish whether their steady state analysis is deficient for any reasons other than unsteadiness in the flow, a detailed re-calculation of their results has been undertaken. The aim of this has been to assess how sensitive is their result for the vortex energy to small changes in the vortex position above the bed, to small changes in the size of the vortex core, and also to the presence of a row of vortices above the rippled bed (as opposed to the single vortex in the entire flow field assumed by Tunstall and Inman).

Tunstall and Inman found that the energy bound up in a vortex depends upon three parameters, namely the height of the vortex centre above the bed (χ_o), the vortex strength (κ) and the radius of the vortex core. The values of these parameters depend, in turn, upon the ripple dimensions. We proceed by assuming that each potential vortex has a rotational core of radius (a_r), such that if the

angular velocity of the rotating core is ω, the vortex strength is $\kappa = \omega a_r^2$. This overcomes the physical difficulty presented by the existence of a singularity at the centre of each vortex in the earlier irrotational analysis. Tunstall and Inman justified their partitioning of the flow into a rigid body rotating core within an irrotational outer flow, with reference to experimental measurements. The procedure has been adopted also by Longuet-Higgins (1981a) and is discussed fully by Milne-Thomson (1968, § 13.10). The analysis of potential plus rotational core vortices is convenient in the present context due to the relative ease with which the energy of such vortices may be calculated. In this section, we follow Tunstall and Inman in assuming that the strengths of vortices generated above the lee slopes of ripples under oscillatory conditions are the same as would occur in steady flow. Thus we base our calculation of the wave energy dissipation rate in oscillatory flow on an assumed quasi-steady flow. In particular, we assume that the vortex energy loss per wave period is given by the product of the energy of each vortex times twice the number of ripples present (since two vortices are formed per period, one on each side of the ripple crest).

The vortex energy in the steady state model is calculated by considering the irrotational and rotational regions of the flow separately. In general, the kinetic energy (T_k) of a fluid is given by

$$T_k = \frac{1}{2} \int_{V_f} \rho_f q^2 \, dV_f \quad , \tag{23}$$

where V_f is the volume of the fluid and q is the fluid speed. In calculating the kinetic energy in the upper ζ-half plane due to the presence of vortices, we initially exclude the inner rotational core of the vortex. Ultimately, the total vortex energy is given by the sum of the separate contributions from the outer irrotational, and inner rotational, flow regions.

7.6 Calculation for the irrotational flow region

For irrotational flow, the fluid speed is such that

$$q^2 = u^2 + v^2 = \phi_x^2 + \phi_y^2 = (\nabla\phi)(\nabla\phi) \, ,$$

and hence, by Green's theorem, Eq (23) may be written

$$T_{kI} = -\frac{\rho_f}{2}\int_S \phi \frac{\partial \phi}{\partial N}\, dS \,, \tag{24}$$

where S is the surface enclosing the fluid, N is the inward directed normal to that surface and the subscript I denotes the irrotational flow region. For two-dimensional flow, the integral in (24) may be reduced to a line integral around the boundary of the flow, times the width of the flow (w), such that

$$T_{kI} = -\frac{\rho_f w}{2}\oint \phi \frac{\partial \phi}{\partial N}\, ds \,. \tag{25}$$

Using the Cauchy-Riemann conditions, we may rewrite (25) in the form

$$T_{kI} = \frac{\rho_f w}{2}\oint \phi \, d\psi \,, \tag{26}$$

which we evaluate to obtain the kinetic energy of the potential flow region. It might be noted that, in a conformal transformation, the kinetic energy of two equivalent flow regions is unchanged and so, for convenience, we perform the calculations which follow for the relatively simple case of the transform plane.

The irrotational vortex energy for a typical ripple wavelength is computed by evaluating the integral in (26) around the path shown in the diagram below. Note that this path excludes the rotational core of radius a_r around the vortex at $\zeta = \zeta_o$ $(= \xi_o + i\chi_o)$, and that the vertical lines AB and GH are separated by the horizontal vortex spacing (a), with points A and H at $\chi = \infty$. The contour used here differs from that of Tunstall and Inman, who simply evaluated the kinetic energy in the entire upper ζ-half plane, excluding only the single rotational vortex core in the flow area. Since the argument which follows is similar to that of Tunstall and Inman (1975) (see also Tunstall (1973)), its full details are not discussed here. Essentially, along BC and FG, the value of the integral is zero since these are streamlines ($d\psi = 0$). On the boundary of the vortex core DE (assumed circular in the ζ-plane) the integral is zero for the same reason. Since along HA the velocity (at infinity) is the free-stream velocity U_o, it follows that, as far as vortex energy is concerned, the contribution from the integral is

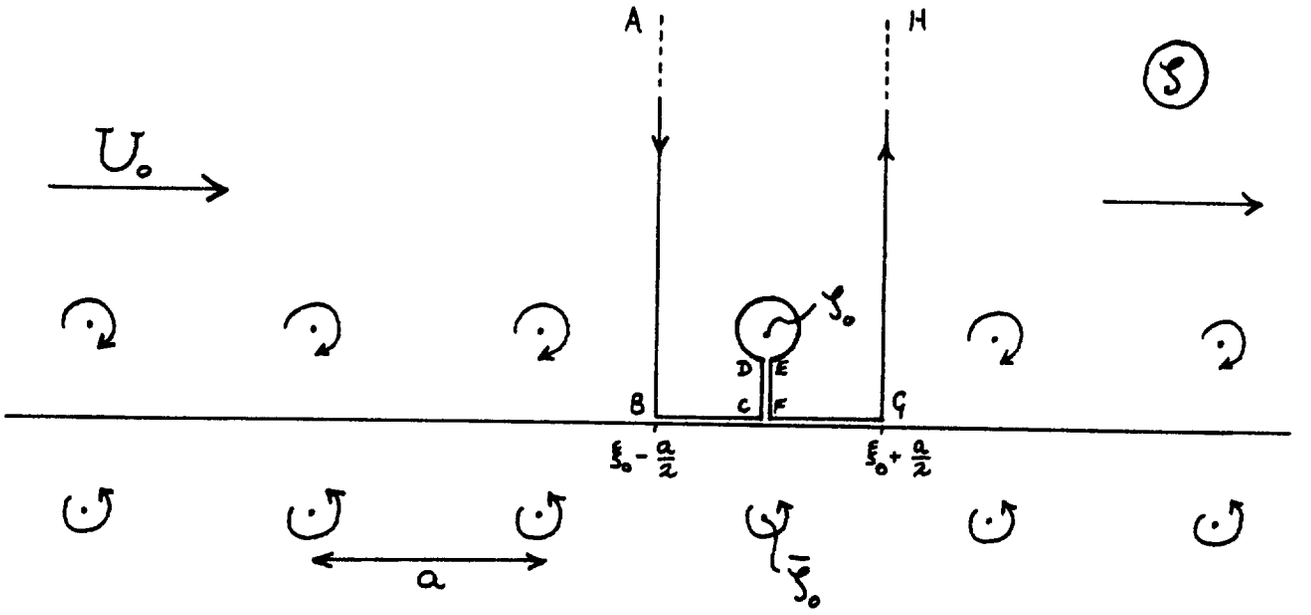

also zero. Finally, on account of the symmetrical arrangement of vortices, the sum of the contributions to the vortex energy from AB and GH is zero. This reduces the expression for the kinetic energy to

$$T_{kI} = \frac{\rho_f w}{2}\left[\int_{CD} + \int_{EF} \phi\, d\psi\right]. \qquad (27)$$

Following Tunstall(1973), we define

$$\zeta = +e^{i\theta}, \quad \zeta - \zeta_o = +_o e^{i\theta_o}, \quad \zeta - \zeta_n = +_n e^{i\theta_n},$$
$$\zeta - \bar{\zeta}_o = R_o e^{i\lambda_o}, \quad \zeta - \bar{\zeta}_n = R_n e^{i\lambda_n},$$

where the subscript n denotes the nth vortex in either the upper or lower row, centred on the vortices at ζ_o and $\bar{\zeta}_o$ respectively, and we write the complex potential (20) in the form

$$\Omega = \phi + i\psi$$
$$= -U_o +\cos\theta + k\left(\theta_o - \lambda_o + \theta_1 - \lambda_1 + \theta_{-1} - \lambda_{-1} + \cdots + \theta_n - \lambda_n + \theta_{-n} - \lambda_{-n} + \cdots\right)$$
$$+ i\left\{-U_o +\sin\theta - k\log\left\{\frac{+_o +_1 +_{-1} \cdots +_n +_{-n} \cdots}{R_o R_1 R_{-1} \cdots R_n R_{-n} \cdots}\right\}\right\}.$$

Note that, as $n \to \infty$, $r_n = R_n$, $r_{-n} = R_{-n}$, $\theta_n = \lambda_n$ and $\theta_{-n} = \lambda_{-n}$. Now, along CD and EF, $\xi = r\cos\theta$ = constant $= \xi_o$, say, so that

$$\phi_{CD} = -U_o\xi_o + \kappa\left(\theta_o - \lambda_o + \theta_1 - \lambda_1 + \theta_{-1} - \lambda_{-1} + \cdots + \theta_n - \lambda_n + \cdots\right) = \phi_o \quad , \text{ say,}$$

and

$$\phi_{EF} = -U_o\xi_o + \kappa\left((\theta_o - 2\pi) - \lambda_o + \theta_1 - \lambda_1 + \theta_{-1} - \lambda_{-1} + \cdots + \theta_n - \lambda_n + \cdots\right) = \phi_o - 2\pi\kappa .$$

It follows that

$$\int_{CD} + \int_{EF} \phi\, d\psi = \int_{CD} \phi_o\, d\psi + \int_{EF} (\phi_o - 2\pi\kappa)\, d\psi = -2\pi\kappa \int_{EF} d\psi .$$

This result arises since θ_o decreases by 2π as the rotational core at ζ_o is encircled once in the clockwise sense. Physically, the integral $\int_{EF} d\psi$ represents the flux crossing EF and, since ψ is a single valued function,

$$\int_{CD} + \int_{EF} \phi\, d\psi = -2\pi\kappa\left(\psi_F - \psi_E\right). \tag{28}$$

Now, at F, we have $\chi = r\sin\theta = 0$, $r_o = R_o$, $r_1 = R_1$, etc, and so $\psi_F = 0$ while, at E, we have $\chi = r\sin\theta = \chi_o - a_r$, $r_o = a_r$, $R_o = 2\chi_o - a_r$, etc, and so

$$\psi_E = -U_o\left(\chi_o - a_r\right) - \kappa \log\left\{\frac{a_r\,(a_r^2 + a^2)\cdots\cdots(a_r^2 + n^2a^2)\cdots\cdots}{(2\chi_o - a_r)\left((2\chi_o - a_r)^2 + a^2\right)\cdots\cdots\left((2\chi_o - a_r)^2 + n^2a^2\right)\cdots\cdots}\right\}. \tag{29}$$

It follows from (27), (28) and (29), that

$$T_{KI} = -\pi\kappa\rho_f w\left[U_o\left(\chi_o - a_r\right) + \kappa \log\left\{\frac{a_r\,(a_r^2 + a^2)\cdots\cdots(a_r^2 + n^2a^2)\cdots}{(2\chi_o - a_r)\left((2\chi_o - a_r)^2 + a^2\right)\cdots\left((2\chi_o - a_r)^2 + n^2a^2\right)\cdots}\right\}\right] \tag{30}$$

in which, for a standing vortex row, U_o is related to κ by (21). Note that, for large n, corresponding terms in the numerator and denominator of the quotient in (30) cancel, and that it is therefore only the initial terms in each infinite product which are important in determining the vortex energy. In the limit $a \to \infty$, Eq (30) becomes

$$T_{kI} = -\pi k^2 \rho_f w \left[\frac{\chi_o - a_r}{2\chi_o} + \log\left(\frac{a_r}{2\chi_o - a_r} \right) \right], \quad (a \to \infty),$$

which is Tunstall and Inman's equivalent result. Equation (30) differs from this result in two respects; firstly, it incorporates a different standing vortex criterion (Eq (21) instead of (17)) and, secondly, the argument of the log-term includes contributions from all the vortex pairs in the row.

7.7 Calculation for the rotational flow region

The remaining part of the calculation of the vortex energy concerns the vortex core itself. As mentioned earlier, we assume that the core is circular in the transform plane and that its radius is a_r. It might be noted, however, that it is permissible to use (27) in cases in which the core is noncircular since, in the derivation of (30), it was assumed only that DE was a streamline of the irrotational motion. In fact, by the nature of the present irrotational model, the core of each vortex in the row is not quite circular as a result of the influence of the image vortex, of all the other vortex pairs in the flow field and of the free-stream flow. The conformal mapping also contributes to the distortion of the rotational core in the physical plane. However,despite these considerations, it is thought that little error is introduced into the present calculations by the assumption of a circular core. This is particularly true the smaller is the radius (a_r) of the core. From experimental results, Tunstall and Inman have suggested that the radius of the inner core is given by $a_r/2b = 0.4$, where 2b is the ripple height. We shall later present results for a range of values of ($a_r/2b$).

We model the situation, as does Tunstall (1973), by assuming that it is legitimate, in the core itself, to add the rotational velocity components to the irrotational components which would be present in the absence of the vortex. The resulting flow field is clearly rotational. The rotational components ($\tilde{u}_r$, $\tilde{v}_r$), associated with the core of the vortex centred at ζ_o in the transform plane, may be expressed by

$$\tilde{u}_r = \frac{\kappa}{a_r^2} (\chi - \chi_o),$$

$$\tilde{v}_r = -\frac{\kappa}{a_r^2} (\xi - \xi_o).$$

The irrotational velocity components within the core are as follows. Firstly, associated with the free stream, we have the velocity components $(\tilde{u}_s, \tilde{v}_s)$ given by

$$\tilde{u}_s = U_0 \quad , \quad \tilde{v}_s = 0 \ .$$

Secondly, associated with all the vortices in both of the infinite rows, except for the vortex at ζ_0 itself, we obtain the velocity components $(\tilde{u}_v, \tilde{v}_v)$ from

$$\tilde{u}_v - i\tilde{v}_v = -\frac{d\Omega_v}{d\zeta} \ ,$$

where (cf (20))

$$\Omega_v = -ik \log \sin\left\{\frac{\pi}{a}(\zeta-\zeta_0)\right\} + ik \log(\zeta-\zeta_0) + ik \log \sin\left\{\frac{\pi}{a}(\zeta-\bar{\zeta}_0)\right\} .$$

Hence, reintroducing the earlier notation, we obtain

$$\begin{aligned}\tilde{u}_v = {} & k\left\{\frac{x-x_1}{r_1^2} + \frac{x-x_{-1}}{r_{-1}^2} + \cdots\cdots + \frac{x-x_n}{r_n^2} + \frac{x-x_{-n}}{r_{-n}^2} + \cdots\right\} \\ & - k\left\{\frac{x+x_1}{R_1^2} + \frac{x+x_{-1}}{R_{-1}^2} + \cdots\cdots + \frac{x+x_n}{R_n^2} + \frac{x+x_{-n}}{R_{-n}^2} + \cdots\right\} \\ & - k\left\{\frac{x+x_0}{R_0^2}\right\},\end{aligned}$$

and (31)

$$\begin{aligned}\tilde{v}_v = {} & -k\left\{\frac{\xi-\xi_1}{r_1^2} + \frac{\xi-\xi_{-1}}{r_{-1}^2} + \cdots\cdots + \frac{\xi-\xi_n}{r_n^2} + \frac{\xi-\xi_{-n}}{r_{-n}^2} + \cdots\right\} \\ & + k\left\{\frac{\xi-\xi_1}{R_1^2} + \frac{\xi-\xi_{-1}}{R_{-1}^2} + \cdots\cdots + \frac{\xi-\xi_n}{R_n^2} + \frac{\xi-\xi_{-n}}{R_{-n}^2} + \cdots\right\} \\ & + k\left\{\frac{\xi-\xi_0}{R_0^2}\right\} .\end{aligned}$$

Again, the contributions to both $\tilde{u}_v$ and $\tilde{v}_v$ from the vortices in the upper and lower rows cancel for large n, and it is therefore only the initial terms in the expansion which are important in determining the velocity field. Note that, in limit $a \to \infty$,

$$\tilde{u}_v = -\kappa \frac{(\chi+\chi_o)}{R_o^2} \quad \text{and} \quad \tilde{v}_v = \kappa \frac{(\xi-\xi_o)}{R_o^2}, \quad (a \to \infty). \tag{32}$$

These velocity components are due only to the lower image vortex at $\zeta = \bar{\zeta}_o$, and are in agreement with the components derived by Tunstall (1973, p 39).

In order to calculate the rotational kinetic energy T_{kR} from (23), we require $q^2 = \tilde{u}^2 + \tilde{v}^2$ where $\tilde{u} = \tilde{u}_r + \tilde{u}_s + \tilde{u}_v$ and $\tilde{v} = \tilde{v}_r + \tilde{v}_s + \tilde{v}_v$. In practice, the components of $\tilde{u}$ and $\tilde{v}$ have been calculated over a grid, and a numerical integration has been performed to obtain T_{kR} from

$$T_{kR} = \tfrac{1}{2} \rho_f w \iint_A q^2 \, dA ,$$

where A denotes the area of the rotational vortex core bounded by the circle $(\xi - \xi_o)^2 + (\chi - \chi_o)^2 = a_r^2$. This may be reduced to the sum of various integrals, from which that representing the free-stream contribution within the core (ie containing the $\tilde{u}_s^2$ term) must be discarded. After further reduction, it may be shown that the vortex energy per wavelength associated with an infinite row of vortex pairs is as follows:

$$T_{kR} = \tfrac{1}{4} \rho_f w \kappa^2 \pi + \tfrac{1}{2} \rho_f w \iint_A (\tilde{u}_v^2 + \tilde{v}_v^2) \, dA + \rho_f w \iint_A \tilde{u}_s \tilde{u}_v \, dA + \rho_f w \iint_A (\tilde{u}_s \tilde{u}_v + \tilde{v}_s \tilde{v}_v) \, dA .$$

A rather greater amount of analytical reduction is possible for the case of a single vortex in the flow (see Tunstall (1973)). However, for the case of an infinite row of vortices, it has been found most practicable, and sufficiently accurate, to proceed by dividing the area of integration A into small elemental squares, and then summing the values of the various integrands calculated at the centre of each square. (For a core of radius a_r, squares of side as great as $a_r/8$ have been found to yield results which are accurate to within approximately 2%.)

The total vortex energy in the steady state problem is given by

$$T_k = T_{kI} + T_{kR} . \tag{33}$$

Having calculated T_k on this basis, Tunstall and Inman proposed that, for the case of a single vortex in the flow field, the vortex energy loss per wave period is given by $\{T_k \cdot 2N_r\}$, that is by the product of the energy of each vortex (T_k) and

twice the number of ripples present ($2N_r$), since two vortices are formed per period, one on either side of the ripple crest. For the case of an infinite vortex row, the same result applies; it will be recalled that, in §7.6, the calculation of vortex energy was made over one ripple wavelength.

7.8 Results for the vortex energy

Results for the vortex kinetic energy (T_k) have been calculated for various physically admissible values of vortex height (χ_o) and rotational core radius (a_r); in particular, values have been taken in the ranges $0.5 \leqq \chi_o/2b \leqq 0.7$ and $0.05 \leqq a_r/2b \leqq 0.7$, where 2b is the ripple height. The experimentally determined values of $\chi_o/2b = 0.6$ and $a_r/2b = 0.4$, quoted by Tunstall and Inman, lie at the midpoints of the respective ranges. In presenting results for the vortex energy (T_k) given by (33), we nondimensionalise T_k in two ways; firstly, following Tunstall and Inman, with respect to $\rho_f w\kappa^2$ and, secondly, with respect to the physically more accessible quantity $\rho_f w(U_o\lambda)^2$, where $\lambda = 2\pi/\ell$ is the ripple wavelength. It will be recalled that U_o and κ are related by Eqs (17) and (21) for the cases of a single vortex pair and an infinite row of vortex pairs, respectively.

For the case of a single vortex in the flow region, the results for the total energy $T_k = T_{kI} + T_{kR}$ are given in Table 12. The calculated values are in agreement with the values presented by Tunstall (1973 , Table 1B) for $0.05 \leqq a_r/2b \leqq 0.6$ and $\chi_o/2b = 0.6$. It might be noted that, while the results for $T_k/(\rho_f w\kappa^2)$ are a function of (χ_o/a_r) only, the results tabulated for $T_k/\rho_f w(U_o a)^2$, in which $a = \lambda$, incorporate the assumption that the ripple steepness $b\ell = 0.15\pi$; that is, using (17) for a single standing vortex pair,

$$\frac{T_k}{\rho_f w (U_o a)^2} = \frac{T_k}{\rho_f w \kappa^2}\left(\frac{2\chi_o}{a}\right)^2 = \frac{T_k}{\rho_f w \kappa^2}\left(\frac{\chi_o}{2b}\cdot\frac{2b\ell}{\pi}\right)^2 = \frac{T_k}{\rho_f w \kappa^2}\left(\frac{\chi_o}{2b}\cdot 0.3\right)^2.$$

For an infinite row of vortex pairs, the equivalent results given in Table 13 depend upon both (χ_o/a_r) and (a/a_r) $(= \lambda/a_r)$; in other words, for a given ripple steepness $(b\ell)$, the results depend upon both $(a_r/2b)$ and $(\chi_o/2b)$. The same nondimensionalisation has been adopted as above, though the condition for a standing vortex row is now (21), such that

$$\frac{T_k}{\rho_f w (U_o a)^2} = \frac{T_k}{\rho_f w \kappa^2\pi^2}\tanh^2\left(\frac{2\chi_o\pi}{a}\right) = \frac{T_k}{\rho_f w \kappa^2\pi^2}\tanh^2\left(\frac{\chi_o}{2b}\cdot 0.3\pi\right).$$

As a check on the calculations, it has been shown that the results in Table 12 are recovered by the method of calculation used for the infinite row, if the vortex spacing a is allowed to become very large (ie much larger than the one ripple wavelength ($a = \lambda$) assumed in the calculations for Table 13).

A comparison of the results in Tables 12 and 13 reveals that, in terms of the more useful quantity tabulated, namely $T_k/\rho_f w(U_o a)^2$, the results for the infinite row are always smaller than those for the single vortex in the flow. For the representative values $\chi_o/2b = 0.6$ and $a_r/2b = 0.4$ suggested by Tunstall and Inman, the difference is about 19%. More generally, however, despite the more realistic physical description provided by the vortex row model, there is rather little difference between the results. What is evident from the tables is that the vortex kinetic energy is dependent mainly upon the core radius (a_r) and the height of the vortex (χ_o) above the bed. This justifies Tunstall and Inman's approach, at least in respect of their assumption of only one vortex in the entire flow field, rather than one vortex per ripple wavelength. However, it provides no explanation for their very low estimate of 7% for the proportion of wave energy loss attributable to vortex formation and shedding. Moreover, despite the quite substantial variations in T_k in Tables 12 and 13, none of the tabulated values is sufficient to produce the order of magnitude increase in the predicted dissipation rate which is necessary to reconcile the present results either with those of Longuet-Higgins (1981a) or with the results from the field experiments discussed in §6. The largest of the tabulated values of $T_k/\rho_f w(U_o a)^2$ is attained with the unrealistically small core radius of $(a_r/2b) = 0.05$.

The implication of the above discussion is that, in certain important respects, the quasi-steady model of Tunstall and Inman (1975) provides an inadequate description of the vortices formed in unsteady flow above a rippled bed. Most importantly, the model does not appear to predict wave energy dissipation rates reliably. One reason for this is that, whether an infinite vortex row, or a single vortex in the flow field, is assumed,the quasi-steady model takes no account of shed vortices present in the flow as a result of vortex shedding in previous wave half-cycles. This is not to say that the model is not helpful in interpreting results such as were obtained in the present field experiments. In fact, the predictions for the streamlines and velocity components in Figs 24 to 30 are probably quite reliable for phase angles in the wave cycle associated with the times of peak free-stream velocity. For example, the model gives a good quantitative idea of the height of influence of vortices above the bed, and it also enables a clear idea to be obtained about the distribution of skin friction on the surface

of a ripple. Evidently, what the quasi-steady formulation fails to predict is the relative importance of skin friction and form drag in unsteady oscillatory flow. (For steady flow, these quatities are in rough agreement whereas, in oscillatory flow, form drag is dominant.) It has been demonstrated in this section also that, whereas peak surface velocities, and hence peak stresses, in nonseparating flow are found in the region of the ripple crests, peak surface velocities in separating flow are found on the lee slopes of the ripples, and are directed towards the crests. Quantitative information of this kind is valuable in interpreting experimental results (§5 and §6) and, more generally, in providing an understanding of the stability of wave-generated sand ripples. (The fact that, in oscillatory cases, sediment is drawn towards the crests from both directions for a large part of each wave cycle enables ripples to grow, at least until an equilibrium is achieved with the restoring influence of gravity.) Ultimately, however, a fully time-dependent description of the phenomenon of vortex formation and shedding is to be preferred over the present quasi-steady description.

§8 CONCLUSIONS

The experiments described in this report represent an extension of the programme of field work on sediment transport of waves described by Davies and Wilkinson (1979) and Davies (1980a and 1983). As in these earlier studies, the central aim has been to make field observations which may be compared with appropriate laboratory results relating to the near-bed oscillatory flow above ripples, and to sediment transport in oscillatory flows. The present comparisons have been of a rather more varied nature than those for the earlier experiments, on account both of the range of conditions monitored in the field, and of the wider experimental objectives of the studies undertaken. The results of two experiments have been described in this report, both of which were carried out at Blackpool Sands in Start Bay. In the first experiment in 1978, observations were made of the near-bed flow, and of the movement of coarse sand on the bed, beneath progressive swell waves in shallow water. In the second experiment in 1980, similar observations were made, but for a bed comprising medium to fine sand, and for a rather more varied range of wave periods. In addition, a number of observations were made of the formation of ripples on an initially flat sand bed. The main conclusions from these two experiments are discussed below.

In §4, sediment threshold motion conditions have been determined in the form of critical values of free-stream velocity amplitude, firstly, for the incipient (sporadic) motion of a few grains here and there on the bed; secondly, for the

general movement of the entire surface layer of sand grains as bedload; and, thirdly, for the suspension of sediment. (Results of the third kind were obtained only for the fine to medium sand beds in the 1980 experiment; the measured wave velocities were insufficient to give rise to suspension of the coarse sand in the 1978 experiment.) The observations of sediment motion were made with an underwater television system, the recordings from which were synchronised with velocity measurements of the wave-induced flow. Some uncertainty has arisen in comparing field results obtained on this basis with previous laboratory results, on account of variations in the definition of sediment threshold motion conditions adopted by different workers. However, as in the previous studies referred to above, the present field results, for irregular waves and mixed grain sizes, have been found to compare quite well with laboratory results for sinusoidal waves and single grain sizes, the threshold criteria in both cases being in terms of free-stream flow parameters. Since previous laboratory results for the threshold of sand motion have generally been for flat sand beds, for the present field studies involving rippled beds it has been necessary to interpret threshold motion conditions with care. In practice, a correction procedure based upon a potential flow argument has been adopted. This has been found to reconcile satisfactorily results for rippled beds in the field and flat beds in the laboratory, at least for cases in which the flow above the ripples was nonseparating.

In §5, a detailed examination has been undertaken of the nature of the oscillatory flow above rippled sand beds. Again, this has been based upon underwater television observations made during both the 1978 and 1980 experiments. Firstly, critical values of measured velocity amplitude have been determined for the onset both of flow instability, and of vortex formation and shedding, above rippled sand beds. Secondly, from the measured velocity records, estimates of the near-bed orbital excursion have been made on a wave-by-wave basis, from which critical orbital excursion values for the onset of instability and vortex formation have been determined. For the irregular measured waves in the field, it has been found that flow instability and vortex formation occur when the near-bed orbital excursion is greater than the ripple wavelength, in accordance with the results of previous laboratory work. This is an important result in connection with the rate at which energy is dissipated in oscillatory flow; energy is dissipated far more rapidly if vortex formation and shedding occurs above a rippled bed, than if it does not. Also described in §5 are certain experimental runs in which equilibrium ripples were allowed to develop on an initially flat sand bed which was exposed to irregular wave action. It has been found that the equilibrium vortex ripples which

formed had characteristics consistent with ripples observed previously in the field by other workers. In general, an understanding of the relationship between the properties of surface waves, and the dimensions of the associated sand ripples, is important if wave energy dissipation rates, and sediment transport rates, are to be quantified. In the field, changes in wave conditions may give rise, after a time lag, to changes in ripple heights and wavelengths. The time lags involved are likely to be most significant during periods of diminishing wave activity; in fact, in the extreme case of a storm which dies away very rapidly, it is possible that a pattern of ripples generated by the highest storm waves may be fossilised on the bed. This is a more complicated situation than that which has usually been considered in laboratory work and it calls for further examination. In the present study, results relating to sediment motion, and to vortex formation and shedding, have been obtained both for equilibrium sand ripples (1980 experiment), and also for fossil ripples associated with some previous wave activity (1978 experiment).

For the contrasting conditions in the 1978 and 1980 experiments, calculations have been made in §6 of the peak bed shear stress in each measured wave half-cycle. On the basis of the synchronous video records obtained with the underwater television system, critical values of stress at the threshold of motion have then been determined. The calculations of stress have been made on the basis of Jonsson's (1967) friction factor (ie drag coefficient) which is a function of the wave Reynolds number and the relative roughness of the bed. Initially, on the basis of these two parameters, the boundary layer has been classified for each wave half-cycle in the experiments. Thus it has been shown that, in the 1978 experiment, the boundary layer was generally transitional (except for the largest waves for which it was smooth turbulent); whereas, in the 1980 experiment, it was generally rough turbulent. In the former case, calculations have been made on the basis that the flow was nonseparating, and that the bed roughness was a function of the sediment grain size. In the latter case, calculations have been made on the basis that the flow was separating, and that the bed roughness was a function of the ripple size. Thus the nature of the near-bed flow has been assumed to be fundamentally different in the two experiments. As far as the bed shear stress is concerned, in the former case the calculated amplitudes of stress are skin friction values, that is values of stress acting directly on the surface layer of sand grains. It has been possible to compare such values calculated at the threshold of sediment motion with appropriate critical values of the threshold stress from Shields' curve. Despite some uncertainty, quite good agreement has been found, and this has confirmed the validity of the approach adopted. (Although Shields' curve is based upon

laboratory results for steady flow, it has been well established that it is legitimate to make comparisons of the above kind with results obtained in unsteady flow.) In the latter case, the calculated amplitudes are of the total stress, comprising the sum of the contributions of skin friction and form drag on the rippled bed. Although in this case it has not been possible to calculate directly the shear stress acting on the surface layer of sand grains, a comparison of the calculated total stress at the observed threshold of sediment motion and the critical threshold stress from Shields' curve suggests an order of magnitude difference between the (larger) form drag and (smaller) skin friction contributions to the total stress. This may be contrasted with the situation in steady flow, in which the total stress on a rippled bed, albeit an asymmetrically rippled bed, is partitioned roughly equally between skin friction and form drag. An immediate implication of the order of magnitude difference between skin friction and form drag is that there is an order of magnitude difference also in the wave energy dissipation rates associated with cases in which the flow above the ripples is separating (and in which there is form drag on the ripples), and cases in which the flow is nonseparating. This relates directly to the earlier discussion of the results in §5.

In order to gain a working understanding of the nature of the velocity field in separating flow over a rippled bed, a two-dimensional irrotational "standing vortex" model has been developed (§7). The general aim of this has been to quantify some of the differences between separating and nonseparating (deep) flow above rippled beds, and to provide some insight into the near-bed processes of sediment motion and entrainment. The particular aims have been to calculate, firstly, near-bed velocities for that part of each wave half-cycle in which the free-stream flow is near its maximum value, and in which a vortex is fully formed above the lee slope of each ripple; and,secondly, the kinetic energy of that vortex in connection with the determination of wave energy dissipation rates. (In principle, the model, which is a simple extension of the single standing vortex pair model of Tunstall and Inman (1975), is more appropriate for application to steady than to unsteady flows. However, its use in the unsteady case may be justified, up to a point, by experimental results.) For nonseparating flow above an idealised naturally rippled bed, streamlines and associated surface velocity components have been calculated which show that the surface velocity in the region of the ripple crest is much enhanced compared with the free-stream velocity, while the velocity in the trough is correspondingly diminished. The associated convergences and divergences of the streamlines above the crests and troughs, respectively, give way to an unperturbed

uniform horizontal flow at about half a ripple wavelength above the mean bed level. Equivalent results for separating flow have been obtained in which the position of the vortex above the lee slope of each ripple has been specified in the model on the basis of previous laboratory work. The streamlines and the surface velocities are fundamentally different from those for nonseparating flow, and it follows that wave energy dissipation rates in the two cases are very different also. Unfortunately, the results of calculations of the vortex kinetic energy, which lead to estimates of the wave energy dissipation rate, appear to be inconsistent with the present experimental findings in respect of the relationship between skin friction and form drag (§6). This is probably due to the fact that the quasi-steady model is inapplicable for phase angles in the wave cycle other than those corresponding to peak values of velocity in the outer free-stream flow. This points to the need for a fully time-dependent model for the study of certain aspects of separating oscillatory flow above sand ripples.

Apart from the very different implications for wave energy dissipation rates in the cases of separating and nonseparating flow, there are also different implications for sediment movement. In general, nonseparating flow is likely to be associated with low waves above nonequilibrium rippled beds, and separating flow with rather higher waves above equilibrium beds. In the nonseparating case, for which the orbital excursion may be supposed to be less than the ripple wavelength and for which the ripples are not in equilibrium with the prevailing flow, bed shear stresses are greatest in the region of the crests where the (tangential) surface velocities are greatest. It is not surprising, therefore, to find sediment motion occurring only in the vicinity of the crests and not in the troughs, as was generally the case in the 1978 experiment. By comparison, in the separating flow case, for which the orbital excursion is greater than the ripple wavelength and the ripples are in equilibrium with the outer flow, bed shear stresses are greatest on the lee slopes of the ripples and are directed towards the ripple crests. The fact that sediment is drawn towards the crests from both directions enables ripples to grow, at least until an equilibrium is achieved with the restoring influence of gravity on the ripple profiles. Further obvious implications for sediment transport arise when vortices are shed from the bed upon flow reversal. If these vortices are sediment laden, vortex shedding is clearly a potent way in which sediment entrainment may occur. Vortex formation and shedding thus serves, firstly, to mobilise and entrain sediment; secondly, to stabilise ripple formations on the bed; and, thirdly, to give rise to high wave energy dissipation rates. Although it has not been possible to compare directly the results in §7 for separating flow with

field measurements, the irrotational model appears to predict the important features of separating flow correctly, and the future development of this model holds out the prospect of an improved general understanding of near-bed processes.

ACKNOWLEDGEMENTS

The results described in this report have been obtained on the basis of field experiments which were made by the author in collaboration with Dr R H Wilkinson, and which were run with the help of the electronics engineers and the diving team at IOS Taunton. At various times, the following members of staff were involved in the field work: Mr G P Le Good, Mr R A Haine, Mr J D Humphery, Mr D H Joyce, Mr J O Malcolm, Mr A J Marks, Mr E J Moore and Dr A P Salkield. All are thanked for their help and hard work.

Data analysis was carried out on the computer by Mrs B L S A Wainwright, Miss J Blower and Mrs L Ellett. The calculations and graph plotting for the theoretical study were carried out by Mr J S Chappell, on a sandwich studentship from the University of Bath. Each of the above was involved also in the analysis of the video records, and they are thanked for their painstaking work.

The illustrations were prepared by Mrs C D Kemp and the report was typed by Mrs J Reeves and Mrs M Ridge.

Finally, Lady A Newmann is thanked for allowing the experiments to be performed at Blackpool Sands.

The work described was supported financially, at least in part, by the Department of Environment.

REFERENCES

BAGNOLD, R A, 1946. Motion of waves in shallow water. Interaction between waves and sand bottoms. Proceedings of the Royal Society, London, Series A, 187, 1-18.

BAKKER, W T, 1975. Sand concentration in an oscillatory flow. Proceedings of the 14th International Conference on Coastal Engineering, 1974. American Society of Civil Engineers, 1129-1148.

BIJKER, E W, VAN HIJUM, E and VELLINGA, P, 1977. Sand transport by waves. Proceedings of the 15th International Conference on Coastal Engineering, 1976. American Society of Civil Engineers, 1149-1167.

BREBNER, A, 1981. Sand bed-form lengths under oscillatory motion. Proceedings of the 17th International Conference on Coastal Engineering, 1980. American Society of Civil Engineers, 1340-1343.

CARSTENS, M R and NEILSON, F M, 1967. Evolution of a duned bed under oscillatory flow. Journal of Geophysical Research, 72, 12, 3053-3059.

CARSTENS, M R, NEILSON, F M and ALTINBILEK, H D, 1969. Bed forms generated in the laboratory under an oscillatory flow: analytical and experimental study. US Army Corps of Engineers, Coastal Engineering Research Center, Technical Memorandum Number 28, 105 pp.

COOK, D O and GORSLINE, D S, 1972. Field observations of sand transport by shoaling waves. Marine Geology, 13, 31-55.

DAVIES, A G, 1979. The potential flow over ripples on the seabed. Journal of Marine Research, 37, 4, 743-759.

DAVIES, A G, 1980a. Field observations of the threshold of sand motion in a transitional wave boundary layer. Coastal Engineering, 4, 23-46.

DAVIES, A G, 1980b. Some interactions between surface water waves and ripples and dunes on the seabed. Institute of Oceanographic Sciences Report, Number 108, 134 pp.

DAVIES, A G, 1982a. On the interaction between surface waves and undulations on the seabed. Journal of Marine Research, 40, 2, 331-368.

DAVIES, A G, 1982b. The reflection of wave energy by undulations on the seabed. Dynamics of Atmospheres and Oceans, 6, 207-232.

DAVIES, A G, 1983. Wave interactions with rippled sand beds, pp 1-65 in Physical Oceanography of Coastal and Shelf Seas by B Johns (Editor). Amsterdam : Elsevier, 470 pp.

DAVIES, A G and WILKINSON, R H, 1977. The movement of non-cohesive sediment by surface water waves. Part 1 : Literature Survey. Institute of Oceanographic Sciences Report, Number 45, 79 pp.

DAVIES, A G, FREDERIKSEN, N A and WILKINSON, R H, 1977. The movement of non-cohesive sediment by surface water waves. Part 2 : Experimental Study. Institute of Oceanographic Sciences Report, Number 46, 80 pp.

DAVIES, A G and WILKINSON, R H, 1979. Sediment motion caused by surface water waves. Proceedings of the 16th International Conference on Coastal Engineering, 1978. American Society of Civil Engineers, 1577-1595.

DINGLER, J R and INMAN, D L, 1977. Wave-formed ripples in nearshore sands. Proceedings of the 15th International Conference on Coastal Engineering, 1976. American Society of Civil Engineers, 2109-2126.

DU TOIT, C G and SLEATH, J F A, 1981. Velocity measurements close to rippled beds in oscillatory flow. Journal of Fluid Mechanics, 112, 71-96.

GRANT, W D and MADSEN, O S, 1982. Movable bed roughness in unsteady oscillatory flow. Journal of Geophysical Research, 87, C1, 469-481.

HOM-MA, M and HORIKAWA, K, 1962. Suspended sediment due to wave action. Proceedings of the 8th International Conference on Coastal Engineering, 1962. American Society of Civil Engineers, 168-193.

HOM-MA, M and HORIKAWA, K, 1963. A laboratory study on suspended sediment due to wave action. Proceedings of the 10th Congress of the International Association for Hydraulic Research, 213-220.

HOM-MA, M, HORIKAWA, K and KAJIMA, R, 1965. A study on suspended sediment due to wave action. Coastal Engineering in Japan, 8, 85-103.

HONJI, H, KANEKO, A and MATSUNAGA, N, 1980. Flows above oscillatory ripples. Sedimentology, 27, 225-229.

HORIKAWA, K and WATANABE, A, 1967. A study on sand movement due to wave action. Coastal Engineering in Japan, 10, 39-57.

HORIKAWA, K and WATANABE, A, 1971. Turbulence and sediment concentration due to waves. Proceedings of the 12th International Conference on Coastal Engineering, 1970. American Society of Civil Engineers, 751-766.

HSIAO, S V and SHEMDIN, O H, 1979. Bottom dissipation in finite-depth water waves. Proceedings of the 16th International Conference on Coastal Engineering, 1978. American Society of Civil Engineers, 434-448.

INMAN, D L, 1957. Wave-generated ripples in nearshore sands. US Army Corps of Engineers, Beach Erosion Board, Technical Memorandum Number 100, 66 pp.

IWAGAKI, Y, and KAKINUMA, T, 1967. On the bottom friction factors off five Japanese coasts. Coastal Engineering in Japan, 10, 13-22.

JOHNS, B, 1975. The form of the velocity profile in a turbulent shear wave boundary layer. Journal of Geophysical Research, 80, 36, 5109-5112.

JONSSON, I G, 1967. Wave boundary layers and friction factors. Proceedings of the 10th International Conference on Coastal Engineering, 1966. American Society of Civil Engineers, 127-148.

JONSSON, I G, 1978. A new approach to oscillatory rough turbulent boundary layers. Technical University of Denmark, Institute of Hydrodynamics and Hydraulic Engineering, Series Paper Number 17, 87 pp. (Also published in Ocean Engineering, 7, 1980, 109-152.)

JONSSON, I G and CARLSEN, N A, 1976. Experimental and theoretical investigations in an oscillatory turbulent boundary layer. Journal of Hydraulic Research, 14, 1, 45-60.

KAJIURA, K 1968. A model of the bottom boundary layer in water waves. Bulletin of the Earthquake Research Institute, 46, 75-123.

KAMPHUIS, J W, 1975. Friction factor under oscillatory waves. Proceedings of the American Society of Civil Engineers. Journal of the Waterway, Port, Coastal and Ocean Division, 101, No WW2, 135-144.

KAMPHUIS, J W, 1978. Attenuation of gravity waves by bottom friction. Coastal Engineering, 2, 111-118.

KENNEDY, J F and FALCON, M, 1965. Wave-generated sediment ripples. Massachusetts Institute of Technology, Department of Civil Engineering, Hydrodynamics Laboratory Report Number 86, 55 pp.

KENNEDY, J F and LOCHER, F A, 1972. Sediment suspension by water waves, pp 249-295 in Waves on Beaches by R E Meyer (Editor). Academic Press, 462 pp.

KNIGHT, D W, 1978. Review of oscillatory boundary layer flow. Proceedings of the American Society of Civil Engineers, Journal of the Hydraulics Division, 104, No HY6, 839-855.

KOMAR, P D, 1974. Oscillatory ripple marks and the evaluation of ancient wave conditions and environments. Journal of Sedimentary Petrology, 44, 1, 169-180.

KOMAR, P D, NEUDECK, R H and KULM, L D, 1972. Observations and significance of deep-water oscillatory ripple marks on the Oregon Continental Shelf, pp 601-619 in Shelf Sediment Transport by D J P Swift, D B Duane and O H Pilkey (Editors). Dowden, Hutchinson and Ross, Inc, Stroudsburg, Pa, 656 pp.

KOMAR, P D and MILLER, M C, 1975. Sediment threshold under oscillatory waves. Proceedings of the 14th International Conference on Coastal Engineering, 1974. American Society of Civil Engineers, 756-775.

LAMBRAKOS, K F, 1982. Seabed wave boundary layer measurements and analysis. Journal of Geophysical Research, 87, C6, 4171-4189.

LAVELLE, J W, YOUNG, R A, SWIFT, D J P and CLARKE, T L, 1978. Near-bottom sediment concentration and fluid velocity measurements on the Inner Continental Shelf, New York. Journal of Geophysical Research, 83, C12, 6052-6062.

LOFQUIST, K E B, 1978. Sand ripple growth in an oscillatory flow water tunnel. US Army Corps of Engineers, Coastal Engineering Research Center, Technical Paper Number 78-5, 101 pp.

LOFQUIST, K E B, 1981. Measurements of oscillatory drag on sand ripples. Proceedings of the 17th International Conference on Coastal Engineering, 1980. American Society of Civil Engineers, 3087-3106.

LONGUET-HIGGINS, M S, 1981a. Oscillating flow over steep sand ripples. Journal of Fluid Mechanics, 107, 1-35.

LONGUET-HIGGINS, M S, 1981b. Contribution to the Discussion. Proceedings of the 17th International Conference on Coastal Engineering, 1980. American Society of Civil Engineers, 3107.

LUKASIK, S J and GROSCH, C E, 1963. Pressure-velocity correlations in ocean swell. Journal of Geophysical Research, 68, 20, 5689-5699.

MACPHERSON, H, 1980. The attenuation of water waves over a non-rigid bed. Journal of Fluid Mechanics, 97, 4, 721-742.

MADSEN, O S and GRANT, W D, 1976. Sediment transport in the coastal environment. Massachusetts Institute of Technology, Department of Civil Engineering Report Number 209, 105 pp.

MANOHAR, M, 1955. Mechanics of bottom sediment movement due to wave action. US Army Corps of Engineers, Beach Erosion Board, Technical Memorandum Number 75, 121 pp.

MATSUNAGA, N, KANEKO, A and HONJI, H, 1981. A numerical study of steady streamings in oscillatory flow over a wavy wall. Journal of Hydraulic Research, 19, 1, 29-42.

MATSUNAGA, N and HONJI, H, 1980. The backwash vortex. Journal of Fluid Mechanics, 99, 4, 813-815.

MILLER, M C and KOMAR, P D, 1980a. Oscillation sand ripples generated by laboratory apparatus. Journal of Sedimentary Petrology, 50, 1, 173-182.

MILLER, M C and KOMAR, P D, 1980b. A field investigation of the relationship between oscillation ripple spacing and the near-bottom water orbital motions. Journal of Sedimentary Petrology, 50, 1, 183-191.

MILNE-THOMSON, L M, 1968. Theoretical hydrodynamics. (5th Edition) London : Macmillan Press Limited, 743 pp.

MOGRIDGE, G R and KAMPHUIS, J W, 1973. Experiments on bed form generation by wave action. Proceedings of the 13th International Conference on Coastal Engineering, 1972. American Society of Civil Engineers, 1123-1142.

NAKATO, T, LOCHER, F A, GLOVER, J R and KENNEDY, J F, 1977. Wave entrainment of sediment from rippled beds. Proceedings of the American Society of Civil Engineers. Journal of the Waterway, Port, Coastal and Ocean Division, 103, No WW1, 83-99.

NEWTON, R S, 1968. Internal structure of wave-formed ripple marks in the nearshore zone. Sedimentology, 11, 275-292.

NIELSEN, P, 1979. Some basic concepts of wave sediment transport. Technical University of Denmark, Institute of Hydrodynamics and Hydraulic Engineering, Series Paper Number 20, 160 pp.

NIELSEN, P, 1981. Dynamics and geometry of wave-generated ripples. Journal of Geophysical Research, 86, C7, 6467-6472.

NIELSEN, P, SVENDSEN, I A and STAUB, C, 1979. Onshore-offshore sediment movement on a beach. Proceedings of the 16th International Conference on Coastal Engineering, 1978. American Society of Civil Engineers, 1475-1492.

NIELSEN, P, GREEN, M O and COFFEY, F C, 1982. Suspended sediment under waves. University of Sydney, Department of Geography, Coastal Studies Unit Technical Report Number 82/6, 158 pp.

PUTNAM, J A and JOHNSON, J W, 1949. The dissipation of wave energy by bottom friction. Transactions of the American Geophysical Union, 30, 1, 67-74.

ROSENTHAL, W, 1978. Energy exchange between surface waves and motion of sediment. Journal of Geophysical Research, 83, C4, 1980-1982.

SAWAMOTO, M, 1980. Flow field over rippled beds induced by wave action. Third International Symposium on Stochastic Hydraulics, 1980, 621-630.

SAWAMOTO, M and YAMAGUCHI, S, 1979. The theoretical modelling on wave entrainment of sand particles from rippled beds. Transactions of the Japan Society of Civil Engineers, 11, 170-171.

SCOTT, T, 1954. Sand movement by waves. US Army Corps of Engineers, Beach Erosion Board, Technical Memorandum Number 48, 37 pp.

SHEMDIN, O, HASSELMANN, K, HSIAO, S V and HERTERICH, K, 1978. Nonlinear and linear bottom interaction effects in shallow water, pp 347-372 in Turbulent Fluxes Through the Sea Surface, Wave Dynamics and Prediction by A Favre and K Hasselmann (Editors). Plenum Publishing Corporation, 677 pp.

SHIBAYAMA, T and HORIKAWA, K, 1980. Laboratory study on sediment transport mechanism due to wave action. Proceedings of the Japan Society of Civil Engineers Number 296, 131-141.

SILVESTER, R and MOGRIDGE, G R, 1971. Reach of waves to the bed of the continental shelf. Proceedings of the 12th International Conference on Coastal Engineering, 1970. American Society of Civil Engineers, 651-668.

SLEATH, J F A, 1970. Velocity measurements close to the bed in a wave tank. Journal of Fluid Mechanics, 42, 1, 111-123.

SLEATH, J F A, 1973. A numerical study of the influence of bottom roughness on mass transport, pp 482-493 in Numerical Methods in Fluid Dynamics by C A Brebbia and J J Connor (Editors). London : Pentech Press, 571 pp.

SLEATH, J F A, 1974. Stability of laminar flow at seabed. Proceedings of the American Society of Civil Engineers, Journal of the Waterways, Harbours and Coastal Engineering Division, 100, No WW2, 105-122.

SLEATH, J F A, 1975a. A contribution to the study of vortex ripples. Journal of Hydraulic Research, 13, 3, 315-328.

SLEATH, J F A, 1975b. Transition in oscillatory flow over rippled beds. Proceedings of the Institution of Civil Engineers, 59, 2, 309-322.

SLEATH, J F A, 1976. On rolling-grain ripples. Journal of Hydraulic Research, 14, 1, 69-81

SLEATH, J F A, 1982a. The suspension of sand by waves. Journal of Hydraulic Research, 20, 5, 439-452.

SLEATH, J F A, 1982b. The effect of jet formation on the velocity distribution in oscillatory flow over flat beds of sand or gravel. Coastal Engineering, 6, 151-177.

SLEATH, J F A, 1982c. Friction coefficients of rippled beds in oscillatory flow. Continental Shelf Research, 1, 1, 33-47.

SMITH, J D, 1977. Modeling of sediment transport on continental shelves, pp 539-577 in The Sea, Volume 6, by E D Goldberg, I N Mc Cave, J J O'Brien and J H Steele. Wiley-Interscience, 1048 pp.

STERNBERG, R W and LARSEN, L H, 1975. Threshold of sediment movement by open ocean waves : observations. Deep-Sea Research, 22, 299-309.

SUNAMURA, T, 1981. Bedforms generated in a laboratory wave tank. Science Reports of the Institute of Geoscience, University of Tsukuba, Section A, Volume 2, 31-43.

SVENDSEN, I A, NIELSEN, P and STAUB, C, 1977. The motion of suspended particles in oscillatory flow. Technical University of Denmark, Institute of Hydrodynamics and Hydraulic Engineering, Progress Report Number 44, 13-18.

TANNER, W F, 1971. Numerical estimates of ancient waves, water depth and fetch. Sedimentology, 16, 71-88.

THIMAKORN, P, 1981. An experiment on clay suspension under water waves. Proceedings of the 17th International Conference on Coastal Engineering, 1980. American Society of Civil Engineers, 2894-2906.

TRELOAR, P D and ABERNETHY, C L, 1978. Determination of a bed friction factor for Botany Bay, Australia. Coastal Engineering, 2, 1-20.

TUNSTALL, E B, 1973. Experimental study of vortices generated by oscillatory flow over rippled surfaces. PhD dissertation, University of California, San Diego, 150 pp.

TUNSTALL, E B and INMAN, D L, 1975. Vortex generation by oscillatory flow over rippled surfaces. Journal of Geophysical Research, 80, 24, 3475-3484.

VAN IEPEREN, M P, 1975. The bottom friction of the sea-bed off Melkbosstrand, South Africa : A comparison of a quadratic with a linear friction model. Deutsche Hydrographische Zeitschrift, 28, 2, 72-88.

VITALE, P, 1979. Sand bed friction factors for oscillatory flows. Proceedings of the American Society of Civil Engineers, Journal of the Waterway, Port, Coastal and Ocean Division, 105, No WW3, 229-245.

WANG, H and LIANG, S S, 1975. Mechanics of suspended sediment in random waves. Journal of Geophysical Research, 80, 24, 3488-3494.

YALIN, S and RUSSELL, R C H, 1963. Similarity in sediment transport due to waves. Proceedings of the 8th International Conference on Coastal Engineering, 1962. American Society of Civil Engineers, 151-167.

ZHUKOVETS, A M, 1963. The influence of bottom roughness on wave motion in a shallow body of water. Bulletin (Izv) of the Academy of Sciences, USSR, Geophysics Series Number 10, 943-948. Translated from Geophysics Series Number 10, 1561-1570.

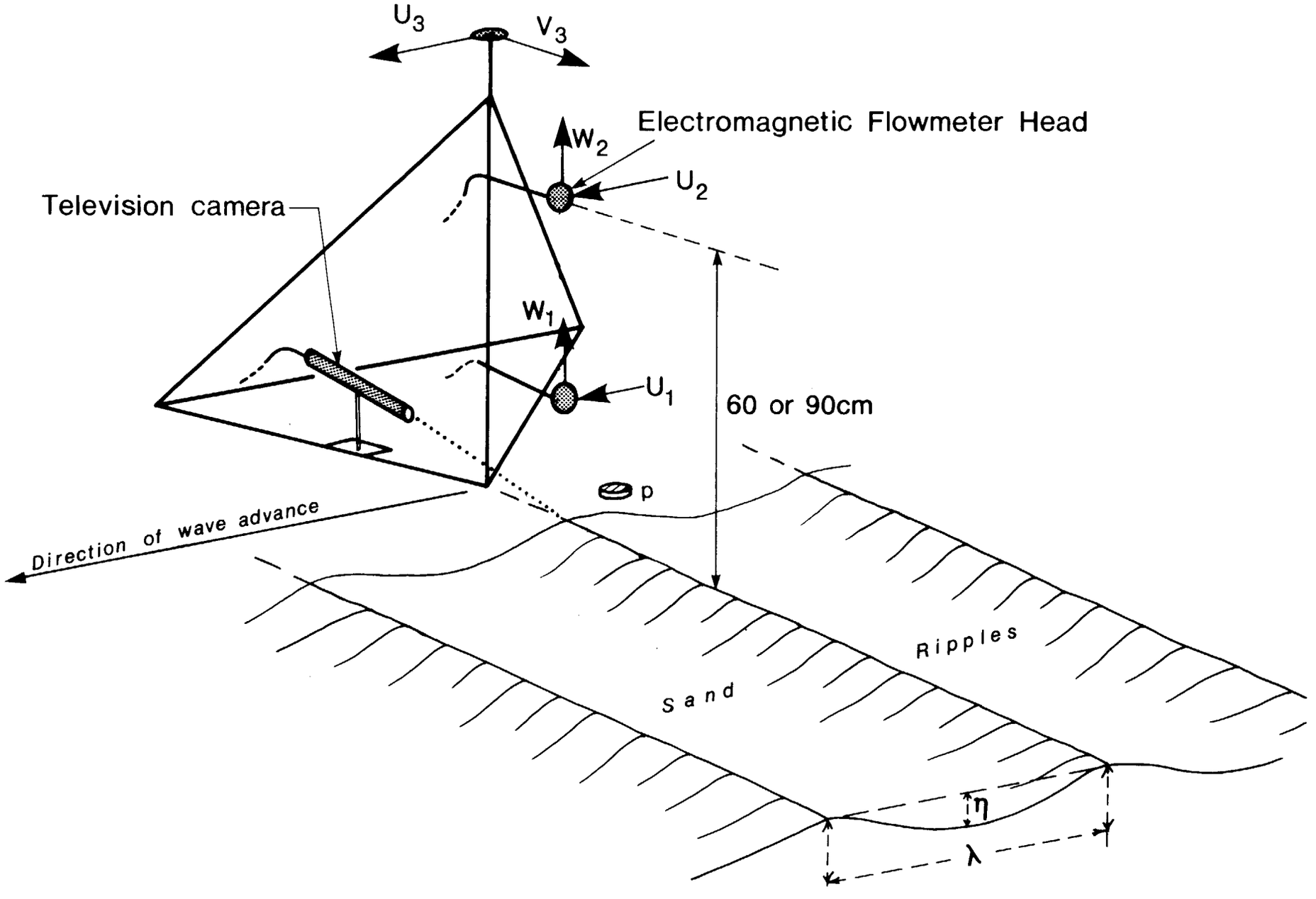

Figure 1 Schematic diagram of the bottom rig.

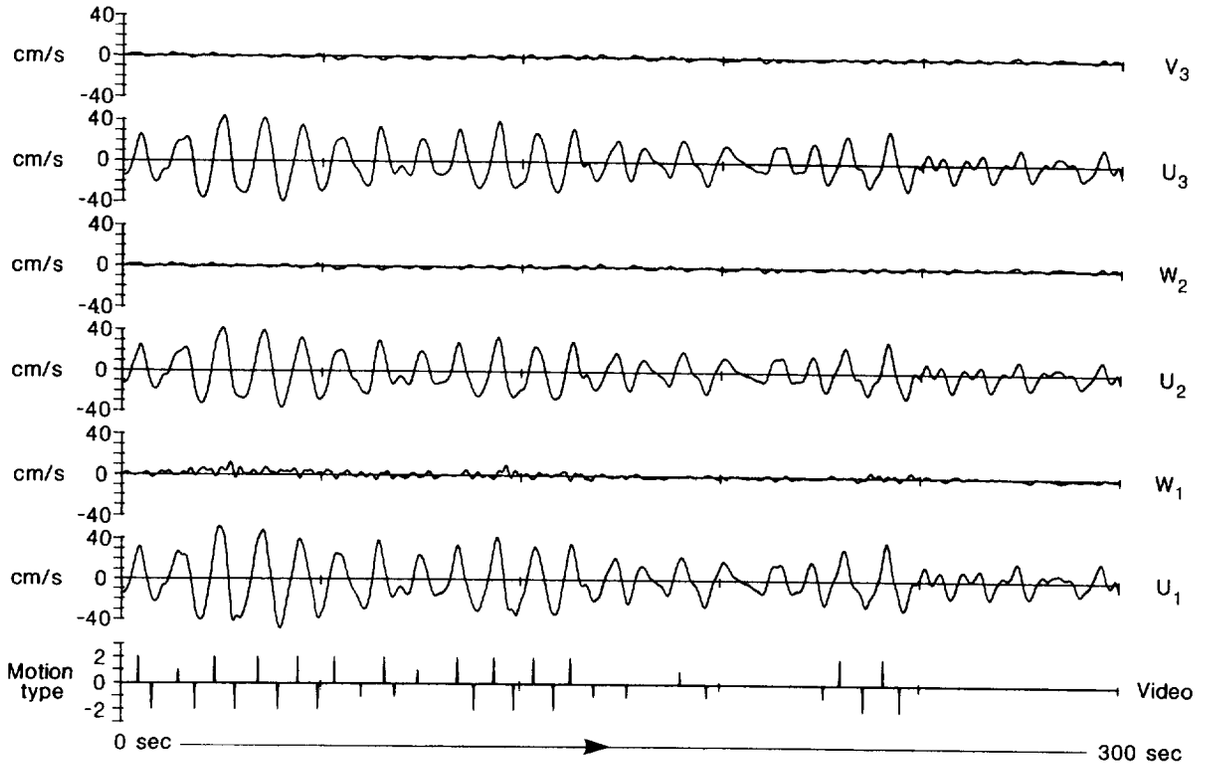

Figure 2(i) Five minute portion of Run 9, 1978. (Water depth ∿ 6.5 m). Sediment motion results appear in the bottom row; the observations from the video records are classified ±1 or ±2, as defined in the text (§4).

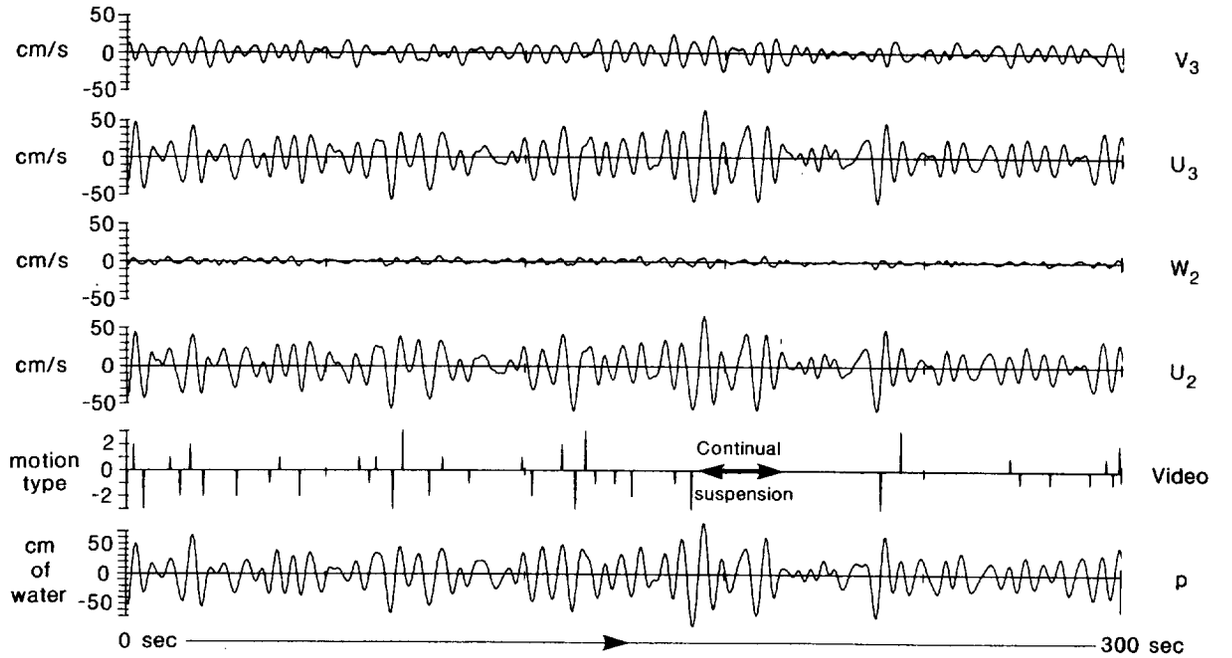

Figure 2(ii) Five minute portion of Run 10, 1980. (Water depth ∿ 6m). Sediment motion results appear in the fifth row; the observations from the video records are classified ±1, ±2 or ±3, as defined in the text (§4).

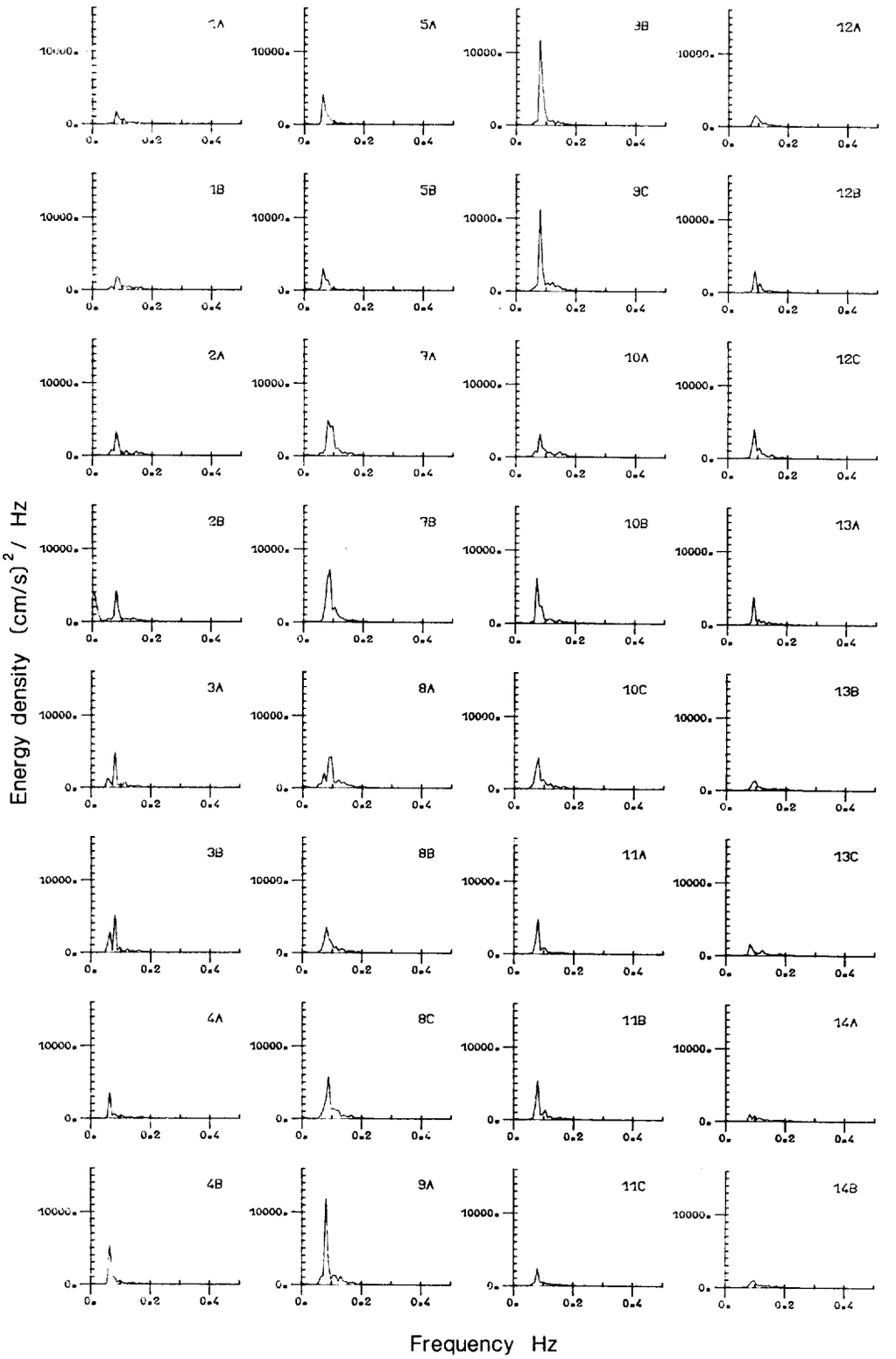

(i)

Figure 3 Energy spectra based on the U_3 component of measured horizontal velocity for the runs of (i) the 1978 experiment and (ii) the 1980 experiment. The measurements were made at nominal heights of 130 cm and 160 cm above the bed, respectively. Run numbers are as indicated (10 minute portions from full 30 minute runs being designated A, B and C).

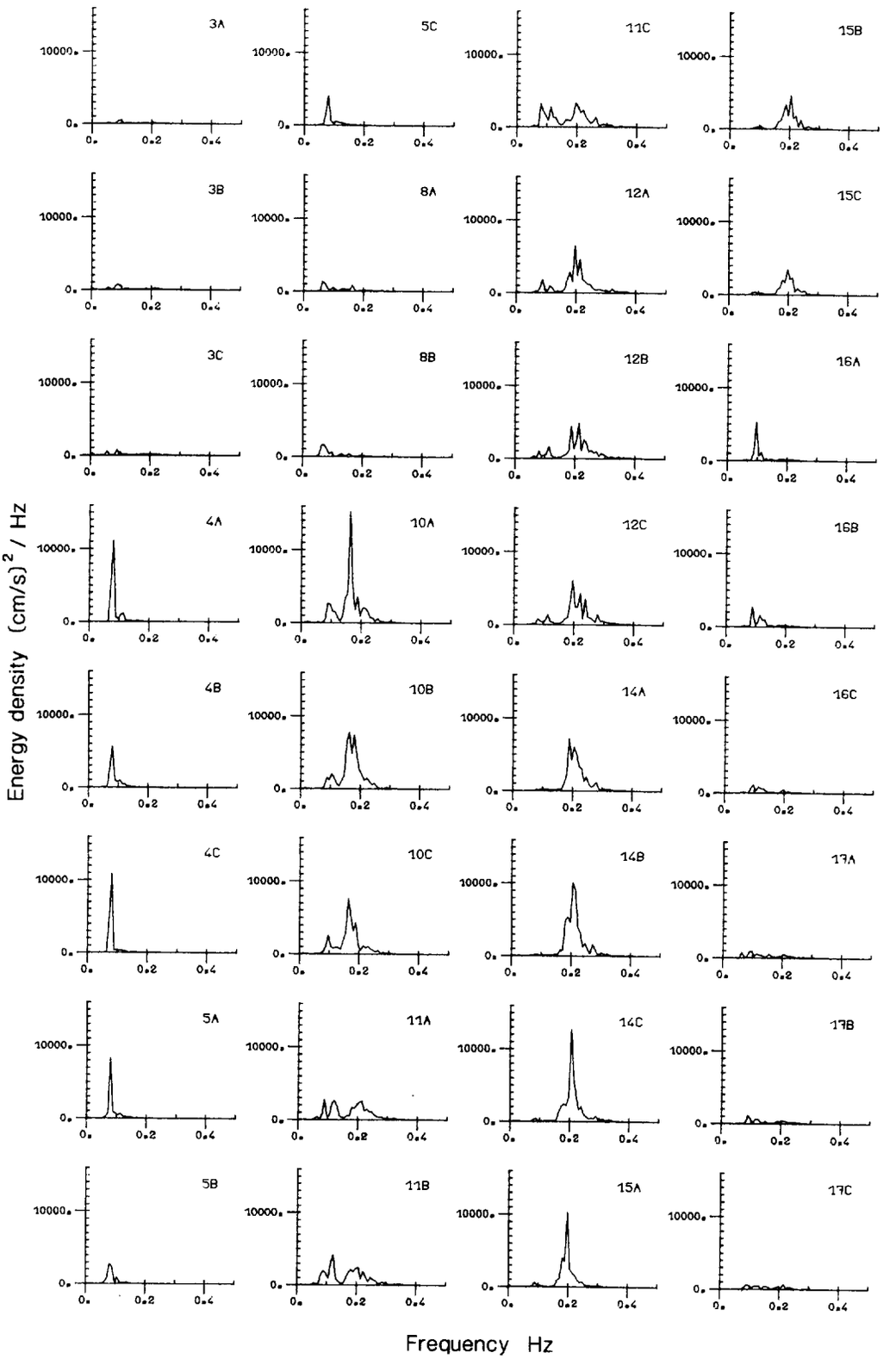
3A
5C
11C
15B
3B
8A
12A
15C
3C
8B
12B
16A
4A
10A
12C
16B
4B
10B
14A
16C
4C
10C
14B
17A
5A
11A
14C
17B
5B
11B
15A
17C
10000.
0.
0.2
0.4
Energy density (cm/s)^2 / Hz
Frequency Hz

3(ii)

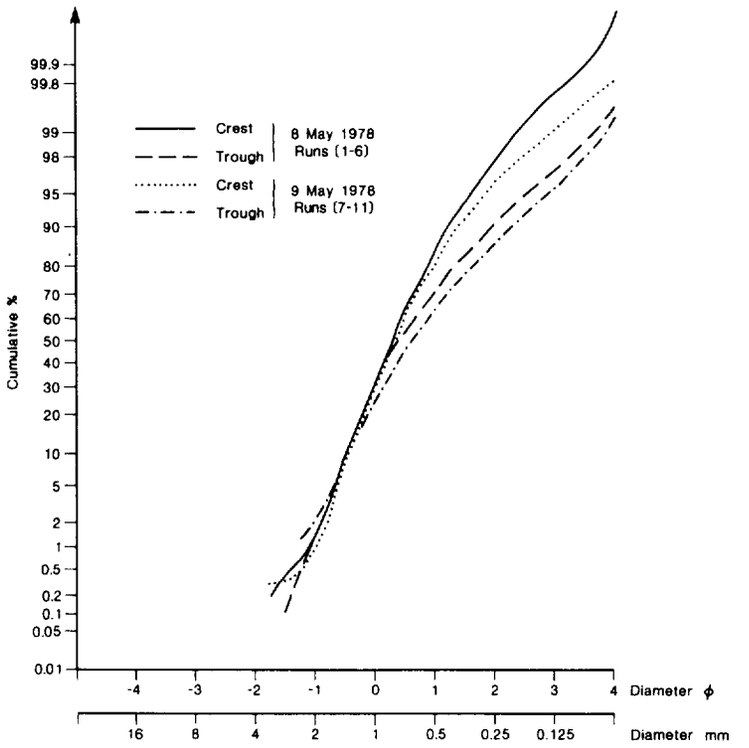

Figure 4(i) Cumulative curves of grain size distribution for the 1978 experiment. The bottom sediment at the crests and troughs for Runs 12-15 was as for Runs 1-11.
Representative grain sizes: D_{10} = 0.038 cm, D_{50} = 0.078 cm, D_{90} = 0.135 cm.

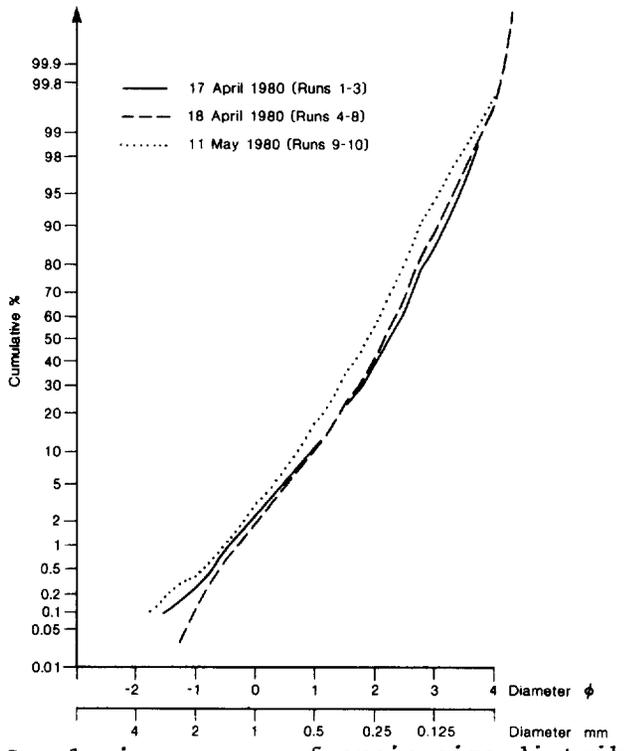

Figure 4(ii) Cumulative curves of grain size distribution for the 1980 experiment. The bottom sediment for Runs 11-17 was as for Runs 9-10.
Representative grain sizes: D_{10} = 0.015 cm, D_{50} = 0.026 cm, D_{90} = 0.062 cm.

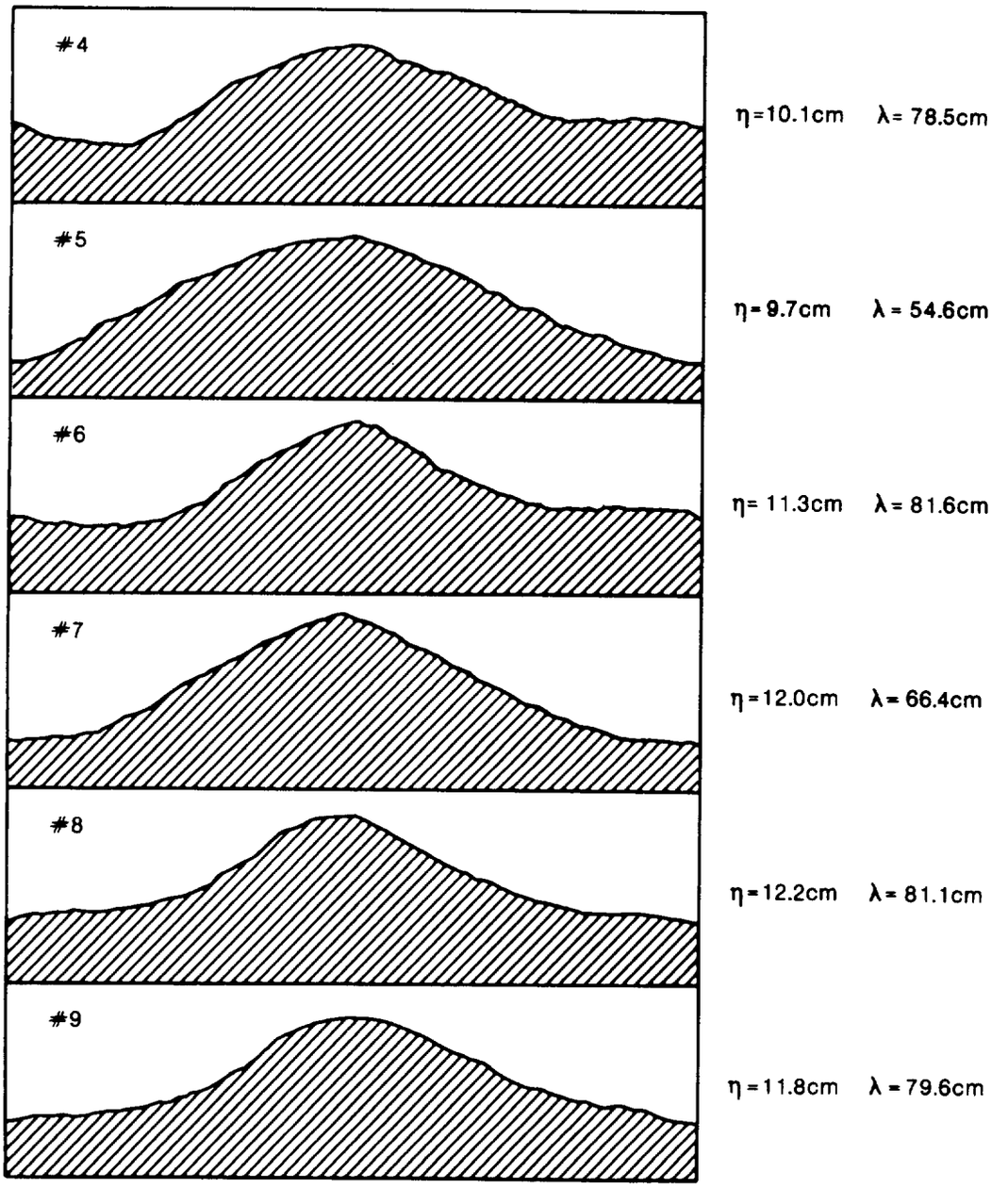

Figure 5(i) Ripple profiles obtained by divers during the 1978 experiment. The profiles are drawn without vertical exaggeration, but have been normalised by their wavelengths.

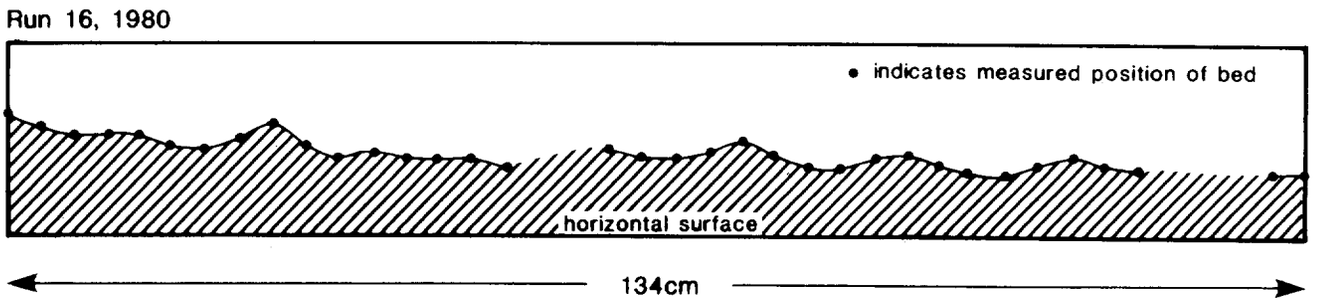

Figure 5(ii) Profile obtained with the "ripple profiler" for Run 16, 1980. The profile is drawn without vertical exaggeration, and with reference to a level horizontal surface. The dashes indicate the absence of data (caused by the failure of certain needles in the array).

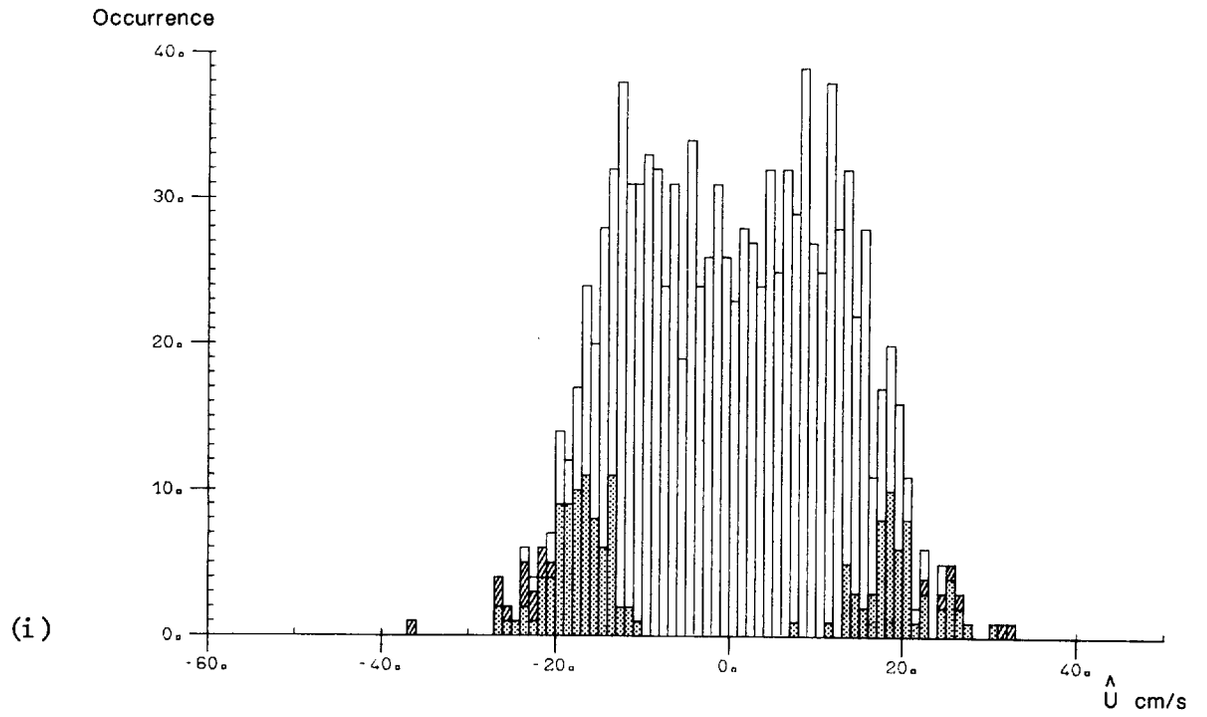

(i)

Figure 6 Histograms for Runs 1 and 3 to 5, 1978, showing the number of values of free-stream velocity amplitude falling within each unit velocity range. The free-stream velocity has been identified, in Figure 6(i), with the measured U-component of horizontal velocity at a height of 130 cm above the bed; in Figure 6(ii), with the total horizontal velocity at this height, defined by $U_T = \text{sgn}(U)\sqrt{U^2 + V^2}$; and, in Figure 6(iii), with the rotated (rectilinear) component of horizontal velocity, U_{ROT}, at the same height. The results are for a rippled bed on which sediment motion was of bedload type and occurred in the region of the crests only. Light shading (dots) denotes "incipient motion"; dark shading (hatching) denotes "general motion". Negative velocity amplitudes relate to motion in the seaward direction, and positive values relate to the shoreward direction.

Representative values: $D_{50} = 0.078$ cm, $\eta = 12$ cm, $\lambda = 74$ cm, $\eta/\lambda \cong 0.16$.

6(ii)

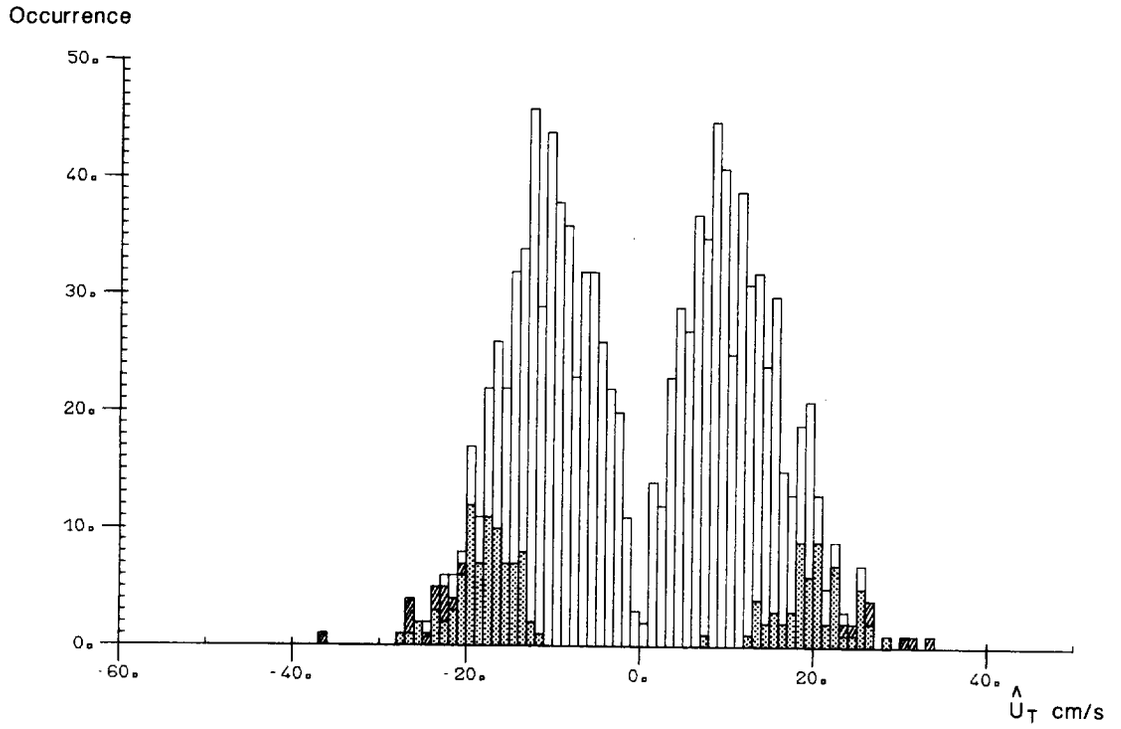
Occurrence
50.
40.
30.
20.
10.
0.
-60.
-40.
-20.
0.
20.
40.
$\hat{U}_T$ cm/s

6(iii)

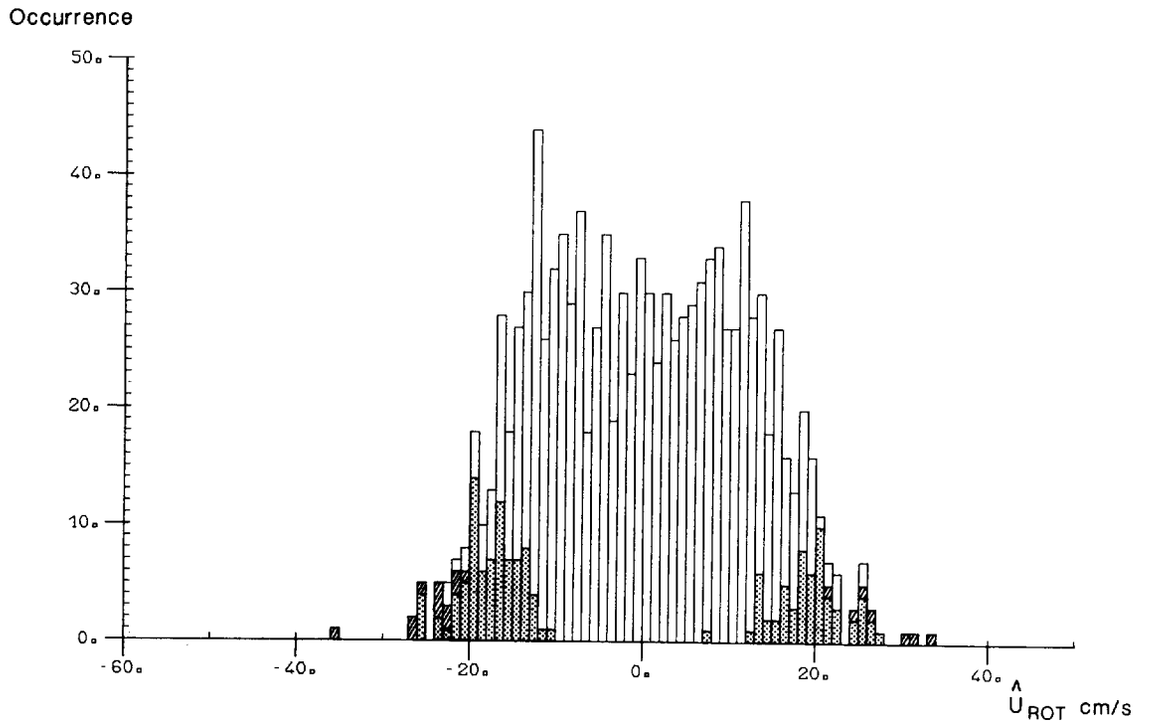
Occurrence
50.
40.
30.
20.
10.
0.
-60.
-40.
-20.
0.
20.
40.
$\hat{U}_{ROT}$ cm/s

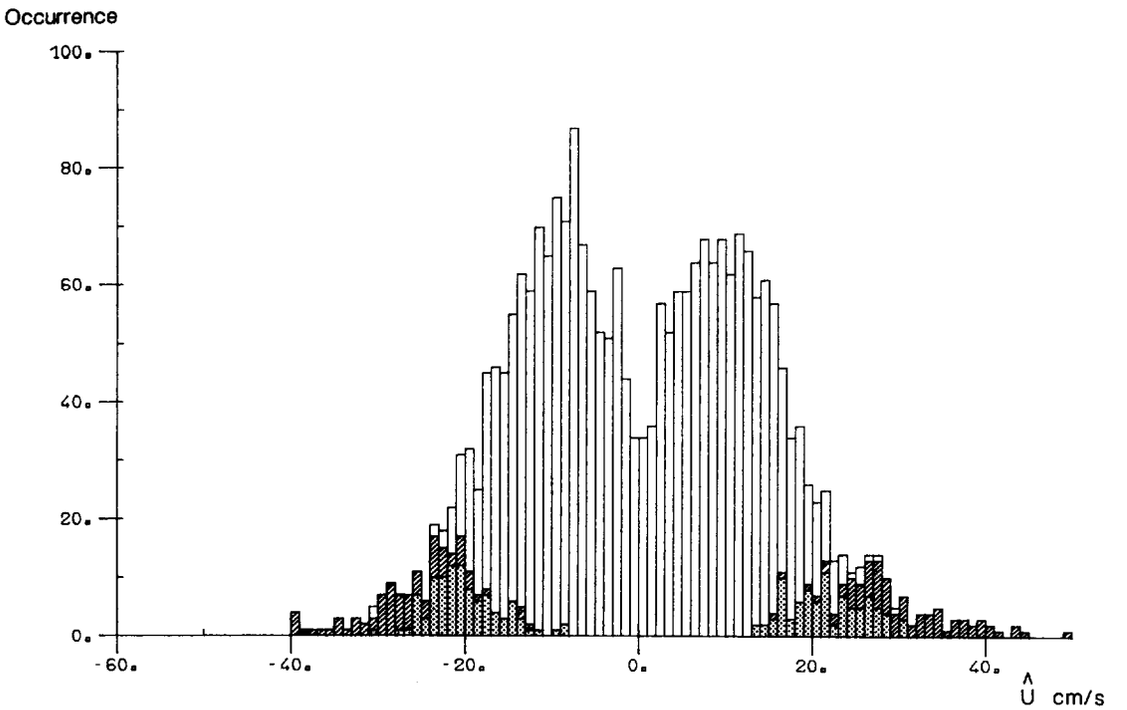

Figure 7 Histogram for Runs 8-14, 1978, showing the number of values of free-stream velocity amplitude falling within each unit velocity range. The free-stream velocity has been identified with the measured U-component of horizontal velocity at a height of 130 cm above the bed (cf Figure 6(i)). Shading is as in Figure 6.

Representative values: D_{50} = 0.078 cm, η = 12 cm, λ = 77 cm, $\eta/\lambda \cong 0.15$.

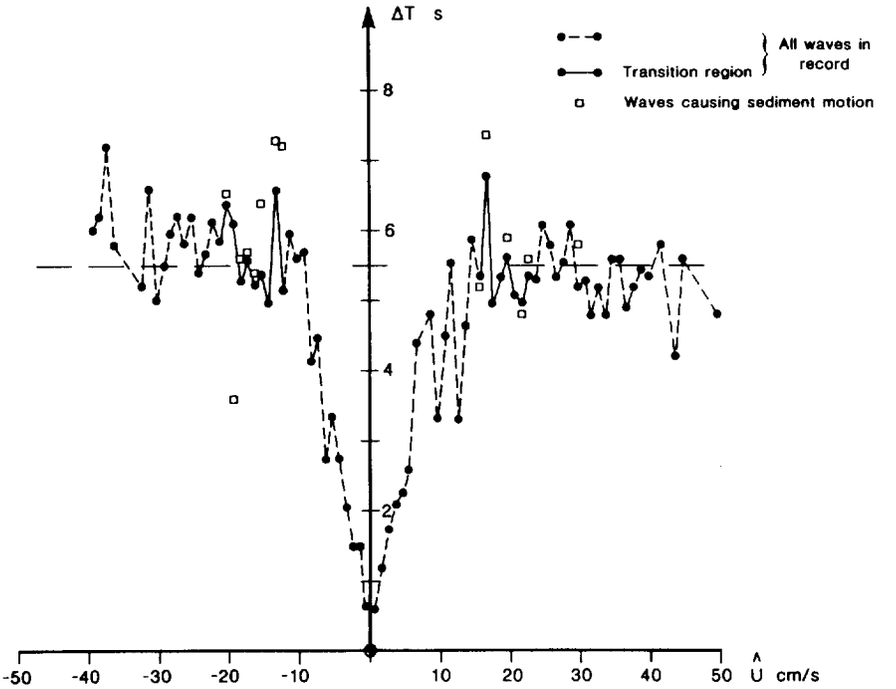

Figure 8 The average wave half-period (ΔT) plotted against horizontal velocity amplitude ($\hat{U}$), for each unit incremental velocity range. The results are for Run 9, 1978, for which the U-component of velocity was measured at a height of 130 cm above the bed. Dots indicate ΔT-values forall the waves in the record. Open squares indicate ΔT-values for the subset of waves in the transition ranges which moved sediment; outside the transition ranges, all the waves moved sediment.

Figure 9 Histograms for individual runs in the 1980 experiment: (i) Run 5, (ii) Run 10, (iii) Run 11, (iv) Run 12, (v) Run 14 and (vi) Run 15. Each histogram shows the number of values of free-stream velocity amplitude falling within each incremental velocity range. The free-stream velocity has been identified with the measured U-component of horizontal velocity at a height of 160 cm above the bed (cf Figures 6(i) and 7). Representative values of grain diameter, and ripple height and wavelength, are listed in Tables 2 and 5. The type of sediment motion is indicated by the shading. Light shading (dots) denotes "incipient motion"; dark shading (hatching) denotes "general motion"; and black shading denotes sediment suspension. When motion was of any of the above types, it occurred over the entire bed surface.

9 (i)

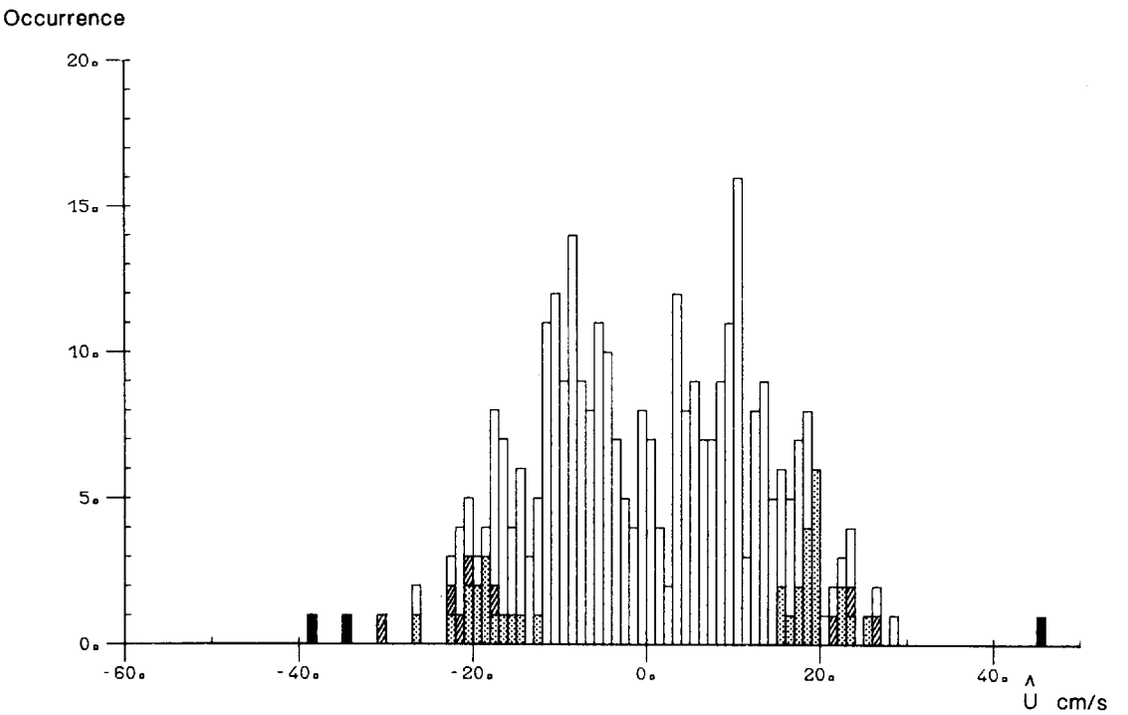
Occurrence
20.
15.
10.
5.
0.
-60.
-40.
-20.
0.
20.
40.
Û cm/s

9(ii)

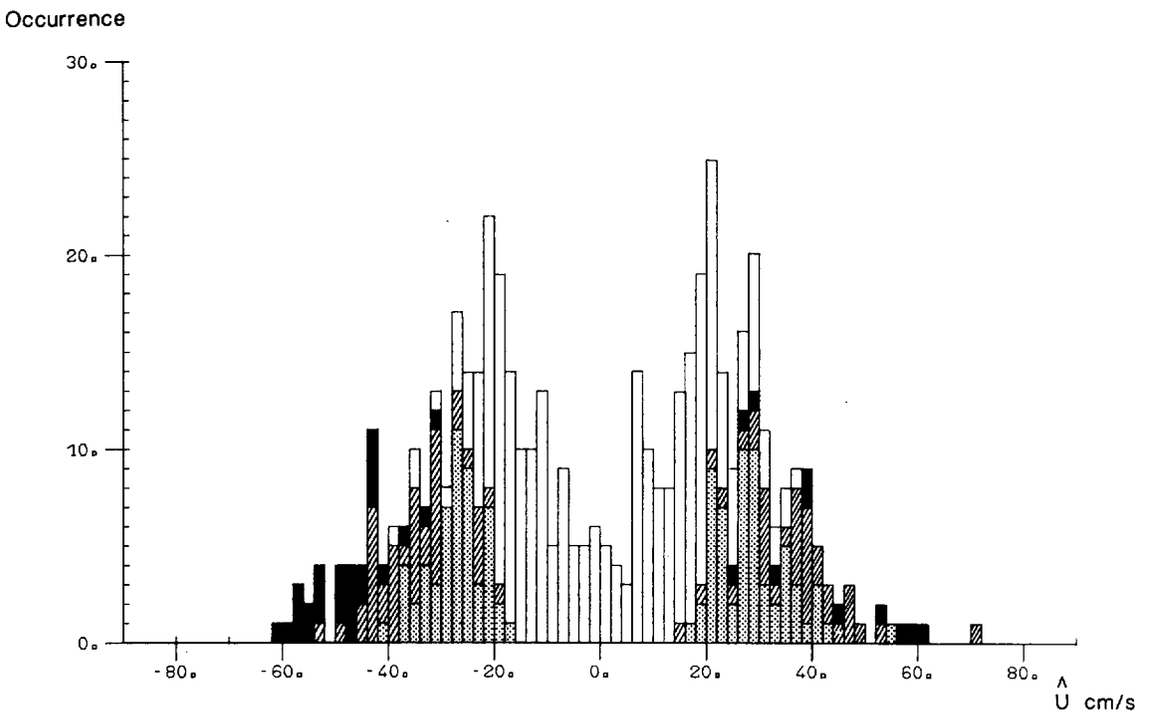
Occurrence
30.
20.
10.
0.
-80.
-60.
-40.
-20.
0.
20.
40.
60.
80.
Û cm/s

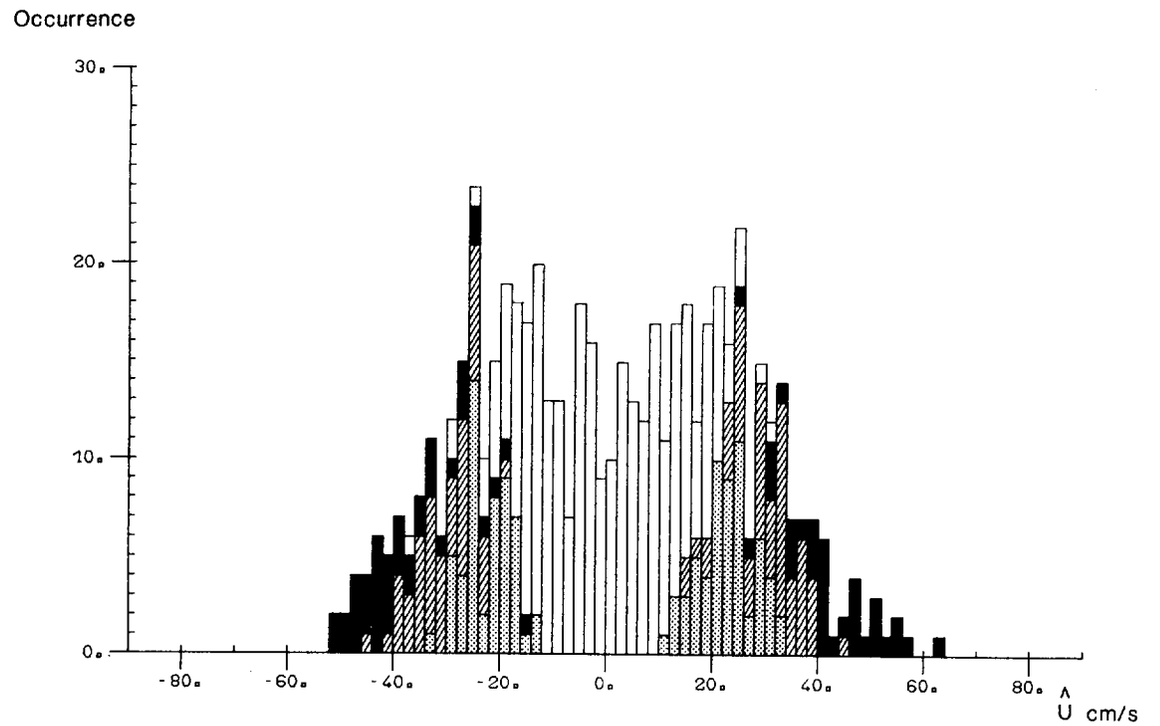
Occurrence
30.
20.
10.
0.
-80.
-60.
-40.
-20.
0.
20.
40.
60.
80.
U cm/s

9(iii)

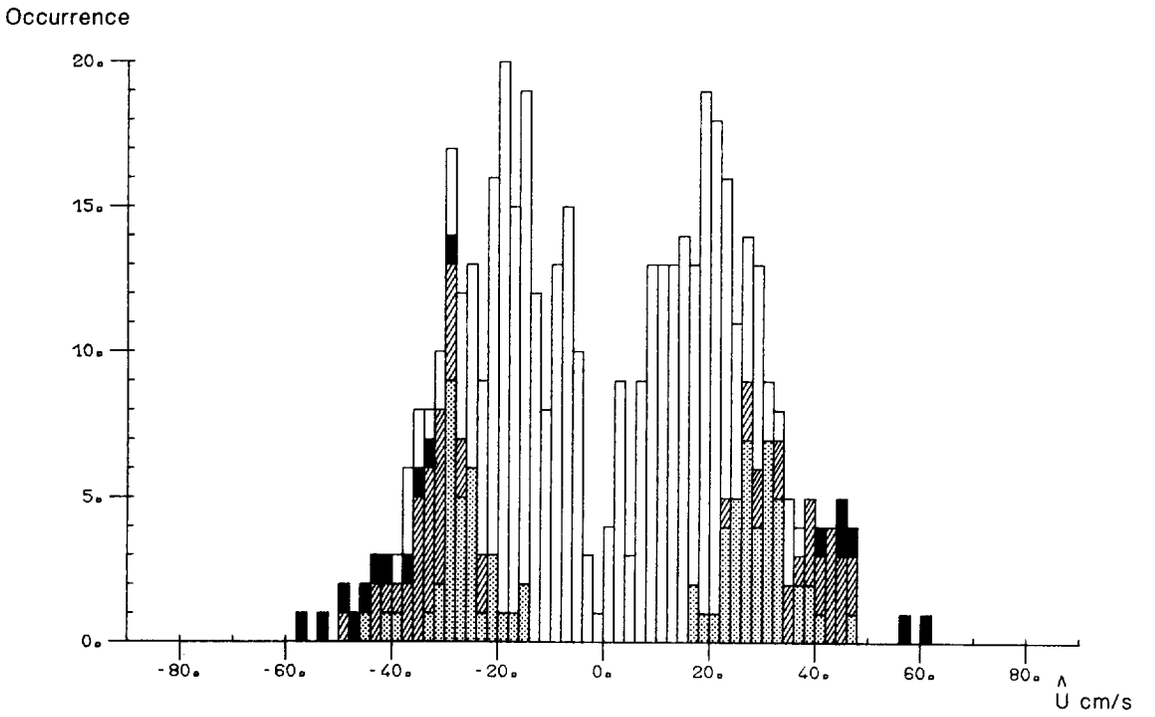
Occurrence
20.
15.
10.
5.
0.
-80.
-60.
-40.
-20.
0.
20.
40.
60.
80.
U cm/s

9(iv)

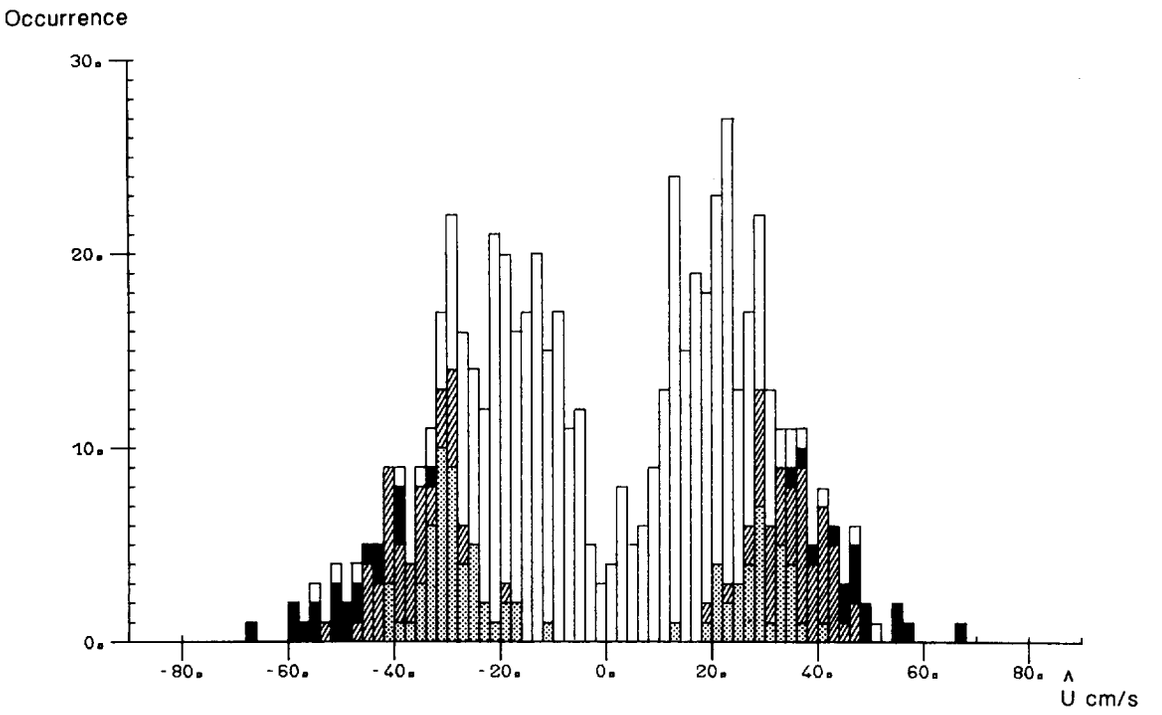
Occurrence
30.
20.
10.
0.
-80.
-60.
-40.
-20.
0.
20.
40.
60.
80.
U cm/s

9(v)

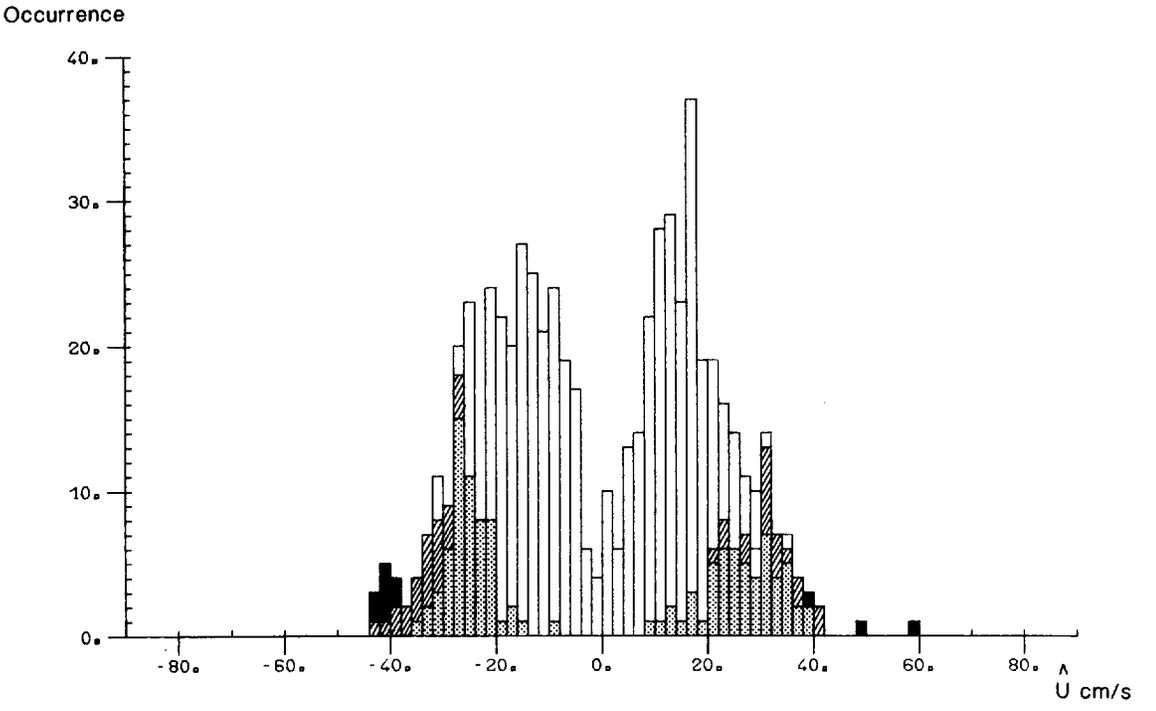
Occurrence
40.
30.
20.
10.
0.
-80.
-60.
-40.
-20.
0.
20.
40.
60.
80.
U cm/s

9(vi)

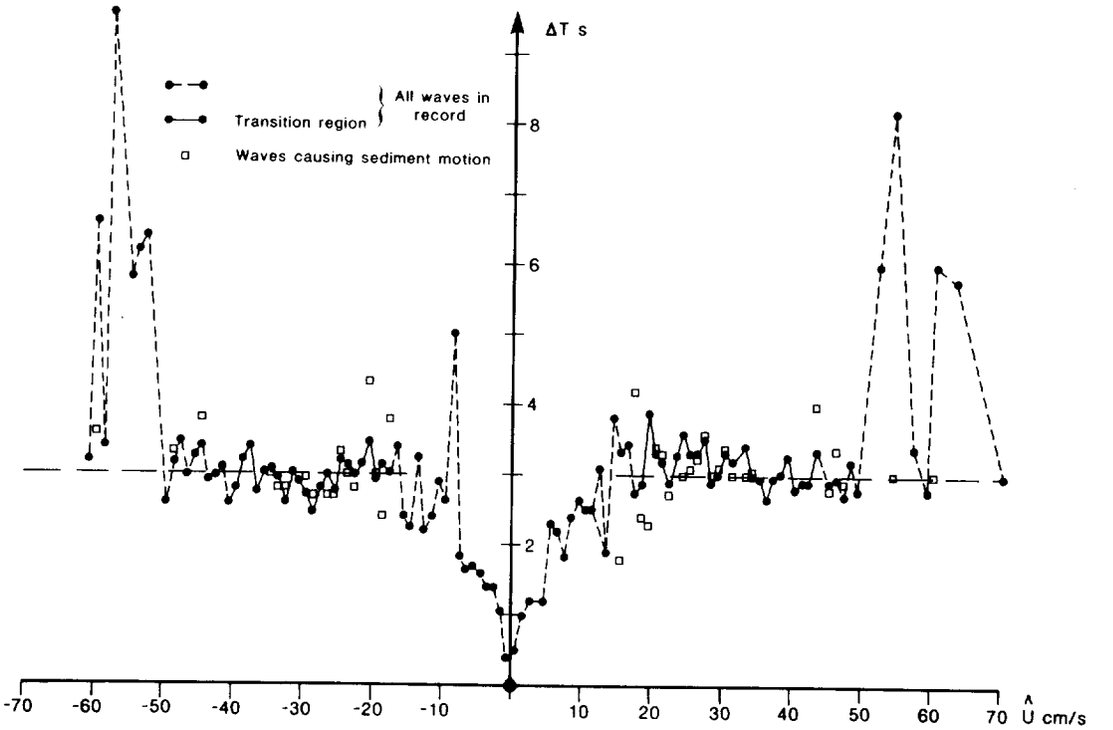

Figure 10 The average wave half-period (ΔT) plotted against horizontal velocity amplitude ($\hat{U}$) for each unit incremental velocity range. The results are for Run 10, 1980, for which the U-component of velocity was measured at a height of 160 cm above the bed. Dots indicate ΔT-values for all the waves in the record. Open squares indicate ΔT-values for the subset of waves in the transition ranges which moved sediment: outside the transition ranges, all the waves moved sediment.

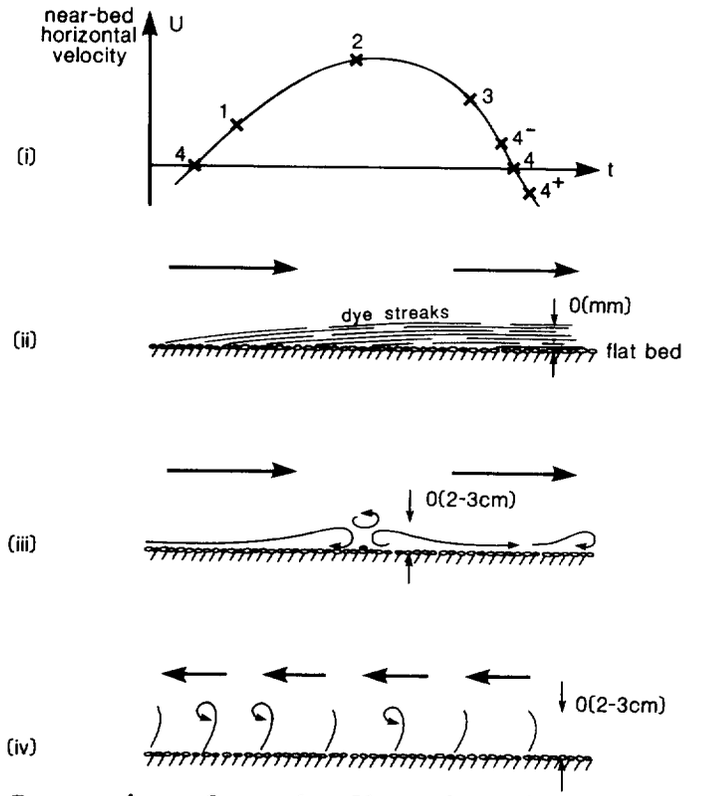

Figure 11 Impressions from the flow visualisation test carried out during Run 6, 1980, above a flat sand bed.

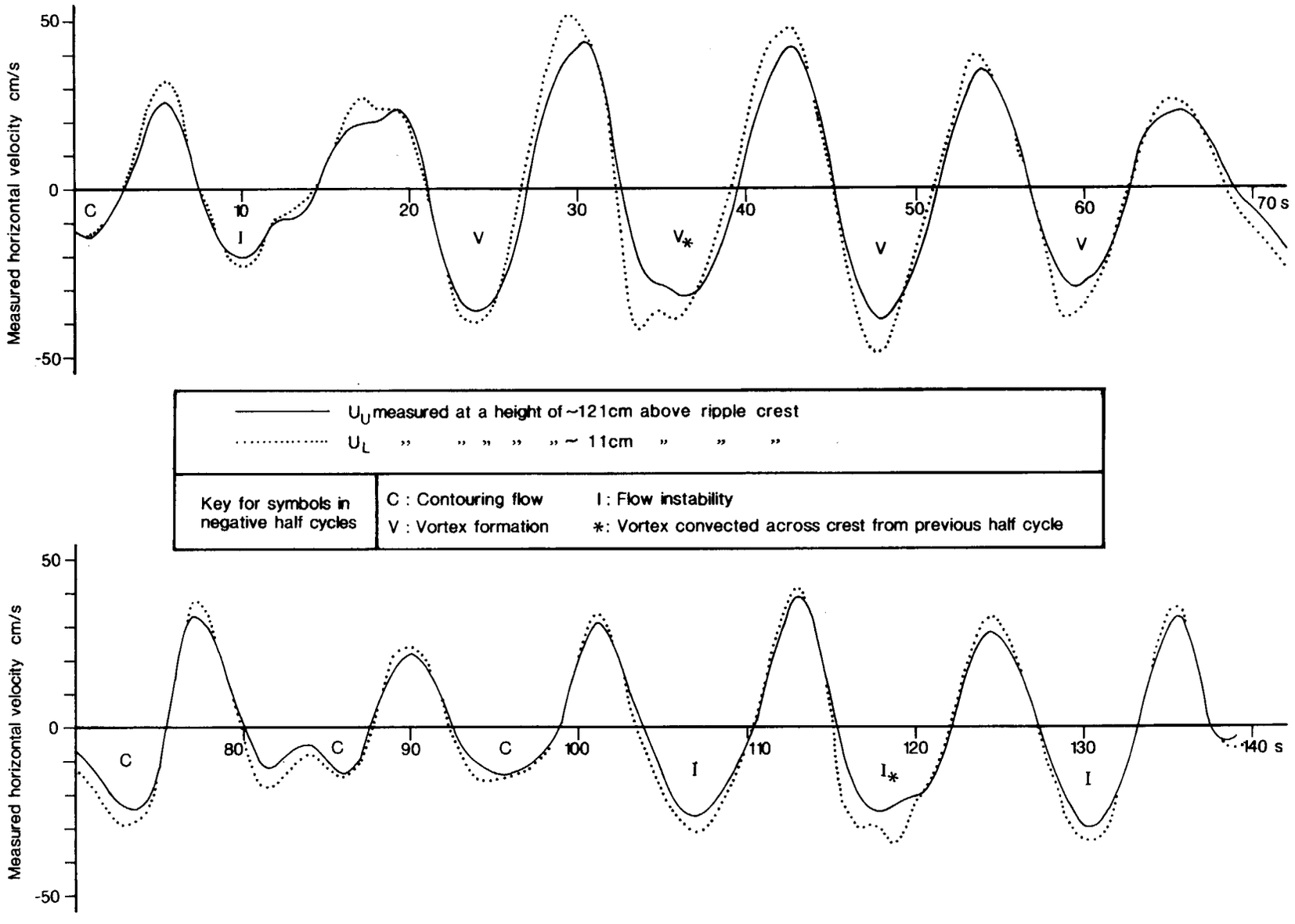

Figure 12 Portion of recorded horizontal velocity data (from Run 9, 1978) made above the crest of a ripple (λ = 74 cm, η = 12 cm). Note that in the two wave half-cycles marked with an asterisk, the lower velocity record has a perturbation which was associated with the passage of a vortex below the lower EM-head at a height of 11 cm above the ripple crest.

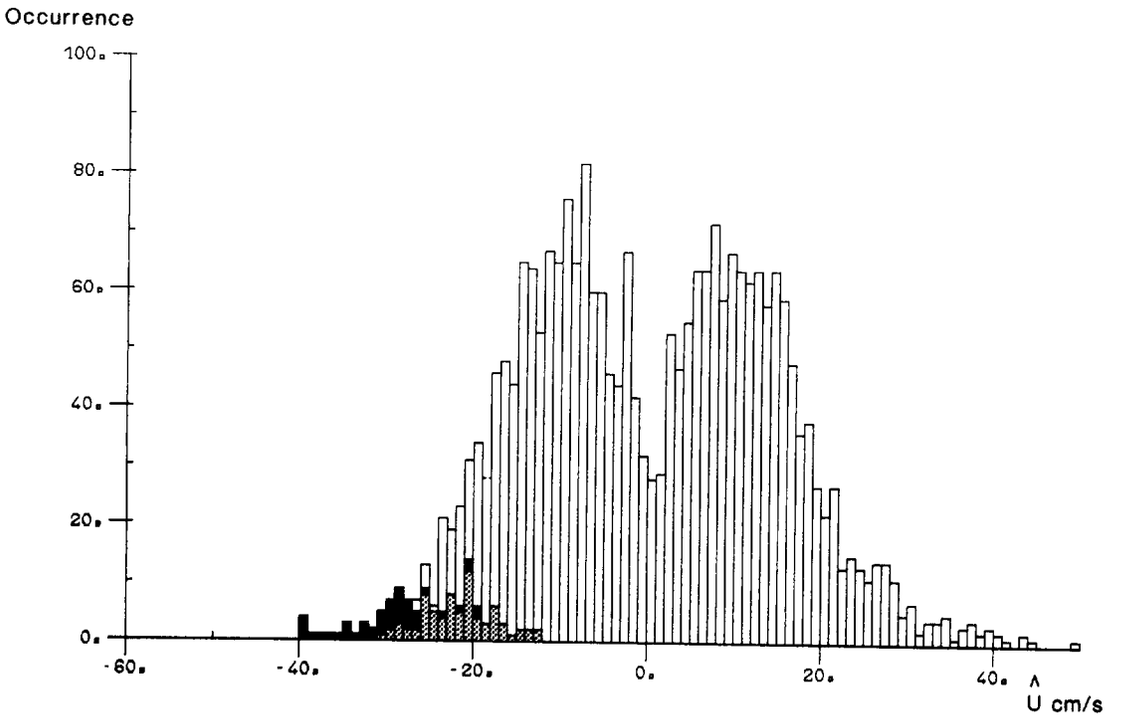

Figure 13 Histogram based upon the measured free-stream velocity ($\hat{U}$) for the same data set as in Figure 7 (Runs 8-14, 1978). Light shading (dots) now denotes flow "instability"; black shading denotes vortex formation. Since the flow above only one side of the ripple was clearly visible on the underwater television records, results for instability and vortex formation are included only for those half-cycles having negative peak velocities.

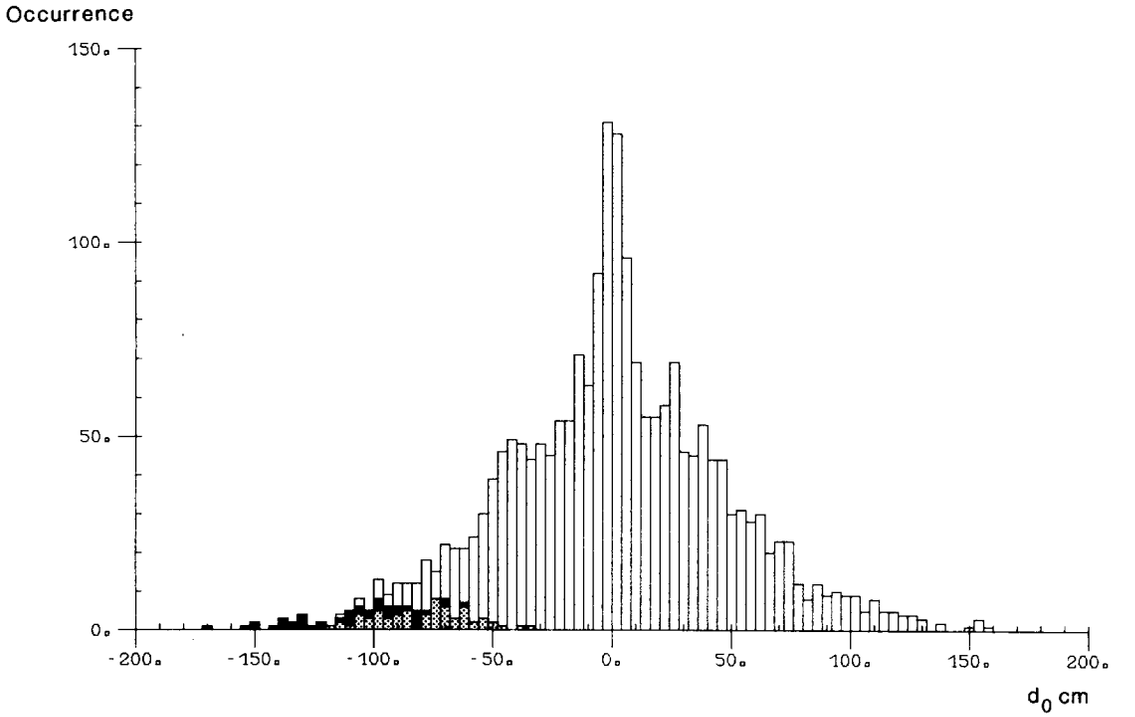

Figure 14 Histogram based upon the calculated orbital excursion (d_o) for Runs 8-14, 1978. Wave half-cycles with double velocity maxima have been excluded. Shading is as in Figure 13.

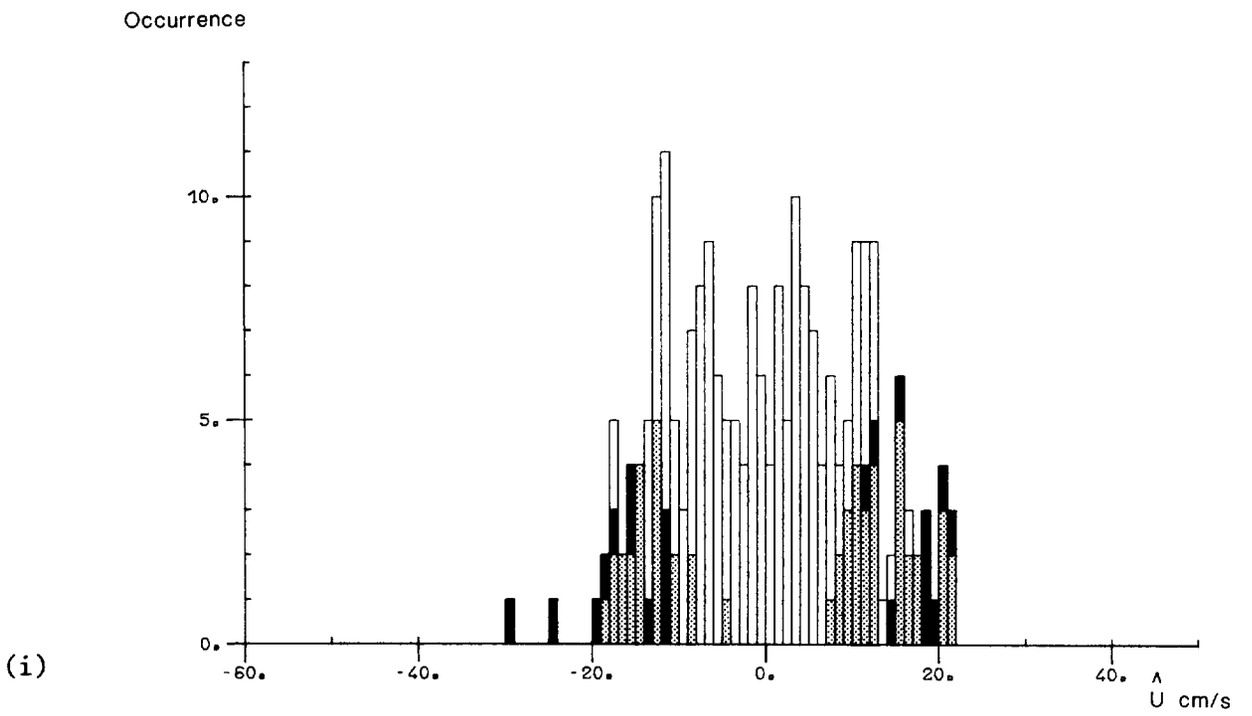

(i)

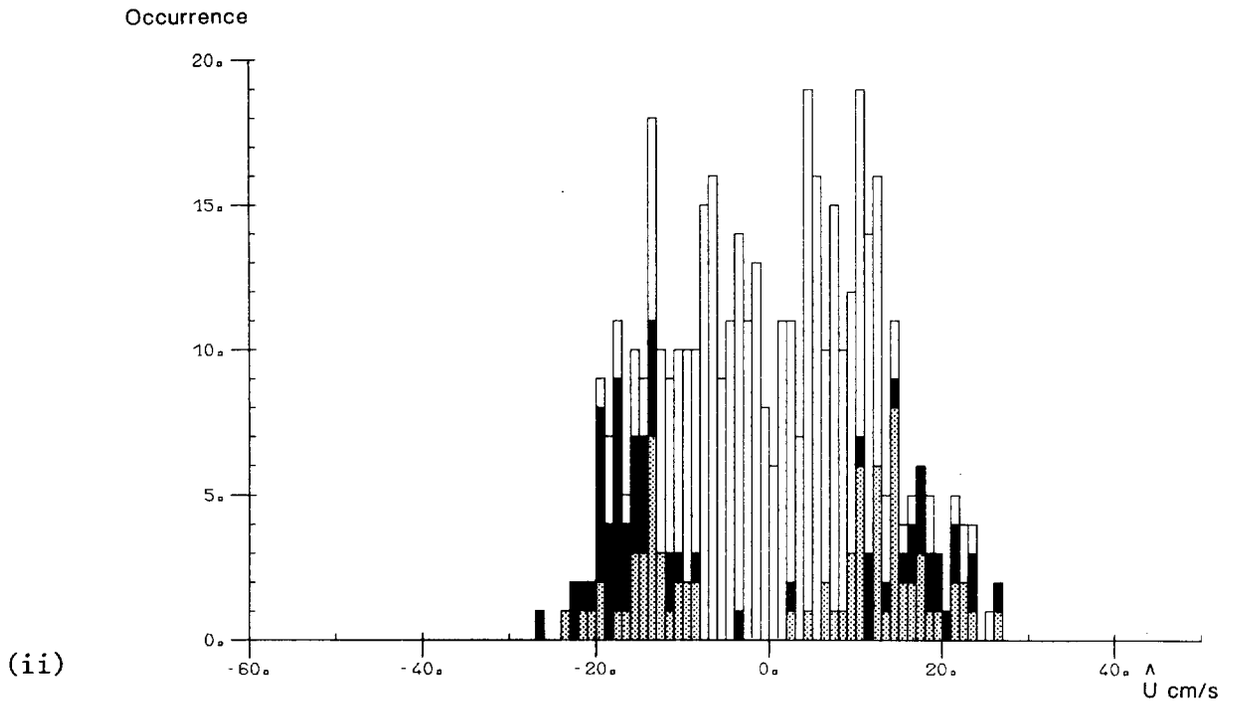

(ii)

Figure 15 Histograms based upon the measured free-stream velocity (U) for (i) Run 8, 1980 and (ii) Run 17, 1980. Shading is as in Figure 13.

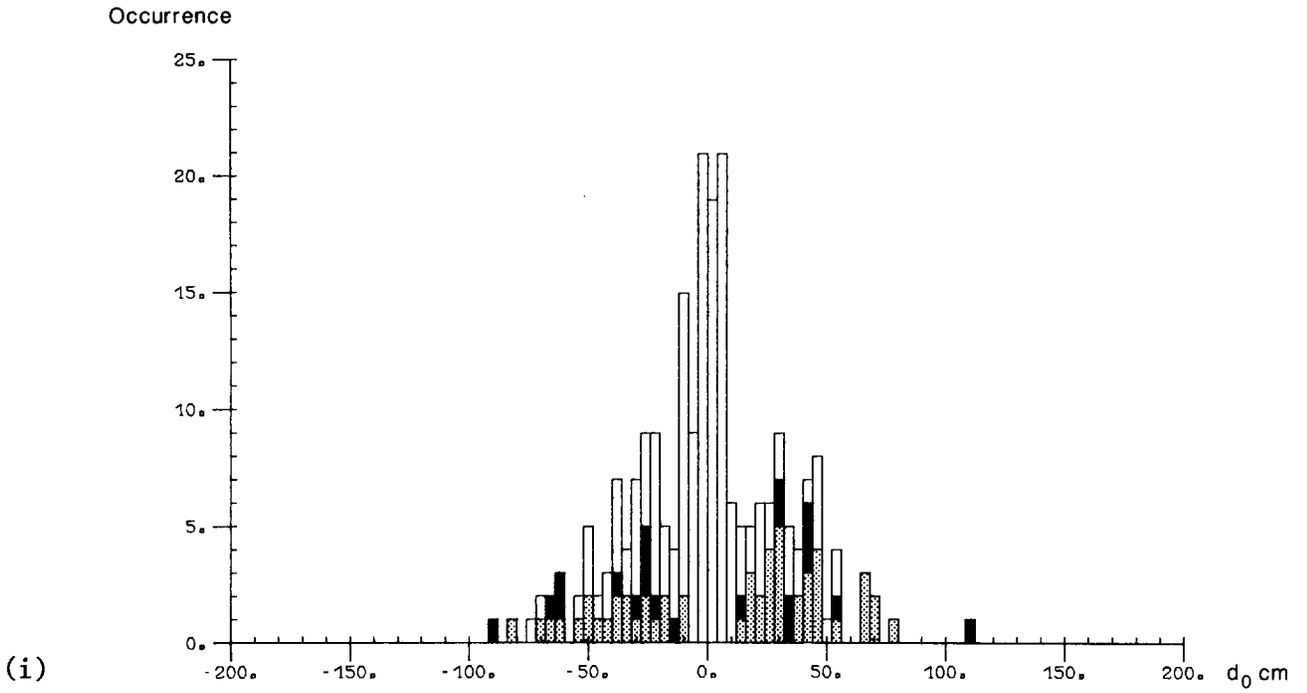

(i)

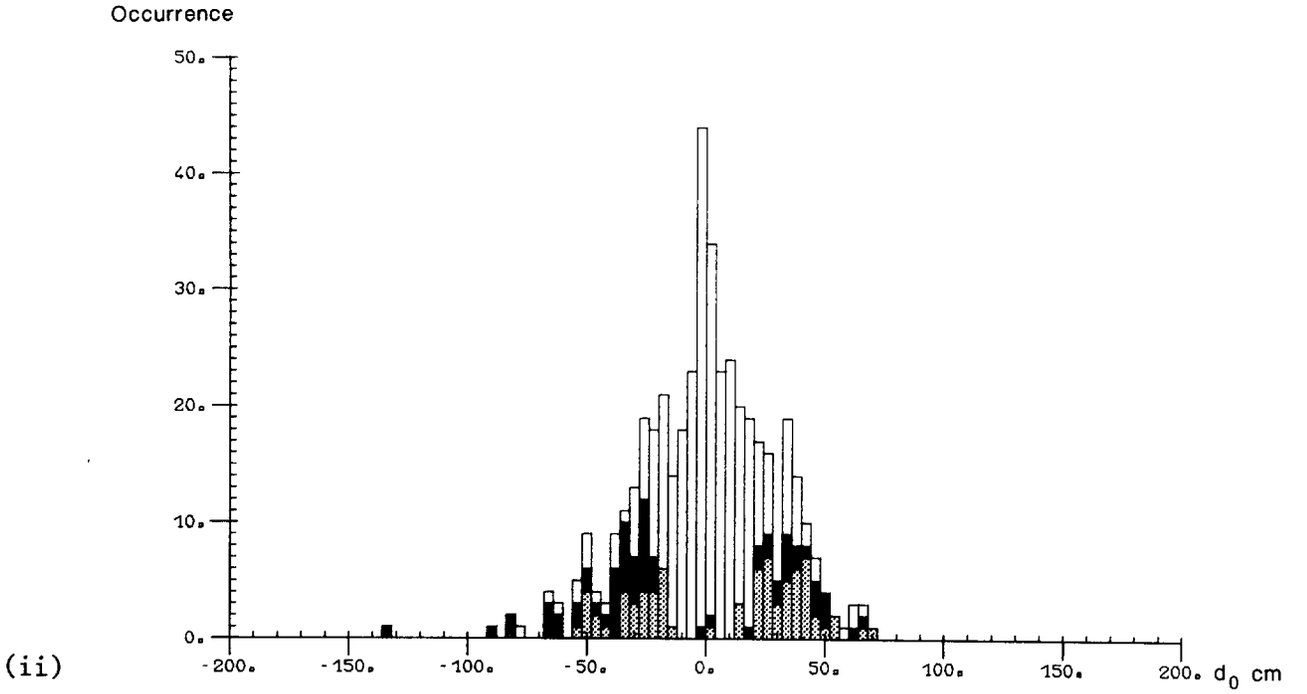

(ii)

Figure 16 Histograms based upon the calculated orbital excursion (d_o) for (i) Run 8, 1980, and (ii) Run 17, 1980. Shading is as in Figure 13.

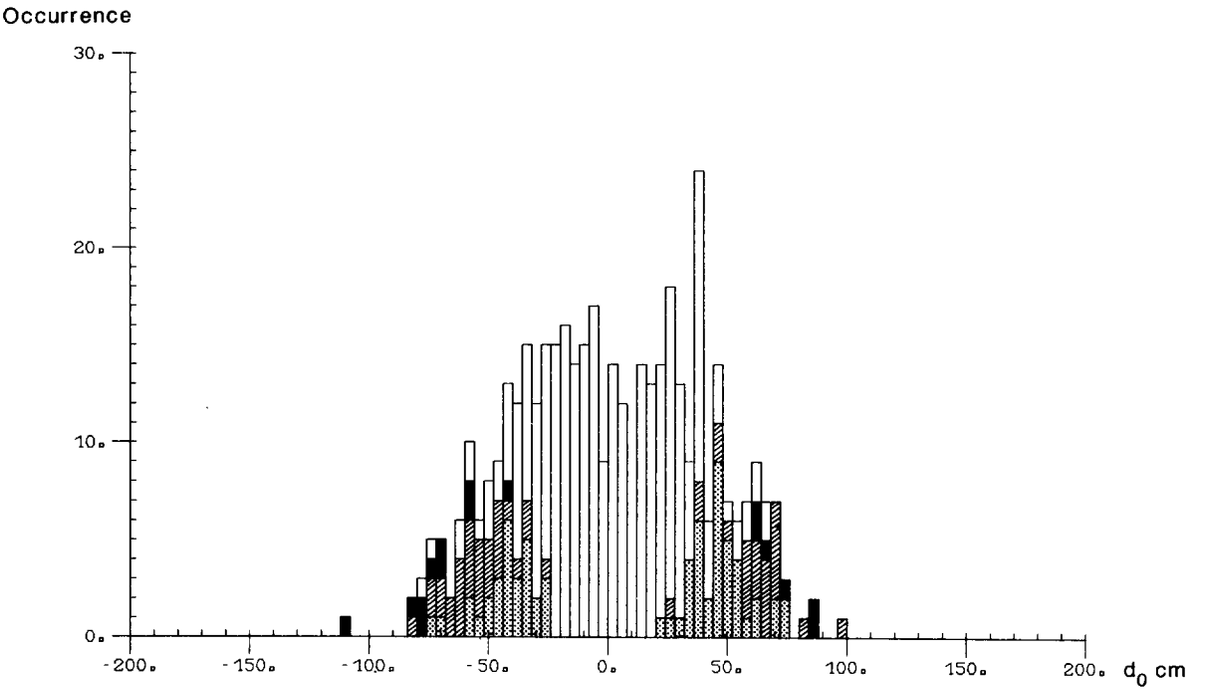

Figure 17 Histogram based upon the calculated orbital excursion (d_o) for Run 12, 1980. Wave half-cycles with double velocity maxima have been excluded. Shading is as in Figure 9.

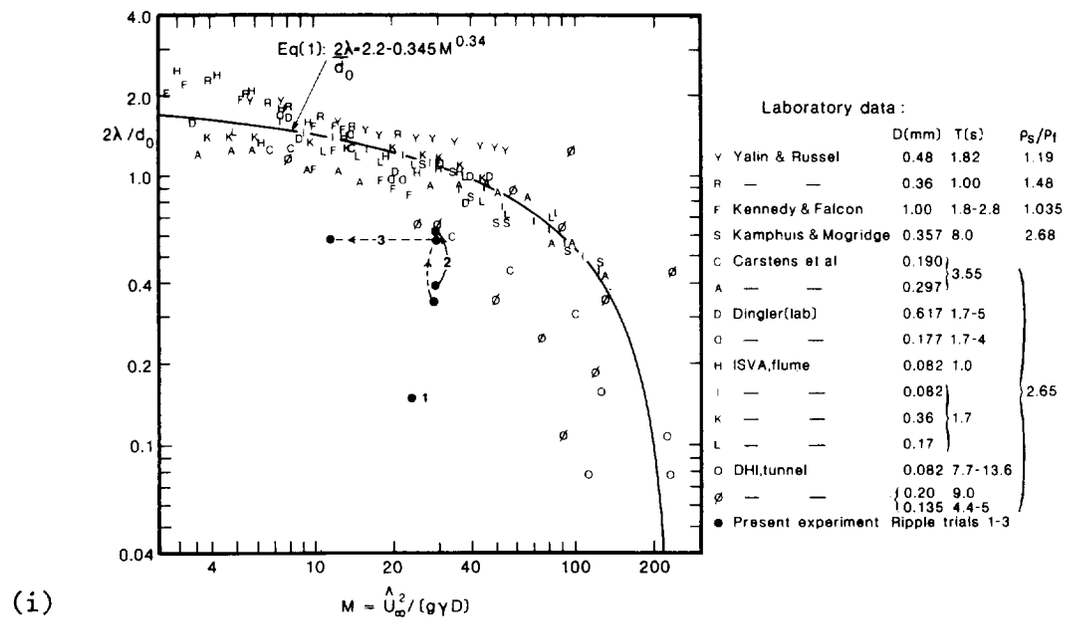

(i)

Figure 18 Results from the ripple formation trials in the 1980 experiment plotted on two graphs presented by Nielsen (1979, Figures 5.16 and 5.17), containing results from (i) previous laboratory studies and (ii) previous field studies. In both cases, the quotient ($2\lambda/d_o$) is plotted against the mobility number M. In Figure 18(i), Nielsen's suggested relationship (Equation (1)) between these quantities for laboratory studies is plotted; in Figure 18(ii), Equation (1) is plotted again, together with Nielsen's suggested relationship (Equation (2)) for field applications.

18(ii)

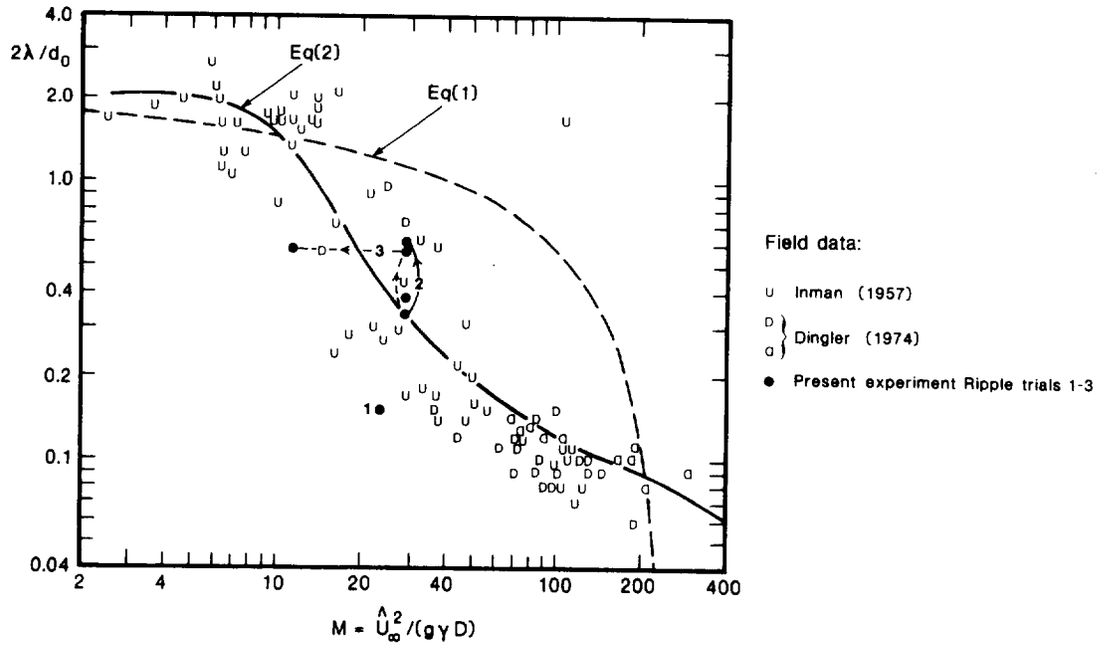

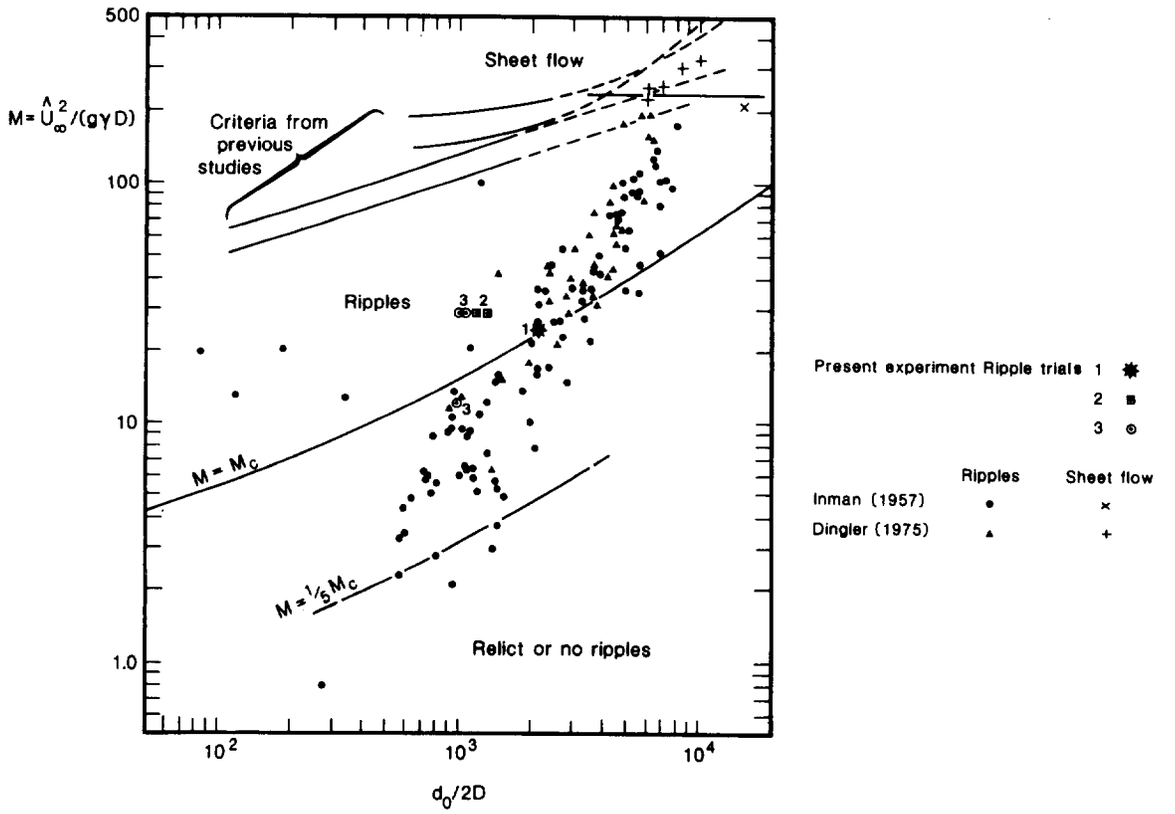

Figure 19 Results from the ripple formation trials in the 1980 experiment shown on a graph presented by Lofquist (1978, Figure 32), in which the mobility number M is plotted against the quotient ($d_o/2D$). This graph delineates the regime of ripple occurrence on the bed. Note that the threshold of sediment motion on a flat bed is indicated by the curve $M = M_c$, and that the boundary between the "ripple" and "sheet flow" regions is defined by criteria proposed by several previous workers (for details, see Lofquist (1978)).

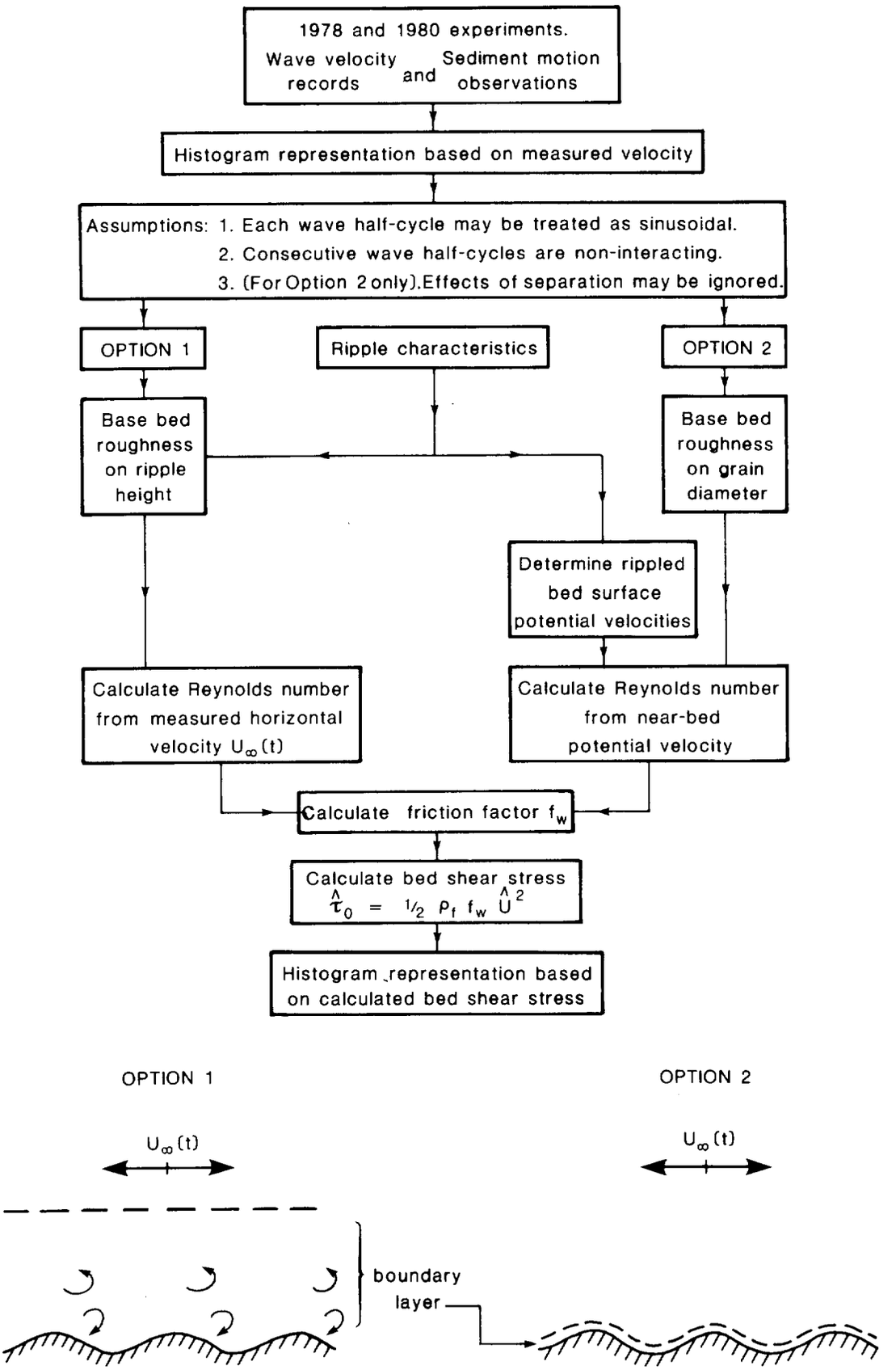

Figure 20 Schematic diagram of the analysis procedures for the 1978 and 1980 experiments.

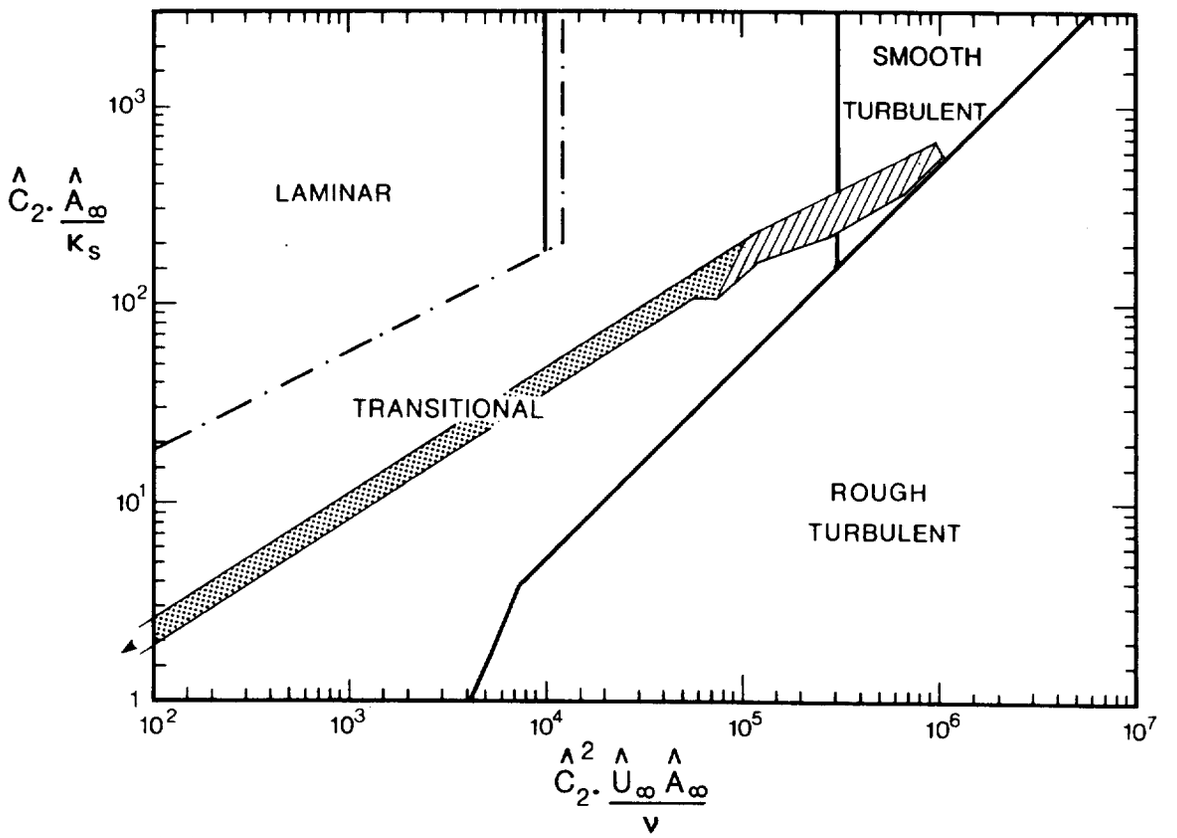

Figure 21 Classification of flow regimes. The shaded area encompasses all the wave half-cycles in Runs 8-14, 1978. The hatched area indicates those half-cycles in which sediment motion was observed. The solid lines indicate Jonsson's (1978) recommended criteria for the boundaries between the transitional and both the laminar and turbulent flow regimes. The dash-dot line indicates Jonsson's (1967) criterion for the boundary between the transitional and laminar flow regimes.

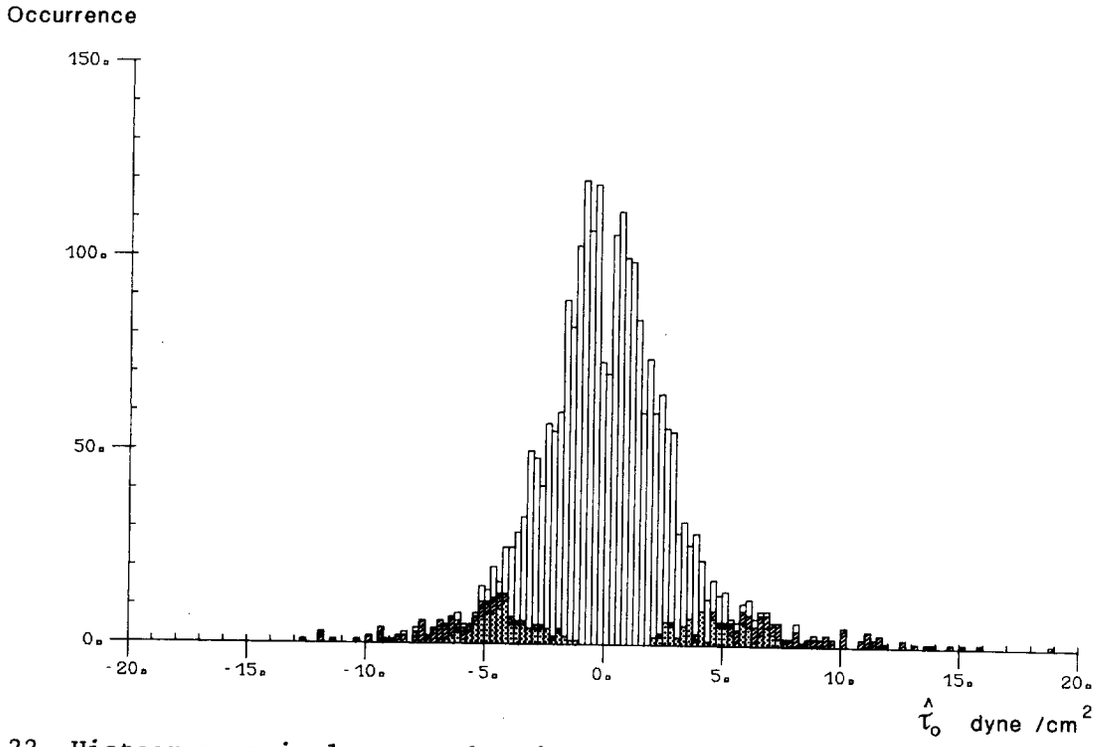

Figure 22 Histogram equivalent to that in Figure 7, but with the amplitude of the calculated bed shear stress (skin friction) plotted on the abscissa (Runs 8 to 14, 1978).

Figure 23 Flow classifications, and histograms based upon the amplitude of the bed shear stress, for the 1980 experiment. In the flow classification diagrams, the shaded areas encompass all the wave half-cycles in each run, and the hatched areas indicate those half-cycles in which sediment motion was observed. The lines delineating the flow regimes are as in Figure 21. In the histograms, light shading (dots) denotes incipient motion; dark shading (hatching) denotes general bedload motion; and black shading denotes sediment suspension. When motion was of any of the above types, it occurred over the entire bed surface. The free-stream velocity has been identified with the measured U-component of horizontal velocity at a height of 160 cm above the bed. Representative values of grain diameter, and ripple height and wavelength, are listed in Tables 2 and 5.

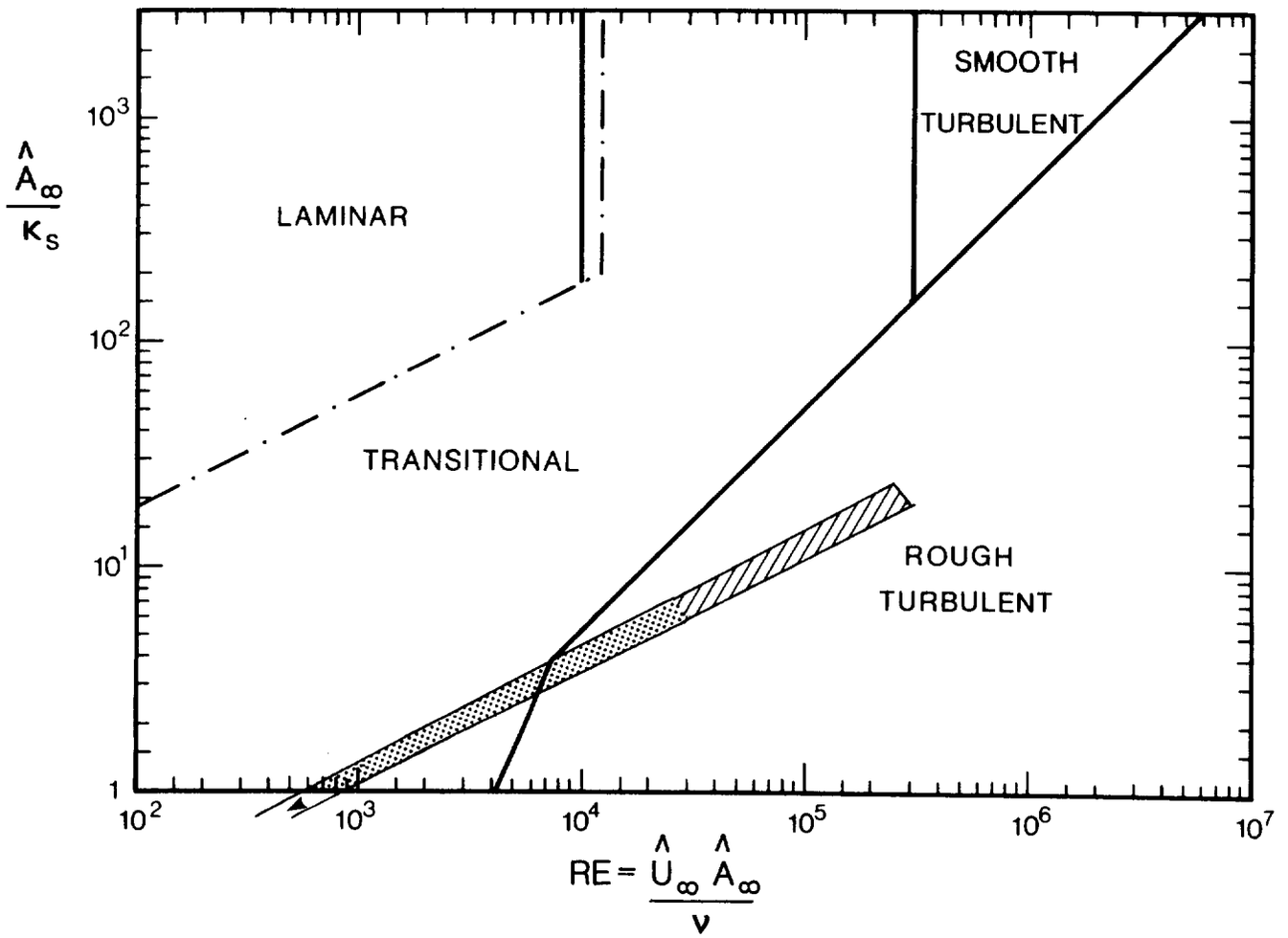

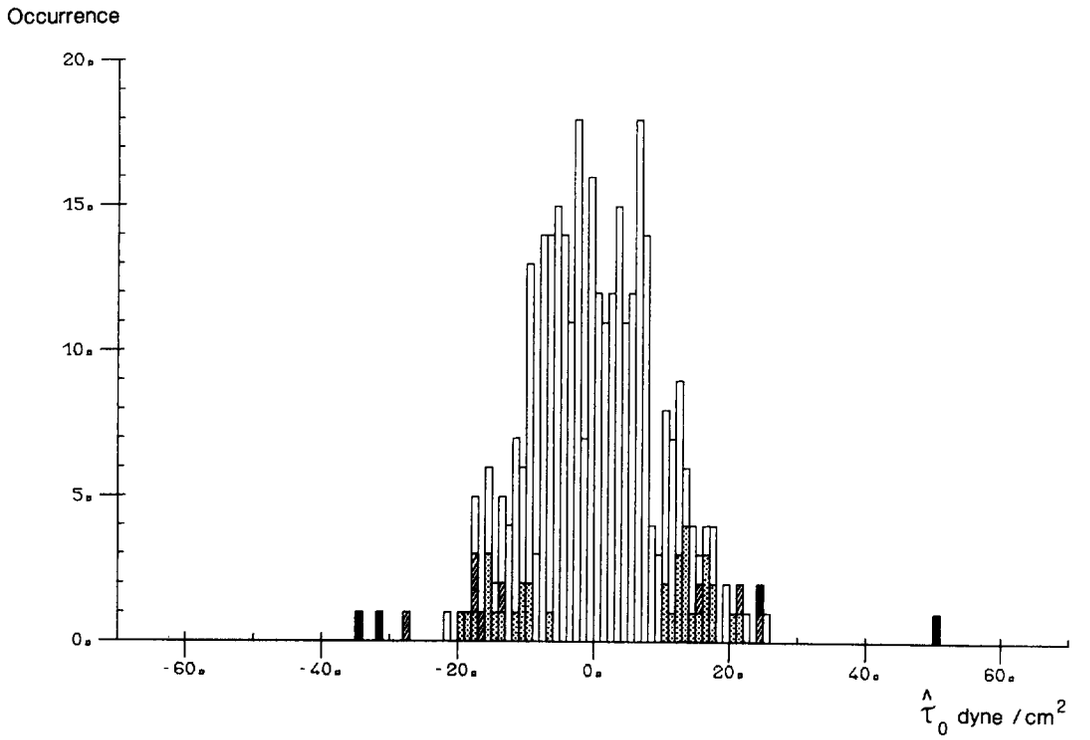

Figure 23(i) Flow classification, and histogram based on the amplitude of the bed shear stress, for Run 5, 1980.

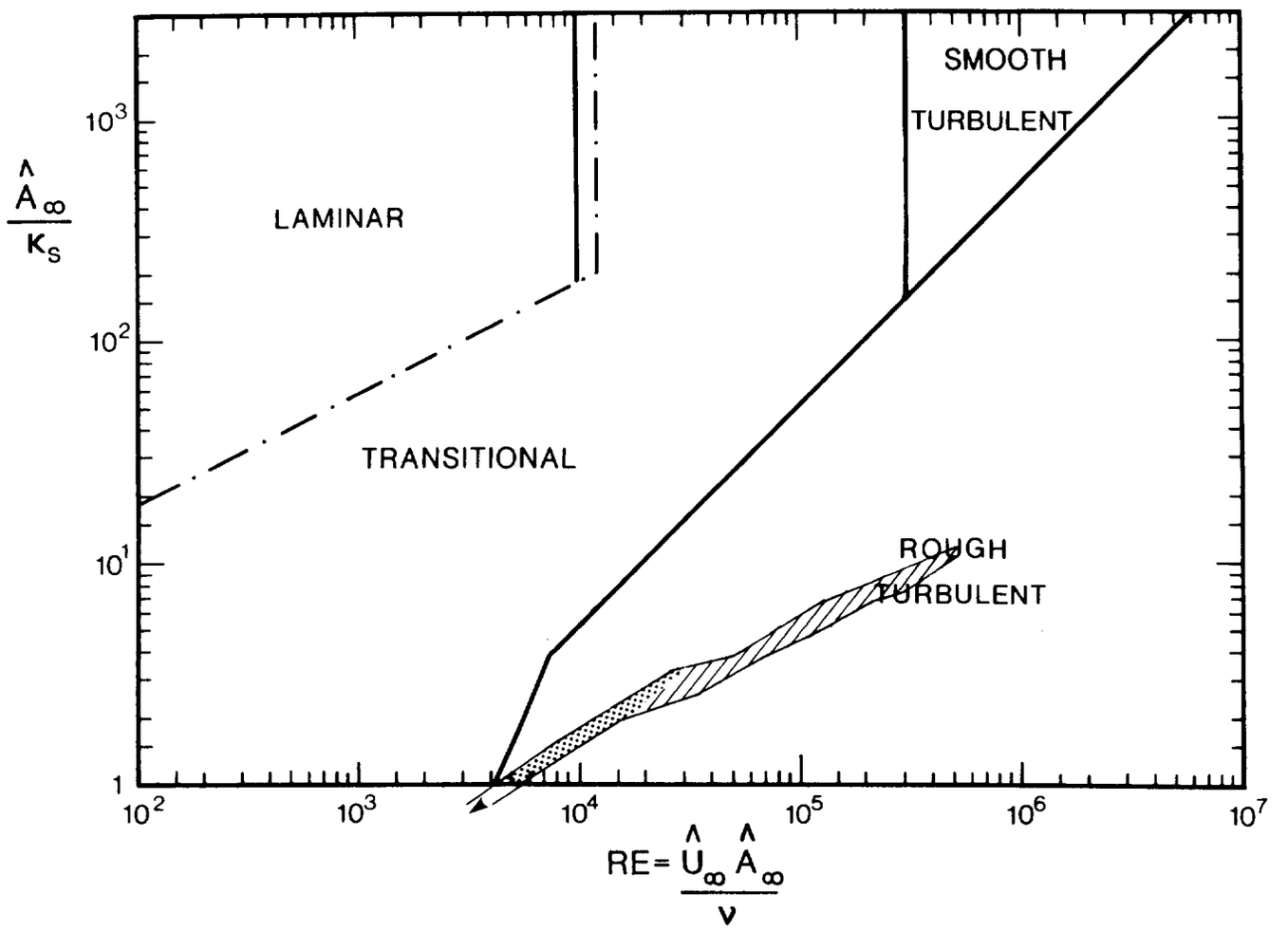

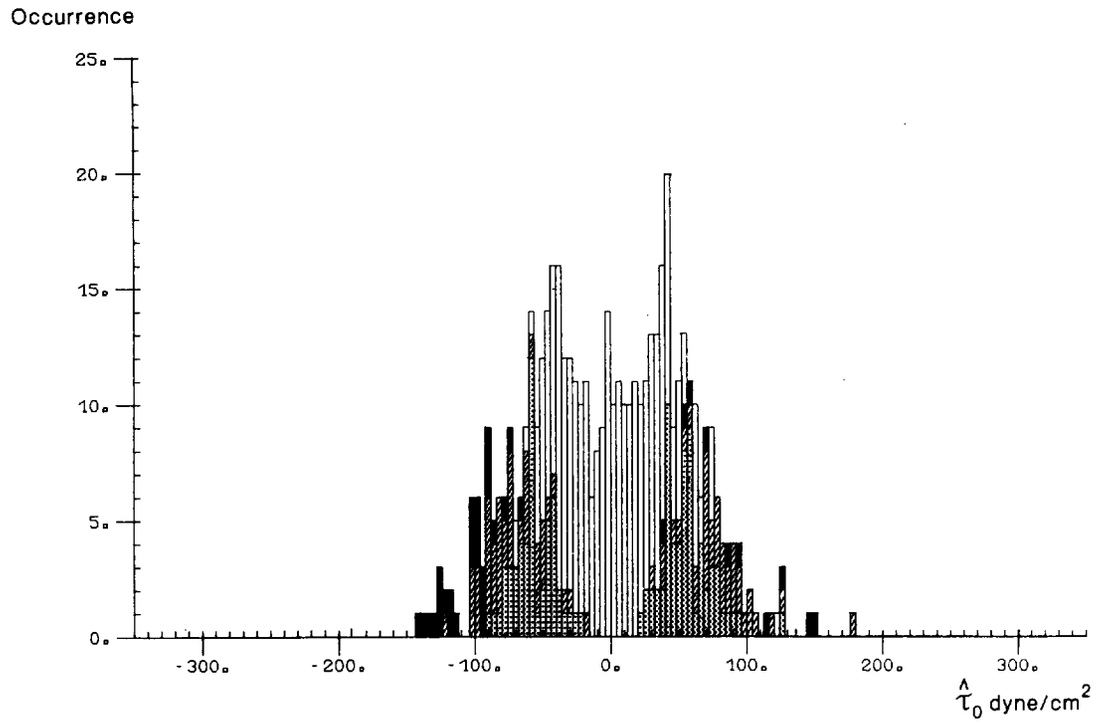

Figure 23(ii) Flow classification, and histogram based on the amplitude of the bed shear stress, for Run 10, 1980.

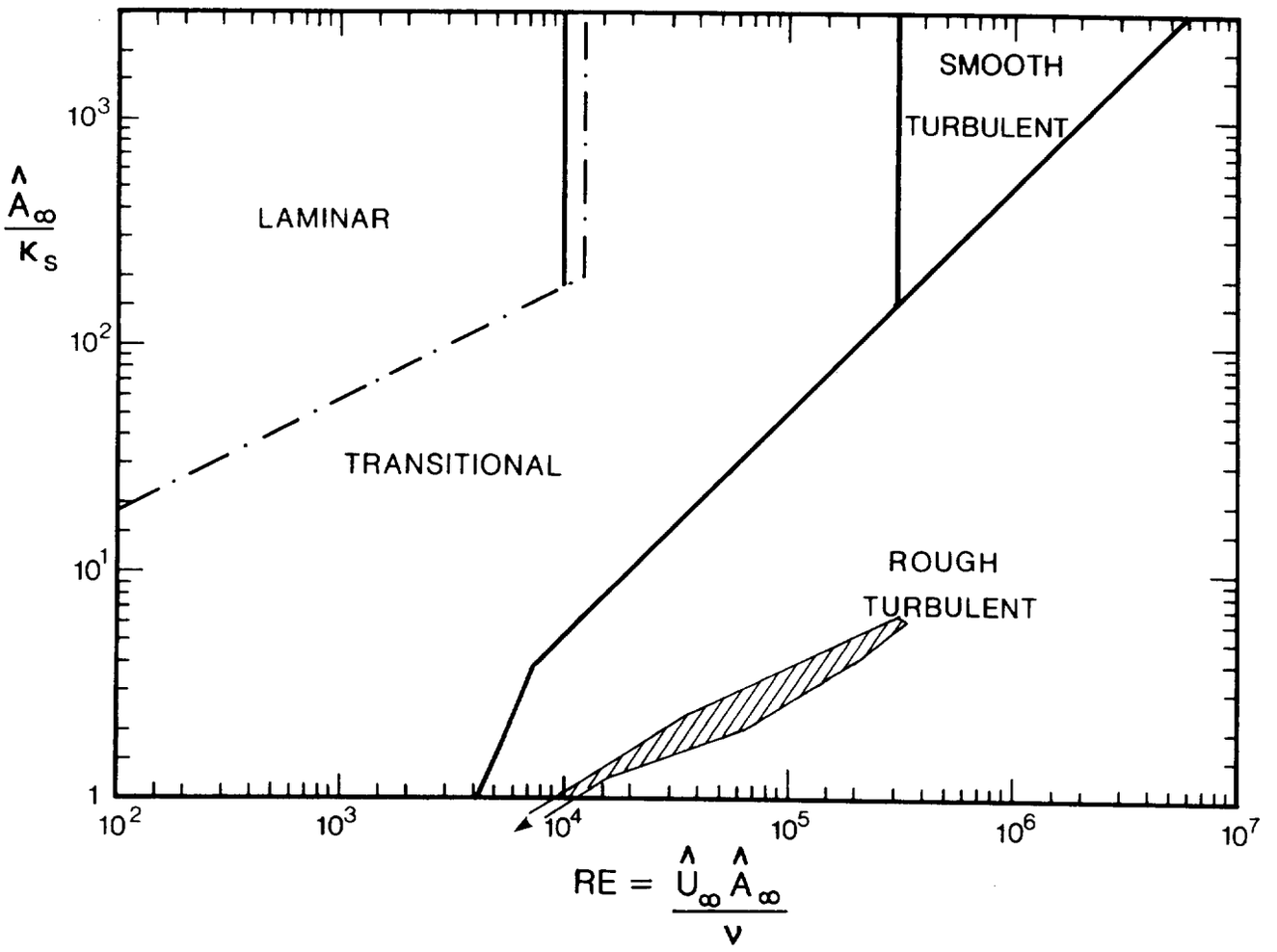

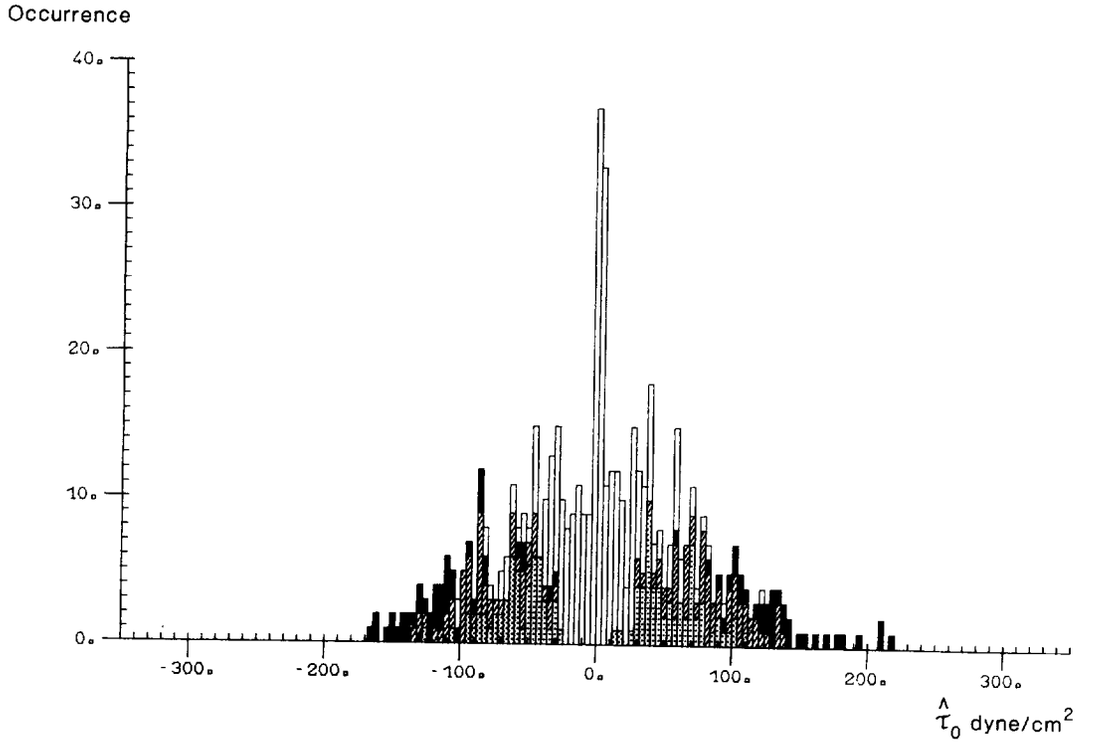

Figure 23(iii) Flow classification, and histogram based on the amplitude of the bed shear stress, for Run 11, 1980.

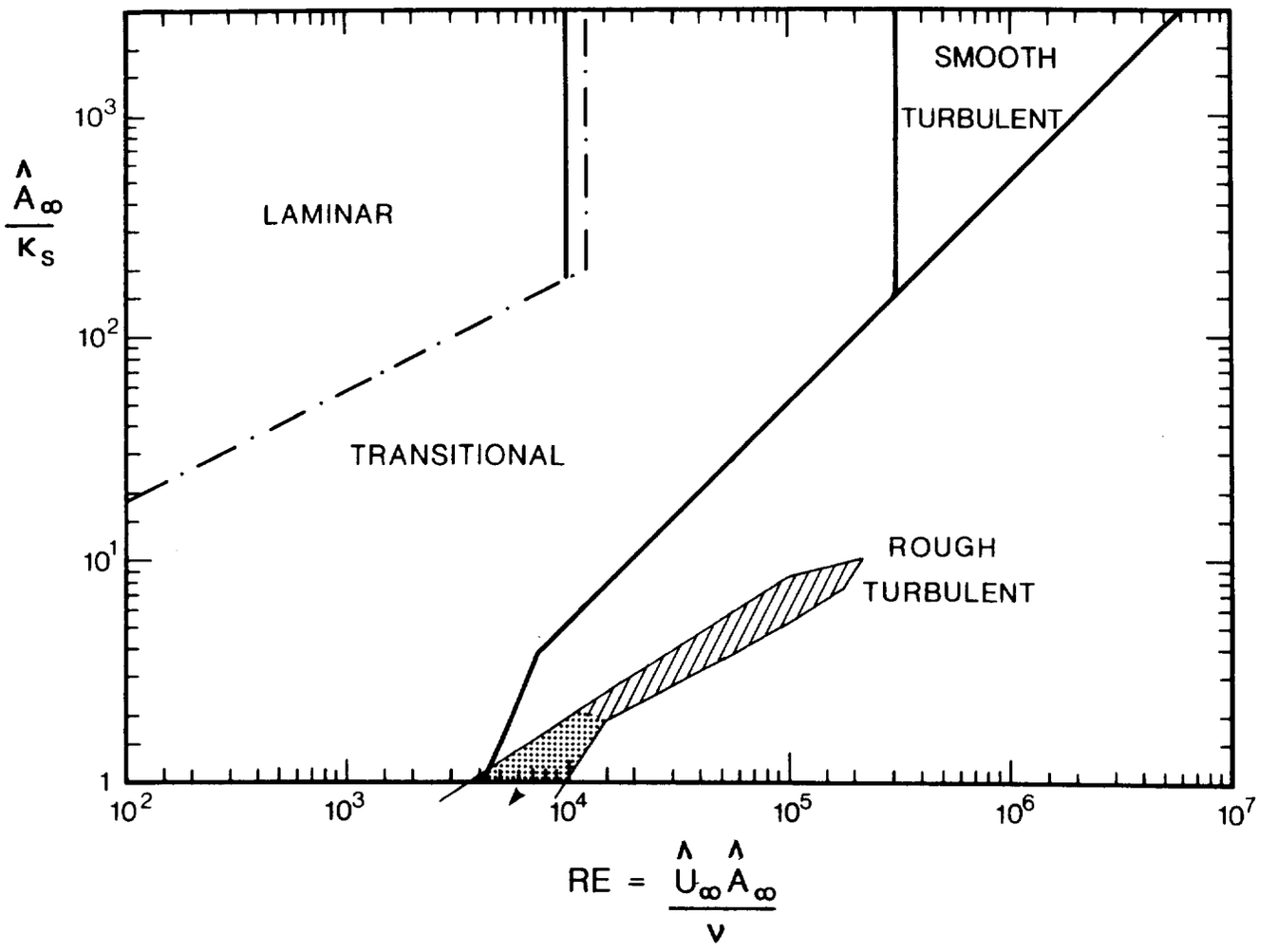

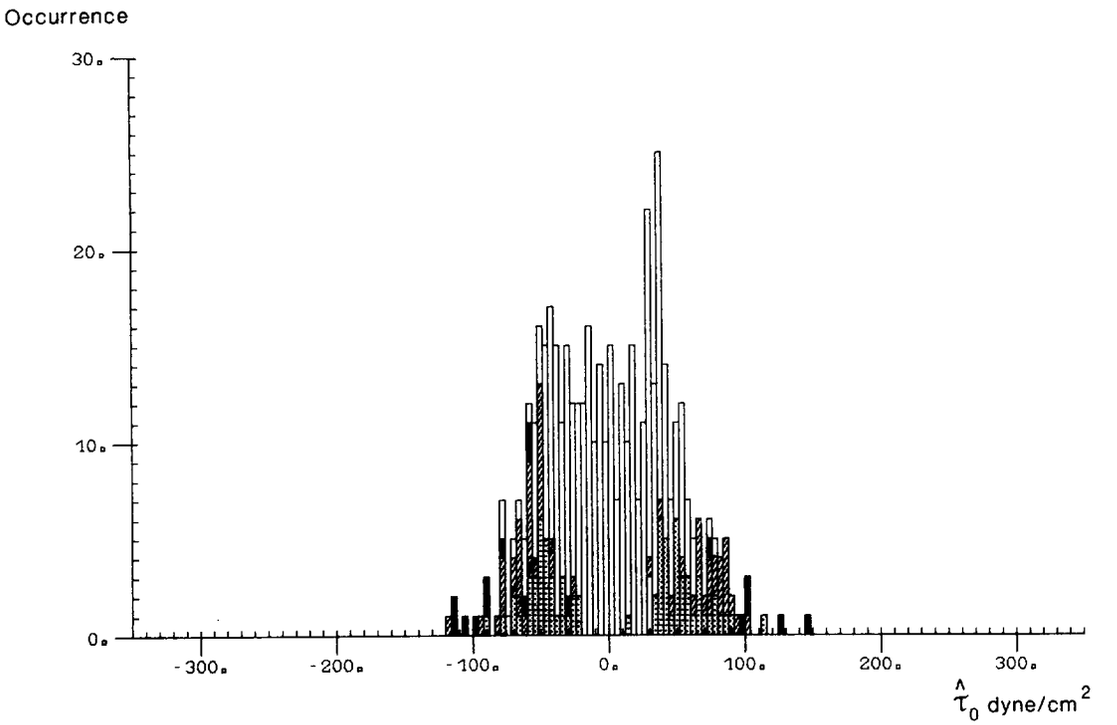

Figure 23(iv) Flow classification, and histogram based on the amplitude of the bed shear stress, for Run 12, 1980.

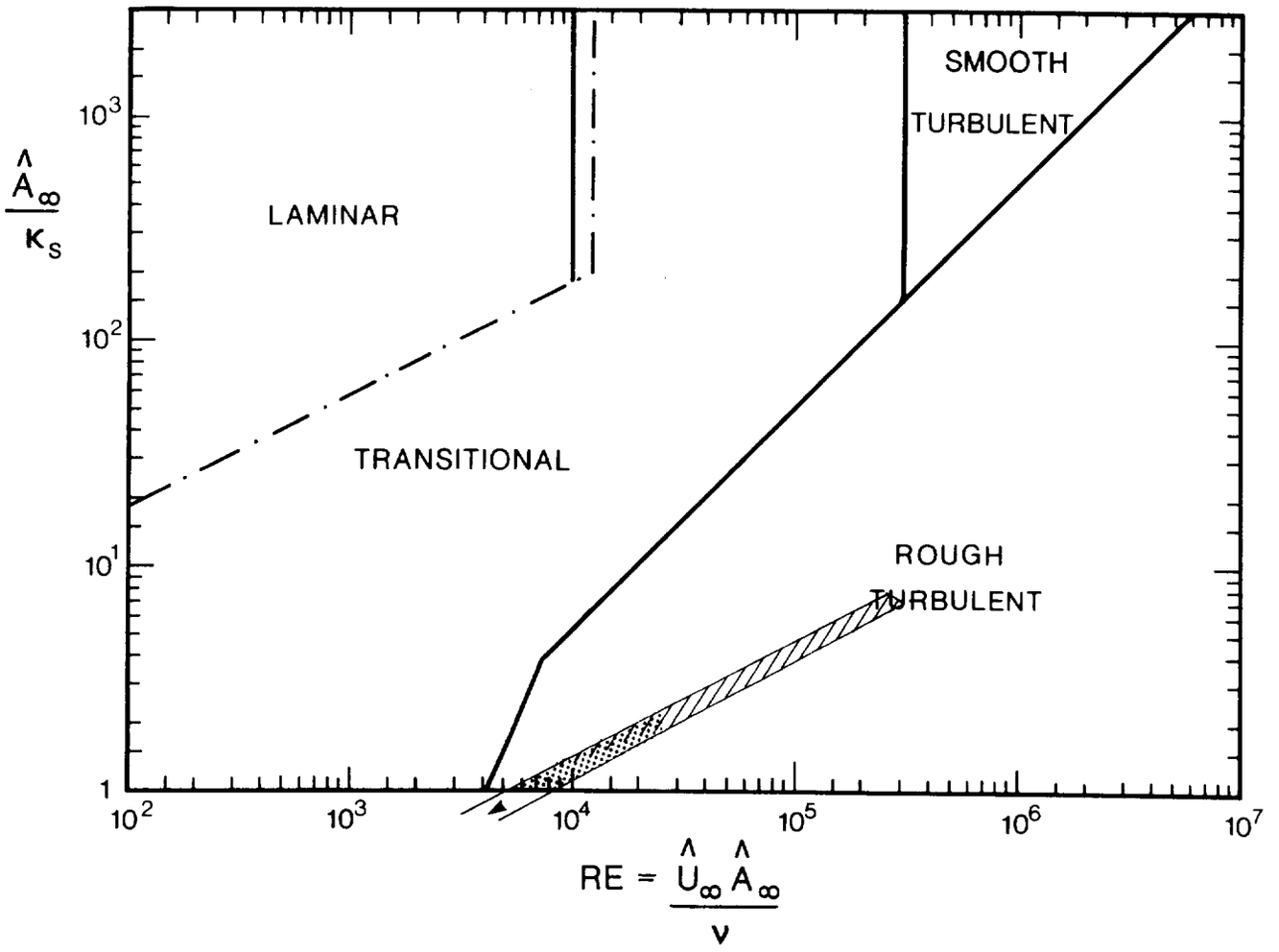

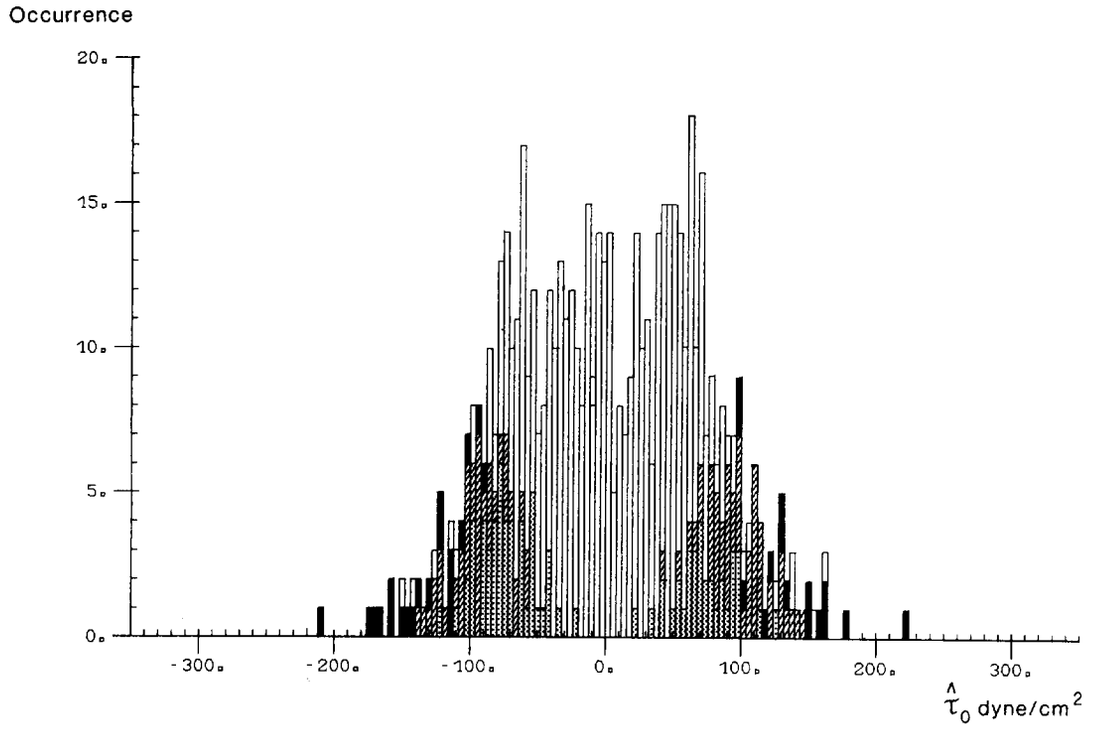

Figure 23(v) Flow classification, and histogram based on the amplitude of the bed shear stress, for Run 14, 1980.

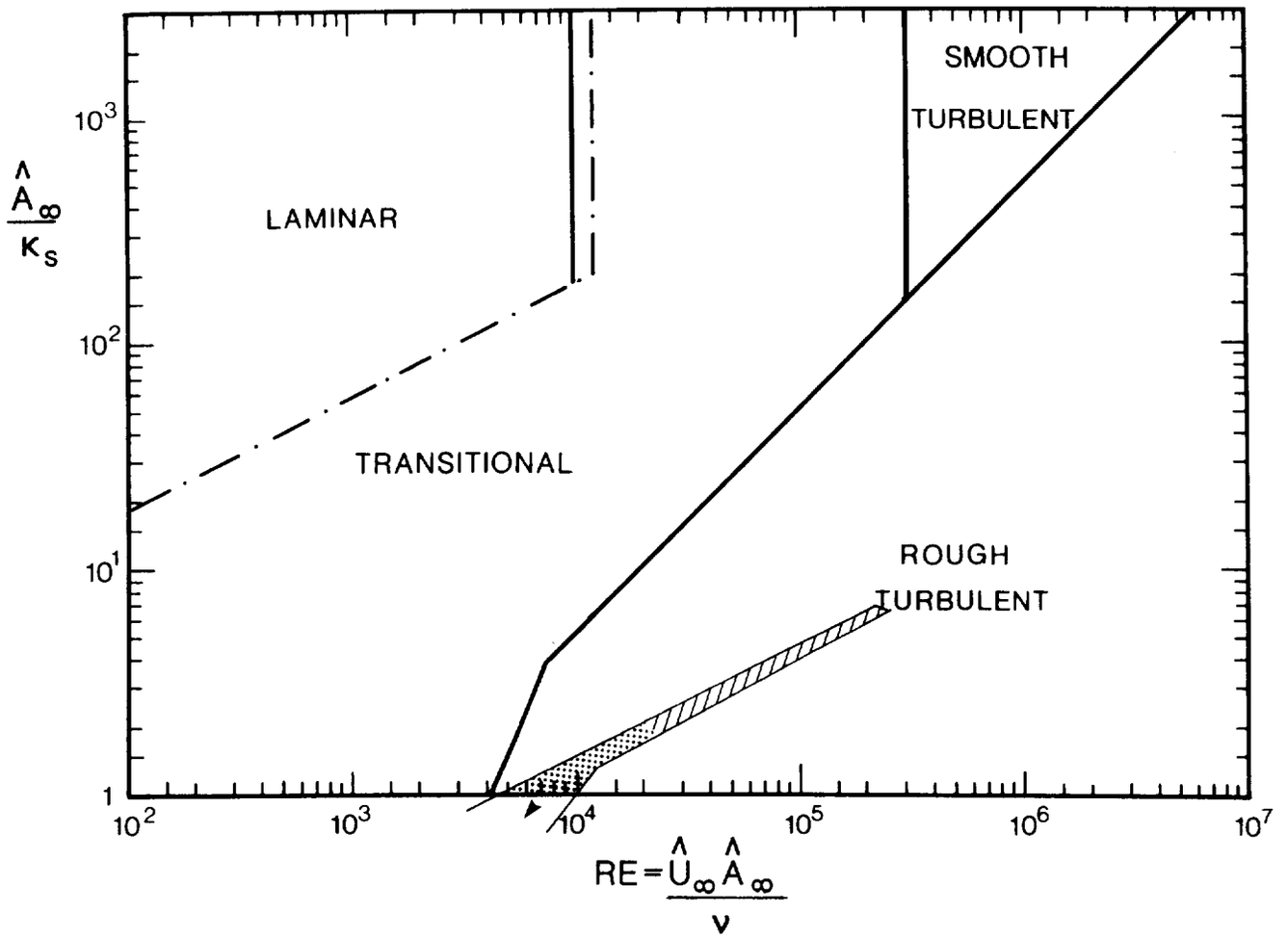

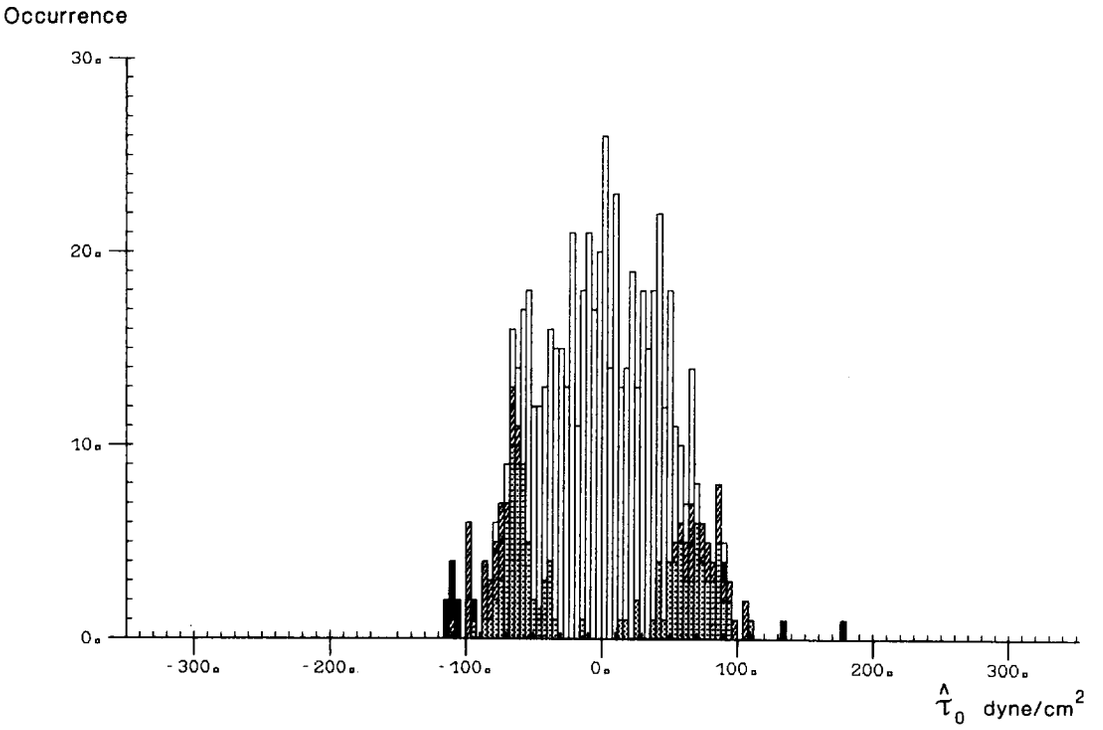

Figure 23(vi) Flow classification, and histogram based on the amplitude of the bed shear stress, for Run 15, 1980.

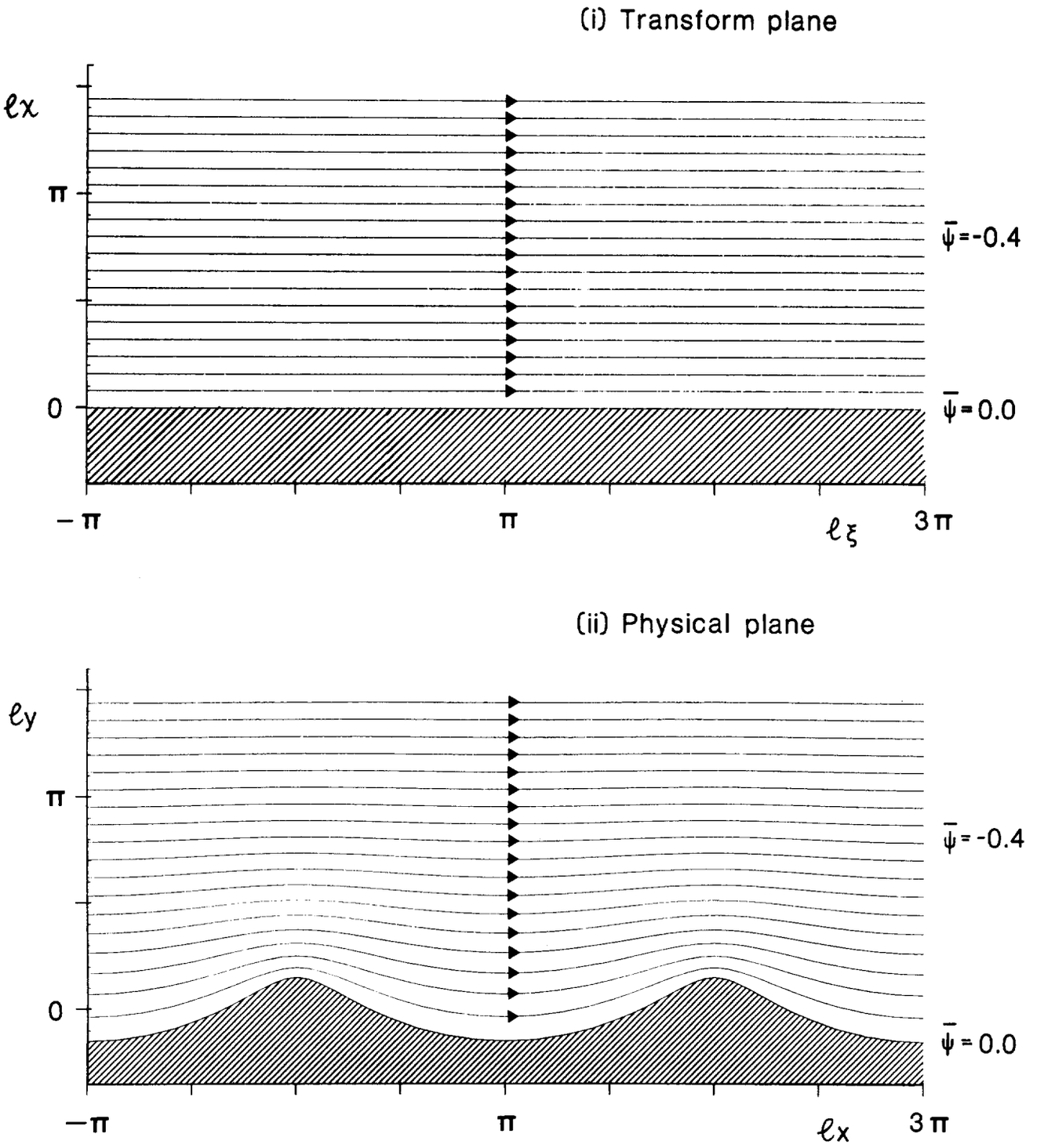

Figure 24 Streamlines of a uniform nonseparating flow in (i) the transform ζ-plane, and (ii) the physical z-plane in which $b\ell = 0.15\pi$.

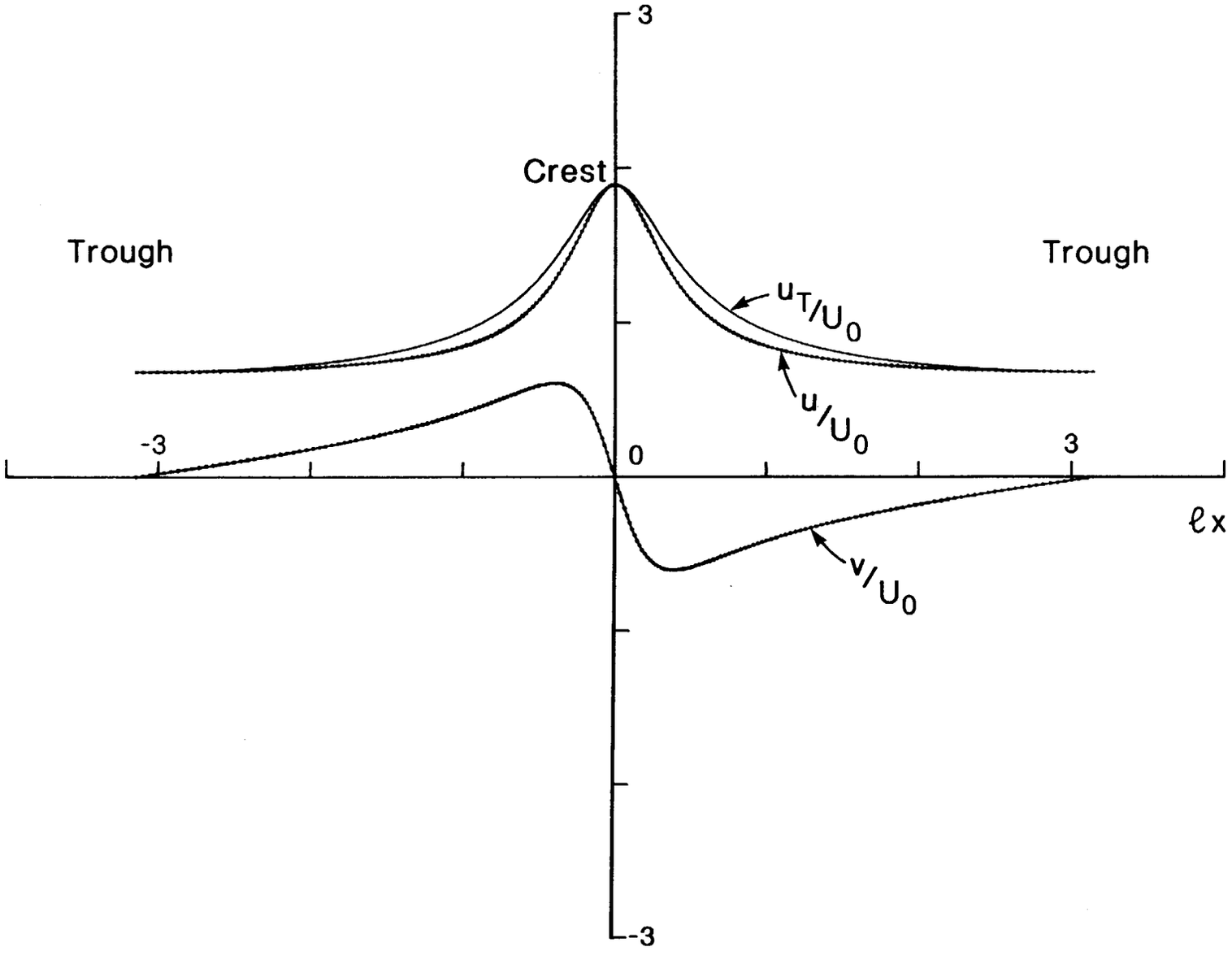

Figure 25 The bed velocity components associated with the nonseparating flow shown in Figure 24(ii) ($b\ell = 0.15\pi$).

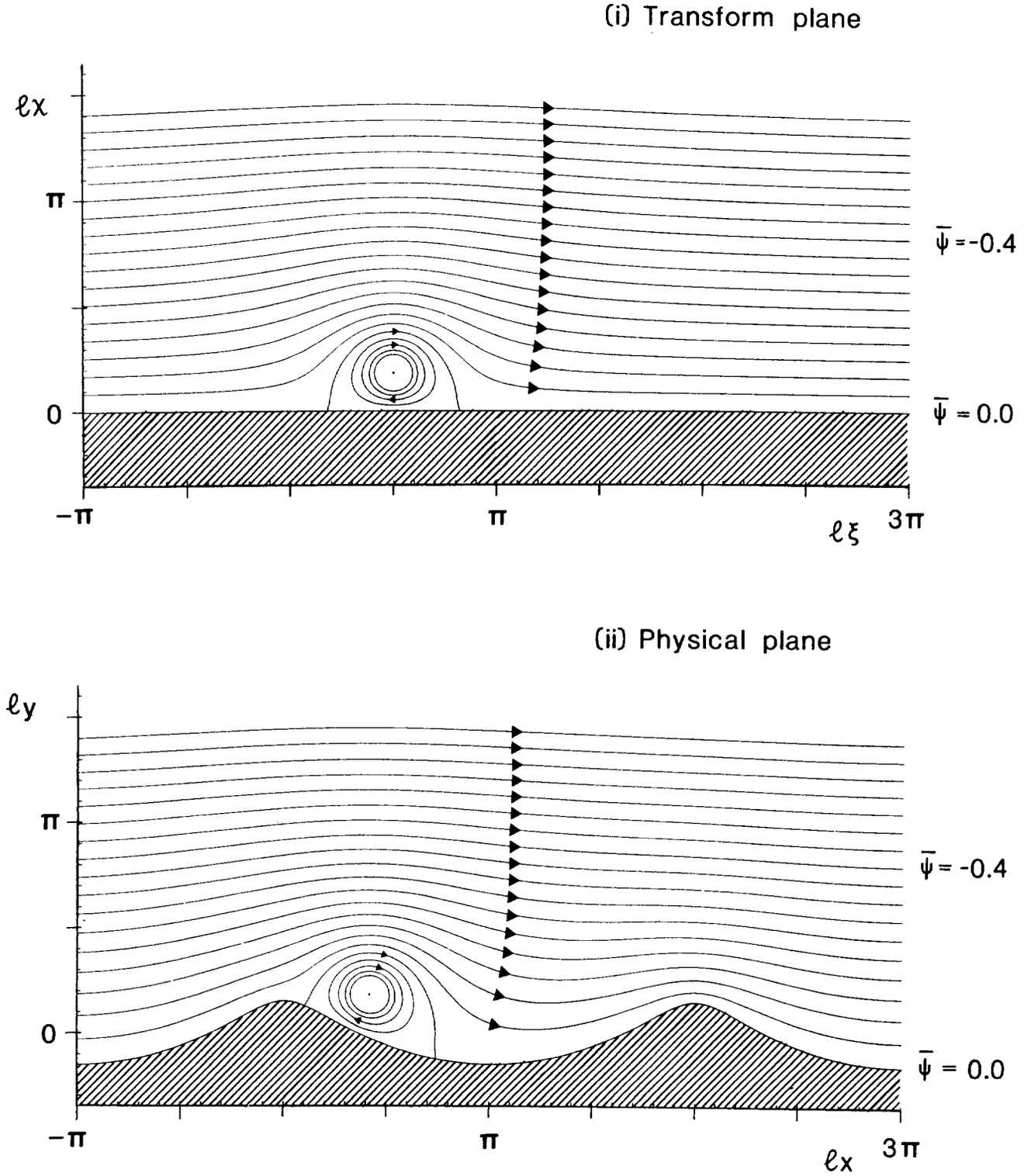

Figure 26 Streamline pattern for the case in which there is a standing vortex above the lee slope of just one ripple in (i) the transform ζ-plane and (ii) the physical z-plane. The flow is otherwise nonseparating. The vortex position in the transform plane is $\ell\xi_o = 0.5\pi$, $\ell\chi_o = 0.18\pi$, with $b\ell = 0.15\pi$.

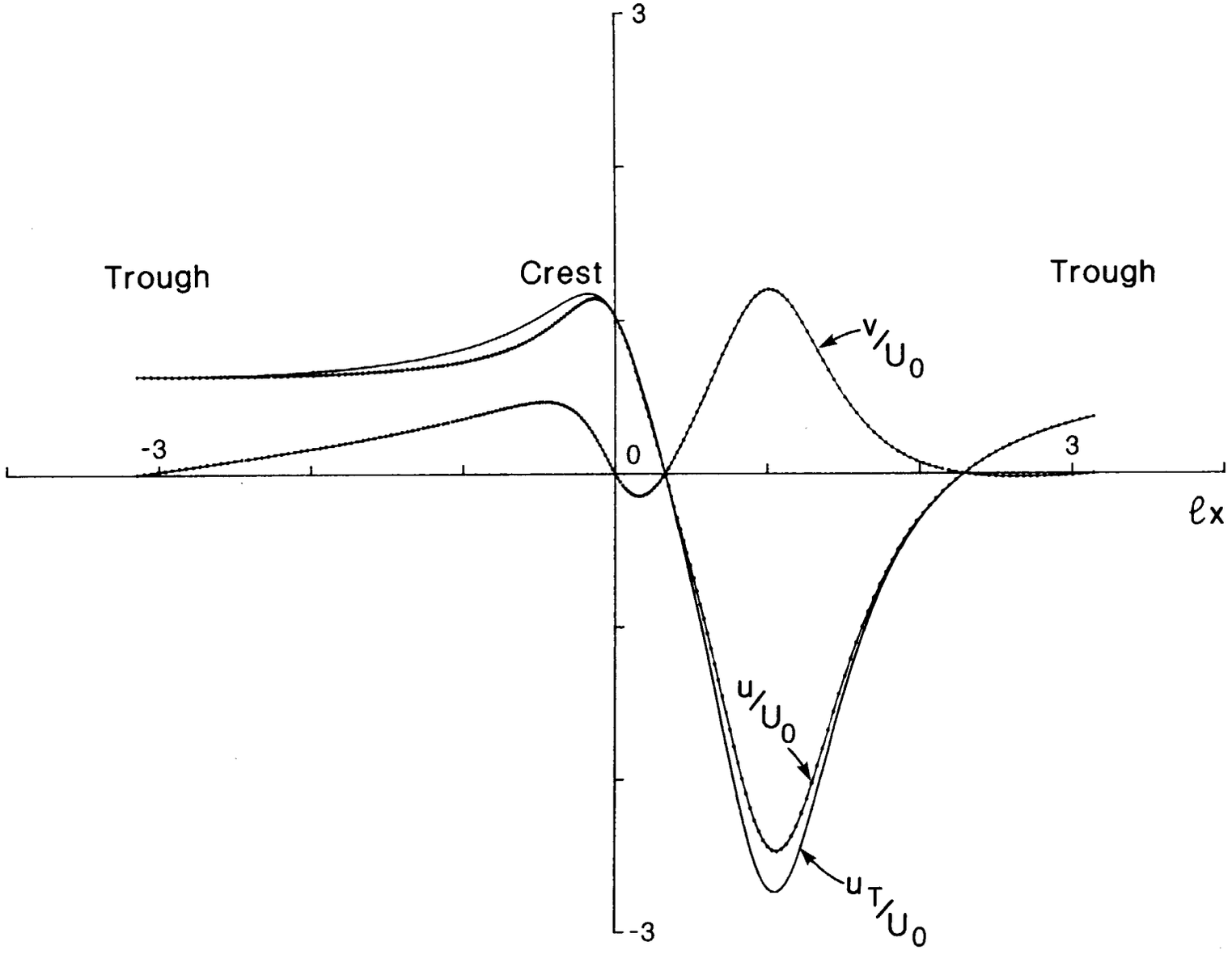

Figure 27 The bed velocity components associated with the flow shown in Figure 26(ii) for $-\pi < \ell x < \pi$ ($b\ell = 0.15\pi$).

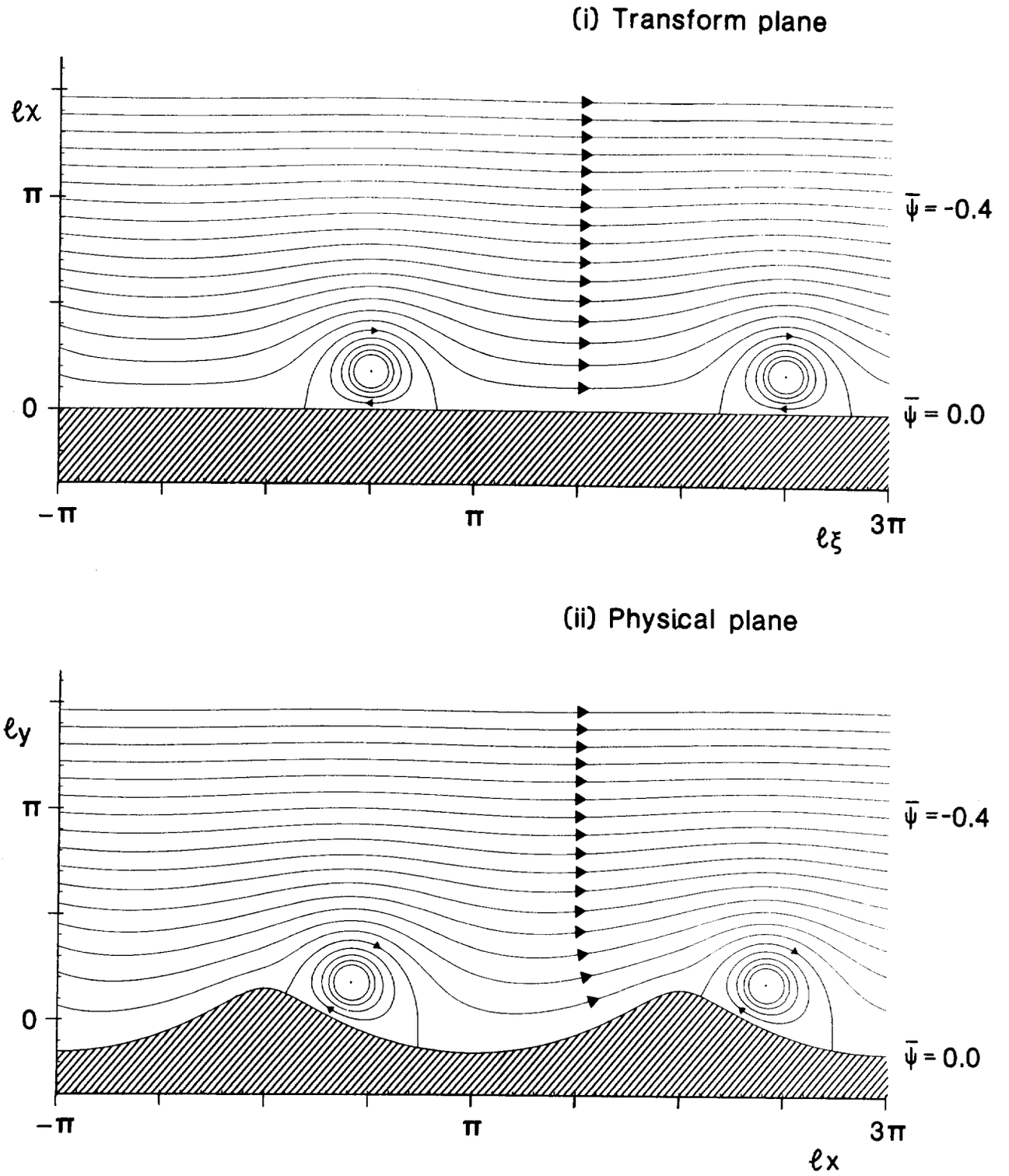

Figure 28 Streamline pattern for the case in which there is an infinite row of standing vortices in (i) the transform ζ-plane and (ii) the physical z-plane. The vortex positions in the transform plane are $\ell\xi_o = 0.5\pi \pm 2m\pi$ (m = integer), $\ell\chi_o = 0.18\pi$, with $b\ell = 0.15\pi$.

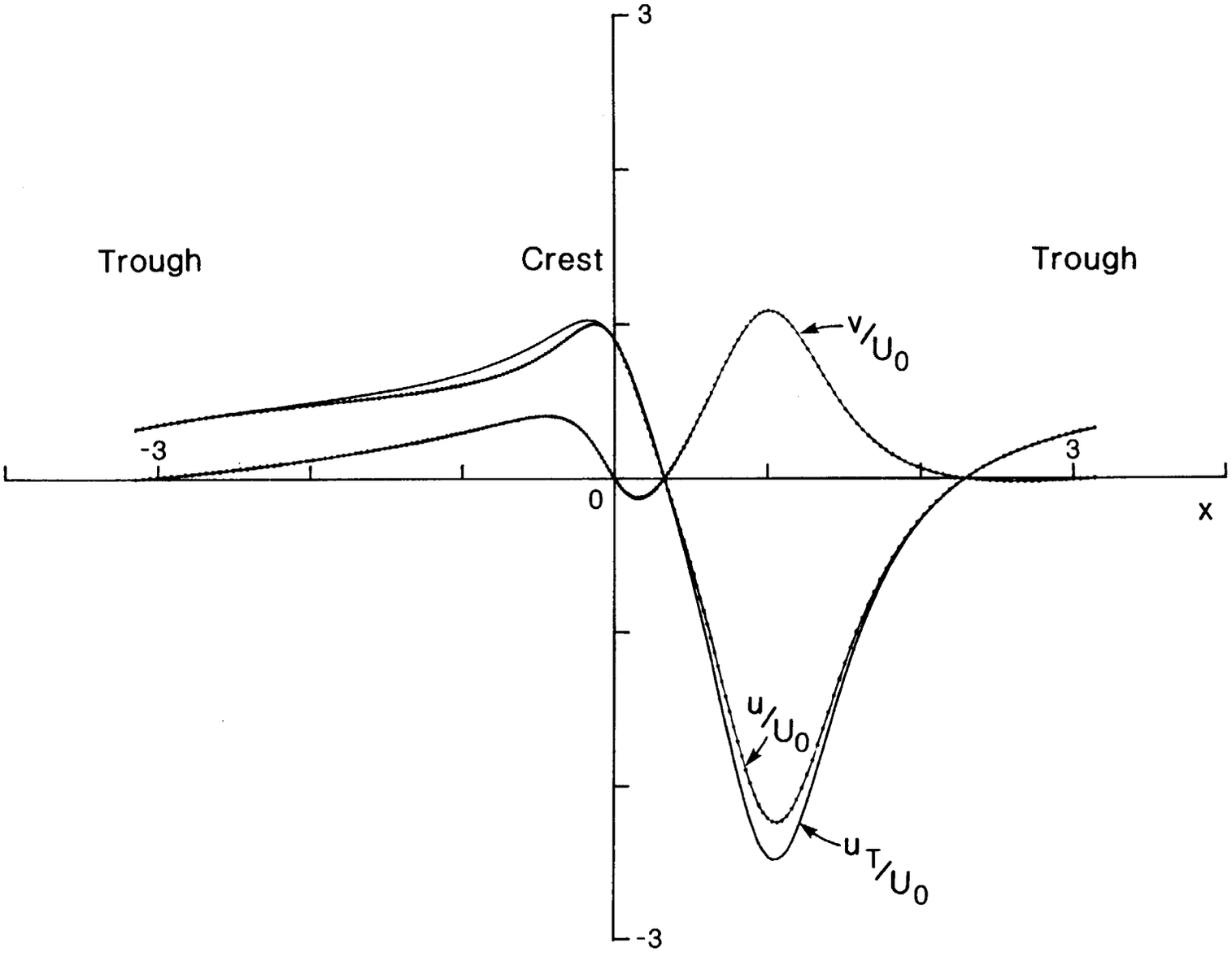

Figure 29 The bed velocity components associated with the flow shown in Figure 28(ii) for a typical ripple wavelength ($b\ell = 0.15\pi$).

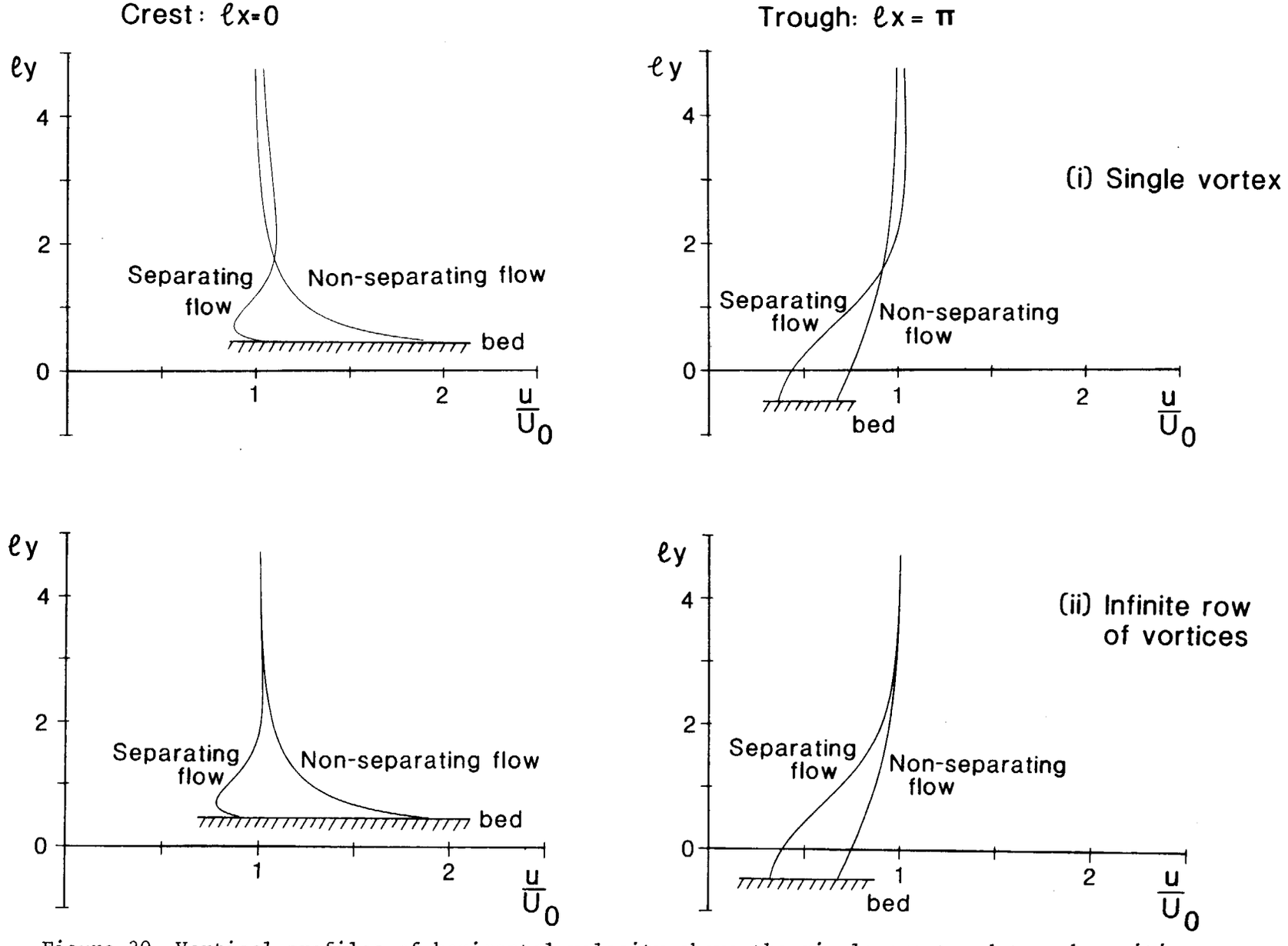

Figure 30 Vertical profiles of horizontal velocity above the ripple crest and trough positions. Each graph shows a comparison of results for separating and nonseparating flow for a ripple of steepness $b\ell = 0.15\pi$. Figure 30(i) shows results for a single standing vortex in the flow, and Figure 30(ii) results for an infinite row of standing vortices.

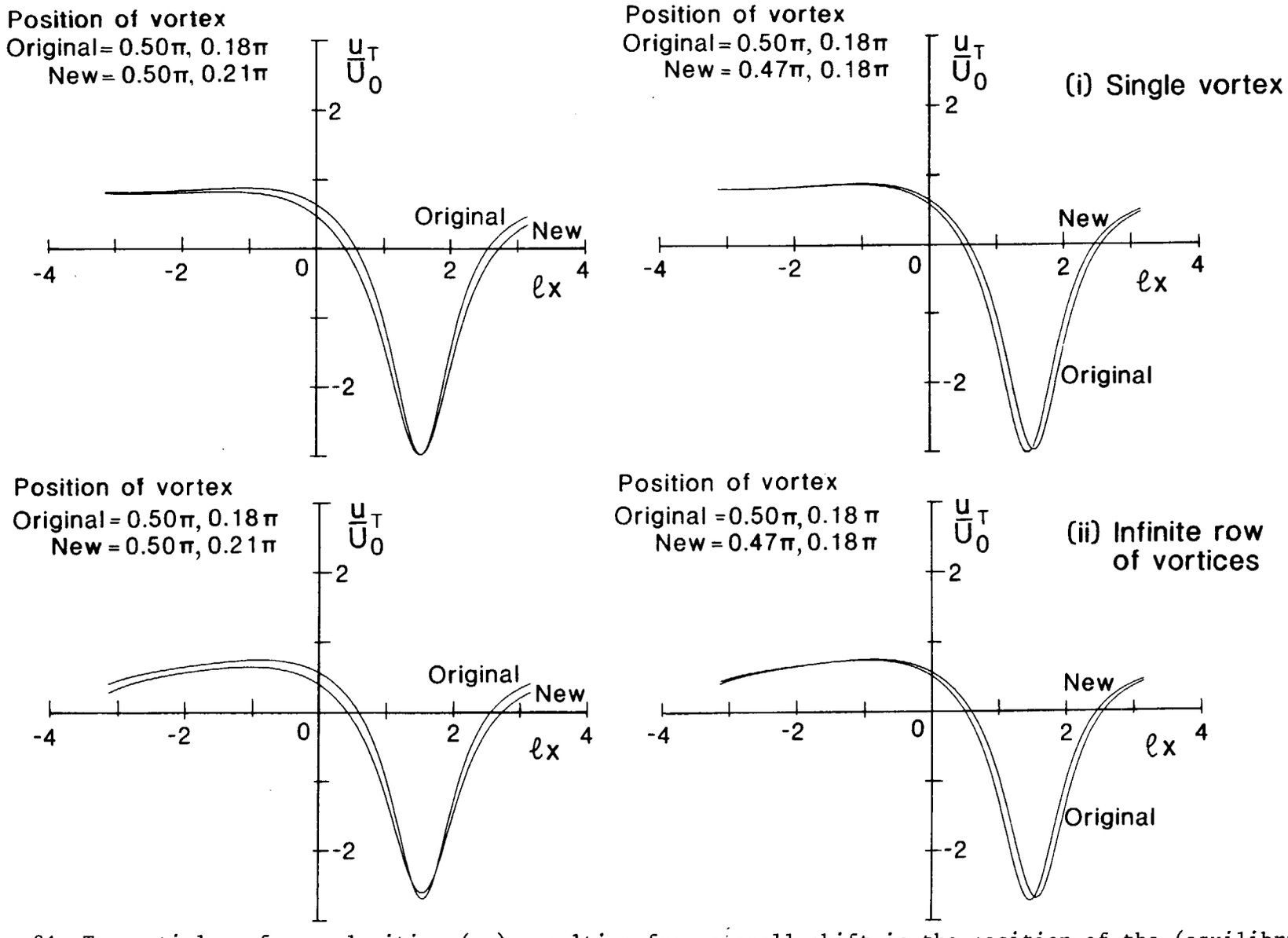

Figure 31 Tangential surface velocities (u_T) resulting from a small shift in the position of the (equilibrium) vortex. The original vortex position in each case is $\ell\xi_o = 0.5\pi$, $\ell\chi_o = 0.18\pi$, and the new position is either $(0.5\pi, 0.21\pi)$ or $(0.47\pi, 0.18\pi)$, as indicated. Figure 31(i) shows results for a single standing vortex in the flow, and Figure 31(ii) results for an infinite row of standing vortices. (Ripple steepness $b\ell = 0.15\pi$).

TABLE 1

BACKGROUND INFORMATION

1978 EXPERIMENT

Date Monday 8 May

Water depth at rig

Time	Depth (m)
1326	5.8
1508	6.4
1628	7.4
1715	8.0
1815	8.6

Experimental runs

Start Time	Run No	Minutes of useful video	Nominal EM Flowmeter heights (cm)	Location of Flowmeters	Comments
1215	1	27	130, 90, 30	Above crest	Flow normal to ripple crests
1328	2	9	130, 90, 20	" "	" " " " "
1403	3	10	130, 90, 20	" "	" " " " "
1527	4	27	130, 90,	" "	Flow at 10°-15° to normal
1630	5	27	130, 90, 20	" "	" " 10°-15° " "
					Actual height of bottom flowmeter = 10.5 cm
1727	6	0	130, 90, 20	Above trough	Flow at 10° to normal.
					Actual height of bottom flowmeter = 19 cm.

Date Tuesday 9 May

Water depth at rig

Time	Depth (m)
1040	8.2
1150	7.0
1207	7.0
1414	5.2
1513	5.5
1624	6.8
1733	7.5

TABLE 1 (cont)

Experimental runs

Start Time	Run No	Minutes of useful video	Nominal EM Flowmeter heights (cm)	Location of Flowmeters	Comments
1111	7	26	130, 90, 20	Above trough	TV view of secondary ripple crest. Flow normal to ripple crests. Actual height of bottom flowmeter = 13 cm
1207	8	25	130, 90, 20	Above crest	Flow normal to ripple crests. Actual height of bottom flowmeter = 11 cm
1248	9	27	130, 90, 20	" "	as for Run 8
1414	10	28	130, 90	" "	as for Run 8
1513	11	27	130, 90	" "	as for Run 8

Date Wednesday 10 May

Water depth at rig

Time	Depth (m)
1308	6.1
1526	5.8
1632	6.6
1715	7.2

Experimental runs

Start Time	Run No	Minutes of useful video	Nominal EM Flowmeter heights (cm)	Location of Flowmeters	Comments
1122	12	22	130, 90	Above crest	Flow normal to ripple crests
1332	13	28	130, 90	" "	" " " " "
1421	14	27	130, 90	" "	" " " " " Actual height of bottom flowmeter = 10 cm
1534	15	0	130, 90, 20	" "	as for Run 14

1980 EXPERIMENT

Date Thursday 17 April

Water depth at rig

Time	Depth (m)
1335	4.2
1654	5.2

TABLE 1 (cont)

Experimental runs

Start Time	Run No	Minutes of useful video	Nominal EM Flowmeter heights	Comments
1315	1	-	160, 60	
1634	2	-	160, 60	Bed flattened at start of run. Sporadic bedload motion. No suspension
1723	3	(30)	160, 60	No sediment motion on rippled bed. Frequent signs of instability and vortex formation

Date Friday 18 April

Water depth at rig

Time	Depth (m)
1150	7.0
1250	5.4
1424	3.8
1618	4.1
1639	4.8

Experimental runs

Start Time	Run No	Minutes of useful video	Nominal EM Flowmeter heights	Comments
1022	4	22	160, 60	
1113	5	29	160, 60	
1250	6	-	160, 60	Bed flattened at start of run. See text (§5) for detailed comments.
1417	7	-	160, 60	See text (§5) for detailed comments.
1613	8	(20)	160, 60	Very occasional sediment movement. Evidence of flow separation.

Date Sunday 11 May

Water depth at rig

Time	Depth (m)
∿1700	∿7 m
∿1900	∿6 m

Experimental runs

Start Time	Run No	Minutes of useful video	Nominal EM Flowmeter heights (cm)	Comments
1656	9	-	160, 60	
1838	10	27	160, 60	Bed flattened at start of run. Dye in TV field of view. Layer of bad visibility above bed

TABLE 1 (cont)

Date Monday 12 May

Water depth at rig

Time	Depth (m)
∿1000	≈5.0
∿1130	4.5
1219	5.0
1407	6.4

Experimental runs

Start Time	Run No	Minutes of useful video	Nominal EM Flowmeter heights (cm)	Comments
0949	11	27	160, 60	
1114	12	18	160, 60	Bed flattened at start of run. Dye in TV field of view
1219	13	-	160, 60	
1307	14	26	160, 60	
1501	15	27	160, 60	

Date Tuesday 13 May

Water depth at rig

Time	Depth (m)
0950	5.3
1213	3.6
1644	8.2

Experimental runs

Start Time	Run No	Minutes of useful video	Nominal EM Flowmeter heights (cm)	Comments
0921	16	13	160, 60	
1211	17	22	160, 60	Dye in field of view

TABLE 2

SAND RIPPLE CHARACTERISTICS

1978 EXPERIMENT

Date	Runs	Ripple No. (Davies 1980b)	Wavelength λ(cm)	Height η(cm)	Steepness (η/λ)
8 May	1-6	4	78.5	10.1	0.129
		5	54.6	9.7	0.178
9 May	7-11	6	81.6	11.3	0.139
		7	66.4	12.0	0.181
10 May	12-15	8	81.1	12.2	0.150
		9	79.6	11.8	0.148
			Mean steepness =		0.154

1980 EXPERIMENT

Date	Runs	Wavelength λ(cm)	Height η(cm)	Comments
17 April	1			No information.
	2,3	6-8	≈2	Ripples formed over the entire bed surface from an initially flattened bed.
18 April	4,5	7-8	1½	Rippled bed as formed overnight.
	6,7	5	¾ - 1	Bed flattened prior to start of Run 6. See text (§5) for detailed comments.
	8	7	1	Ripples increasingly sharp-crested with time.
11 May	9	12-15	≈2	Rather confused three-dimensional ripple pattern.
	10	11-16	2-3	Bed flattened prior to start of run.
12 May	11	20	6-7(?)	Rippled bed as formed overnight. Confused ripple pattern close to the rig; two-dimensional pattern outwards from instruments.
	12			Bed flattened prior to start of run. Following flattening, divers reported an almost immediate development of "lines of shell" on the bed, in the usual sense of "rolling grain" ripple development. Short ripples developed during the run.
		10	1-2	Ripple dimensions prior to Run 13.
	13			Ripple development continued.
	14,15	12-18	4-6(?)	Following Run 14, ripple pattern close to the rig confused, but pattern two-dimensional outwards from instruments. Probable ripple height in TV-field of view ≈3½ cm.
13 May	16	15-20	3-4½(?)	Rippled bed as formed overnight. Well defined ripples with sharp crests. Ripple profiler used (see Fig 5(ii)).
	17	15-20	3-4½(?)	

TABLE 3

RESULTS FOR VELOCITY MEASURED IN THE HORIZONTAL PLANE ABOVE THE RIG

Run Number		U-Variance $(cm/s)^2$	V-Variance $(cm/s)^2$	RATIO	ANGLE OF ROTATION ψ_r (rad)
1978	1	63.17	7.81	0.124	0.116
	2	163.80	no information	-	-
	3	137.61	14.08	0.102	0.070
	4	74.72	14.80	0.198	0.118
	5	74.26	23.77	0.320	0.137
	7	175.84	29.46	0.168	-0.093
	8	148.25	22.88	0.154	0.056
	9	213.31	24.31	0.114	0.028
	10	116.12	14.82	0.128	0.015
	11	93.35	20.18	0.216	-0.116
	12	71.39	12.16	0.170	0.082
	13	61.58	7.29	0.118	-0.002
	14	47.48	19.55	0.412	-0.431
1980	3	33.87	5.52	0.163	0.036
	4	141.49	15.85	0.112	-0.003
	5	85.19	10.71	0.126	-0.113
	8	67.00	9.45	0.141	0.100
	10	423.32	88.11	0.208	0.291
	11	292.46	39.66	0.136	0.067
	12	302.19	27.30	0.090	-0.106
	14	396.14	24.79	0.063	-0.012
	15	209.56	31.67	0.151	-0.006
	16	101.83	37.80	0.371	-0.512
	17	68.17	14.10	0.207	-0.324

TABLE 4

SEDIMENT THRESHOLD VELOCITY AMPLITUDE RESULTS

1978 EXPERIMENT

Runs	Duration (min)	Parameter	Estimated velocity amplitude ranges for each sediment motion type (cm/s): 1	2	3
1-5	100	U_3	9-27	21- ?	no suspension
1 and 3-5	91	U_T	12-28	22- ?	" "
1 and 3-5	91	U_{ROT}	11-27	21- ?	" "
8-14	184	U_3	11-29	14- ?	" "
8-14	184	U_T	11-30	17- ?	" "

Note. The results have been averaged for the + and - directions of motion.

LABORATORY THRESHOLDS

Runs	Representative period of waves moving sediment 2.ΔT(s)	Grain size (cm)	Threshold velocity amplitude (cm/s): BAGNOLD	MANOHAR Incipient	MANOHAR General	KOMAR AND MILLER
1,8,12	10	D_{90}=0.135	41	40	44	42
		D_{50}=0.078	32	36	40	33
		D_{10}=0.038	24	31	34	24
3,11	12	0.135	43	40	44	43
		0.078	34	36	40	34
		0.038	25	31	34	26
4	13	0.135	45	40	44	44
		0.078	35	36	40	35
		0.038	26	31	34	26
5	14	0.135	46	40	44	44
		0.078	36	36	40	35
		0.038	26	31	34	27
9,10	11	0.135	42	40	44	42
		0.078	33	36	40	34
		0.038	25	31	34	25
13,14	9	0.135	40	40	44	41
		0.078	31	36	40	33
		0.038	23	31	34	23

TABLE 5

SEDIMENT THRESHOLD VELOCITY AMPLITUDE RESULTS

1980 EXPERIMENT

Run Number	Duration (min)	Parameter	Estimated velocity amplitude ranges for each sediment motion type (cm/s): 1	2	3	Representative period of waves moving sediment 2. ΔT (s)	Grain size (cm)	Threshold velocity amplitude (cm/s): BAGNOLD	MANOHAR Incipient	MANOHAR General	KOMAR AND MILLER
3	(30)	U_3	>19-? (No motion)				D_{90} = 0.052	25	33	37	27
		U_T	>20-?			(8)	D_{50} = 0.021	17	28	31	18
							D_{10} = 0.011	13	24	27	15
4	22	U_3	11-(29)	20-?			D_{90} = 0.052	29	33	37	29
		U_T	11-(30)	21-?		12	D_{50} = 0.0225	20	28	31	21
							D_{10} = 0.012	15	25	27	17
5	29	U_3	14-24	(21)-?	(34)-?		D_{90}				
		U_T	14-24	(22)-?	(34)-?	12	D_{50}	as for Run 4			
							D_{10}				
8	(20)	U_3	>22-? (Almost no motion)				D_{90} = 0.052	27	33	37	28
		U_T	>22-?			(10)	D_{50} = 0.0025	19	28	31	20
							D_{10} = 0.012	14	25	27	16
10	27	U_3	17-40	19-50	(37)-?		D_{90} = 0.062	25	34	38	28
		U_T	21-41	26-51	(41)-?	6	D_{50} = 0.026	17	29	32	18
		U_{ROT}	19-41	22-51	(36)-?		D_{10} = 0.015	13	26	29	15
11	27	U_3	13-31	22-40	(28)-?		D_{90}				
		U_T	14-32	22-40	(29)-?	6	D_{50}	as for Run 10			
		U_{ROT}	13-31	21-40	(27)-?		D_{10}				
12	18	U_3	15-37	27-45	(40)-?		D_{90} = 0.062	23	34	38	27
		U_T	17-37	27-46	(41)-?	5	D_{50} = 0.026	16	29	32	17
		U_{ROT}	17-37	27-45	(40)-?		D_{10} = 0.015	13	26	29	14
14	26	U_3	17-39	27-47	(37)-?		D_{90}				
		U_T	17-39	27-47	(37)-?	5	D_{50}	as for Run 12			
							D_{10}				
15	27	U_3	14-36	24-41	(44)-?		D_{90}				
		U_T	14-36	25-43	(46)-?	5	D_{50}	as for Run 12			
							D_{10}				
16	13	U_3	10-22	15-?			D_{90} = 0.062	28	34	38	30
		U_T	12-25	19-?		9	D_{50} = 0.026	19	29	32	20
		U_{ROT}	9-24	18-?			D_{10} = 0.015	15	26	29	17
17	22	U_3	12-?				D_{90} = 0.062	26	34	38	29
		U_T	12-?			7	D_{50} = 0.026	18	29	32	19
							D_{10} = 0.015	14	26	29	16

Notes:
1. Results have been averaged for the + and - directions of motion.
2. Velocity values in brackets are rough estimates.
3. Wave period values in brackets are for the waves with the largest velocity amplitudes.
4. The tabulated results are based upon histograms equivalent to those in Fig 9, but drawn with unit (cm/s) incremental widths.

TABLE 6

THRESHOLD RESULTS FOR THE ONSET OF FLOW INSTABILITY AND VORTEX FORMATION

1978 EXPERIMENT

Runs	Duration (min)	Estimated ranges of free-stream velocity amplitude (cm/s) for:		Estimated ranges of orbital excursion (cm) for:	
		Instability	Vortex formation	Instability	Vortex formation
1-5	100	12 -(26)	(25)- ?	38 -(122)	(118)- ?
8-14	187	12 - 30	19 - ?	34 - 118	62 - ?

NOTES : 1. Velocity amplitudes relate to U_3 component of free-stream velocity measured at a height of 130 cm above the bed.

2. Orbital excursion results : wave half-cycles with double velocity maxima have been excluded.

3. Values in brackets are rough estimates.

TABLE 7

THRESHOLD RESULTS FOR THE ONSET OF FLOW INSTABILITY AND VORTEX FORMATION

1980 EXPERIMENT

Runs	Duration (min)	Estimated ranges of free-stream velocity amplitude (cm/s) for:		Estimated ranges of orbital excursion (cm) for:	
		Instability	Vortex formation	Instability	Vortex formation
3	27	9 - 19	(8)- ?	14 - (58)	(18)- ?
8	13	8 - 20	11 - ?	12 - (80)	22 - ?
11	27	no information	19 - ?	no information	18 - ?
16	13	no information	12 - ?	no information	38 - ?
17	15	7 -(24)	9 - ?	14 - (62)	20 - ?

Notes : 1. Velocity amplitudes relate to the U_3 component of free-stream velocity measured at a height of 160 cm above the bed.

2. Results have been averaged for the + and - directions of motion.

TABLE 8

RIPPLE FORMATION TRIALS : 1980 EXPERIMENT

Trial number	Run number	Representative free-stream velocity amplitude † $\hat{U}_\infty$ (cm/s)	Representative period of waves moving sediment (sec)	Grain size $D = D_{50}$ (cm)	Mobility number †† M	Orbital excursion d_o (cm)	Ripple wavelength λ (cm) (mean) (cm)	Ripple height η (cm)	$\frac{2\lambda}{d_o}$	$\frac{d_o}{2D}$	Type of wave spectrum	Comments
1	2						6-8 (7)	∿2				No video
	3	(>20)	(8)	0.021	(>12)	(>51)	6-8 (7)	∿2	(<0.27)			Bad video. No sediment motion.
												overnight.
	4	(30)	12	0.023	24	100	7-8 (7½)	1½	0.15	2.1×10^3	SINGLE PEAK	
	5	(30)	12	0.023	(24)	(100)	7-8 (7½)	1½	(0.15)	2.1×10^3	SINGLE PEAK	
2	10	35	6	0.026	29	70	11-16 (13½)	2-3	0.39	1.35×10^3	SINGLE PEAK	
												overnight.
	11	35	6	0.026	29	64	20	6-7	0.62	1.23×10^3	POLYMODAL	
3	12	35	5	0.026	29	60	10	1-2	0.33	1.15×10^3	SINGLE PEAK /POLYMODAL	
	13			0.026								No video.
	14	35	5	0.026	29	54	12-18 (15)	4-6	0.56	1.04×10^3	SINGLE PEAK	
	15	35	5	0.026	29	52	12-18 (15)	4-6	0.58	1.00×10^3	SINGLE PEAK	
												overnight.
	16	22	9	0.026	12	60	15-20 (17½)	3-4½	0.58	1.15×10^3	POLYMODAL	
	17	(22)	7	0.026	(12)	(60)	15-20 (17½)	3-4½	(0.58)	1.15×10^3	POLYMODAL	

Notes: † Values taken at centre of bedload range (general motion). Values in brackets : too few general motion observations for reliable results.

†† Mobility number $M = \hat{U}_\infty^2/\{g\gamma D\}$

TABLE 9

SEDIMENT THRESHOLD STRESS AMPLITUDE RESULTS

1978 EXPERIMENT

Runs	Duration (min)	Estimated stress amplitude ranges for each sediment motion type (dyne/cm²)		
		1	2	3
1 and 3-5	91	1.25-6.125	4.5- ?	no suspension
8-14	184	1.625-7.25	4.0- ?	no suspension
Equivalent results in terms of Shields' parameter θ' based upon the median grain diameter:				
1 and 3-5	91	0.010-0.047	0.035- ?	no suspension
8-14	184	0.013-0.056	0.031- ?	no suspension

Notes : 1. The results have been based on the U-component of horizontal velocity measured at a height of 130 cm above the bed.

2. Results have been averaged for the + and - directions of motion.

3. Shields' parameter $\theta' = \hat{\tau}'_o/(g\rho_f\gamma D) = \frac{1}{2}f_w M$. The calculated results represent the skin friction on the bed in the vicinity of the ripple crests.

TABLE 10

SEDIMENT THRESHOLD STRESS AMPLITUDE RESULTS

1980 EXPERIMENT

Run number	Duration (min)	Angle of misalignment ψ_r (rad)	Ripple heights η(cm)	η'(cm)	Bed roughness k_s	Parameter	Estimated stress amplitude ranges for each sediment motion type (dyne/cm²) 1	2	3
3	(30)	0.036	-	1.0	$3.57\eta'$	U_3	>20-?	(No motion)	
4	22	-0.003	-	1.1	$4\eta'$	U_3	7-(26)	15-?	
					$3.57\eta'$	U_3	7-(22)	14-?	
					$3.57\eta'$	U_T	7-(23)	14-?	
					$3.57\eta'$	U_{ROT}	7-(22)	14-?	
					$3\eta'$	U_3	6-(20)	13-?	
5	29	-0.113	1.5	1.1	4η	U_3	13-(27)	(25)-?	(36)-?
					$4\eta'$	U_3	11-(21)	(20)-?	(29)-?
					$3.57\eta'$	U_3	10-20	(19)-?	(28)-?
					$3.57\eta'$	U_T	10-21	(19)-?	(28)-?
					$3.57\eta'$	U_{ROT}	10-20	(18)-?	(27)-?
					$3\eta'$	U_3	9-18	(17)-?	(25)-?
8	(20)	0.100	-	1.0	$3.57\eta'$	U_3	>21-?	(Almost no motion)	
10	27	0.291	-	1.9	$4\eta'$	U_3	26-100	50-122	(70)-?
					$4\eta'$	U_T	26-108	54-126	(76)-?
					$4\eta'$	U_{ROT}	18-106	54-128	(74)-?
					$3.57\eta'$	U_3	22-92	44-114	(64)-?
					$3.57\eta'$	U_T	26-100	50-118	(68)-?
					$3.57\eta'$	U_{ROT}	18-98	50-120	(66)-?
					$3\eta'$	U_3	22-80	40-100	(54)-?
					$3\eta'$	U_T	22-88	48-104	(60)-?
					$3\eta'$	U_{ROT}	14-86	44-106	(60)-?
11	27	0.067	6.5	2.9	4η	U_3	22-156	(46)-236	(78)-?
					$4\eta'$	U_3	22-124	32-150	(74)-?
					$4\eta'$	U_T	22-136	36-152	(80)-?
					$4\eta'$	U_{ROT}	18-128	32-152	(78)-?
					$3.57\eta'$	U_3	20-108	30-136	(68)-?
					$3.57\eta'$	U_T	22-116	32-136	(74)-?

(cont)

TABLE 10 (cont)

SEDIMENT THRESHOLD STRESS AMPLITUDE RESULTS

1980 EXPERIMENT

					$3.57\eta'$	U_{ROT}	18-110	30-136	(72)-?
					$3\eta'$	U_3	20-92	26-120	(58)-?
					$3\eta'$	U_T	20-98	28-120	(64)-?
					$3\eta'$	U_{ROT}	16-94	26-120	(62)-?
					$2\eta'$	U_3	14-64	22-88	(42)-?
					$2\eta'$	U_T	14-70	22-88	(48)-?
					$2\eta'$	U_{ROT}	14-68	20-88	(44)-?
12	18	-0.106	-	1.4	$4\eta'$	U_3	26-90	56-93	(84)-?
					$4\eta'$	U_T	26-90	56-96	(84)-?
					$3.57\eta'$	U_3	26-84	52-88	(78)-?
					$3.57\eta'$	U_T	26-84	52-88	(78)-?
					$3.57\eta'$	U_{ROT}	26-86	50-86	(78)-?
					$3\eta'$	U_3	22-72	44-76	(68)-?
					$3\eta'$	U_T	22-72	44-76	(68)-?
14	26	-0.012	-	2.1	$4\eta'$	U_3	46-114	62-156	(102)-?
					$4\eta'$	U_T	46-116	66-156	(102)-?
					$3.57\eta'$	U_3	42-104	56-142	(94)-?
					$3.57\eta'$	U_T	42-106	58-142	(94)-?
					$3.57\eta'$	U_{ROT}	42-104	56-140	(94)-?
					$3\eta'$	U_3	34-92	48-126	(82)-?
					$3\eta'$	U_T	36-94	52-126	(82)-?
15	27	-0.006	5	2.1	4η	U_3	44-168	116-?	(238)-?
					$4\eta'$	U_3	38-98	68-?	(106)-?
					$4\eta'$	U_T	42-100	70-?	(106)-?
					$3.57\eta'$	U_3	36-96	58-?	(94)-?
					$3.57\eta'$	U_T	40-90	64-?	(98)-?
					$3.57\eta'$	U_{ROT}	36-90	58-?	(94)-?
					$3\eta'$	U_3	32-78	50-?	(82)-?
					$3\eta'$	U_T	36-78	54-?	(86)-?
16	13	-0.512	-	2.5	$4\eta'$	U_3	17-41	25-?	
					$3.57\eta'$	U_3	14-37	23-?	
					$3.57\eta'$	U_T	17-43	26-?	

(cont)

TABLE 10 (cont)

SEDIMENT THRESHOLD STRESS AMPLITUDE RESULTS

1980 EXPERIMENT

					$3.57\eta'$	U_{ROT}	18-41	26-?
					$3\eta'$	U_3	10-32	20-?
17	22	-0.324	-	2.5	$4\eta'$	U_3	(21)-?	
					$3.57\eta'$	U_3	(19)-?	
					$3.57\eta'$	U_T	(19)-?	
					$3.57\eta'$	U_{ROT}	(19)-?	
					$3\eta'$	U_3	(19)-?	

Notes. 1. Results have been averaged for the + and - directions of motion.

2. Stress values in brackets are rough estimates.

3. The ripple height η' is equal to one seventh of the ripple wavelength (λ) (see Table 2).

TABLE 11

BED SURFACE VELOCITIES FROM THE IRROTATIONAL FLOW MODEL, FOR AN INFINITE ROW OF VORTEX PAIRS

Ripple steepness $b\ell$	Vortex position (for separating flow) $\ell\xi_o$	$\ell\chi_o$	Position on ripple in physical plane ℓx		Non-separating flow $u/U_o = u_T/U_o$	Separating flow u_T/U_o	Stagnation points ℓx	ℓx
0.05π	0.5π	0.06π	0	crest	1.186	1.104	1.096	1.748
			$\pm\pi$	trough	0.864	0.804		
			-0.187	velocity	-	1.113		
			1.411	maxima	-	-2.929		
0.10π	0.5π	0.12π	0		1.458	1.080	0.668	1.975
			$\pm\pi$		0.761	0.564		
			-0.200		-	1.129		
			1.241		-	-2.740		
0.15π	0.5π	0.18π	0		1.891	0.900	0.326	2.294
			$\pm\pi$		0.680	0.323		
			-0.172		-	1.026		
			1.053		-	-2.482		
0.2π	0.5π	0.24π	0		2.691	0.504	0.093	2.744
			$\pm\pi$		0.614	0.115		
			-0.138		-	0.771		
			0.839		-	-2.204		

TABLE 12

KINETIC ENERGY CALCULATED FOR A SINGLE VORTEX IN THE FLOW

Radius of rotational vortex core $(a_r/2b)$	Height of vortex centre $(\chi_o/2b)$	Kinetic energy $T_k/\rho_f w\kappa^2$	Kinetic energy $T_k/\rho_f w(U_o a)^2$
0.05	0.50	8.617	0.1939
0.10	0.50	6.415	0.1443
0.15	0.50	5.100	0.1147
0.20	0.50	4.136	0.0930
0.25	0.50	3.356	0.0755
0.30	0.50	2.684	0.0604
0.35	0.50	2.079	0.0467
0.40	0.50	1.516	0.0341
0.45	0.50	0.977	0.0220
0.50	0.50	0.451	0.0101
0.05	0.60	9.193	0.2978
0.10	0.60	6.998	0.2267
0.15	0.60	5.696	0.1845
0.20	0.60	4.751	0.1539
0.25	0.60	3.996	0.1294
0.30	0.60	3.356	0.1087
0.35	0.60	2.790	0.0904
0.40	0.60	2.275	0.0737
0.45	0.60	1.793	0.0581
0.50	0.60	1.334	0.0432
0.55	0.60	0.889	0.0288
0.60	0.60	0.451	0.0146
0.05	0.70	9.678	0.4268
0.10	0.70	7.489	0.3302
0.15	0.70	6.194	0.2731
0.20	0.70	5.260	0.2319
0.25	0.70	4.520	0.1993
0.30	0.70	3.899	0.1719
0.35	0.70	3.356	0.1480
0.40	0.70	2.868	0.1264
0.45	0.70	2.418	0.1066
0.50	0.70	1.996	0.0880
0.55	0.70	1.594	0.0703
0.60	0.70	1.206	0.0532
0.65	0.70	0.826	0.0364
0.70	0.70	0.451	0.0199

Note. 1. Ripple steepness $b\ell = 0.15\pi$

TABLE 13

KINETIC ENERGY CALCULATED FOR A MEMBER OF AN INFINITE ROW OF VORTICES

Radius of rotational vortex core $(a_r/2b)$	Height of vortex centre $(\chi°/2b)$	Kinetic energy $T_{k/\rho_f w\kappa^2}$	Kinetic energy $T_{k/\rho_f w(U_o a)^2}$
0.05	0.50	8.612	0.1683
0.10	0.50	6.409	0.1252
0.15	0.50	5.091	0.0995
0.20	0.50	4.125	0.0806
0.25	0.50	3.340	0.0652
0.30	0.50	2.663	0.0520
0.35	0.50	2.052	0.0401
0.40	0.50	1.481	0.0289
0.45	0.50	0.934	0.0182
0.50	0.50	0.397	0.0077
0.05	0.60	9.490	0.2521
0.10	0.60	6.990	0.1856
0.15	0.60	5.685	0.1510
0.20	0.60	4.737	0.1258
0.25	0.60	3.978	0.1056
0.30	0.60	3.333	0.0885
0.35	0.60	2.761	0.0733
0.40	0.60	2.238	0.0594
0.45	0.60	1.747	0.0464
0.50	0.60	1.278	0.0339
0.55	0.60	0.822	0.0218
0.60	0.60	0.371	0.0098
0.05	0.70	10.241	0.3468
0.10	0.70	7.478	0.2533
0.15	0.70	6.181	0.2093
0.20	0.70	5.245	0.1776
0.25	0.70	4.500	0.1524
0.30	0.70	3.874	0.1312
0.35	0.70	3.324	0.1126
0.40	0.70	2.828	0.0958
0.45	0.70	2.370	0.0802
0.50	0.70	1.938	0.0656
0.55	0.70	1.524	0.0516
0.60	0.70	1.123	0.0380
0.65	0.70	0.730	0.0247
0.70	0.70	0.340	0.0115

Notes. 1. Ripple steepness bl = 0.15π

2. The vortex spacing is equivalent to one ripple wavelength ($a = \lambda$).